Physical Encapsulation of Interface Bilayers

Stephen Andrew Sarles

Dissertation submitted to the Faculty of the
Virginia Polytechnic Institute and State University
in partial fulfillment of the requirements for the degree of

Doctor of Philosophy
in
Mechanical Engineering

Donald J. Leo, Chair
Daniel J. Inman
Raffaella De Vita
James R. Heflin
Scott T. Huxtable
David Needham

8th April 2010
Blacksburg, Virginia

Keywords: lipid bilayer, physical encapsulation, regulated attachment method,
encapsulated interface bilayer

Physical Encapsulation of Interface Bilayers

Stephen Andrew Sarles
Virginia Polytechnic Institute and State University
Donald J. Leo, Advisor

ABSTRACT

This dissertation presents the development of a new form of biomolecular material system which features interface lipid bilayers capable of hosting a wide variety of natural and engineered proteins. This research builds on the droplet interface bilayer (DIB) platform which first demonstrated that, through self-assembly, lipid-encased water droplets submersed in oil can be physically connected to form a liquid-supported lipid bilayer at the droplet interface. Key advantages of the DIB method over previous bilayer formation techniques include the lack of a supporting substrate which simplifies bilayer formation and the ability to connect many droplets to form 'cell-inspired' networks which can provide a collective utility based on the compositions and arrangement of the droplets. The research present herein specifically seeks to overcome three limitations of the original droplet interface bilayer: limited portability due to lack of droplet support, the use of externally supported electrodes to electrically probe the network, and the requirement that in order to form DIB networks, aqueous volumes must be individually dispensed and arranged.

The approach presented in this document is to provide increased interactions between the contained liquid phases and a supporting substrate in order to achieve both increased usability through refined methods of packaging and *in situ* interface formation which eliminates the need to create individual droplets. *Physical encapsulation* is defined as the the use of a solid substrate to contain both liquid phases such that the aqueous volumes are physically supported on one length scale ($10 - 1000\mu$m) while not inhibiting the self-assembly of phospholipids at the oil/water interface occurring on a much smaller length scale ($1 - 10$nm).

Physically-encapsulated droplet interface bilayers are achieved by connecting lipid-encased droplets within a substrate that tightly confines the positions of neighboring droplets. A term called the *packing factor* is introduced to quantify the ratio of the aqueous volumes per the total compartment volume. Physically-encapsulated droplet interface bilayers formed in high packing factor substrate (30%) that also features integrated electrodes demonstrate all of the properties that unencapsulated DIBs exhibit (electrical resistances greater than 1GΩ, failure potentials between $|200 - 300|$mV, and the ability to host transmembrane proteins) but these confined assemblies can be moved, shaken, and even completely inverted. Additionally, a structured experiment to quantify the durability of interface bilayers shows that encapsulated and unencapsulated droplet interface bilayers can both survive $3 - 7$g of lateral acceleration prior to bilayer failure, but have different modes of failure. Encapsulated DIBs tend to rupture, while unencapsulated DIBs completely separate.

Physical encapsulation is also shown to permit the *in situ* formation of durable interface bilayers when the substrate is made from a flexible material. The importance of this approach stems from the fact that, by using the substrate to locally partition a single aqueous volume into multiple volumes, there is no need to arrange individual droplets. This method of bilayer formation is termed the *regulated attachment method (RAM)*, since the separation and subsequent reattachment of the aqueous volumes is regulated by the opening and closing of an aperture within the flexible substrate. In this dissertation, a mechanical force is used to directly modulate the aperture dimension for controlling both the initial formation and final size of the interface. With the demonstrated advantages of portability and controlled attachment offered by physical encapsulation, encapsulated lipid bilayers are formed within a completely sealed flexible substrate. A key aspect of this final work is to demonstrate that both the organic and aqueous phases can be stabilized internally, creating a complete material system that features tailorable interface bilayers.

To Kelsey, Mom, Dad, and Ben

Acknowledgments

Many people have contributed tremendously to the work that comprises this dissertation[1]. I would especially like to thank my advisor, Dr. Don Leo, for his guidance, encouragement, and friendship. Dr. Dan Inman also deserves special recognition for his advice and friendship—and for always having a good (and often WV-related) joke on hand. I would also like to thank Dr. Randy Heflin, Dr. Scott Huxtable, Dr. David Needham, and Dr. Raffaella De Vita, for their insights and recommendations that has benefited this work. Beth Howell has been instrumental in my work and deserves many thanks for her assistance. My many CIMSS colleagues (both former and present) deserve special thanks for their friendships, technical advice, and willingness to lend a hand. Finally, I would like to acknowledge those that have supported me from the beginning, my family. My wife, Kelsey, my parents, and brother were all too vital in providing me with love, support, patience, and good food along the way.

Andy Sarles

Virginia Polytechnic Institute and State University

8th April 2010

[1]The author would also like to acknowledge financial support offered through Office of Naval Research (N000140810654) as well as supplemental funding from the Virginia Space Grant Consortium (VSGC).

Table of Contents

List of Figures

List of Tables

Chapter 1

Introduction and Literature Review

The diversity in both the structure and function of living organisms and natural materials provides both inspiration for new designs and benchmarks for comparing realized prototypes. Scientists have long studied nature to better understand how plants and animals function and consequently, their efforts have led to a vast array of technological milestones. In 1674 Anton Van Leeuwenhoek, a microscope lens grinder, discovered microorganisms in a drop of water, establishing the study of microbiology and bacteriology that continues today. Frederick Banting and his colleagues (1920's) identified the hormone insulin and its role in balancing blood sugar, thereby creating an effective and necessary treatment of diabetes and saving millions of lives. More recently, the mapping of the human genome, which includes $20 - 25$ thousand genes, marks continued progress and hope toward screening, treating, and curing of a large number of chronic conditions and diseases [1]. In a similar light, scientists and engineers have begun to create bio-inspired materials and devices to solve difficult problems, including flapping and morphing wing designs for flight control of small aircraft used in unmanned surveillance [2, 3], implantable heart replacement systems such as the AbioCor [4, 5], and synthetic ligament tissues and novel drug delivery systems made from natural

spider silk [6, 7, 8], to name a few. A bio-inspired design process involves first identifying how nature has evolved to tackle specific challenges and then using either synthetic or natural materials to construct assemblies that share structure and/or function with their biological kin in order to combat similar tasks [9].

The highly-unique, extensively-networked, and naturally-hierarchical construction and operation of the cellar structures of plants and animal provides a wealth of inspiration for creating novel sensors [10, 11, 12], actuators [13], nano-machines [14, 15, 16], energy-conversion units [17, 18], and assembly and organization guidelines [19]. Proteins are biomolecules in cells that facilitate nearly all of the crucial metabolic processes within the cell. Several of the roles that these molecules play include acting as pumps, selective gates, switches, catalysts, receptors, and motors, along with being structural elements in membranes and producing genetic material for sustaining the identity of the cell. The function(s) of a given protein is directly related to its structure, and so changes to its chemical makeup affect its inherent abilities. Biologists have studied the activities of many proteins from nature and more recently, biochemists and genetic engineers have developed precise methods for creating new mutations of existing proteins. Yet, the use of functional proteins in commercially available applications is limited and often the reason for this limitation is that proteins must exist in an environment which mimics that found in a cell. Without this condition, many proteins can not adopt their functional configuration and thus, can not carry out their inherent tasks.

This work seeks to extend our capabilities as engineers and material scientists in being able to properly host and make use of a diverse selection of biological molecules, including proteins, for creating new bio-inspired device concepts. Specifically, efforts to understand how to assemble biomolecules into functional structures and then preserve this configuration for long-term use will be addressed. Methods to characterize these phase-separated assemblies and techniques that increase our understanding of how biological molecules can be arranged

for increased functionality are also developed.

1.1 Bio-inspiration from Cells

A specific subset of bio-inspired scientific research is geared toward the study of individual plants and animal cells, including the underlying biomolecules that comprise them. With its its roots in traditional biology, efforts to understand the link between structure and function of these biomolecules (specific types and functions of these components will be provided later) enables scientists and engineers to create new materials and devices that offer similar functionality and diversity. First, the basic structure of the eukaryotic cell, found in plants, animals, fungi, and protists, is reviewed in order to better understand the specific inspiration derived from these organisms.

1.1.1 The Eukaryotic Cell

Eukaryotes are organisms whose cells are organized into complex structures, including the nucleus, and which are enclosed by cell membranes [20, 21]. In contrast, prokaryotic cells found in bacteria, are much simpler structures characterized by a nearly-featureless internal volume, called the cytoplasma, which is enclosed by a plasma membrane and lacking a cytoskeletan. As a result of their compartmentalized form, eukaryotic cells feature specific power plants called mitochondria (in animals) and chloroplasts (in plants); whereas the production of energy in prokaryotic cells is a function of the cell as a whole. These differences in organization also lead to different modes of species transport within the cytoplasm. The movement of macromolecules in prokaryotes is dominated by diffusion through the water-based cytosol, while eukaryotes depend on a network of endomembranous organelles including

the endoplasmic reticulum, the Golgi apparatus, lysosomes, and vacuoles connected via mobile vesicles [21, 22]. Eukaryotes also posses mechanoenzymes that convert metabolic energy in the form of adenosine-triphosphate (ATP) into mechanical work through hydrolysis. The highly-organized nature of eukaryotic cells showcases how hierarchical assembly of molecules into membranes, membranes into organelles, and networked organelles into functioning cells produces complex, yet efficient building blocks.

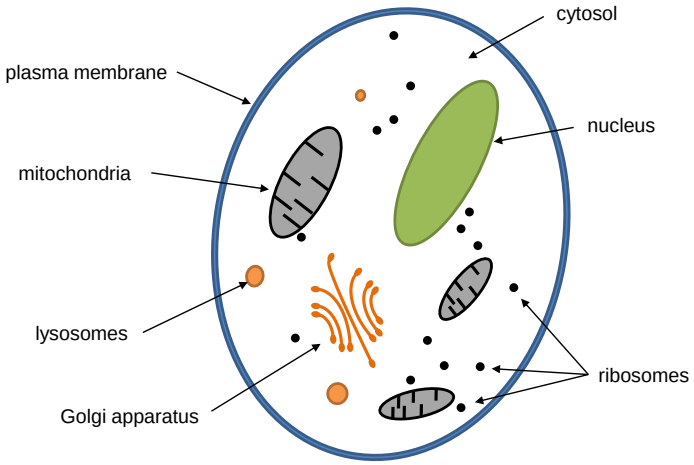

Figure 1.1: The cellular structure of eukaryotes features many internal compartments within the cytoplasm, including the nucleus, which contains the genetic information of the cell and regulates gene expression.

The simplified schematic of a eukaryotic cell in Figure 1.1 shows some of the primary organelles contained within the plasma membrane. The roles of these organelles are specific, from energy-production in the mitochondria, to the processing and packaging of biomolecules such as proteins and lipids that are produced within the cell in the Golgi apparatus, to the translation of proteins from RNA in the ribosomes and the digestion of organelles, food particles, and bacteria in lysosomes. These structures work in harmony to carry out the primary roles of the cell: growth of the organism, through cell division and sustaining life through metabolic processing of nutrients [21].

1.1.2 Cell Membrane: A Selective Barrier

A key feature of both eukaryote and prokaryote cells is the cell membrane. This water-insoluble structure serves to define the outer boundaries of the cell and, in eukaryotic cells, cell membranes also define the sizes and shapes of the organelles within the cytoplasm. The composition of the cell membrane allows it to simultaneously block diffusion and enable selective transport of species into and out of the cell. Harold describes the dual-natured purpose of the cell membrane in more general terms. "To stay alive you have to be able to hold out against equilibrium, maintain imbalance, bank against entropy, and you can only transact this business with membranes in our kind of world" [21].

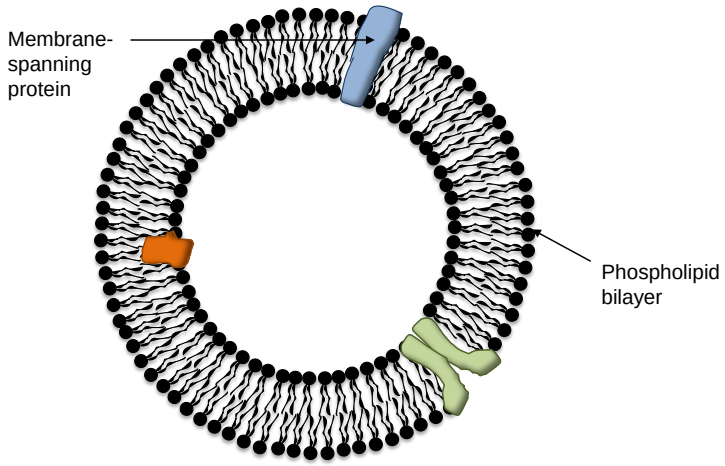

Figure 1.2: The cell membrane structure is defined by a bilayer arrangement of phospholipid molecules but also contains proteins, cholesterol (not shown), and other biomolecules.

The primary structural elements of a cell membrane (shown in Figure 1.2) are phospholipid molecules organized into a *lipid bilayer* (or bilayer lipid membrane (BLM)), though other molecules including carbohydrates, cholesterol, proteins, and metallic ions are present in living cell membranes [23]. Selective transport of species through this ultra-thin (only $5-7$nm thick) membrane is aided via the proteins that bind to and reside within the cell membrane. This composite structure is not a static assembly but fluid-like, allowing diffusion

of lipids and protein in the plane of the membrane [24]. The properties and functions of phospholipid molecules and bilayers and the relationship between structure and function of proteins embedded in these membranes are examined below in greater detail.

1.1.3 Phospholipids and Lipid Bilayers

Lipids are defined as biological material soluble in organic solvents, such as ether or chloroform [25]. Lipid molecules are amphiphatic structures (meaning "hating both") in that part of the molecule does not like to be around water while the rest does not like to be in a nonpolar environment [22]. The term amphiphilic, meaning "loving both," can also be used since the hydrophilic region of the molecule orients towards the aqueous phase while the hydrophobic (or lipophilic) sections of the molecule are sequestered from water. More generally, lipid molecules fall into a category of molecules known as surfactants, or surface active agents, as they reduce the interfacial tension at the interface between two fluids [26]. Phospholipids are a type of lipid molecule characterized by a phosphate-based polar head group that attaches to a glycerol molecule through a phosphodiester link [22]. The glycerol molecule then links the hydrophilic head group to one or two hydrophobic acyl tail groups. Figure 1.3 shows the chemical structure for diacyl saturated (i.e. zero double bonds in the hydrocarbon chain) phosphatidylcholine (PC) molecule having identical 16-carbon tails. Not all phospholipids, however, have identical hydrocarbon chains. Phospholipids can have two dissimilar hydrocarbon chains per molecule and one or both of these chains can be unsaturated [22, 27]. Phosphatidylethanolamine (PE), phosphatidylserine (PS), and phosphatidylglycerol(PG) are additional head groups common to phospholipids native to plant and animal cells.

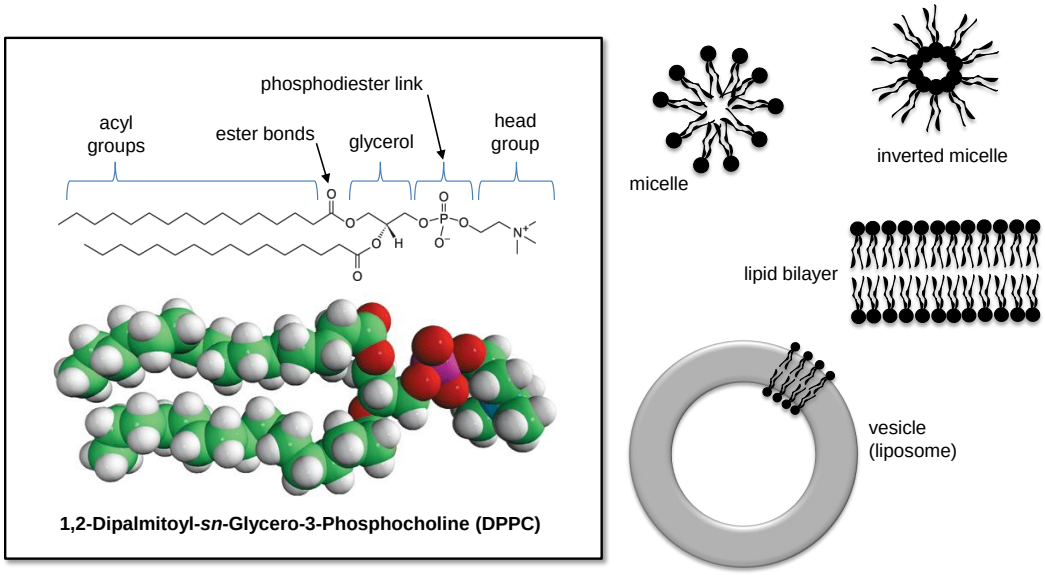

Figure 1.3: Phospholipids, such as DPPC, consist of a hydrophilic head group and two hydrophobic fatty acid tails. Amphiphilic molecules including phospholipids can self-assemble into ordered arrangements due to the hydrophobic effect.

Self-Assembly of Amphiphiles

Lipid molecules, due to their amphiphilic nature, spontaneously organize into various mesoscopic structures. In water, phospholipids can form aggregates called micelles, planar lipid bilayers, and spherical lipid bilayers known as vesicles or liposomes, where the head groups shield the oil-loving tails from the surrounding polar environment (see Figure 1.1.3). In an nonpolar solvent, inverse micelles are formed, with the tails of the lipid molecules facing outward. The organizational drive, which Tanford termed the Hydrophobic Effect [28, 29], is present whenever there is a "sufficiently high concentration of amphiphilic molecules (or ions) containing a polar or charged group at one end, attached to a relatively large hydrocarbon moiety...The opposing thermodynamic preferences of the two ends of such a molecule are most simply satisfied by self-association to form an aggregate with the hydrocarbon chains in the middle, avoiding contact with water as much as possible, and the hydrophilic polar groups at the surface ..." [28]. This desire to reach a thermodynamic equilibrium arises not

just because of an attraction of like molecules, but primarily due to repulsion forces between the water and the hydrophobic regions of the lipids.

Accordingly, the chemical composition as well as the size and shape of the lipid molecules determines which types of organized structures are formed [30, 25, 31, 32]. Small surfactant molecules form stable micelles in water when the concentration of the surfactant is greater than what is termed the critical micelle concentration (cmc). Two-tailed phospholipids, however, prefer to form bilayer structures, either planar bilayers or vesicles [22]. Furthermore, inverse micelles are more stable as small aggregates in a nonpolar solvent and thus, no equivalent CMC is observed for these mixtures [33]. Hydrophobic interactions not only drive the initial formation of ordered assemblies, but also play a role the fluid-like nature of the lipid bilayer [24] and in determining the location and insertion mechanism of proteins into the bilayer [28, 34, 30, 32, 35].

Physical Properties of Lipid Bilayers

The physical properties of lipid bilayers have been studied extensively in order to understand how the environment in cell membranes facilitate an enormous diversity of biomolecules that conduct nearly all of the vital processes that are performed in living organisms. Several notable papers that offer a more in-depth look at the physical nature of these structures include those by Evans [36], Needham, et al [37, 38, 39, 40] and McIntosh and Simon [35]. The discussion presented here serves merely to introduce the concept of a fluid membrane and highlight how the properties of the membrane are linked to structure and manner of assembly.

The chemical structure of the lipid molecules as well as the manner in which they are bound together in the membrane govern the physical properties of bilayer lipid membranes.

Phospholipid bilayers are ultra-thin liquid-crystalline membranes formed through the spontaneous self-assembly of amphiphilic lipid molecules in water in order to minimize free energy [37, 36]. These structures exhibit great resistance to change in molecular surface density [36] and the individual molecules interact nonspecifically through long-range electrostatics, electrodynamic and solution forces, including van der Waals interactions, electric double-layer repulsion, and hydrophobic interactions. These nonspecific forces permit mobility of the lipids in the plane of the membrane and influence the surface density of the lipid molecules (phospholipids occupy approximately $65\mathring{A}^2$ per molecule [40]). Substituting different types of lipids into a membrane affects the thickness and elasticity of the membrane, as well as the the fluidity of the bilayer (a function of hydrocarbon chain order). The relative size and shape of lipid molecules also affect the intrinsic radius of curvature, which is the propensity to lie flat or bends toward or away from water [31, 34, 32, 41].

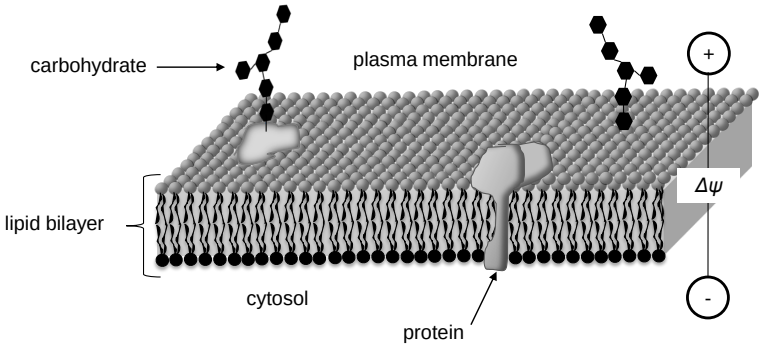

Figure 1.4: The fluid mosiac structure of a cell membrane is a conglomerate structure including integral membrane proteins carbohydrates (black hexagonal complexes attached to the proteins) embedded in a lipid bilayer. $\Delta\Psi$ represents the transmembrane potential, which is negative inside (cytosol side) of the cell.

A phospholipid bilayer, much like traditional engineering materials such as metals and polymers, exhibits a phase-transition temperature that causes changes to the material properties of the membrane[25, 42]. Lamellar phases of phospholipids can exist as either "anisotropic fluid acyl chains or solids with crystallized chains" [36]. The fluid nature of a liquid-crystalline

bilayer transforms into a viscous gel state when the temperature plunges beneath the transition temperature, T_C. Fluid bilayers, like cell membranes at physiological temperatures, facilitate the mobility of lipids and proteins into, out of, and within the membrane necessary for carrying out many metabolic processes [22, 35]. However in the gel-state, the membrane literally loses its fluidity. Frozen cell membranes are susceptible to cracking, which puts at risk the contents of the cell. The temperature at which this transition occurs is dependent on the chemical structure and size of the hydrocarbon tails and on head group chemistry. Generally, phospholipid molecules with longer hydrocarbon tails can achieve a packing state of higher-order than that of short-chained lipids and thus have higher transition temperatures [42, 25, 43]. Measured gel-liquid crystalline temperatures in diacyl, saturated phosphatidylcholine molecules indicate an increase of approximately 20^oC for each two-carbon added to the acyl group [42]. Conversely, an increase in the degree of unsaturation in the hydrocarbon chains results in a dramatic reduction in the transition point. The inclusion of a single unsaturated fatty acid at the first or second carbon in the glycerol backbone lowers the transition temperature from 41^oC for dipalmitoyl phosphatidylcholine (DPPC) to -5^o for the palmitoyl-oleoyl phosphatidylcholine (POPC). The transition temperature is also affected by the head group species. Phosphatidylethanolamine (PE) molecules display T_C values 20^oC higher than the corresponding lipid molecule with a phosphatidylcholine head group [25, 42].

1.1.4 Proteins: Nature's Polymers

Proteins are biomolecules that carryout nearly all of the functions of the cell and, while most of these functions depend on the ability of the protein to recognize specific molecules called ligands through binding [22, 44], proteins can also be structural elements, such as keratin in hair and fibroin in silk, they can be enzymes such ATPase that hydrolyze chemical energy, and, when residing in the cell membrane, they can transport matter (pumps and ion

channels) as well as send and receive information [21, 23]. In addition, one of the key tasks of proteins is to synthesis new DNA [22]. The enormous diversity offered by proteins is a result of their construction; proteins are built from a palette of only 20 amino acid monomers that each has its own shape and chemical properties, yet proteins be assembled together in a countless number of combinations and lengths. The term *peptide* is used to describe polymers containing less than 50 amino acid monomers, while *polypeptide* is used to describe longer chains of amino acids. Proteins are generally large molecules, with molecular weights ranging from a few kilodaltons (kDa) to hundreds of kDa [22].

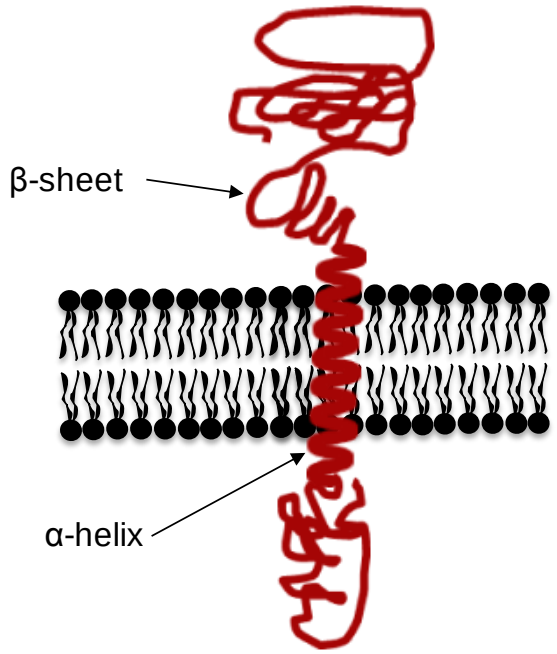

Figure 1.5: The tertiary structure of a transmembrane platelet derived growth factor receptor protein shows the complexity and relative size of a protein structure (reproduced from [21]).

Structure and function are intimately linked in proteins. The linear sequence of amino acids that comprise a given protein is called the primary structure. Hydrogen bonding between successive amino acids cause local organizations of the protein backbone called secondary structures, which include α-helix and β-sheets (see Figure 1.5). Functionality,

though, is derived from the protein adopting, or "folding into," a three-dimensional, or tertiary, structure which is unique to a given protein. The process of a protein folding into this three-dimension configuration is largely driven by hydrophobic interactions of the amino acids (some are hydrophilic while others are hydrophobic) with each other, the protein backbone, and with surrounding water molecules. For example, proteins fold into a globular shape in water in which the hydrophobic segments are clustered in the center of the protein. Similarly, transmembrane proteins can bind to and even self-insert into lipid bilayers, such that hydrophobic segments can interact with the hydrocarbon core of the membrane. The tertiary structure of a protein is held together by hydrogen bonds, electrostatic interactions, van der Waals forces, and hydrophobic interactions of the amino acids [21, 28].

A specific class of proteins function as integral membrane proteins (Figure 1.5), linking opposites sides of the bilayer for the transport of mass and information. Segments of amino acids within these elements may pass through the hydrophobic core of the membrane multiple times and even aggregate with other integral membrane proteins to form multi-molecular (quaternary) structures. Alpha-hemolysin (α-HL) is one transmembrane protein that forms aggregates of seven called heptamers in order to construct a conductive water channel through the thickness of the bilayer [45, 46, 11, 47].

1.2 A Comparison of Functional Biomolecules and Traditional Active Materials

The previous sections introduced the basic composition and structure of the eukaryote cell common to both plants and animals. Specifically, the properties of the cell membrane, a composite structure composed of a lipid bilayer and other biomolecules including proteins,

were examined in order to better understand the environment that functional biomolecules require in order to carry out their tasks. A key concept that governs many of the properties of these material elements is what Tanford termed the *Hydrophobic Effect* [28]. These repulsive interactions are the driving force for the formation of the bilayer and the spontaneous folding of a protein into its tertiary structure, whether in water or in a cell membrane, and they help to determine the fluid nature of a cell membrane.

The ability to study proteins requires they be reconstituted into a lipid bilayer, which mimics the cell membrane. Furthermore, with the capability to form a lipid bilayer, natural proteins and those genetically-engineered in a lab can be used to develop new protein-based technologies. The key relationship between structure and function defines the operating characteristics (i.e. input stimulus versus output response) of these macromolecules and the nearly-endless number of combinations of amino acids used to make proteins ensures that engineers have only begun to find ways to use this functionality. The methods for formation and characterization of bilayer lipid membranes will be introduced in an upcoming literature review, but first, a comparison between biomolecules and tradition active materials reveals similar input-output relationships (Figure 1.6).

The table shown in Figure 1.6 presents the input stimulus and output response of common active materials including piezoelectric ceramics, ionic polymer transducers, and shape memory alloys. The first two materials couple mechanical strain to an electric field, while shape memory alloys create mechanical strain through crystal reorientation in response to a change in temperature. Proteins that reside in in a lipid bilayer (Figure 1.6) also provide links between multiple forms of energy in order to conduct various metabolic tasks. ATPase enzymes convert the chemical energy found in adenosine-triphosphate (ATP) into a proton current [48], while $At\mathrm{SUT}_4$ proteins respond to a pH gradient by co-transporting sucrose and water molecules through the bilayer [49]. Since each protein has a different structure

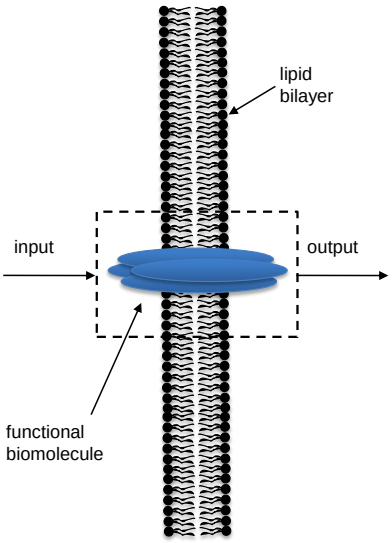

Active element	Input	Output
Piezoelectric	electric field/strain	strain/electric field
Ionic polymer transducer (IPT)	electric field/strain	strain/electric field
Shape memory alloy (SMA)	temperature-stress	strain
ATPase[1]	ATP (chemical energy)	proton current
$AtSUT_4$[2]	pH gradient	sucrose/H_2O co-transport
bacteriorhodopsin (bR)[3]	light energy	proton current
MscL[4]	increase in membrane tension	conductance increase (channel opens)

1. V. B. Sundaresan, S. A. Sarles, D. J. Leo, "Chemoelectrical energy conversion of adenosine triphosphate", presented at *Active and Passive Smart Structures and Integrated Systems 2007, San Diego, California, USA,* ***2007.***
2. V. B. Sundaresan, D. J. Leo, *Sensors and Actuators B: Chemical* ***2008, 131, 384.***
3. T.-J. M. Luo, R. Soong, E. Lan, B. Dunn and C. Montemagno, *Nat Mater* ***4:220-224 (2005).***
4. S. I. Sukharev, P. Blount, B. Martinac, F. R. Blattner and C. Kung, *Nature* ***368:265-268 (1994).***

Figure 1.6: The input-output relationship inherent in proteins are not so different from those found in traditional active engineering materials.

and this structure then determines its unique function, substituting proteins that reside in a bilayer for a different type of biomolecule results in a different transduction behavior. Others have shown that the protein bacteriorhodopsin (Br) produces a proton current by absorbing photons from light [18] and the large conductance mechanosensitive channel, MscL, found in *E. Coli* prokaryote cells increases the ability of ions to move through the channel in response to a mechanical strain in the membrane, like a bio-strain gage.

This comparison highlights the similar input-output relationships that complex biomolecules share with traditional active materials. The key difference between these two classes of material elements is that there exists a much greater diversity in transduction mechanisms with biological molecules than currently exists in the traditional engineering materials. By building the capability to form lipid bilayers for hosting these molecules, a new class of active materials that rely on their inherent abilities awaits.

1.3 Literature Review

The formation of a bilayer (or "black") lipid membrane (BLM) is necessary for investigating and assembling integral membrane proteins for use in protein-powered device concepts [50, 51, 23]. This $5 - 7$nm thick artificial phospholipid bilayer mimics the environment of a cell membrane, providing a suitable environment for the reconstitution of proteins [50, 52, 53, 54, 23]. The following literature survey reviews the origins of BLM research, methods of bilayer formation, characterization techniques and experimental results, and the device concepts that have been developed using lipid bilayers. This information is presented in a format designed to highlight the long-term efforts and continued interest in forming synthetic analogs to natural cell membranes. These structures offer the unique environment necessary for reconstituting functional biomolecules, but also present many challenges in creating macro-scale functionality and achieving long-term durability from nano-scale molecular assemblies.

1.3.1 History of Bilayer Lipid Membranes

The term "black lipid membrane" originates from observations of soap films at the air-water interface performed by Robert Hooke and Isaac Newton in the 17th century [51, 23]. These famous individuals observed that the mono- and bimolecular films formed from soap and lipid molecules, respectively, did not reflect transmitted light due to their ultra-thin structures, thus having a black appearance. Hooke's and Newton's original findings provided evidence that molecules had the ability to self-assemble into ordered structures on the molecular scale. The ordering and reduced surface tension of an air-water interface by fatty-acids, such as those found in cooking oils, were later observed by Benjamin Franklin in 1774, Agnes Pockels in 1891 [55], and Langmuir in the early 20th century [23]. Gorter and Grendel (1925) proposed the first description of a bimolecular lipid leaflet when they determined that the

lipids extracted from red blood cells covered an area twice that of the surface area of the cells [56]. Years later Rudin discovered a similar "black membrane" could be formed using natural lipids underwater and that "excitability-inducing molecules" (proteins) lowered the electrical resistance of the membrane through "penetration and/or formation of channels" [50]. This seminal work established not only a method for creating lipid bilayers and reconstituting proteins *in vitro* across a porous support separating two aqueous chambers, but it also established the use of electrical measurements to characterize these assemblies.

1.3.2 Methods of Lipid Bilayer Formation

Several bilayer formation techniques have evolved over the last fifty years of research. These methods each make use of the amphiphilic properties of the phospholipid molecules in order to aid assembly. A vast majority of lipid bilayers are formed on a supporting synthetic substrate and, in these cases, the methods used also take into account the surface properties and geometry of the supporting material in order to further facilitate bilayer formation. Common supporting structures in BLM research have included steel wire loops [50, 52], Teflon sheets containing single apertures [57, 58, 59, 60, 61], porous micro-filter membranes made from polycarbonate, cellulose, or glass fibers [62, 63, 64, 65, 66, 67], porous ceramic alumina [68, 69], and solid planar substrates made from glass, gold, and silicon [70, 71, 72, 73, 74]. The selection of the material type and geometry of this support structure affects how the bilayer assembles, and in some cases, determines which procedure(s) can be used to form the membrane. The most commonly used techniques for forming bilayers include lipid folding, Langmuir-Blodgett (LB)/Langmuir-Schaefer (LS), vesicle fusion, and lipid painting. The use of a supporting substrate is not a requirement, however, as the recently-developed droplet interface bilayer (DIB) method creates liquid-supported bilayer lipid membranes at the interface of adjacent water droplets submerged in a nonpolar medium.

Lipid Folding

Lipid folding, also known as the Montal-Mueller (MM) technique, is a common technique for reconstituting a lipid bilayer membrane across an aperture formed in a hydrophobic material (such as Teflon or silicon) separating two chambers filled with aqueous electrolyte solution [60]. First, a lipid solution of phospholipids dissolved in an organic solvent such as pentane or chloroform is spread across the surface of the aqueous medium at a level below that of the aperture to form a monolayer of lipids at the air/water interface. A lipid bilayer is then formed when the lipid monolayers on each side of the septum "fold" together across the aperture as the levels of electrolyte solutions in each chamber are raised simultaneously (see Figure 1.7). This method requires a hydrophobic substrate in order to anchor the lipid bilayer to the supporting substrate because of the "tails-up" orientation that each lipid monolayer first assumes at the air/water interface. This method also requires precise control of the fluid levels in each chamber in order to fold the monolayers together and can be used to form bilayers across single pores ranging in size from 0.2μm to 3mm [57, 58, 59, 60, 61].

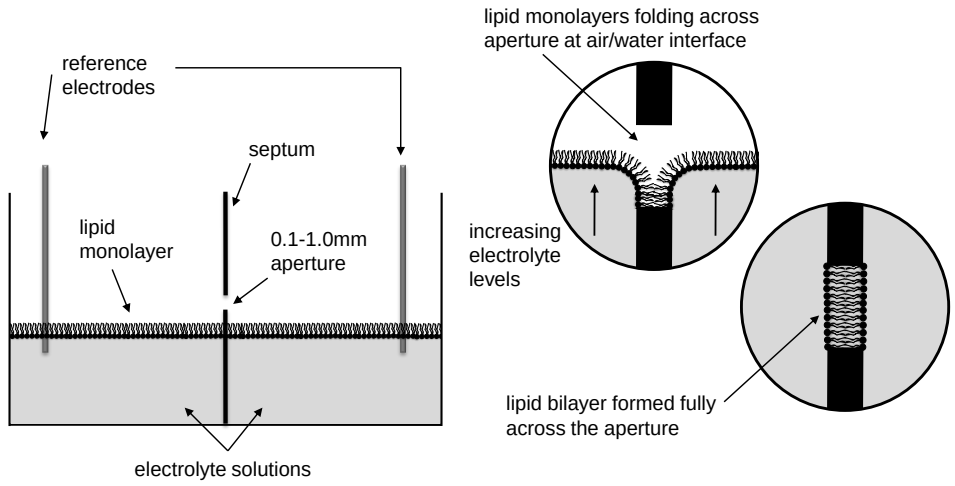

Figure 1.7: The lipid folding technique creates a bilayer across the pore of a septum that separates two aqueous chambers.

The lipid folding method has mostly been used for studies involving the formation of a pla-

nar BLMs across a single pore in order to host other biomolecules for various ion channel gating [61, 72] and protein function experiments [70, 69]. However, Mayer, et al used the lipid folding technique for forming BLMs over three separate pores arranged vertically in the same Teflon membrane [61]. Nikolelis and Siontorou also used lipid folding when they developed a biosensor that detects acetylcholine, urea, and penicillin by flow injection through micro-bilayers supported on porous filters [62]. They chose lipid folding over other forming techniques in order to eliminate the effects of unevaporated solvent from the lipid solution that can possibly and adversely affect BLM formation, stability, and protein functionality. In general though, applications and studies that require large-area lipid bilayers, or multiple supported BLMs, use other techniques for forming horizontal bilayers on a different type of support.

Langmuir-Blodgett and Langmuir-Schaefer

In the 1930s, Iving Langmuir and Katharine Blodgett developed a technique, later known as the Langmuir-Blodgett (LB) method, for depositing monolayers of amphiphilic molecules on solid surfaces. Their early work demonstrated that stearic acids [75], calcium stearate [76], and barium-copper stearates [77] could be deposited in successive layers to form thin films on glass. Simply, their technique involved spreading a monomolecular layer of amphiphilic molecules onto the surface of a water bath and then by lowering and raising a glass slide vertically through the air-water interface, the hydrophilic regions of the molecules would adhere to the glass. A second dipping cycle into the water formed a bilayer film, since the lifting motion attracted molecules oriented with their hydrophobic region toward this first layer. A variation of this technique, called the Langmuir-Schaefer (LS) method, assembles the second layer by moving the glass slide horizontally across the surface of the water at a constant pressure [78].

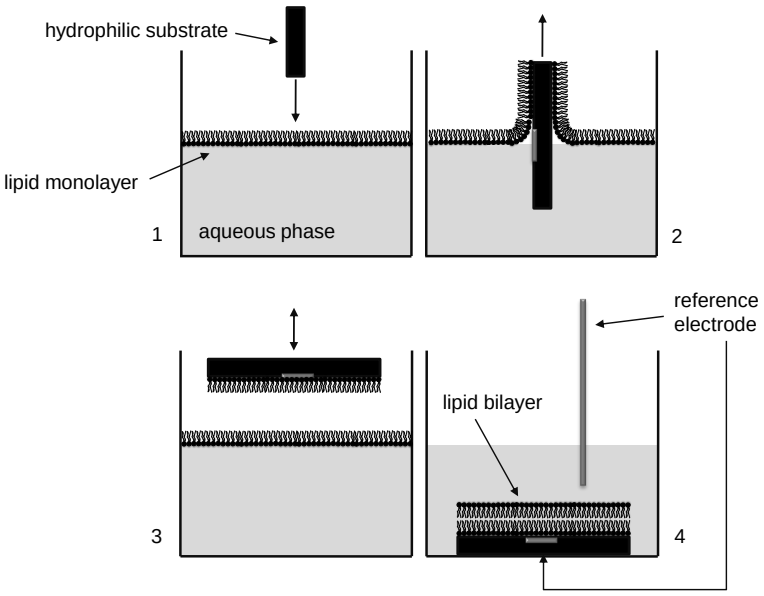

Figure 1.8: Lipid bilayer formation on a hydrophilic substrate using a combined LB-LS technique.

The formation of a bilayer lipid membrane using LB/LS techniques is shown in Figure 1.8. In the first block, the formation of a phospholipid monolayer is spread across an aqueous phase. When the hydrophilic support is then lifted out of the medium (2), a monolayer forms with the headgroups oriented toward the support on both sides. The LS technique is then employed to complete the BLM by lowering and pulling the support horizontally across the surface of the lipid-coated aqueous subphase (3). The LB technique with vertical "dipping" is traditionally not used for lifting the second monolayer because phospholipid headgroups have such a high affinity for the water subphase. Rather than lifting a second lipid monolayer, the first monolayer is stripped away from the support by the lipid molecules floating on the water surface [79].

While this method is a simple idea and can produce great repeatability in layer formation for many materials, the use of LB/LS on phospholipid membranes has not endured as much success. The quality of BLMs formed by LB have not shown nearly as much consistency as

those formed by lipid painting [79]. Incorporating integral membrane proteins into the BLM provides additional challenges [71]. Kalb, et al, used LB to deposit an initial phospholipid onto quartz, but then employed a second method called vesicle fusion in order to obtain a complete BLM with embedded proteins [80].

Vesicle Fusion

Eukaryote cells use vesicle formation and fusion in order to efficiently package proteins and lipids in the Golgi apparatus for delivery to the plasma membrane and other endomembranes within the cytoplasm, as well as for secretion of macromolecules from the cell [22, 81]. A similar process has been developed that creates lipid vesicles and then transfers them to a desired surface in order to build a lipid bilayer or to a preexisting bilayer to facilitate protein and lipid insertion [82, 83]. Aside from bilayer formation, vesicles (liposomes) are also used for controlled drug-delivery capsules [84, 85, 86], nanoreactor platforms [87], and novel biosensors [12].

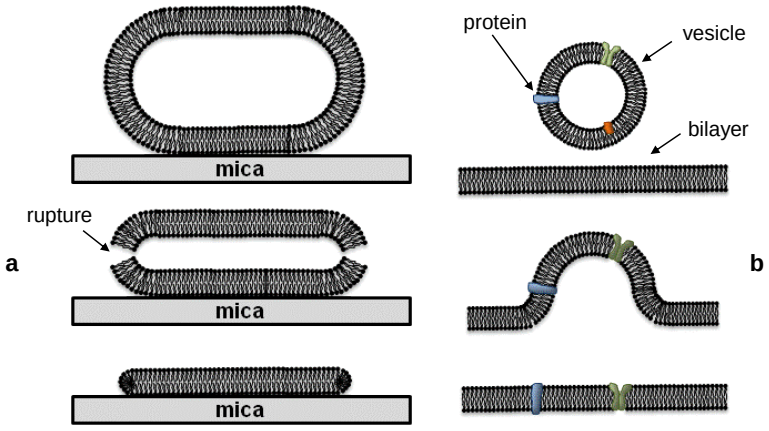

Figure 1.9: The formation of supported lipid bilayers is achieved by the rupture of vesicles at the surface of the mica substrate [82] (a). Vesicles can also be used to transport other biomolecules into a preexisting lipid membrane [83] (b).

The vesicle fusion technique for assembling bilayer lipid membranes is a multi-step process

[88, 89, 90] beginning with vesicle formation. First, a lipid solution is dissolved in an organic solvent such as chloroform. The solvent is then evaporated, leaving a dry lipid film. The lipid film is subsequently re-hydrated with an aqueous buffer solution, which initiates the self-assembly of the phospholipid molecules into vesicles. Sonication and/or vortexing [91, 80], multiple freeze/thaw cycles [91, 80, 92, 83, 93], and extrusion [91, 80, 88] through small pores further promote the formation of vesicles and help to obtain vesicles of a more uniform size distribution. In addition, the number of lamellar layers in the vesicles can be controlled by varying the number of extrusion cycles and/or sonication conditions (power and time) [88]. The incorporation of transmembrane proteins into lipid vesicles is possible by adding the protein into the initial lipid solution [91, 82, 83]. Liposomes are then transfered onto a supporting substrate such as gold, glass, mica, and quartz in order to induce vesicle rupture and BLM formation shown in Figure 1.9. Many variations of this process also exist, though the basic technique is to coat the vesicle solution onto a clean, surface-treated substrate and let it incubate for some amount of time. Finally, the lipid covered substrate is rinsed with buffer solution to remove excessive layers of lipids, leaving a planar BLM supported by the substrate.

Kalb, et al devised a variation of this formation technique in order to reduce interactions between integral membrane proteins and the hydrophilic support, thus preserving the lateral mobility of these proteins within the BLM [80]. First, their method consisted of forming a phospholipid monolayer using the Langmuir-Blodgett technique onto a quartz slide. Then, vesicles produced via extrusion were absorbed onto the supporting monolayer to complete BLM formation and safely incorporate proteins into the membrane.

Lipid Painting

Probably the least scientific of the bilayer formation techniques is a method called lipid painting. As the name suggests, planar BLMs are formed with an instrument used to physically spread a solution of phospholipids dissolved in an organic solvent onto a supporting substrate. The solvent is necessary for the lipids to remain fluid-like for obtaining better coverage when painted. The solvent then drains away or evaporates, leaving a film of lipid molecules. Self-assembly into an ordered configuration does not occur until the lipid-covered substrate is immersed in an aqueous medium. At this point, the quest to minimize free energy driven by hydrophobic interactions leads to ordered assemblies of lipids. When the supporting structure is given a hydrophilic surface treatment, a planar bilayer is favorable as the polar headgroups of one side of the bilayer orient toward the substrate (see insert in Figure 1.10).

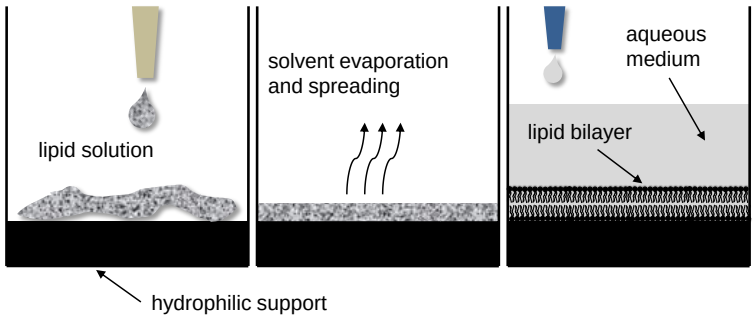

Figure 1.10: Lipid painting relies heavily on the amphiphilic nature of the phospholipid molecules in order to construct a bilayer structure. Selecting a supporting substrate with appropriate geometric and surface properties is necessary to achieve a lipid bilayer.

Several works on the formation of lipid bilayers have utilized the lipid painting technique. Thompson, et al used this method to form many small BLMS across the pores of several commercially available filter membranes [63]. O'Boyle, et al also used lipid painting for forming a planar BLMs supported by porous substrates in order to demonstrate a change in ion

permeability through the membrane as a function of protein antigen-antibody-complement reactions. Similar work with gramicidin D K^+ ion channels inserted into BLMs formed by the painting technique was also conducted by Dhoke, et al [67]. A slightly different form of lipid painting has also been used to form BLMs supported by hydrophobic substrates similar to the one shown in Figure 1.7. In 1967, Lauger, et al pipetted a lipid solution across the 3mm diameter pore in a Teflon membrane submerged in aqueous medium to form a bilayer lipid membrane [57]. Specifically, they used a 1% solution of egg lecithin (egg phosphatidylcholine (PC)) lipids dissolved in *n*-decane and coated the aperture using a Teflon tube. Unlike the steps illustrated in Figure 1.10, this process does not allow for solvent evaporation and the resulting bilayer retains some amount of organic solvent in the hydrophobic core of the membrane.

The primary advantage of using lipid painting is its simplicity; this method takes full advantage of the self-assembly nature of phospholipid molecules. However, bilayer thinning, instability, and protein denaturization are potential defects caused by leftover solvent remaining in the BLM [62, 64]. The advantage of solvent-less lipid solutions is that the properties of the BLM are dominated by the lipid molecules in study and not from any polar solvent remaining in the hydrophobic core of the membrane [94]. White had this in mind when he formed "solvent-free" BLMs by painting a lipid solution containing squalene, which does not remain in the bilayer as much as other small molecule polar solvents[95, 37].

Liquid-Supported Lipid Bilayers

The role of the substrate in most bilayer formation techniques is to provide an anchoring platform to which the bilayer can adhere. The substrate helps to define the size and shape of the bilayer and the planar configuration of the membrane provides easy access to both sides of the bilayer. This substrate, however, can hinder the mobility of the molecules within

the membrane [96] and as a result affect protein function. Further, the use of supported or suspended BLMs in device concepts are often limited by the fragility of the membrane and formation demands great attention to the geometry and surface chemistry of the supporting substrate which can complicate BLM formation. Two recently-developed methods enable the formation of bilayer lipid membranes without the constraints of a synthetic support. Instead, liquid oil/water interfaces provide a fluid interface for hosting self-assembled lipid molecules.

Droplet Interface Bilayers - In this scheme, a lipid monolayer assembles at the oil/water interface of water droplets submerged in an organic solvent. A bilayer is then formed when the droplets are brought into contact, excess solvent is removed, and the two opposing lipid monolayers thin to a two-molecule thick structure (Figure 1.11). Funakoshi, et al first attempted this technique as initial validation that intersecting aqueous and lipid solution streams can be used to form BLMs within microfluidic channels [97]. Holden, et al refined and expanded the approach to demonstrate that this technique produces BLMs that last for days and even that droplets can be arranged and rearranged to form stable networks of nanoliter-volume water droplets interconnected by DIBs [98]. The droplets used in these experiments were approximately 700μm in diameter (200nL in volume), producing interface sizes on the order of $200-300\mu$m in diameter. These researches later determined that that the phospholipids can be added to either the oil or water phase in order to form monolayers for stabilizing the droplet interface. In addition, the incorporation of transmembrane proteins including alpha-hemolysin and bacteriorhodopsin into the water phase proved that other biomolecules can self-insert into the bilayer interface [98, 99].

One drawback of the DIB method is that in order to validate the formation of a bilayer and confirm protein activity via electrical measurements (BLM characterization techniques are described in more detail in Section 1.3.3), a process far easier for traditional planar

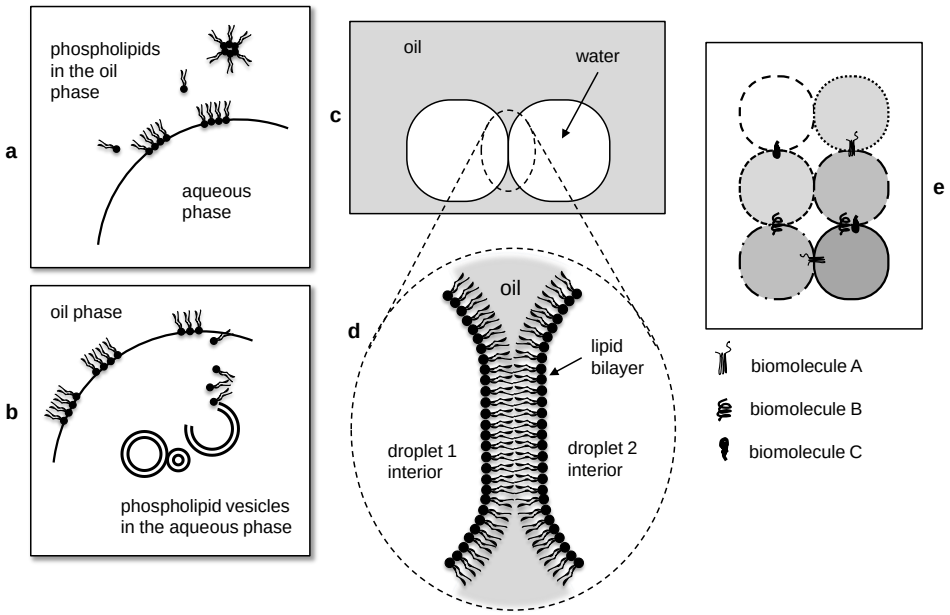

Figure 1.11: Droplet interface bilayers are formed at the interface of large inverse micelles created when lipid molecules self-assemble at the oil/water interface of water droplets submerged in organic solvent (1). Funakoshi, et al validated this technique before developing automated bilayer formation from crossing aqueous and organic streams in a micro-fluidic prototype [97]. Researchers at Oxford and Duke Universities advanced the method several steps further in demonstrating that a DIB can be formed at the interface of droplets when either the lipid molecules are dissolved in the nonpolar organic phase ("lipid-out") [98, 99] or added as vesicles to the aqueous interior of the droplets ("lipid in") [93] (3). Holden, et al also demonstrated that the droplet interface bilayer technique provides a method for creating large biomolecular networks composed of multiple interface bilayers connecting many adjacent droplets [98] (4).

BLMs, electrodes must be inserted into each droplet. Holden, at al made use of precise positioning equipment for manipulating wire-type electrodes which were inserted into the droplets. Agarose, a hydrophilic gel, was used to coat the tip of the electrode which provided a better anchoring point for the droplet during positioning and aided insertion into the droplets [98].

Droplet on Hydrogel Bilayers - A similar bilayer formation technique that relies on the self-assembly of a lipid monolayer at an oil-water interface is the droplet on hydrogel

bilayer (DHB) method. Opposing lipid monolayers form at the oil-agarose and oil-water interfaces of hydrogel and a water droplet, respectively (Figure 1.12), which then allows bilayer formation to take place when the lipid-encased droplet is lowered onto the lipid-covered hydrogel. This work was also developed at Oxford University and the creators used total internal reflectance fluorescence (TIRF) microscopy to visualize the horizontal contact area and electrical measurements to validate BLM formation and protein activity.

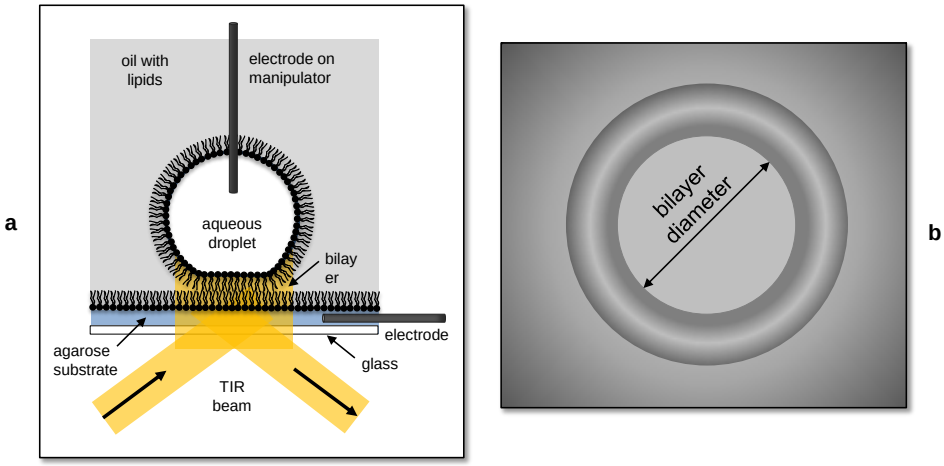

Figure 1.12: Illustrations show how the DHB method enables BLM formation at the interface of a water droplet and a hydrogel surface (a) and how the diameter of the resulting bilayer can be visualized using TIRF microscopy (b) [100, 96, 101].

The advantages of unsupported bilayer lipid membranes include the relative ease in which they can be formed, their stability (Holden noticed that droplet interface bilayers could last weeks [98]), and the ability to achieve various configurations of single bilayers and even functioning networks of biomolecules. However, because the bilayer is not formed on a supporting substrate, the size of the interface must be controlled through droplet manipulation via the electrodes. Further, the insertion of a specific number of proteins into these bilayers is an added challenge.

1.3.3 Lipid Bilayer Characterization Techniques

In parallel with much of the early research during the 1960s on how to form stable BLMs, methods for characterizing bilayers both with and without proteins were also developed. These techniques were used to first verify formation, but also to determine the size and quality of the membrane, develop an understanding of the physical properties of the bilayer, and to establish and validate theoretical models of these molecular assemblies [52, 60]. Additionally, bilayer characterization techniques are also aimed observing the activities of embedded integral membrane proteins. The primary modes for characterizing lipid bilayers include electrical measurements to track the flow of ions through a membrane, mechanical testing of material properties, including strength and fluidity, of the bilayer, and imaging techniques for visualizing the mobility of species. A brief look at these primary techniques and a sampling of published results are presented in this section.

Electrical Interrogation of Lipid Bilayers

One of the main roles of a plasma cell membrane is to provide a selective barrier for regulating ion transport into and out of the cytoplasm. While the bilayer itself blocks transport, integral membrane proteins facilitate the selective transport of ions across the membrane. As a result, electrical measurements are widely used to track the flow of ions in order to characterize the sealing ability of the bilayer and record transmembrane protein activity.

Voltage-Clamp - Voltage-clamp measurements, in which the voltage applied across the bilayer is prescribed and the resulting current is measured, have been used extensively for quantifying the electrical resistance of bilayer lipid membranes [50, 52, 57, 102] and recording the gating behavior proteins and ion channels [50, 60, 103, 104, 105, 106, 98, 99]. Commercially available voltage and current sources are available, though many of researchers devel-

oped there own systems in house. Measurements of bilayer lipid membranes without proteins indicate that these molecular assemblies have a very high electrical resistance, ranging from $10^4 - 10^8 \Omega \cdot \text{cm}^2$, when normalized per the membrane area. The electrical capacitance of a membrane, which is a function of the dielectric permittivity of the phospholipid molecules and the area and thickness of the bilayer, ranges from $0.1 - 1.0 \mu\text{F/cm}^2$. These quantities dictate that as the bilayer grows in area, the resistance decreases and the capacitance increases. Conversely, bilayers formed over very small pores (i.e. those with small membrane area), exhibit very large resistances on the order of $10^9 - 10^{12}\Omega$ (GΩ−TΩ) and small capacitances from $10^{-12} - 10^{-9}$F (pF−nF). In many early measurements, both the size of the bilayer and the capacitance were measured independently, but more-recently well-established membrane capacitances for a given phospholipid are used to estimate bilayer size directly from measurements of nominal capacitance.

Bilayer characterization also provides a way to verify that the materials and formation process provide a suitable environment for hosting transmembrane proteins. A very high BLM resistance is required in order to measure the small changes in conductance produced by single and few inserted proteins, which can range from a few pS (10^{-12}S) for gramicidin D channels to nS (10^{-9}S) for alamethicin oligomers and alpha-hemolysin heptamers [74, 69, 106] under an applied constant voltage. The importance of a highly-resistive bilayer is that the activity of single and few proteins can be monitored in response to controlled conditions including pH, electrical field, concentration gradients, and ligand binding events.

Electrical Impedance Spectroscopy (EIS) - Electrical impedance spectroscopy has also been used by many to characterize the electrical impedance of bilayer membranes with and without proteins over a wide frequency range. These measurements produce estimates of the resistance and capacitance of the bilayer but also provide information about how the bilayer assembles onto synthetic substrates [107, 108, 73, 68, 69, 59, 58, 48, 109, 110].

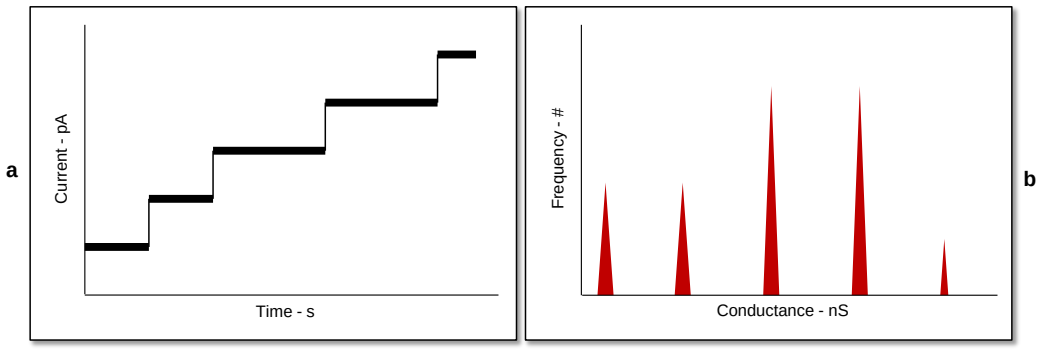

Figure 1.13: An example of a voltage-clamp measurement (often called a single channel recording) shows the step-wise changes in current resulting from the insertion of individual proteins, such as alpha-hemolysin (αHL) heptamers, under an applied electric field (a). The histogram representation (b) is commonly used to show the discrete levels of current that are measured and are used to compute estimates of electrical conductance for a single proteins.

Impedance analysis is not typically used to investigate the insertion of single or few proteins, rather it is a technique that can be used to witness the aggregate effect of many proteins within a bilayer that collectively permeabilize the membrane [111, 70, 112, 67].

Cyclic Voltammetry (CV) - Cyclic voltammetry is a third electrical characterization technique used for directly examining the current flowing through a system as a function of an increasing and decreasing voltage. This method is often useful for examining redox, or electron transfer, reactions of chemicals and also in demonstrating the diode-like behavior exhibited by many proteins [107]. CV was first applied to the area of BLM research by Tien, when he formed a lecithin-cholesterol BLM saturated with TCNQ (7,7',8,8'-tetracyano-*p*-quinodimethane) in order to demonstrate electron transfer through a bilayer [113]. The use of CV has grown with increased interest in using supported BLMs for sensing and energy conversion processes that require electron transfer to a metal electrode [114, 115, 107, 116]. CV can also be used to characterize the electrochemical parameters of biomembrane bound species such as enzymes, pigments, dyes, poisons, drugs, etc. that contribute to the transfer of electrical energy from biological events [107, 102].

Mechanical Characterization of Lipid Membranes

Two of the primary goals for quantifying the mechanical properties of bilayer lipid membranes is to understand the forces that hold them together and give them their fluidity and to be able to predict the strength of a membrane as a function of composition and environmental conditions. The approaches for characterizing the mechanical properties include analyses of entire vesicles, suspended planar BLMs, and lipid monolayers. A few of the most well-known techniques are described in this section.

Micromechanical Vesicle Aspiration - A method for measuring the thermal transitions, cohesion, elasticity, and surface rigidity of closed bilayer membranes (large vesicles: $10 - 200\mu$m in diameter) was developed by Kwok and Evans in the late 1970's and early 1980's [117]. This technique utilizes a glass micropipette and controlled suction pressure to study the thermo-mechanical behavior and colloidal interactions of phospholipid vesicles *in situ*. Two major advantages of this mechanical characterization technique is that organic solvents used in lipid solutions for forming planar bilayers are not present in solvent-free liposomes and the induced stress and temperature of the vesicles can be controlled independently in order to full examine the multiple structural phases of lipid bilayers [36, 38, 39].

The results of the studies by Kwok, Evans, and Needham using this technique highlighted that lipid bilayers are highly expandable materials and the mode of area dilation depends on the temperature-related structural phases of the membrane. Bilayers in the fluid phase (L_α) and the corrugated intermediate solid ($P_{\beta'}$) phases dilate due to an expansion of the phospholipid acyl chains with temperature, whereas expansion of the solid phase, $L_{\beta'}$ is also a function of chain tilt. These works also quantified the elastic modulus, K, of the membranes as a function of composition and temperature; solid phase bilayers exhibited significantly higher elastic moduli than the corresponding fluid phase. Further, the measure-

ments demonstrated that the incorporation of cholesterol molecules into the bilayer increases the stiffness of the membrane and raises bilayer tension at vesicle rupture by an order of magnitude [36, 39].

Pressurization of Planar Bilayers - A complementary method for measuring the mechanical strength of suspended planar bilayer lipid membranes was developed at Virginia Tech. This work sought to measure directly the failure pressure that causes rupture of lipid bilayers formed over pores in a synthetic substrate[118] as a way to quantify the strength of suspended lipid bilayers used in a protein-powered device concept [13, 110]. A stepper-motor was used to drive a piston to incrementally increase the pressure applied to the aqueous solution on one side of the bilayer and measured using a pressure transducer. Electrical impedance measurements, as well as fluorescence imaging, were used to verify the formation and subsequent rupture of 1-Stearoyl-2-Oleoyl-*sn*-Glycero-3-Phosphatidylcholine (SOPC) lipid bilayers. The pressure that caused failure was found to be inversely related to the diameter of the pores over which the membranes were formed, suggesting that smaller pores were favorable for forming robust bilayer-based device concepts.

Monolayer Formation and Characterization - The properties of single lipid monolayer formed at an air/water or oil/water interface have also been studied. Monolayers comprise each leaflet of a bilayer and thus methods to study this single layer can provide understanding of a full bilayer. A direct property measured in all of these works is the interfacial tension at the polar/nonpolar fluid interface. Amphiphilic phospholipid molecules assemble at this interface, lowering the difference in surface energies of the two phases. Horizontal surface balances and Wilhelmy plate balances in a Langmuir trough are often used to directly measure the tension of lipid monolayer at the interface [119], though more sophisticated techniques were developed to measure the formation of surfactant monolayers at much smaller interfaces inside a micropipette [120, 40]. This approach enabled the surface tension, γ ($\mathrm{mN/m^{-1}}$), to

be determined through the Laplace equation

$$\Delta P = \frac{2\gamma}{R_c} \tag{1.1}$$

by applying a known pressure, ΔP (Pa), across a curved interface between the two phases (air/water or oil/water) within a micropipette and measuring the resulting radius of curvature, R_c (μm). With a smaller interfacial area than that for traditional Langmuir-type troughs, the dynamic adsorption of molecules to the interface and the equilibrium interfacial tension can be monitored and measured quickly.

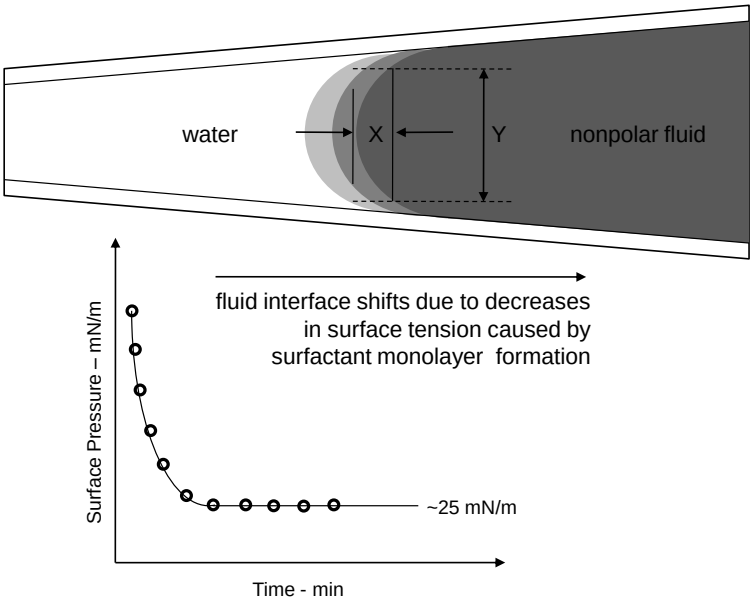

Figure 1.14: The micropipette technique developed by Lee, et al at Duke University has the ability to accurately measure the dynamic and equilibrium surface tensions at the interface of two fluids within a micropipette [120].

Lee, et al demonstrated the rate of adsorption of phospholipid molecules from vesicles in the water phase to the air/water interface and the equilibrium surface tension are functions of the temperature relative to the gel-to-liquid crystallization transition temperature of a given lipid (recall that this transition temperature is dependent on bilayer composition - see Section

1.1.3). However, lipids in the fluid phase, L_α, display nearly identical adsorption rates of 50mN/m min^{-1} and equilibrium interfacial tensions of 25mN/m, regardless of phospholipid type.

Optical Techniques

Several optical techniques have also been used to provide additional proof of formation, measure the fluidity of the lipid molecules, monitor the "flipping" of phospholipid molecules from one side of the membrane to the other, and even visualize proteins and ion channels directly. Montal and Mueller (1962) reported that their reconstituted lipid bilayers were invisible in transmitted light, hence the term "black lipid membrane" [50]. Their observations,in conjunction with electrical measurements of the bilayer, confirmed that ultra-thin bilayer structures are not visible in reflected light. Since then, approaches to visualize these molecular assemblies by tagging lipids and proteins with fluorescent molecules have been used for fluorescence recovery after photobleaching (FRAP), fluorescence resonance energy transfer (FRET), and total internal reflection fluorescence (TIRF) microscopy, all of which can be used to image the assembled bilayer and reconstituted proteins. An additional technique called vibration sum frequency generation uses principals of non-linear optics to examine the formation of lipid monolayers at dissimilar interfaces.

Fluorescence Imaging Techniques - Fluorescence images are obtained from molecules that emit fluorescent light at a particular wavelength when excited by incident light at different wavelength. One specific technique, called fluorescence recovery after photobleaching (FRAP), excites fluorescently-tagged lipid molecules by exposure to fluorescent light focused through an aperture. After some time in "dark" conditions, the emission detected via a photo-multiplier is used to view the previously bleached area. Fainting that occurs between bleaching and viewing is then related to the lateral diffusion of the dye molecules

in the membrane and can be used to quantitatively measured the fluidity of the bilayer [121, 88, 71, 70]. In a similar fashion, Hwang, et al used fluorescently tagged lipids to monitor the "flip-flop" of phospholipid molecules from one side of the half of the bilayer to the other half in asymmetric droplet interface bilayers [93].

Fluorescence resonance energy transfer (FRET) is a powerful technique based on Förster transfer of energy from a donor fluorescent molecule to an acceptor molecule [122]. The efficiency of the energy transfer is highly dependent on the distance between the two molecules, thus making this technique especially useful in tracking the relative distances between two dye molecules. FRET has been used to study a number of biological processes including measuring DNA, tracking the folding and unfolding of proteins, and studying macromolecular interactions [122]. Cha, et al demonstrated that FRET can be used to study the various voltage-dependent conformations of labeled subunits of a *Shaker* potassium channel [123]. Borisenko, et al used a combination of FRET and traditional electrical measurements to simultaneously record the formation of gramicidin ion channels in a bilayer lipid membrane [124].

Total internal reflection fluorescence microscopy (TIRFM) is a third fluorescence technique method used to observe the adsorption, fusion, and desorption kinetics of fluorescent-labeled molecules. This method focuses one or more laser beams (e.g. argon ion laser) through a quartz prism which is completely internally reflected at the quartz-buffer interface. This technique is used to selectively excite nearby fluorescent molecules, and the emission that is observed is proportional to the amount of bound fluorophore. Kalb, et al used TIRFM in order to look at the adsorption rate of lipid vesicles onto a POPC monolayer supported by quartz [80]. Heron, et al also used this method for measuring the diffusion of phospholipids within droplet on hydrogel (DHB) bilayers [100] and later for obtaining simultaneous single channel current measurements and fluorescence images of calcium ions passing through

alpha-hemolysin channels in DHBs [125].

Vibration Sum Frequency Generation - Vibration sum frequency is second-order non-linear optics technique that relies on the principal that spatial and temporal overlapping of two intense optical fields at different frequencies induces polarization. The polarization generates an electrical field which is dependent on the molecular vibrations of the molecules at the interface [27]. When the incident optical fields are scanned across an IR spectrum suitable for the interface in study, changes in the molecular arrangements of the molecules can be determined. Smiley and Richmond used this technique for observing the formation of monolayer assembly at air/water and liquid-liquid interfaces and observed that longer acyl chains result in the retention of more oil in the hydrocarbon region of the monolayer [27, 126]. Walker also used this same technique to measure changes in dynamic surface tension and investigate how the local structuring of water molecules are affected by the ordering of phosphlipids at a water-tetrachloride (CC_4) interface [127].

1.3.4 Early-Stage Bilayer-Based Devices

Recently, interest in using biological molecules such as phospholipids, proteins, and ion channels has led to the development of several types of bio-inspired materials and devices: chemical sensors [128, 62, 129, 74], rotary motors [130, 15, 131], and bio-transistors [132]. In most of these works, proteins reconstituted into an artificial bilayer lipid membrane (BLM) formed on either a solid support or suspended across one or many pores in a synthetic material are the active elements in the device. Since bilayers formed in these trials demonstrate very high electrical resistances, necessary for studying single and few proteins in the membrane, the systems were used primarily for molecular sensing applications. Other works including those at Virginia Tech have concentrated on scaling the functions of individual

proteins to general larger-scale outputs, such as energy-conversion.

Sundaresan, et al used ATPase enzymes and $At\text{SUT}_4$ proteins reconstituted into bilayer lipid membranes to use the chemical energy in adenosine triphosphate (ATP) to pump sucrose and water across lipid membranes formed across the pores of a porous support [13, 110]. The ATPase enzymes hydrolyze available ATP in this concept, establishing a pH gradient across the membrane which triggers co-transport through $At\text{SUT}_4$ proteins. A second device concept relying on reconstituted proteins to emerge from this work used ATPase enzymes alone to convert the chemical energy in ATP into electricity that was sourced to an external circuit [48]. The Biocell—as it is named—produced $1 - 2\mu\text{W/cm}^2$ of lipid membrane and per 15μl of ATPase enzyme added to the system.

1.4 Motivation and Plan for Developing New Biomolecular Material Systems

Reimhult and Kumar in their recent review article of bilayer-based sensing platforms formed from micro- and nano-porous substrates suggested that many of the current bilayer-based technologies for creating functional devices are limited by the fragility of the bilayers for long-term use, the inability to effectively reconstitute bilayers across a large number of pores needed to prevent electrical leakage currents, and the limitation that supported bilayer systems quickly dehydrate and not longer work in air [129]. An additional observation of the works reviewed in this chapter also indicate that current device concepts contain one type of protein capable of usually one task. The ability to integrate the functions of many proteins, each within their own lipid bilayers, into one device provides additional challenges.

The droplet interface bilayer (DIB) method (see Section 1.3.2 for more information) devel-

oped by researchers at Oxford and Duke offers several unique possibilities that are unavailable using supported bilayers and avoids many of the issues related to the formation of lipid bilayers on synthetic substrates mentioned above. In their seminal paper, Holden, et al demonstrated that large networks of aqueous droplets can be assembled, where the interface between adjacent droplets is a liquid-supported lipid bilayer that is capable of hosting proteins. They demonstrated that alpha-hemolysin proteins could be used as sensors to detect the presence of specific biomolecules and also showed that bacteriorhodopsin proteins residing in separate interfaces can work in concert to generate electrical current from light energy [98]. Their reported results also indicate that networks of DIBs are quite stable, lasting weeks without bilayer degradation and even allowing the rearrangement of droplets to create new bilayer interfaces. Biomolecular networks formed via the DIB technique offer the ability to tailor the contents of each droplet, control which interface bilayers contain proteins, and allow for nearly endless arrangements of the modular droplets. Yet, the original DIB platform does not directly translate into a complete material system capable of demonstrating network-level functionality and engineering durability.

Nonetheless, a truly unique form of active materials can be achieved based on the formation and stabilization of interface bilayers and the inherent functionality of integral membrane proteins that regulate the transport and conduction of ions within the network. In this dissertation we present results that enable the development of a new class of smart material that utilizes the transport properties of biomolecules as the transduction mechanism. Our work is inspired by the fact that biological networks utilize charge and mass transport as a means of producing very complex functions such as cell signaling, system regulation, tissue regeneration, and healing. The ultimate goal of our work is to utilize similar physical processes to engineer a new class of durable material that can be tailored to provide novel types of stimulus-responsive behavior in material systems. As shown in Figure 1.15, the

types of stimulus-responsive behavior we are envisioning consist of responses to common physical stimuli such as sound, force, heat, and light. As is the case for biological systems, biomolecular material systems will utilize the transport properties of interface bilayers to create complex input-output relationships that lead to new types of functional behaviors in materials. In this manner we will create a truly hierarchical system that utilizes the properties of materials and the activities of biomolecules at very small length scales to enable complex system behaviors at larger length scales.

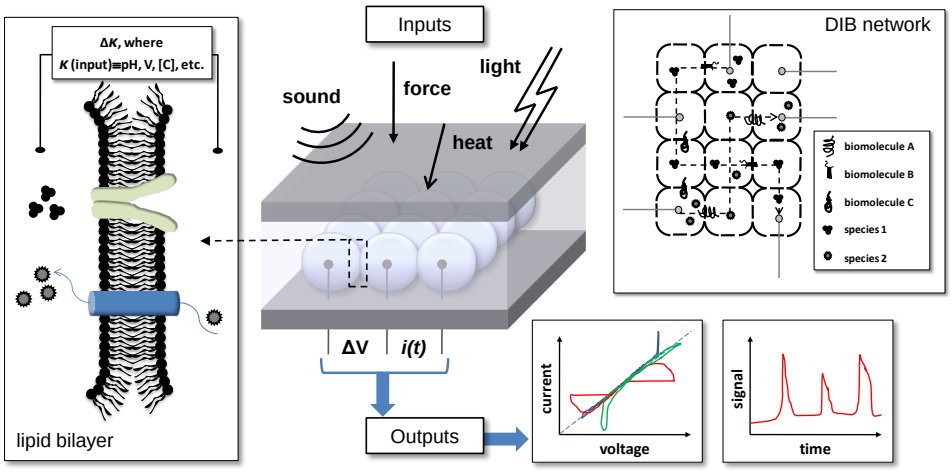

Figure 1.15: Active materials that utilize the transport properties of biomolecules are constructed from networks of interface bilayers. Proteins incorporated into specific bilayer interfaces in the network determine the input/output transduction relationship to multiple stimuli.

The primary thesis presented in this work demonstrates that through physical encapsulation, functioning interface bilayers can be formed in durable materials through refined methods that enable control over bilayer size, formation location, and network configuration. This document tracks the advances made since the inception of the original DIB platform for assembling, characterizing, and encapsulating biomolecular networks. While DIBs provide a suitable starting point for the development of hierarchically-structured materials, it is a technique not without limitations. The works discussed in this paper specifically seek to

extend the durability, usability, and refinement of cell-inspired biomolecular networks and the resulting contributions demonstrate that physically-encapsulated interface bilayers can be formed within durable materials, without the need for discrete dispensing and arrangement of droplets and at the interface of non-spherical aqueous volumes. These efforts depart significantly from the original DIB method but intentionally carry-over many of its attractive qualities: simplicity, stability, and network modularity.

1.4.1 Research Goals and Contributions

This dissertation documents the development of a new class of material consisting of organized biological molecules through the formation, characterization, and encapsulation of liquid-supported interface bilayers. The scientific contributions of these efforts provide an increased knowledge base for assembling a wide range of composite material systems based on principles of phase separation and self-assembly. Notable contributions distinguishing this work from that of others are detailed below.

- Feedback control strategies are used to demonstrate an alternative method for prescribing specific current-voltage behavior of lipid bilayers, where both the properties of the interface and the chosen control authority dictate closed-loop performance.
- Physically-encapsulated droplet interface bilayers contained within high packing factor substrates featuring integrated electrodes retain the critical properties of the original DIBs but demonstrate increased portability—physical encapsulation allows DIB networks to survive handling, violent shaking, and even complete inversion.
- The durability of droplet interface bilayers is quantified for the first time and modes of failure are correlated to the level of interaction the aqueous volumes have with the supporting substrate.

- A new approach, called the regulated attachment method (RAM), is developed for controlled interface bilayer formation within flexible substrate. This method makes use of a deformable substrate to internally separate and reattach lipid-encased aqueous volumes for bilayer formation and through control of the deformation, allows the size of the bilayer to be varied in reversible fashion.

- A method for stabilizing both the aqueous and oil phases within PDMS is developed to maintain the necessary oil/water interface within sealed substrates. The combined use of a non-swelling fluorocarbon oil and a solution-phase surface modification procedure to maximize wetting by the oil phase enables retention and proper phase separation of the liquids contained in PDMS.

- Bilayer formation within a completely sealed substrate is demonstrated for the first time. Interfaces formed using perfluorodecalin as the oil phase demonstrate high electrical resistances and failure potentials consistent with unencapsulated DIBs and enable the measurement of single channel protein recordings.

1.5 Document Overview

This introductory chapter provided the inspiration and background information on cellular structures along with an extensive review of lipid bilayer formation and characterization techniques. The state-of-the-art bilayer-based device concepts were also reviewed, motivating the creation a new class of active materials consisting of physically-encapsulated interface bilayers. The organization of the following document builds a case for graduating the fundamental concepts of bilayer formation at a liquid-liquid interface established by the DIB technique to more-complex material systems that feature biomolecular networks assembled within durable materials. The research efforts presented herein are primarily experimental

and are presented in an order that reflects the chronological progress of this technology.

Chapter 2 prefaces the experimental work presented in this dissertation with a brief discussion of the experimental measurement techniques used to study interface bilayers, with special attention given to the protocols and equipment used to make each measurement and the interpretation of data. Chapter 3 focuses on characterization and tailoring of of transport across droplet interface bilayers. Specifically, single bilayers formed at the interfaces of two-droplet pairs are examined as this system represents the basic building block of larger biomolecular networks. We investigate how the current-voltage relationships of these model systems can be tailored using both biomolecules reconstituted into the interfaces as well as external feedback control.

Physical encapsulation of interface bilayers is first introduced in Chapter 4 as a method for creating more usable DIB networks within solid substrates. Chapter 5 introduces the the regulated attachment method (RAM), a concept that builds on the benefits of using a supportive solid substrate to form durable interface bilayers *in situ* within a flexible substrate. This work specifically deviates from the original DIB in that individual droplets are not dispensed and/or arranged to form bilayers, and it is this feature that enables the creation of a new form of internally-structure materials for hosting biomolecular assemblies. The work presented in Chapter 6 combines physical encapsulation, microfabrication techniques, and RAM to create encapsulated interface bilayers stabilized internally within a sealed substrate. A surface modification procedure is developed to eliminate oil absorption into the bulk PDMS substrate and to maximize wetting by a fluorocarbon oil phase such that both aqueous and oil phases properly phase separate within the material. Lastly, Chapter 7 closes with a summary of the contributions and conclusions of the work.

Chapter 2

Measurement Techniques and Interpretation of Experimental Data

Constructing biomolecular assemblies with a bottom-up approach can often result in the formation of very small organized structures. For example, lipid bilayers have measured thicknesses of a mere $5 - 7$nm and many transmembrane protein molecules have dimensions on the order of nanometers. Optical methods provide limited results given the small length scales of these assemblies, therefore electrical characterization techniques are widely-used instead.

Several methods for electrically characterizing lipid bilayers and measuring the activities of single and few proteins residing in these bilayers were introduced in the literature review in the previous chapter (Section 1.3.3). These techniques provide validation of bilayer formation and have been used extensively for measuring the discrete changes in selectivity and ionic conductivity that individual protein molecules incur on lipid membranes.

This chapter provides a more-detailed look at three types of electrical characterization tech-

niques and special attention is given to both the protocols employed for making the measurements and the interpretation of experimental data. A solid understanding of the characterization techniques used in this work is deemed critical since the work presented in this dissertation is predominantly experimental in approach. This discussion establishes a foundation for comparing measurements obtained on liquid-supported interface bilayers to those obtained from lipid bilayers formed using previous methods.

2.1 The Representative Circuit: A Single Droplet Interface Bilayer

As a basis for the following discussion, a representative circuit shown in Figure 2.1 is defined that consists of a single droplet interface bilayer (DIB) formed between two lipid-encased droplets submersed in oil. Each droplet contains an electrolyte solution containing dissociated ions of a common salt, such as sodium chloride (NaCl) or potassium chloride (KCl) and also may contain phospholipid vesicles and/or proteins. The conductive electrodes used in this system extend through the oil phase and pierce into the aqueous interior of the droplets for both droplet positioning and electrical measurements. Phospholipid molecules incorporated into either liquid phase result in the formation of a lipid monolayer at the oil/water interface surrounding each droplet. A liquid-supported interface bilayer is then formed when the separated droplets are brought into contact. Bilayer thinning follows as excess oil is first removed from between the two opposing monolayers and the monolayers "zip" together due to van der Waals forces [133, 134, 135].

A unique quality of droplet interface bilayers compared to many lipid bilayer systems is the lack of a supporting substrate. This feature not only simplifies bilayer formation but also

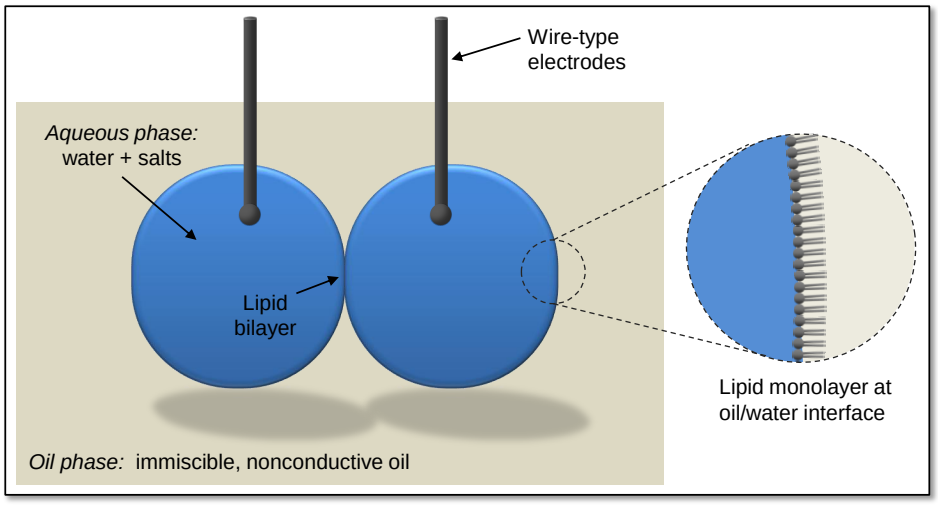

Figure 2.1: The droplet interface bilayer is a method for creating durable, liquid-supporting lipid bilayers at the interface of connected, lipid-encased aqueous droplets submersed in oil. Self-assembly processes drive the formation of a lipid monolayer at each oil/water interface, enabling bilayer formation upon contact. Impaling electrodes are used to position droplets in a network as well as to access the conductive aqueous medium contained within each droplet for electrical characterization of the interface.

contributes to the stability of the interface. Additionally, the lack of a supporting substrate in favor of a liquid support reduces the number of contributing factors that affect the electrical response measured for DIBs. By using a non-conducting organic solvent such as hexadecane for the oil phase, the only conductive path between electrodes positioned in separate droplets is through the aqueous phase and across the bilayer(s).

The image in Figure 2.2a shows the electrical components that contribute to the measured response. The electrode-electrolyte solution interface for each electrode is modeled as a resistor, R_{el}, in parallel with a capacitor, C_{el} [108]. The aqueous electrolyte solution within each droplet contributes to the circuit a series resistance, R_s, whose value is dependent on the chemical composition and concentration of the volume [69]. The bilayer also affects the flow of ions. In an ideal case, in which a pure lipid bilayer provides a perfect electrical seal between the droplets, the interface is modeled as pure capacitor due to its ability to separate,

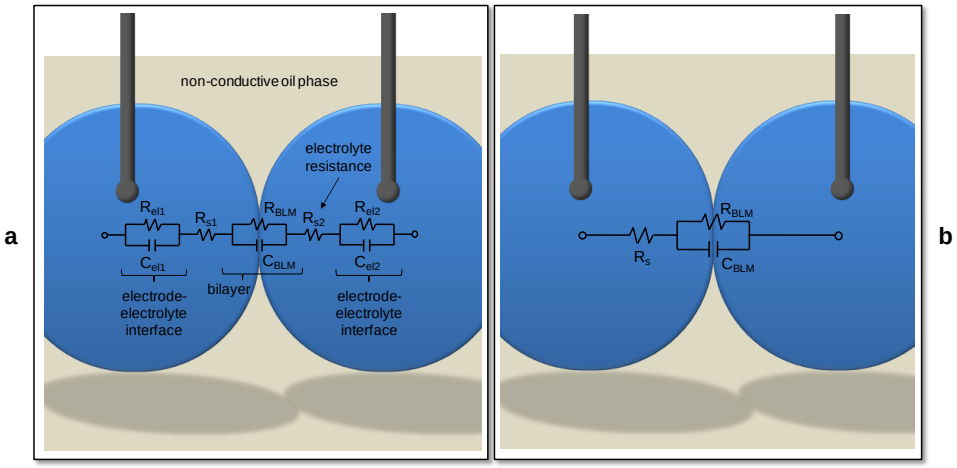

Figure 2.2: The conductive pathway existing between electrodes positioned in separate droplets passes through the bilayer, each electrolyte-electrode interface, and electrolyte within the droplets (a). A reduced circuit model only contains the resistance of electrolyte solution and the influence of the lipid bilayer (b).

but not transport, charge. However, real bilayers have finite resistance values and so both resistive and capacitive terms are used to describe the interface. Likewise, the resistance of the electrolyte solution and the electrode-electrolyte interface components are included on the opposite side of the bilayer within the second droplet.

The use of reversible electrodes (commonly silver-silver chloride) promotes efficient ion exchange and prevents electrical double layers from forming at the surface of the electrode in chloride-based electrolyte solutions results in electrode-electrolyte interfaces that have negligible resistance and capacitance values. Furthermore, the two series resistances for each electrolyte solution can be added to obtain an equivalent resistance. With these simplifications, the complete circuit model condenses to the form shown in Figure 2.2b, where only the interface bilayer and the electrolyte solutions affect the flow of ions. In contrast, electrical models of supported bilayers assembled directly on supporting substrates are more-complex and include additional terms that describe the contributions (typically capacitive in nature) of the substrate [73, 68]. For the following discussion on measurement techniques and data

interpretation, measured responses are expected to correspond to the simplified DIB circuit shown in Figure 2.2b.

2.2 Experimental Setup for Bilayer Measurements

In addition to substrate fabrication and materials preparation, which are described as needed in the following chapters, the experimental setup used to form and characterize interface bilayers requires suitable electrodes and a low-noise workstation for obtaining quality measurements. Reversible, silver-silver chloride (Ag/AgCl) electrodes are used because they freely exchange mobile chloride ions with the electrolyte solutions contained within the droplets. As a result, Ag/AgCl electrodes do not contribute significantly to the impedance of ion flow occurring between the electrodes and thus, do not alter the assumed circuit model across a single bilayer shown in Figure 2.2b. Additionally, this type of electrode is used because it does not develop a sizable Nernst Potential when placed in chloride-based electrodes [136, 137], which ensures proper control of the voltage applied to the system.

Silver-silver chloride (Ag/AgCl) electrodes are fashioned from 125μm-thick silver wire (Goodfellow). Ball-shaped ends are formed at the tips of the electrodes (see Figure 2.1) using a butane lighter; these profiles provide an anchoring point for attaching the droplets to the electrodes. Electrodes are chlorided for $30 - 60$ minutes in household bleach until they turn dark gray in color and then rinsed with water. The ball-ends are then dipped in molten 5% (w/v) agarose gel (Sigma) in order to provide a hydrophilic surface that aids in electrode insertion into the droplets and free exchange of ions at the electrode surface [98, 93]. In later studies that do not require the need to position and probe individual droplets, Ag/AgCl electrodes are fashioned directly from 125μm-thick silver wire, without ball-shaped ends or agarose gel.

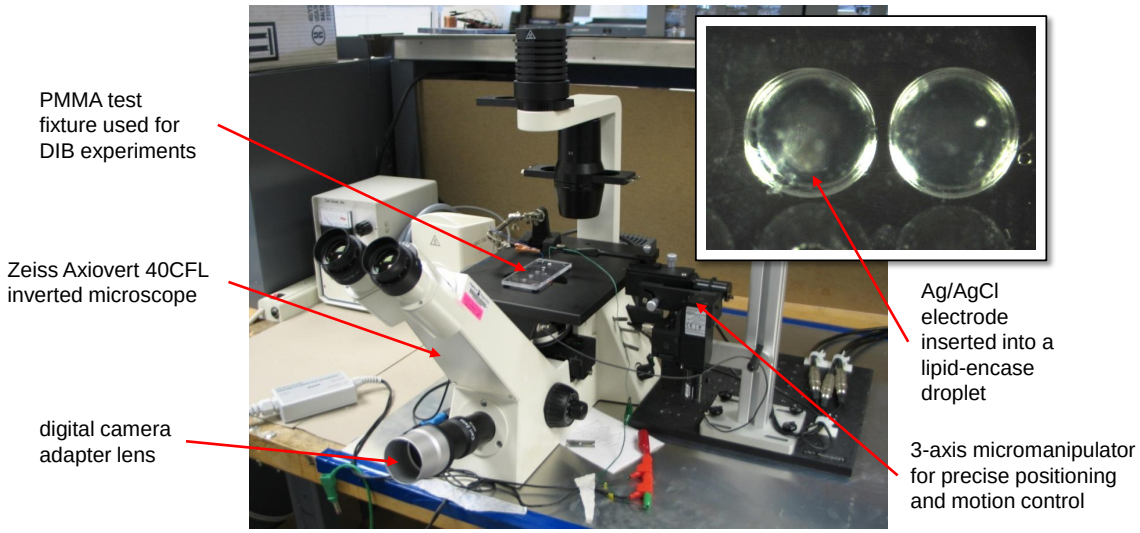

Figure 2.3: The standard workstation for forming and characterizing interface bilayers includes an inverted microscope, 3-axis micromanipulator, digital camera, and Faraday cage (not shown).

A low-noise testing environment is critical for being able to resolve very small levels of current flowing through highly-resistance interface bilayers. Tests are conducted on a Axiovert 40CFL (Carl Zeiss) inverted microscope such the biomolecular networks can be viewed through the 5X objective and images can be obtained with a Canon G6 digital camera and digital camera adapter attached to the microscope. A 3-axis stepper motor-drive (joystick-controlled) micromanipulator (SM325, WPI Inc.) is used in various ways to provide droplet positioning and controlled substrate motions in later studies. A homemade Faraday cage surrounding the entire workstation is grounded to an earth ground connection on either the Autolab or AxoPatch amplifier in order to minimize the addition of noise into the electrical measurements. An image of this workstation is shown in Figure 2.3.

2.3 Electrical Characterization Techniques

The primary techniques used to characterize lipid bilayers throughout this dissertation include electrical impedance spectroscopy (EIS), cyclic voltammetry (CV), and chronoamperometry measurements. These techniques enable the researcher to verify bilayer formation, extract estimates of the values of electrical resistance and capacitance of the membrane, as well as characterize the responses of the membranes and/or proteins to varying transmembrane potentials.

2.3.1 Electrical Impedance Spectroscopy

Electrical impedance spectroscopy (EIS) is the study of how the electrical impedance, or the opposition to the flow of current (or ions), of a system varies with frequency. The complex electrical impedance, Z, has units of Ohms (Ω) and is defined in the following expression as the ratio of complex voltage, V, to complex current, I,

$$Z(\omega) = V(\omega)/I(\omega) \tag{2.1}$$

where, ω is the excitation frequency in radians per second (rad/s). In the case where the impedance of a system behaves like a pure resistor (i.e. $Z(\omega) = R$), Equation 2.1 can be rewritten as Ohm's Law

$$V = IR. \tag{2.2}$$

As a result, the measured current in a purely resistive circuit produced is equally proportional to the applied voltage at any excitation frequency and so the relationship is not written as

a function of frequency. However, the electrical impedances of most physical systems are functions of frequency, indicating that additional frequency-dependent circuit elements, such as capacitors and inductors, contribute to the total complex impedance. The impedance of a pure capacitor, C, is given by the expression $Z(\omega) = 1/j\omega C$, where j is the imaginary unit, while the impedance of an inductor, L is likewise given by the expression $Z(\omega) = j\omega L$.

Furthermore, because the impedance of many physical systems is not a single component, but instead a combination of terms, the circuit model for a system is not always known. EIS, then, provides a way to measure the total complex impedance of a system in order to obtain an understanding of which type of electrical phenomena occur in specific frequency regions. With this knowledge, one can begin to assign the measured electrical behavior to actual physical processes, such as charge separation and transport, that result from the applied potential.

Displaying Measured Electrical Impedance Data

Complex impedance data are typically displayed in one of two ways, a Bode diagram which plots both the magnitude and phase of the measured impedance versus the excitation frequency, or a Nyquist diagram which plots the magnitude of the imaginary impedance versus the magnitude of the real impedance for the measured frequency points. The magnitude, $|Z|$, and phase, θ, of the complex impedance are given by

$$|Z(\omega)| = \left[(real\,(Z(\omega)))^2 + (imag\,(Z(\omega)))^2 \right]^{1/2} \tag{2.3}$$

and

$$\theta(\omega) = tan^{-1}\left(\frac{imag\,(Z(\omega))}{real\,(Z(\omega))}\right). \tag{2.4}$$

Figure 2.4a summarizes the impedance contributions of the three most common electrical elements and provides analytical expressions for the magnitude and phase of each.

a

Element	Impedance Expression, Z(ω)	Real component	Imaginary component	Magnitude of Impedance, |Z| (Ω)	Phase of Impedance, θ ( )
Resistor	$Z_R(\omega)=R$	R	--	R	0
Capacitor	$Z_C(\omega)=1/j\omega C$	--	$-1/\omega C$	$1/\omega C$	-90
Inductor	$Z_L(\omega)=j\omega L$	--	ωL	ωL	90

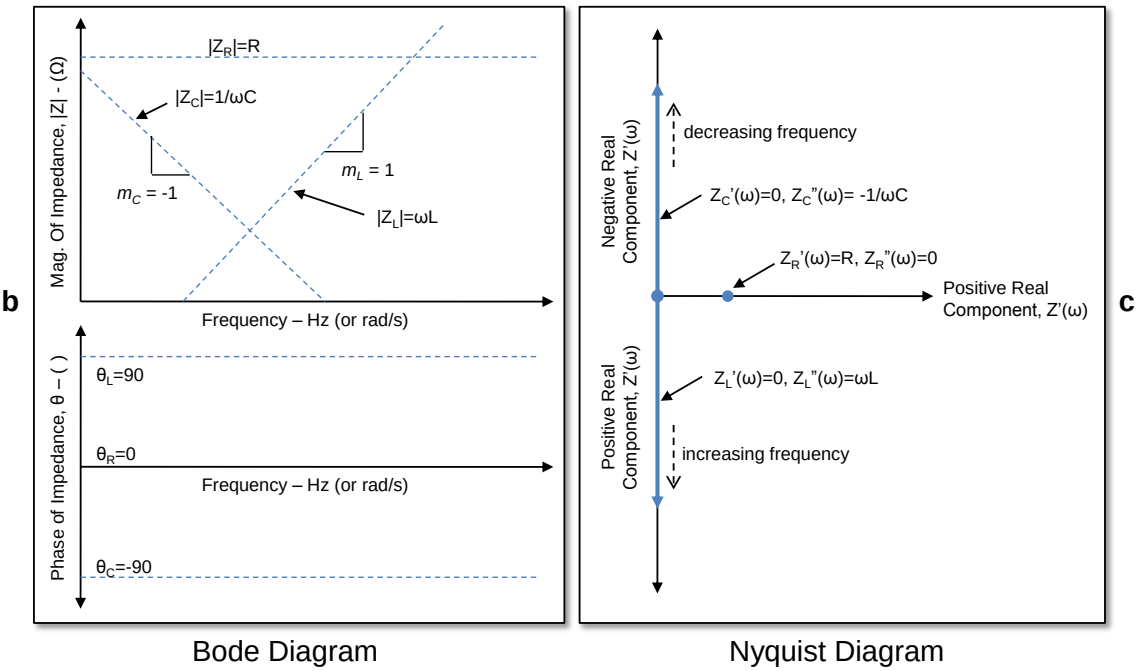

Figure 2.4: Expressions for the complex impedance, $Z(\omega)$, the real and imaginary components of impedance, as well as the magnitude, $|Z(\omega)|$, and phase, $\Theta(\omega)$ are provided for three common circuit elements: a resistor, capacitor, and inductor (a). The complex electrical impedance of each element is displayed in Bode (b) and Nyquist (c) representations.

Bode and Nyquist diagrams are also provided in Figure 2.4b,c to illustrate how the impedance of each element varies with frequency. A resistor has a constant magnitude of impedance, $|Z_R(\omega)| = R$, and a phase of 0^o across the entire frequency spectrum in the Bode represen-

tation, but only marks a single point, $Z'_R = R$ on the abscissa of the Nyquist diagram. A capacitor demonstrates a frequency dependent response with a steadily-increasing magnitude of impedance (slope of -1 on a log-log scale) for decreasing frequencies and a constant phase angle of -90^o. In a reversed fashion, an inductor exhibits an increasing magnitude of impedance with increasing frequency (slope of $+1$) and a phase angle of 90^o. These two elements produce vertical lines on a Nyquist plot, with the capacitor only contributing negative imaginary impedance values and the inductor producing only positive values of imaginary impedance. Discrete frequency points are not shown in a Nyquist diagram, but as a general trend increasing magnitudes of imaginary impedance correspond to increasing and decreasing frequencies, respectively, for capacitors and inductors.

Bode Diagram for the Electrical Impedance of a DIB

To better understand how EIS data is displayed for multi-element systems, we will study the case of the single droplet interface bilayer (shown in Figure 2.2b). First, we will develop an expected impedance response and then compare it to experimental data for a DIB in order to show how the values of each circuit element can be deduced from the measurement. Though the impedance of a DIB can also be plotted in a Nyquist diagram, only Bode representations are used from this point forward since EIS data in this dissertation is presented in a Bode format. The electrical impedance for a single DIB shown in Figure 2.2b can be written as

$$Z_{DIB}(\omega) = \frac{R_{BLM}}{1 + j\omega R_{BLM} C_{BLM}} + R_s \tag{2.5}$$

where, R_{BLM} and C_{BLM} are the resistance and capacitance of the bilayer, respectively, and R_s is the total resistance of the electrolyte solution within the droplets on both sides of the bilayer. Instead of developing analytical expression for the real and imaginary components

of this expression, we can use a graphical approach to illustrate the contribution of each element in the system. For this example, we first assume that the solution resistance is non-zero and several orders of magnitude less than the resistance of the bilayer. This assumption is valid since electrolyte resistances for common salt concentrations are typically on the order of $1-10\text{k}\Omega$, while a bilayer resistance is often greater than $1\text{G}\Omega$ [23, 69]. With these relative values in mind, we can draw lines that represent the magnitude and phase of impedance for both resistive terms on the Bode plot (Figure 2.5a).

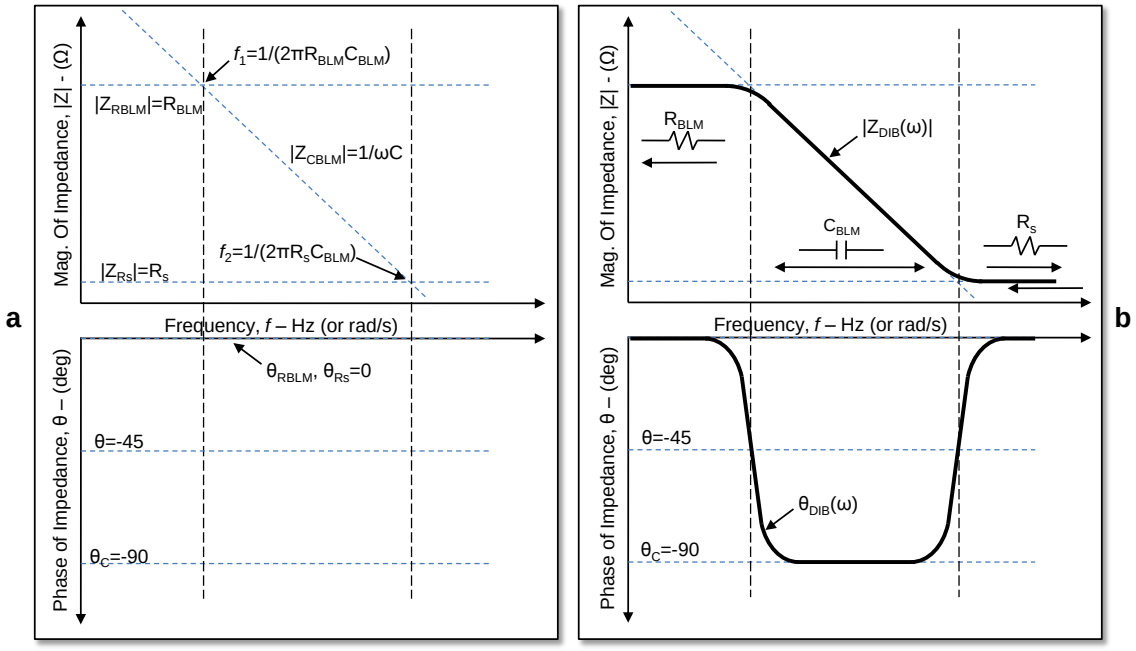

Figure 2.5: Constructions lines for each of the elements in the reduced DIB circuit are first drawn on the magnitude and phase plots of a Bode diagram in a graphical approach for understanding DIB impedance (a). The combined magnitude and phase of impedance of a DIB is then drawn by following the construction line that refers to the element of lower impedance for terms connected in parallel (R_{BLM} and C_{BLM}) and the element of higher impedance for terms connected in series (R_s and C_{BLM}) (b).

Additionally, a construction line with a slope of -1 is drawn on the magnitude plot for the capacitance of the bilayer and a line representing -90^o is also sketched on the phase plot. The intersections between the magnitude of impedance line for the capacitor and the two

resistance asymptotes define the transition frequencies, f_1 and f_2, in the system, where at each intersection the phase is equal to -45^o. In both cases, the frequency at which this occurs is related to the product of the capacitance, C and the intersecting resistance, R_{BLM} or R_s. Vertical lines are drawn at these frequencies in order to help estimate the phase transitions for combined phase response.

Recalling that current flows through the least resistive element in a parallel circuit and is limited by the element with the highest impedance for components connected in series, we can use the asymptotes sketched in Figure 2.5a to approximate the impedance of a DIB across the entire frequency range. The solid black lines in Figure 2.5b show the shape of the magnitude and phase for a single DIB whose impedance is described by Equation 2.5. Note that at both transitions frequencies, the phase passes through a value of -45^o. Figure 2.5b shows that in some frequency regions, the system is dominated by a single component. Specifically, at low frequencies (often $<$ 1Hz for real lipid bilayers) the lipid bilayer is essentially a pure resistor while at very high frequencies, only the solution resistance, R_s, plays a role in the measured impedance for the network [68, 69]. Between the two transition frequencies, the system acts like a pure capacitor of value C_{BLM}.

Protocol for EIS Measurements

The electrical impedance of a system is experimentally measured by applying an AC potential (typically sinusoidal) of known amplitude, $|V|$ and recording the resulting current flow. This process is repeated many times at different excitation frequencies in order to obtain a complete impedance spectrogram. Throughout this dissertation, EIS measurements are obtained on interface bilayers using an Autolab PGSTAT12 Potentiostat/Galvanostat (Eco Chemie) with FRA (Frequency Response Analysis) software (version 4.97). This device is operated in two-electrode mode (RE and CE-labeled leads are tied together and WE and

S-label leads are also tied together) to apply a voltage and measure the resulting current between electrodes inserted into neighboring droplets. A typical routine consists of applying a 5mV (RMS) sinusoidal voltage at 30 equally-spaced (log-scale) frequencies between 500kHz to 10mHz. Autolab measures the complex current and then computes the real and imaginary components of the impedance at each frequency.

EIS Data Interpretation

Sample EIS data for a single DIB acquired with Autolab and then plotted in Matlab is shown in Figure 2.6a. Much like the anticipated response sketched in Figure 2.5, the data displays a high frequency asymptote that is several orders of magnitude lower than the low-frequency asymptote assigned to the resistance of the bilayer.

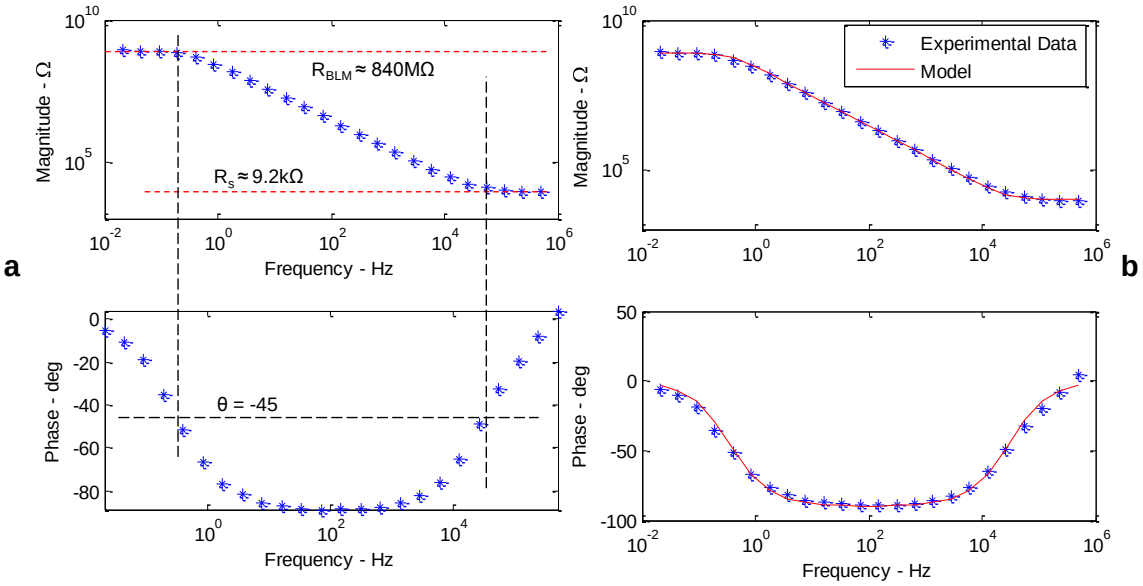

Figure 2.6: Electrical impedance data points collected on a single DIB demonstrate a similar response to the sketched behavior in Figure 2.5b (a). A non-linear least squares fitting routine is applied to the data in order to extract estimates of membrane resistance and capacitance and electrolyte resistance that produce a close-fitting simulated response (b).

Visual inspection of the data shows that the electrolyte solution has a resistance of approx-

imately 9kΩ and the bilayer has a resistance of 840MΩ (marked by the horizontal dashed lines on the magnitude versus frequency plot). An estimate of the capacitance can be obtained using the expression for either transition frequency in Figure 2.5a, however a different approach is used to extract estimates of resistance and capacitance from EIS data for the remainder of this work. A non-linear least squares fitting routine that mimics the same Fit Approximation function in the FRA software is used. This code (example Matlab script is provided in Appendix A) minimizes the approximation error between the measured experimental data and a simulated set of impedance points for all measured frequencies (defined by Equation 2.5) by optimizing the values of bilayer resistance, bilayer capacitance, and solution resistance. The approximation error weighs all data points equally in a manner defined by Boukamp [138] that prevents large-valued impedance points from dominating the fit error used in the optimization procedure. Figure 2.6b shows the results of applying the fitting procedure to the same set of impedance data. The red line overlays nearly perfectly on the blue data points, indicating that the assumed expression of the DIB impedance is appropriate. The results of the fit to this particular set of data estimates that the bilayer has a resistance and capacitance of 817MΩ and 557pF, respectively, while the solution resistance is approximately 9.6kΩ.

The importance of obtaining these values lies the physical phenomena they represent. The resistance of a bilayer is a measure of its ability to prevent the transport of ions across the interface. Higher values of resistance ($> 1G\Omega$) indicate a better seal as a result of more complete lipid monolayer assembly prior to formation. A bilayer with a low value of resistance is often called a "leaky" bilayer [139], since ions can pass through the core of the membrane even in the absence of proteins used to promote transport. In a later section on single channel current recordings, the importance of having very high bilayer resistances is discussed in terms of being able to measure the activities of very few proteins within the

membrane.

The measured capacitance provides a direct indication of the areal size of the bilayer. A lipid bilayer is modeled as a parallel plate capacitor, whose capacitance is given by

$$C = \epsilon_0 \epsilon_r A/t, \tag{2.6}$$

where ϵ_0 is the permittivity in a vacuum ($\epsilon_0 = 8.854 \times 10^{-12}$F/m), ϵ_r is the relative dielectric permittivity of the hydrocarbon core of the membrane ($\epsilon_r \approx 2$ [139]), A is the area of the bilayer, and t is the thickness of the hydrocarbon core ($t \approx 3 - 5$nm, [139]). Accordingly, the area-normalized capacitance, defined as the ratio of the dielectric permittivity to the thickness of the hydrocarbon core of the membrane, is constant for a given type of bilayer, since both parameters are determined by the type of phospholipid molecules that make up the membrane. For our purposes in deducing the area of the bilayer from measurements of nominal capacitance, published values of normalized capacitance for the type of phospholipid bilayer that we form are used directly. Phospholipid bilayers made from 1, 2-diphytanoyl-*sn*-glycero-3-phosphocholine (DPhPC), the lipid used for all experiments in this work, have reported normalized capacitance values of 0.6μF/cm^2 [140, 98]. Thus, a measured capacitance of 557pF corresponds to an approximate membrane area of 9.72×10^{-4}cm^2. Many times in this document, the size of the bilayer is expressed as an equivalent diameter instead of an area, in order to provide a better feel for the size of the bilayer. The shape of the interface is assumed to be circular, though the actual interface geometry is not known or directly seen upon bilayer formation. An area of 9.72×10^{-4}cm^2, nevertheless, corresponds to an equivalent bilayer diameter of 344μm.

2.3.2 Cyclic Voltammetry

Cyclic voltammetry (CV) is a second tool used frequently throughout this work for studying voltage-dependent behaviors of lipid bilayers. CV measurements consist of cycling an applied potential between two different values and measuring the resulting current along the way. This electrical technique is commonly found in many electrochemical studies, where the current measured provides information on the state of reactions, including oxidation-reduction processes, which can occur at different rates depending on the applied voltage. More related to this field of work, Tien used cyclic voltammetry to study how electron-transfer processes can be prescribed in cell-like membranes by incorporating TCNQ (7,7,8,8-tetracyano-p-quinodimethane) compounds into suspended lipid bilayers [113].

For our purposes, we use cyclic voltammetry to specifically characterize the current-voltage relationships of liquid-supported lipid bilayers both with and without proteins. CV is also used to record the potential at which liquid-supported lipid bilayers rupture due to an applied electric field.

Protocol for Performing CV Measurements

Since CV is used to characterize properties of the bilayer, particularly, the ability for proteins to alter the current-voltage relationship of the membrane as well as failure caused by an applied electric field, the voltage is varied slowly in order to target the region of the frequency spectrum (see Figure 2.6b) where the measured electrical impedance is dominated by only the electrical resistance of the interface.

CV measurements are performed with an Autolab PGSTAT12 and GPES (General Purpose Electrochemistry Software) software (version 4.97). The prescribed voltage is applied by connecting the leads wired a two-electrode configuration directly to the electrodes that insert

into the aqueous solutions on each side of the bilayer. The standard protocol for implementing CV on lipid bilayers consists of starting a scan at 0V, ramping the applied potential to a positive vertex, then decreasing the potential to a negative voltage of the same magnitude, and finally returning the potential to 0V. A scan rate of 2.5mV/s, with incremental voltage steps of 0.3mV, is used consistently in this work as it minimizes the contribution of bilayer capacitance into the measurement. Typical vertex potentials of ±100mV are used for studying the current-voltage relationship of bilayers with and without proteins while a positive apex potential of +500mV is selected for conducting bilayer failure measurements.

Displaying and Interpretting CV Data

Figure 2.7 provides representative current-voltage data obtained through CV on a single droplet interface bilayer. The plot on the left (Figure 2.7a) shows that the measured current varies linearly with the applied voltage for levels less than |100mV| and that the measured current at 0V is nonzero. This second point is explained by the fact that the Autolab system consistently measures non-zero currents at 0V, but for the purposes of studying current-voltage relationships the nominal value of current is often of little importance. The slope of the black dashed line that approximates this relationship marks the conductance (measured in Siemens, S) of the bilayer, and thus, the inverse of the slope provides a secondary way to estimate the resistance of the membrane with units of Ohms (Ω). The slope for this particular set of data is approximately 1.1pS, which corresponds to an approximate resistance of more than 800GΩ.

Figure 2.7b provides a second current-voltage trace for the same membrane taken to much higher positive voltage. This measurement is performed to intentionally induce bilayer rupture at large potentials. The trace shows that the bilayer demonstrates much the same current-voltage behavior for potentials less than 200mV. At higher potentials small spikes in

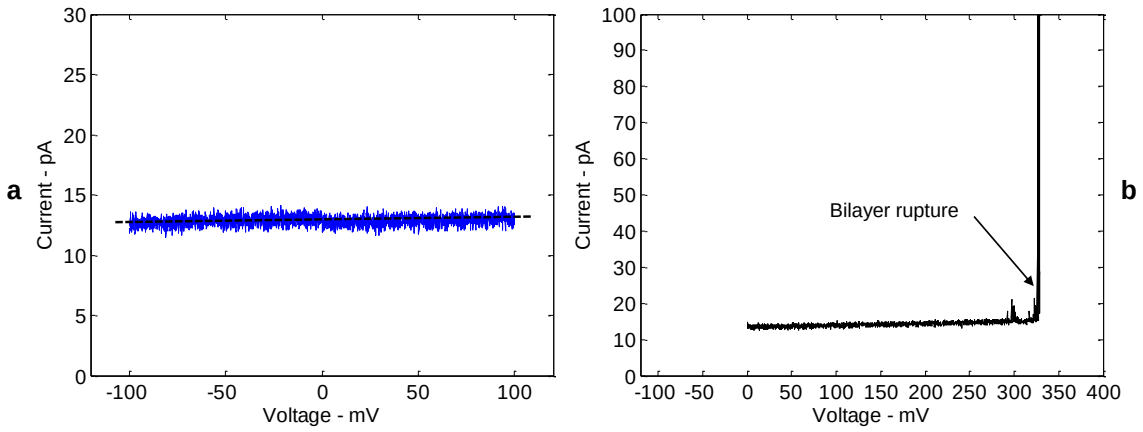

Figure 2.7: Current-voltage traces (a,b) obtained with CV measurements can be used to detect voltage-dependent behavior of the membrane, such as protein activity (not shown) or bilayer rupturing, as shown in (b).

current are observed, and then finally at a potential of 330mV the current increases to an unrecoverable level due to failure of the interface and coalescence of the droplets. This large increase in current up to several μA (peak not shown) is expected since now the dominant impedance between the electrodes is the low resistance of the electrolyte (only several kΩ in magnitude). While these data for a pure lipid bilayer do not exhibit much voltage-dependent current response at potentials less than $\pm$100mV, later studies with lipid bilayers containing protein molecules display significantly different behavior.

2.3.3 Chronoamperometry

Chronoamperometry is the measurement of current versus time for an applied potential. Throughout this work, two primary forms of chronoamperometry are used: current measurements of protein gating due to an applied dc voltage and square-wave current measurements induced by an applied triangular voltage waveform used to track changes in membrane capacitance.

Single Channel Recordings

Single channel recordings is the process of measuring the changes in current through a lipid bilayer induced by the insertion or gating activities of transmembrane proteins. Though the term suggests that the measurement is made for only one protein in the bilayer, it also applies to the measurement of a small number of proteins in the bilayer. The key distinction with this type of measurement is that the concentration of proteins in the bilayer needs to be low enough that at any one point in time, the activities of a single protein can be observed. As a result, this technique is widely-used to showcase the quality of a lipid bilayer, since an unregulated flow of ions through "leaky" membrane obscures the observation of current transients attributed to individual protein molecules. In the literature, the typical goal for bilayer formation is to produce a membrane with a resistance greater than 1GΩ (higher is always better), such that $10^{-12} - 10^{-9}$A (pA-nA) levels of current due to protein activity can only be attributed to flow through the protein itself rather than through the membrane.

Protocol for Single Channel Recordings

Two different pieces of equipment are used to record single channel current measurements of lipid bilayers containing proteins. The Autolab PGSTAT12 operated with GPES software (chronoamperometry configuration) is used to measure the insertion of proteins with slow insertion dynamics, as opposed to molecules that rapidly open and close within the bilayer. The standard protocol for making this type of measurement with the Autolab equipment consists of applying a constant voltage (typically $40 - 100$mV) and measuring the resultant current for an extended period of time. A fixed sampling rate of 10Hz or less is available with the Autolab for acquiring current data.

An AxoPatch200B patch clamp amplifier and Digidata 1440A data acquisition system (Molec-

ular Devices) controlled with AxoScope software are used for conducting single channel measurements of proteins with faster dynamics. This device is specifically designed for conducting low-level current measurements at high sampling frequencies and uses a cooled headstage unit to provide extremely low noise levels during the measurement. Single channel measurements of proteins in bilayers are obtained with the amplifier operated in the whole-cell configuration ($\beta = 1$) and the two silver-silver chloride electrodes are connected directly to the positive voltage and ground connections on the tethered headstage unit. Sampling rates as high as 250kHz can be used, through a wide range of lower sampling rates are also available for capturing slower events. Measured current is often filtered at 1kHz using an integrated analog filter within the amplifier.

Displaying and Interpreting Single Channel Recordings

Unlike the current-voltage relationships of pure lipid bilayers, the incorporation of active proteins into a membrane results in a composite membrane that behaves differently from lipid-only bilayers under the similar conditions. Single channel recordings are typically displayed in two forms: a current versus time graph and a histogram to illustrate the distinct levels of measured current.

The data shown in Figure 2.8 illustrates that the measured current for a bilayer containing proteins is not a static value. The measurement on the left corresponds to a bilayer with alpha-hemolysin channels which insert into the bilayer for a period of time, creating a conductive channels in the membrane. The measured stepwise increases and decreases in current, then, correspond to the addition and subtraction of αHL proteins into and out of the bilayer. The histogram shows the three dominant levels of current measured in this time period. Conductance values for the proteins are often computed by dividing the magnitude of the step-wise changes in current by the applied potential. In this example, a 6pA shift

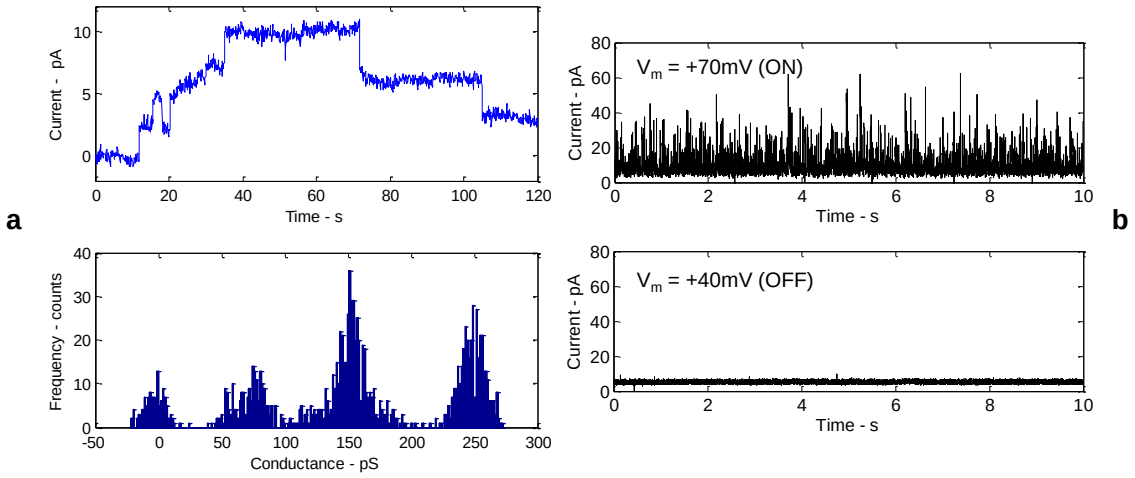

Figure 2.8: Alpha-hemolysin (αHL) insertion activity is measured as step-wise changes in the current flowing through a bilayer (a), while rapid gating activity of alamethicin channels depends on the applied voltage (b).

measured in response to an applied potential of 40mV corresponds to a conductance of 1.5nS.

In contrast to αHL recordings, the current traces in Figure 2.8b are obtained from a bilayer containing a high concentration of alamethicin proteins which insert into the membrane and then rapidly open and close (i.e. gates) under an applied potential. At this concentration, step-wise increases in conductance due to individual gating events are not easily recorded, though the measurement still shows the rapid opening and closing caused by these voltage-activated molecules. Faster sampling and/or less protein in the bilayer is expected to produce cleaner single channel recordings of alamethicin. The lower trace confirms that this phenomenon is voltage-dependent, where applied potentials less than some critical value (+70mV for alamethicin) do not result in gating activity in the membrane. In both cases, however, having a bilayer with a very high electrical resistance is required in order to resolve the small increases in current caused by individual proteins.

Square-Wave Current Measurements

The capacitance of a membrane can be tracked in real-time through a second form of chronoamperometry measurement. In this procedure, the current-voltage relationship for a capacitor ($I = CdV/dt$, where the current, I, flowing through a capacitor of capacitance, C, is proportional to the time rate of change of the applied voltage, dV/dt) is used directly to estimate capacitance from real-time current measurements. Per this relationship, the application of a constantly increasing or decreasing voltage across a capacitor produces a steady-steady current value proportional to the value of the capacitance and the rate of voltage change. Similarly, a symmetric triangle waveform voltage centered about 0V produces a square-wave current through the capacitor. The use of this type of technique enables the capacitance of the membrane (proportional to its areal size, see Equation 2.6) to be tracked in real-time. A specific situation where this measurement is useful is during the initial formation of a droplet interface bilayer. Prior to contact, the capacitance of the oil phase is negligible. But once the excess oil is removed and the two opposing lipid monolayers thin to a bilayer structure, the capacitance increases sharply and then grows as the thinned bilayer continues to expand radially.

Protocol for Real-Time Capacitance Measurements

Square-wave current measurements are conducted using the AxoPatch200B and Digidata 1440A in whole cell mode with the applied voltage signal produced externally and routed into the AxoPatch via the external control connection on the back panel of the device. A Hewlett Packard 3314A outputs a 0.5V triangular wave at 100Hz (a frequency where the bilayer is purely capacitive–see Figure 2.6a), such that with a signal gain of 20mV/V for incoming signals into the AxoPatch, a triangle wave of 10mV in amplitude at the same

driving frequency is applied to the electrodes. Current is sampled at 5kHz and low-pass filtered at 1kHz using the front panel control on the amplifier.

Interpretation of Real-Time Capacitance Measurements

The measured current and applied voltage are both recorded using AxoScope software. Estimates of capacitance are computed within the same software (using Math functions on the incoming current signal), by dividing the measured current by the time rate of change of the applied voltage ($dV/dt = 4Af = 4$, for an applied voltage amplitude, A, of 10mV and a driving frequency, f, of 100Hz). Additional post-processing can also be performed to estimate bilayer size as described in Section 2.3.1. A representative real-time capacitance measurement of initial bilayer formation is shown in Figure 2.9.

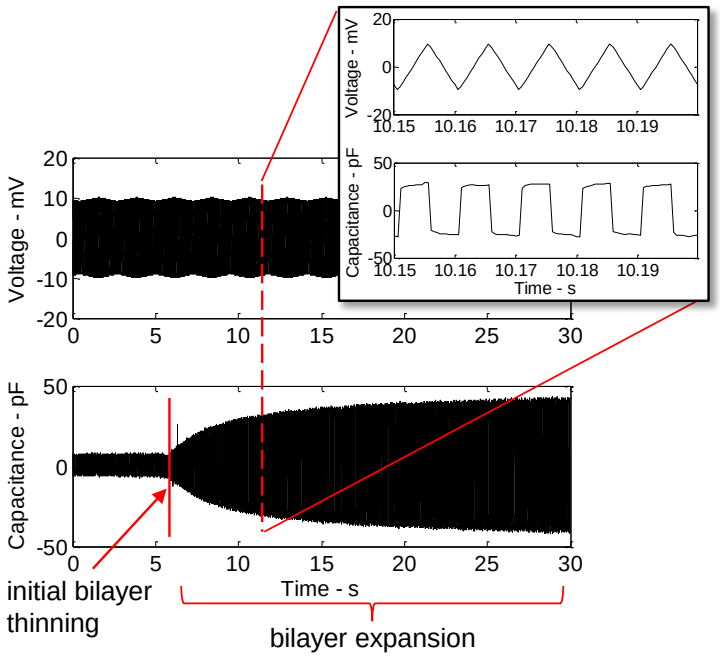

Figure 2.9: The magnitude of the measured square-wave current is directly proportional to the capacitance, and thus the area, of a droplet interface bilayer. Real-time measurements show both the initial thinning and subsequent expansion of the interface.

The figure shows that at approximately the 6-second mark, the magnitude of the capacitance increases sharply when the bilayer first thins and the grows steadily over the next 30 seconds as the area of the interface expands. The inset shows that the shapes of the applied voltage and measured current signals do not change during the measurement. Only the magnitude of the measured current (and computed capacitance) changes due to the formation of lipid bilayer between the electrodes. This type of measurement can also be used to track changes in bilayer size as well as record the complete separation of the monolayers that join to form the interface.

2.4 Chapter Summary and Conclusions

The techniques described in this chapter form a basic understanding of the electrical measurements used to characterize lipid bilayers. Interpretation of representative data demonstrated how collected data are analyzed in the context of evaluating whether a given bilayer creates the proper environment for hosting functional biomolecules. The following chapters employ these techniques frequently to characterize interface bilayers formed within engineering materials.

Chapter 3

Fundamental Studies in Tailoring Transport in Droplet Interface Bilayers

Droplet interface bilayers form the basic building block of biomolecular material systems, where each droplet can be thought of as an artificial cell, or *cell-mimic*. These "cells" communicate with other "cells" through ionic transport processes that occur across the lipid bilayer formed between neighboring droplets. The composition and properties of the host bilayer, then, determines the selective regulation of species and signals transported from one cell volume to the next.

In this chapter[1], single and multi-bilayer DIB networks are studied to investigate how desired transport processes can be prescribed in a network of droplets. First, the electrical properties of pure lipid droplet interface bilayers formed using both *lipid-out* and *lipid-in* practices

[1]Note: This chapter presents a modified and expanded version of the published paper "Tailored current-voltage relationships of droplet interface bilayers using biomolecules and external feedback control" [141].

are investigated with electrical impedance spectroscopy (EIS) and cyclic voltammetry (CV) techniques in order to better understand the role of the host bilayer. Second, we demonstrate that the transport properties (defined by the current-voltage relationship) of the bilayer can be tailored using biological molecules as well as external feedback control strategies. Alpha-hemolysin (αHL) proteins from *Staphylococcus aureus* and alamethicin channels from the fungus *Trichoderma viride* are reconstituted into specific droplets such that self-insertion of the molecules occurs from the aqueous interior of the droplet into designated interface bilayers. Bilayers containing either of the two types of proteins display different current-voltage characteristics, showcasing the convenience for using the inherent functions of the protein to tailor the transport properties of the entire interface. In a novel approach, feedback control is applied in two different fashions to customize the transport dynamics of DIBs for both current tracking and voltage control. This initial set of experiments establishes a toolkit for analyzing and customizing specific interfaces within complex functional networks.

3.1 Experimental Methods

3.1.1 Materials

Droplet interface bilayers are formed using either the *lipid-out* method, where phospholipids are dissolved into the oil phase, or the *lipid-in* method, with phospholipids incorporated as vesicles into the aqueous buffer solution that constitutes each droplet volume [93]. Lipid-out droplet interface bilayers (DIBs) are formed using the procedures developed by Holden, et al [98, 99, 101]. The aqueous droplets contain 10mM MOPS (Sigma), 100mM NaCl (Sigma), pH7 buffer solution and 1, 2-diphytanoyl-*sn*-glycero-3-phosphocholine (DPhPC) synthetic lipids purchased as lyophilized powder (Avanti Polar Lipids, Inc.) are dissolved in hexadecane

(Sigma) to form a 10mg/ml lipid stock solution for the oil phase. Aqueous droplets used to form lipid-in DIBs contain a 2mg/ml solution of DPhPC phospholipid vesicles in 10mM MOPS (Sigma), 100mM NaCl (Sigma), pH7 buffer solution. The phospholipid vesicles are prepared as described elsewhere [93] and are stored at $3 - 8^{o}$C for several weeks during testing. It should be noted that salt concentrations on the order of 100mM are commonly used within the aqueous phases for many of the measurements of whole membrane properties (i.e. EIS, bilayer rupture, aggregate protein activity) performed in this work. However, higher salt concentrations are used at times for amplifying the measured current in several single channel measurements and for repeating conditions that others have used in their own work. Reversible silver-silver chloride (Ag/AgCl) electrodes are fashion for DIB positioning and electrical interrogation as discussed in Section 2.2.

3.1.2 Formation of Droplet Interface Bilayers

First, a well machined into a poly(methyl methacrylate) (PMMA) tray is filled with $40 - 50\mu$l of the oil phase (either phospholipid/hexadecane solution for lipid-out DIBs or pure hexadecane for lipid-in DIBs) (Figure 3.1). Two 300nl droplets of the corresponding aqueous solution are then pipetted into the oil phase. A silver-silver chloride (Ag/AgCl) electrode coated with hydrophilic agarose gel (Sigma) is immediately inserted into each droplet for subsequent positioning and electrical measurements. Initially, the electrodes are positioned such that the droplets do not touch in order to allow for the amphiphilic lipid molecules present in either phase to adsorb to the oil/water interface, forming a lipid monolayer around each droplet. Holden, et al found that droplet interface bilayers can be produced repeatedly when the monolayers are allowed to "stabilize" for 30 minutes [98], however, our results indicate several hours are needed to establish stable lipid bilayers from well-packed lipid monolayers when using DPhPC phospholipids dissolved in hexadecane. In contrast, lipid-

in DIBs require only 5 minutes of stabilization prior to bilayer formation [93, 142]. The electrodes are repositioned following monolayer formation in order to bring the droplets into physical contact (Figure 3.1b). A bilayer forms spontaneously within a few minutes once excess oil is removed from between the droplets, permitting thinning of the two opposed monolayers [143]. In the specific context of DIB formation, droplets are commonly said to "zip" together to form an interface bilayer (Figure 3.1c). More-complex networks of DIBs are made in a similar fashion by dispensing and connecting additional lipid-encased droplets.

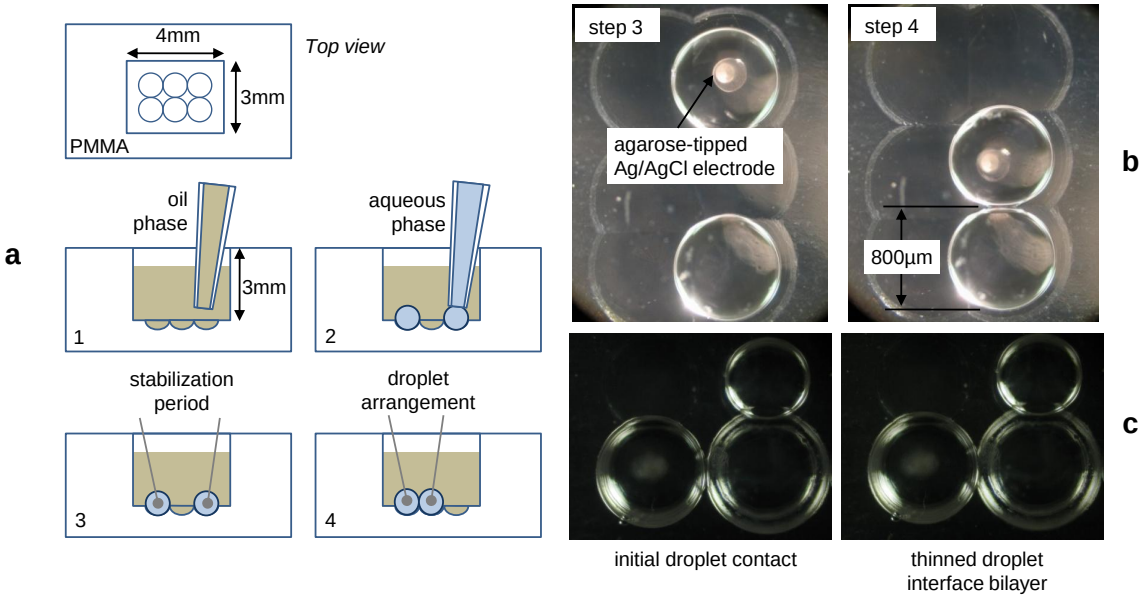

Figure 3.1: droplet interface bilayers are formed when aqueous droplets (300nl each) are pipetted (a.2) into the oil phase within a well (a.1). An agarose-tipped Ag/AgCl electrode is inserted into each droplet and the droplets are kept separated (a.3, b). After sufficient time to allow for lipid monolayer assembly at the oil/water interface. the electrodes are repositioned to bring to the droplets into physical contact (a.4, b). A bilayer forms when excess organic solvent is extracted from between the droplets and the two lipid monolayers "zip" together (c).

Electrical impedance spectroscopy (EIS) and cyclic voltammetry (CV) are used to characterize the electrical properties of droplet interface bilayers with and without proteins. The standard protocols described for performing each measurement with the Autolab equipment

are described in detailed in Chapter 2, Sections 2.3.1 and 2.3.2. The 3-axis stepper-motor controlled micromanipulator is used to move one of the electrodes for precise droplet positioning throughout the study while the other electrode is held stationary by a "helping hands"-style wire holder.

3.2 Characterization of Single, Lipid-Only DIBs

3.2.1 *Lipid-out* Droplet Interface Bilayers

Electrical impedance and cyclic voltammetry measurements (Figure 3.2a, b) are first conducted on DPhPC droplet interface bilayers that do not contain proteins. EIS measures the resistance to charge transport across the droplet interface positioned between the electrodes within neighboring droplets. When no bilayer forms (and the droplets remain separate), EIS measurements indicate an "open circuit" response. When the droplets coalesce, the measurement records a low resistance of the lipid-electrolyte solution. Measured membrane resistance values vary from $100\text{M}\Omega - 10\text{G}\Omega$ while equivalent bilayer diameters range from $200 - 500\mu$m for 300nl droplets.

Figure 3.2b shows the specific resistance (resistance $\times$ membrane area) and equivalent diameter of the lipid bilayer versus time for successive EIS measurements on three different DIB formation trials. Without proteins in these bilayers, the three trials show that the resistance increases with time (up to 200%), yet the size of the bilayer undergoes a much smaller change (less than 25%). Tracking bilayer size confirms that changes to the nominal resistance are not due solely to changes in bilayer size.

Finally, cyclic voltammetry is used to characterize the electrical limits of droplet interface bilayers. In these measurements, the current flowing through the membrane is measured for

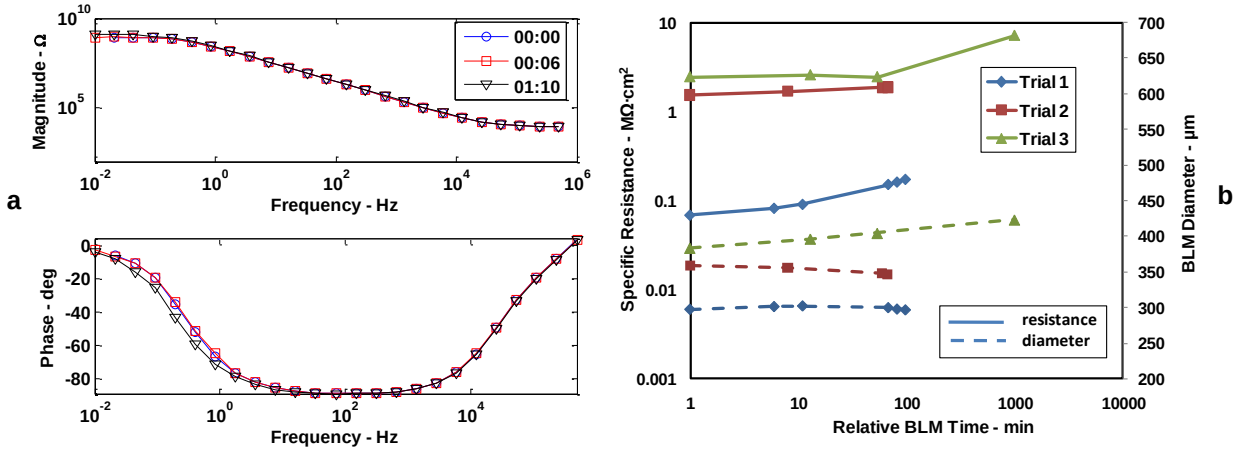

Figure 3.2: The magnitude and phase of the electrical impedance versus frequency for a droplet interface bilayer without proteins measured over time (a). The specific resistance ($M\Omega \cdot cm^2$) and equivalent membrane diameter (μm) for three DPhPC droplet interface bilayers measured in time (b).

a steadily-increasing voltage until rupture, marked by a large spike in the current due to the failure of the membrane resistance. Cyclic voltammetry measurements show the measured current flowing through a lipid bilayer for an increasing and decreasing applied potential from -100mV and +100mV (Figure 3.3a). Subsequent electrical measurements on the system following bilayer rupture and immediate droplet coalescence show the response of the electrolyte resistance since the lipid membrane that previously stabilized the interface no longer exists. The data shown in Figure 3.3b illustrates that lipid-out DIBs fail at applied potentials ranging from $100 - 250$mV, values lower than those measured for bilayer lipid membranes formed using other techniques. DPhPC bilayer lipid membranes formed across the pore of a supporting substrate in two separate studies using the folding technique exhibited failure potentials of $390 - 410$mV [140, 144]. The lipid bilayers formed in these separate studies were smaller, however, which may contribute to a more durable lipid membrane (the apertures in the supporting substrate ranged from $100 - 250\mu$m, resulting in a bilayer with an even smaller diameter when the formation of an annulus of lipid solution around the rim

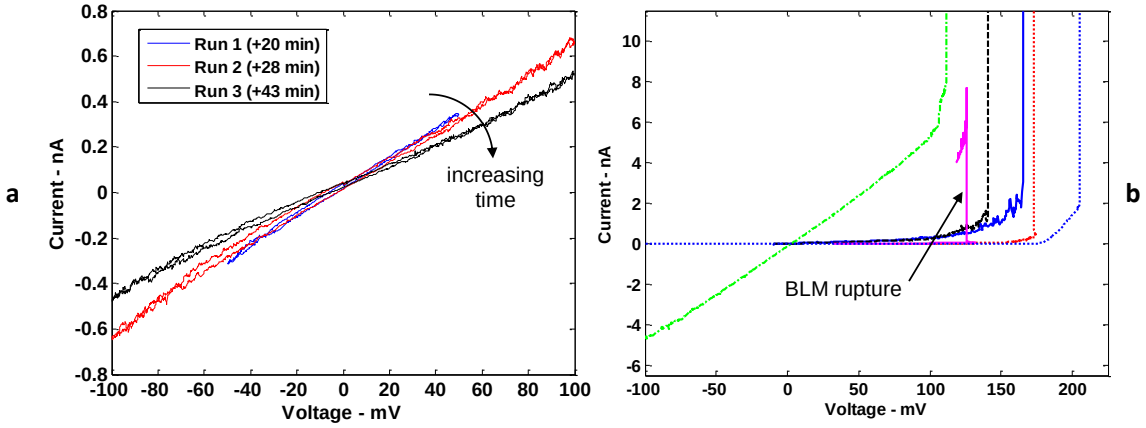

Figure 3.3: Current versus voltage plotted for three successive CV measurements on a single lipid-only DIB (a). Failure potentials for DIBs are marked at the point where current increases abruptly (b). Note: The relative time markers indicate the time (in hr:min format) after the two droplets first come together to form a bilayer lipid membrane.

of the pore is considered [57, 145]). In contrast, the diameters of droplet interface bilayers formed in this study are twice as large. The combination of a much larger membrane area and a varying degree of monolayer assembly may have contributed to the lower failure potentials measured for lipid-out droplet interface bilayers.

3.2.2 *Lipid-in* Droplet Interface Bilayers

The formation of singe, lipid-in DIBs at the interface of adjacent aqueous droplets is again confirmed using electrical impedance spectroscopy (EIS) and cyclic voltammetry (CV) measurements. Values of electrical resistance and capacitance of the membrane are extracted from the data in the same fashion as described above. The impedance data presented in Figure 3.4a corresponds to a lipid bilayer with an initial resistance of 2.5GΩ that increases to more than 14GΩ by the third measurement. The capacitance of the bilayer is estimated to be $11 - 12$pF and the computed equivalent diameter for this interface is computed to be 50μm.

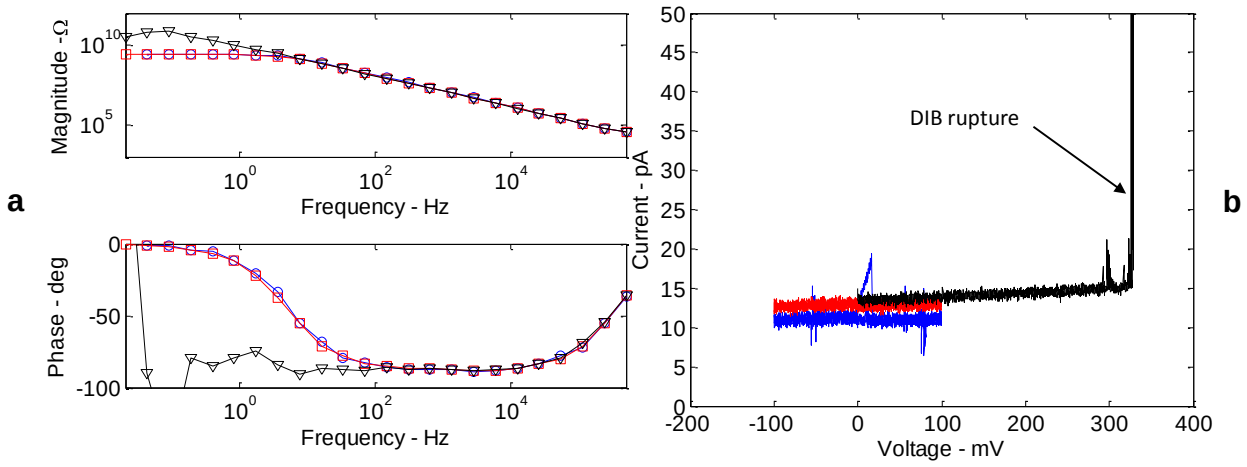

Figure 3.4: Representative electrical impedance (a) and cyclic voltammetry (b) data measured on a single droplet interface bilayer. Both the magnitude and phase of the electrical impedance versus frequency are plotted for three successive measurements on the same DIB. Three cyclic voltammetry measurements are also shown, with the third measurement inducing bilayer rupture at an applied potential greater than 300mV.

Cyclic voltammetry measurements also confirm the higher bilayer resistance formed aqueous containing phospholipid vesicles. The current-voltage relationship shown in Figure 3.4b of a pure DPhPC bilayer without proteins is highly linear for applied potentials up to the observed failure potential at approximately 330mV. Again, the failure potential is marked by a sharp, irreversible increase in current measured when the bilayer ruptures and the droplets coalesce. The average measured capacitance and equivalent interface diameter of additional *lipid-in* bilayers is approximately 360pF and 260μm, respectively. The average specific resistance measured for these bilayers is 7MΩ·cm^2 ($n = 9$), while the average failure potential recorded for a subset of these trials is 340mV ($n = 4$).

The measured electrical resistance and bilayer failure potentials indicate that the addition of phospholipid vesicles into the aqueous droplets results in the assembly of a tightly-packed lipid monolayer that translates into the formation of highly-resistive, stable bilayers. This improved bilayer formation is attributed to the fact that phospholipid contained within the droplets experience a smaller adsorption distance to the oil/water interface than lipid

molecules dissolved in the external oil phase. On average the specific bilayer resistances measured for single, lipid-in DPhPC droplet interface bilayers is nearly $10\text{M}\Omega\cdot\text{cm}^2$. Moreover, these interfaces rupture at applied voltages higher than 300mV (Figure 3.4). Lipid-out DPhPC droplet interface bilayers characterized in the initial tests produced specific membrane resistances ranging from $0.1 - 10\text{M}\Omega\cdot\text{cm}^2$, though very few of these trials produced bilayers having nominal resistances greater than $1\text{G}\Omega$, and failed at electrical potentials between $100 - 200\text{mV}$.

3.3 Tailoring Transport with Biomolecules

The incorporation of proteins into a droplet interface bilayer results in a membrane with selective transport functionality. The following discussion examines the current-voltage relationships measured for two different proteins incorporated into single DIBs as well as three-droplet, two-bilayer networks.

3.3.1 Single DIBs containing Alpha-Hemolysin

Alpha-hemolysin (αHL) from the bacteria *Staphylococcus aureus* (Sigma) causes lysis, or cell death, by the breaking the cell membrane through the formation of water-permeable ion channels that span the thickness of the membrane [46]. These proteins are dissolved in the aqueous buffer of one droplet (*cis*) in a droplet interface bilayer pair. Three different concentrations of αHL are used in this study: 10μg/ml, 5μg/ml, and 1μg/ml are dissolved in the aqueous buffer solution and kept refrigerated for up to a week. These concentrations are significantly higher than those used in studies aimed at discerning single or few-protein insertion events [98, 99, 106] because it is desired to cause and record large-scale changes to

the current-voltage relationships of the lipid bilayers.

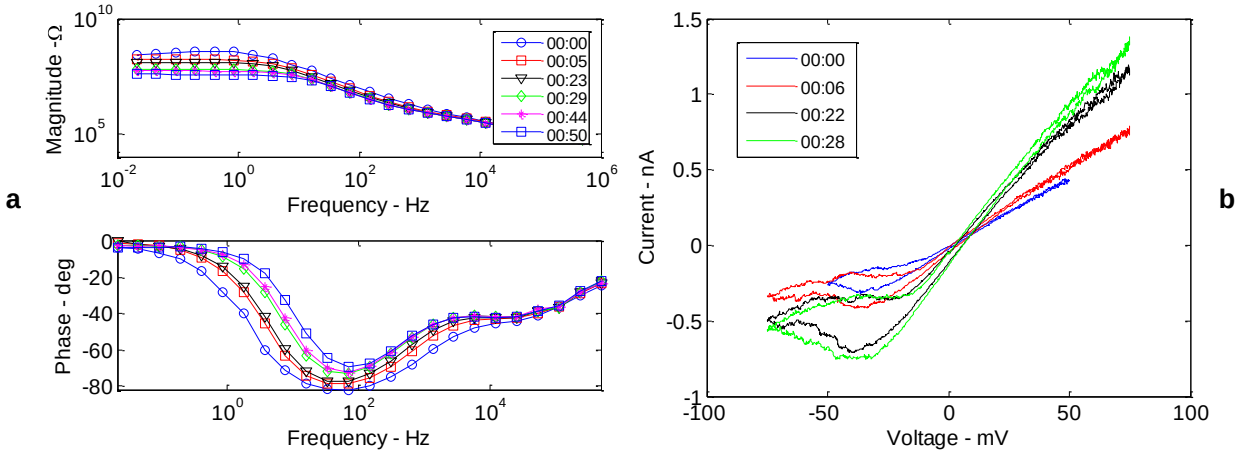

Figure 3.5: EIS (a) and CV (b) measurements for a single droplet interface bilayer in which one droplet contained 5μg/ml αHL dissolved in buffer solution (designated as the *cis* side of the membrane). The positive (working) electrode is placed in the droplet without protein (*trans*).

Figure 3.5 illustrates the measured effects of 5μg/ml αHL in buffer solution added to one droplet in the droplet-pair. Successive electrical impedance spectroscopy measurements in Figure 3.5a show a reduction in the near-dc resistance of the lipid membrane. Furthermore, cyclic voltammetry measurements indicate that the incorporation of the ion channels into the membrane alters the current-voltage relationship compared to bilayers which do not incorporate αHL. Comparing Figure 3.3a and Figure 3.5b, we see that the incorporation of the αHL into the bilayer produces a nonlinear current-voltage relationship that exhibits an inflection point in the current at voltages less than approximately -20mV. The cyclic voltammetry data also indicates that the conductance (as measured by the slope of the current-voltage curve) of the lipid membrane containing ion channels increases over time as additional αHL channels incorporate into and porate the membrane. This response is consistent with the decreasing low-frequency magnitudes of impedance observed with EIS.

The insertion and activity of αHL ion channels in droplet interface bilayers is witnessed as

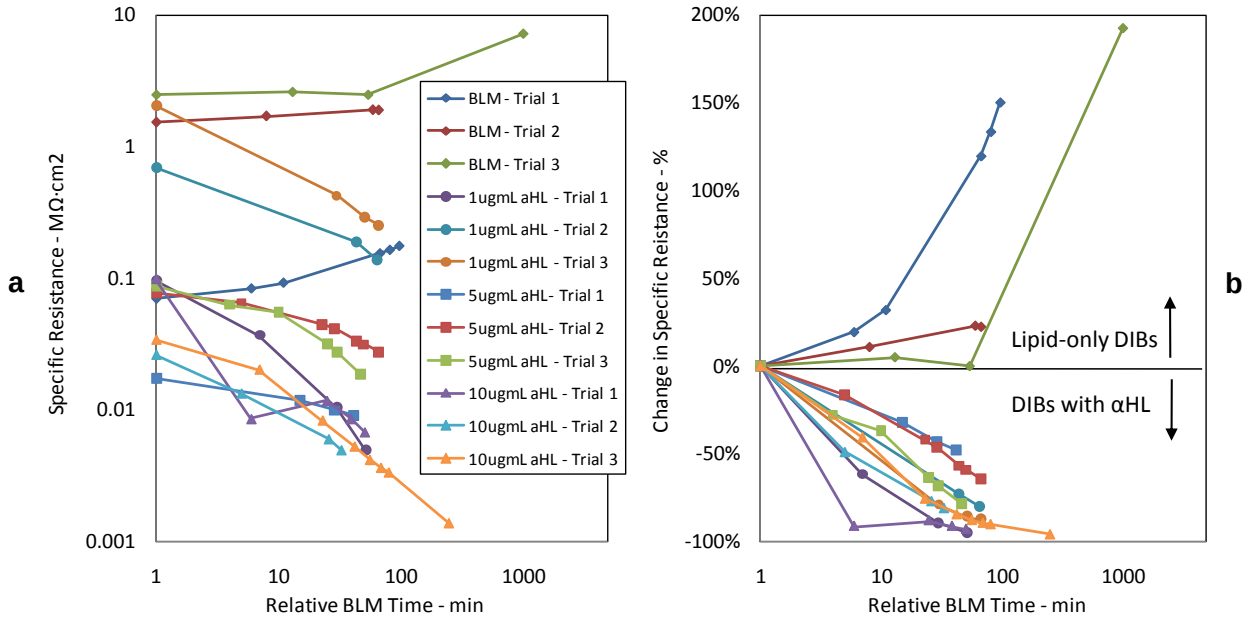

Figure 3.6: Specific resistance ($M\Omega{\cdot}cm^2$) (a) and change in specific resistance (%) (b) versus time after BLM formation for droplet interface bilayers containing varying amounts of αHL (10μg/ml, 5μg/ml, and 1μg/ml).

both a continual reduction in the resistance of the bilayer as well as a nonlinear current-voltage relationship measured with CV. Song, et al characterized the structure and function of the 33kDa αHL ion channel from the *Staphylococcus aureus* bacteria and provided evidence that a water-pore forms when seven αHL monomers aggregate on the lipid surface to form a heptamer [46]. The heptamer then inserts through the lipid bilayer, creating an anion-selective water-channel. The data shown in Figure 3.5, and in Figure 3.6 for three different concentrations of ion channels, indicate that the insertion of a large number of αHL heptamers reduces the effective resistance of a lipid bilayer. Measured initial specific resistances of droplet interface bilayers range from $0.01 - 10 M\Omega{\cdot}cm^2$ (Figure 3.5b), and these values then decreased by more than an order of magnitude in the first $1 - 2$ hours after BLM formation. The final resistance values measured for αHL-degraded lipid membranes range from a $1 - 100 M\Omega{\cdot}cm^2$. It is envisioned that at some point, the bilayer becomes saturated

with functioning ion channels and its resistance either reaches a minimum value or the membrane fails and the droplets coalesce. This process in nature is called lysis, or cell death by breaking of the membrane [46]. In contrast, the measured values of resistance for lipid membranes without ion channels increase over time.

Alpha-hemolysin ion channels residing in the interface bilayers display non-linear current-voltage response during cyclic voltammetry measurements. Partial rectification of the ion current is seen at negative potentials below roughly -40mV in Figure 3.5b. Others have witnessed similar asymmetric, rectification of the ionic current through alpha-hemolysin ion channels reconstituted in bilayer lipid membranes and have attributed this behavior to an asymmetric charge distribution of the amino acid residues along the transmembrane pore [47, 146, 147]. Furthermore, Menestrina characterized the voltage-dependent conductance of αHL ion channels, finding that the ion channel is inhibited by divalent and trivalent cations [148]. In these studies, however, no inhibition was seen for the monovalent sodium cations present in the aqueous buffer solution.

3.3.2 Lipid Bilayers with Alamethicin

The results demonstrated with alpha-hemolysin provide credible evidence that the insertion of proteins into a lipid bilayer produces variations in the current-voltage relationship of the membrane. To further illustrate that this altered response is protein dependent, a second series of tests are performed using the protein alamethicin. Alamethicin is a 2kDa ion channel that binds to and partially inserts into a bilayer as a monomer and then upon application of voltage, inserts through the hydrophobic core of the membrane [91, 149]. The instability of the hydrophilic amino acids in the peptide chain then drives aggregation ($3 < n < 12$ per bundle) with other monomers to form a cation-selective, voltage-dependent ion channel

[91, 150]. In addition to alamethicin insertion into lipid-out DIBs, parallel measurements are conducted to investigate and confirm protein insertion into droplet interfaces from aqueous droplets containing phospholipid vesicles and proteins. We expand the scope of this study to also investigate two-sided insertion (i.e. when both droplets contain proteins) and also present measurements of protein activity within multi-bilayer DIB networks formed from three droplets connected serially.

Alamethicin insertion into *lipid-out* DIBs

Purified alamethicin from the fungus *Trichoderma viride* (Sigma and A.G. Scientific) is reconstituted into both *lipid-out* and *lipid-in* DIBs in a similar manner. Alamethicin proteins are stored in ethanol at 0.1% (w/v) and this stock solution is diluted further to a final concentration of 1μg/ml alamethicin in aqueous buffer. The electrical impedance and cyclic voltammetry measurements on bilayers containing alamethicin confirm this behavior (Figure 3.7).

The observed nonlinear current-voltage behavior (Figure 3.7a) agrees well with measurements of alamethicin in supported bilayer lipid membranes [91, 69, 151, 152, 106]. Protein activation (opening) consistently occurs at potentials (relative to the cis side of the membrane) between -25mV and -80mV for the concentrations used in these tests. Often successive cyclic voltammetry measurements on the same bilayer with alamethicin show little change over time, indicating that a large percentage of the proteins that incorporated into the BLM do so before the first cyclic voltammetry measurement (usually within $10-20$ minutes after BLM formation). This behavior is expected, since alamethicin monomers are known to bind to and partially insert into a bilayer prior to the application of voltage [91, 149]. The measured data support this behavior, suggesting that the alamethicin monomers attach to the lipid monolayer prior to bilayer formation and, therefore, are poised and ready to insert upon the

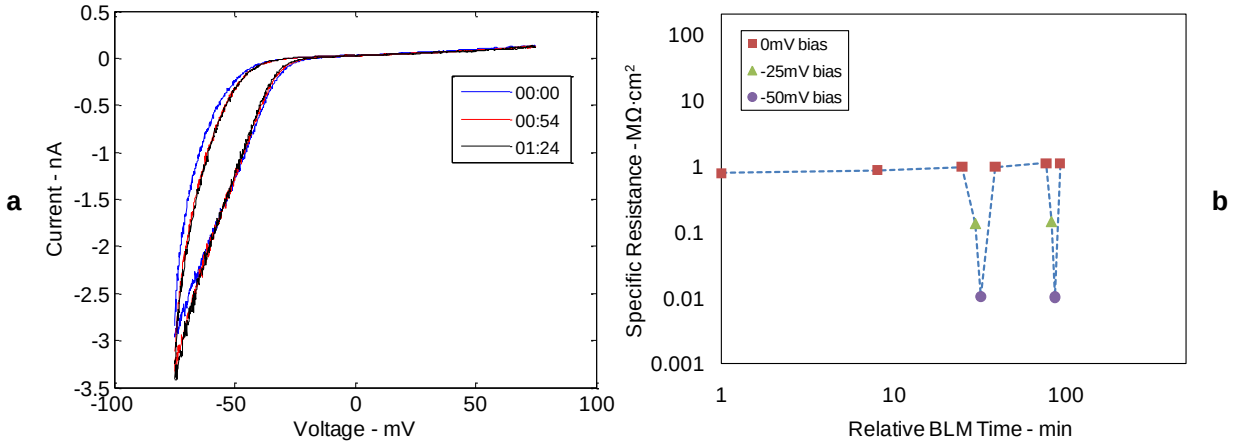

Figure 3.7: The current-voltage relationship (a) and the specific bilayer resistance versus time (b) measured for an interface bilayer with 1μg/ml alamethicin added to one droplet. EIS measurements are performed at three different biasing potentials (0mV, $-$25mV and $-$50mV) and demonstrate the ability to toggle the resistance of the bilayer with an applied bias potential.

first voltammetry measurement. The measured hysteresis seen in the cyclic voltammetry measurements is attributed to both the opening/closing rates of the ion channels as well as the applied voltage ramp rate [153, 152]. Vodyanoy's work also indicated that adsorbed alamethicin monomers can alter the geometric capacitance of a bilayer and that the charging and discharging of the total capacitance is affected by the corresponding rates of alamethicin adsorption and desorption from the membrane [151].

The positive (working) electrode in these tests is placed in the droplet containing only buffer solution (*trans*), therefore an applied potential more negative than $-$50mV is required to open all alamethicin channels. Bilayers containing alamethicin produced small nonzero ($<$ 5mV) open-circuit potentials, further indicating that the applied voltage causes pore opening in the alamethicin channels and that in the open-circuit configuration, the ion channels are in a closed state. The specific membrane resistance is reversibly varied from 1MΩ·cm^2 at 0mV in the closed state to 0.1MΩ·cm^2 at $-$25mV in a partially-open state and to 0.01MΩ·cm^2 at $-$50mV in a fully open state (Figure 3.7b). The bilayer is returned to its open-circuit

state between EIS measurements, verifying that the reduction in the specific resistance at -50mV was not dependent on a previous measurement -25mV. Furthermore, the resistance of the bilayer in the closed state remained steady, and in some trials increased slightly, over the duration of the test as excess lipid molecules in the surrounding lipid solution continue to pack into each monolayer. Measurements on additional DIB pairs ($n = 9$) containing alamethicin in one droplet further support the current-voltage relationship of alamethicin in a bilayer shown in Figure 3.7. In all tests, the conductance of the membrane increased $2-3$ orders of magnitude by alamethicin activation.

Alamethicin in single, *lipid-in* DIBs

In these tests, alamethicin/ethanol stock solution is first diluted further to a concentration of 100μg/ml alamethicin in 10mM MOPS, 100mM NaCl, pH 7 buffer solution. Droplets containing alamethicin consist of a 50:2 (v:v) vesicle solution-protein solution mixture. The first set of experiments focuses on the current-voltage response of alamethicin within single droplet interface bilayers formed from two droplets. Figure 3.8 shows the results of the EIS and CV measurements on three different single DIBs: without alamethicin in either droplet, with alamethicin in only one droplet, and with alamethicin in both droplets.

EIS measurements in Figure 3.8a for the three cases show a very similar impedance signature for droplet interface bilayers measured using a small applied potential (5mV RMS). Each of the three trials produced a bilayer with an electrical resistance greater than 10GΩ and an interface ranging from $250-350\mu$m in diameter. Cyclic voltammetry measurements, however, show that differences in the current flowing through the interfaces arise as a function of voltage. Figure 3.8b shows that the conductance (measured by the slope of the current-voltage curve) of a bilayer containing alamethicin increases when the voltage of the droplet containing alamethicin is at a potential approximately +60mV relative to the opposite side. For

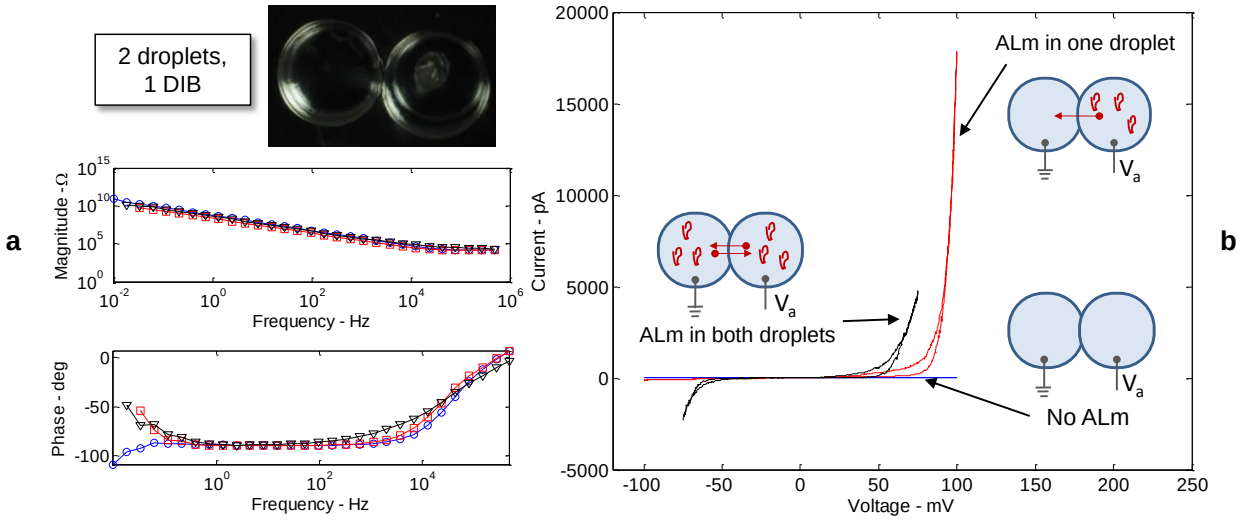

Figure 3.8: Electrical impedance and cyclic voltammetry measurements on single, *lipid-in* droplet interface bilayers with and without proteins. The blue (circles) traces refer to EIS and CV measurements of a pure lipid DIB, the red (squares) traces correspond to a two-droplet network that contains alamethicin (ALm) proteins in the right droplet, and the black (triangle) traces refer to alamethicin incorporated into both droplets. The arrows in the sub-figures indicate the direction of protein insertion from within the droplet interiors.

example, when alamethicin is incorporated into the right droplet in a two-droplet network and the voltage in this droplet is higher than 60mV, the slope of the current-voltage curve increases greatly. Incorporating alamethicin proteins into both droplets produces a symmetric voltage-dependent conductance (black trace). The measured current traces shows that the voltage-dependent change in conductance is reversible; bilayers containing alamethicin resume a state of high resistance for applied potentials approaching 0V.

The voltage-dependent conductance of alamethicin proteins in droplet interface bilayers confirms the ability to reconstitute proteins into *lipid-in* DIBs in the presence of phospholipids vesicles within the droplets. The final concentration of alamethicin in each 300nl droplet in this study is 3.8μg/ml, which is comparable to the 1μg/ml concentration used in alamethicin measurements in *lipid-out* DIBs. A similar voltage-dependent conductance is measured in this study via CV at applied potentials greater than +60mV in the droplet containing the

alamethicin. The conductance of the membrane (the slope of the current-voltage curve) in both the *OFF* state when the proteins are closed and during the *ON* state are approximated by applying a linear regression to both regions of the red trace (denoting alamethicin added to just one droplet) in Figure 3.8b. In the *OFF* state, the conductance of the membrane is approximately 317pS, which corresponds to an equivalent membrane resistance of 3.2GΩ. This approximated resistance is consistent with the estimated bilayer resistance value of 9GΩ measured via EIS. The *ON* state conductance of the membrane at potentials close to +100mV increases to 750nS. Thus, the resistance of the membrane with the proteins activated is only 1.3MΩ, a three order-or-magnitude decrease in resistance to current flow. The cyclic voltammetry data also shows that once this potential is removed, the membrane returns to its original, highly-resistive closed state. One unknown in this study is the precise number of proteins that self-insert into the bilayer during the measurements. Unlike αHL channels of known and constant conductance, alamethicin channels aggregate in the bilayer to form bundles of varying size and so single values of conductance can not be used to estimate the number of proteins present.

Alamethicin in multi-DIB networks

A second subset of experiments are performed in order to measure the current-voltage relationships of alamethicin incorporated into multi-DIB networks. *Lipid-in* DIBs are again used in this brief study as the higher bilayer resistance that are obtained provides a more stable droplet network. Four configurations are tested: three droplets without alamethicin, alamethicin incorporated into the end droplet, alamethicin added to the central droplet, and alamethicin proteins in all three droplets.

The activation of alamethicin proteins in larger biomolecular networks is affected by the presence of additional lipid membranes in the network. EIS measurements (not shown)

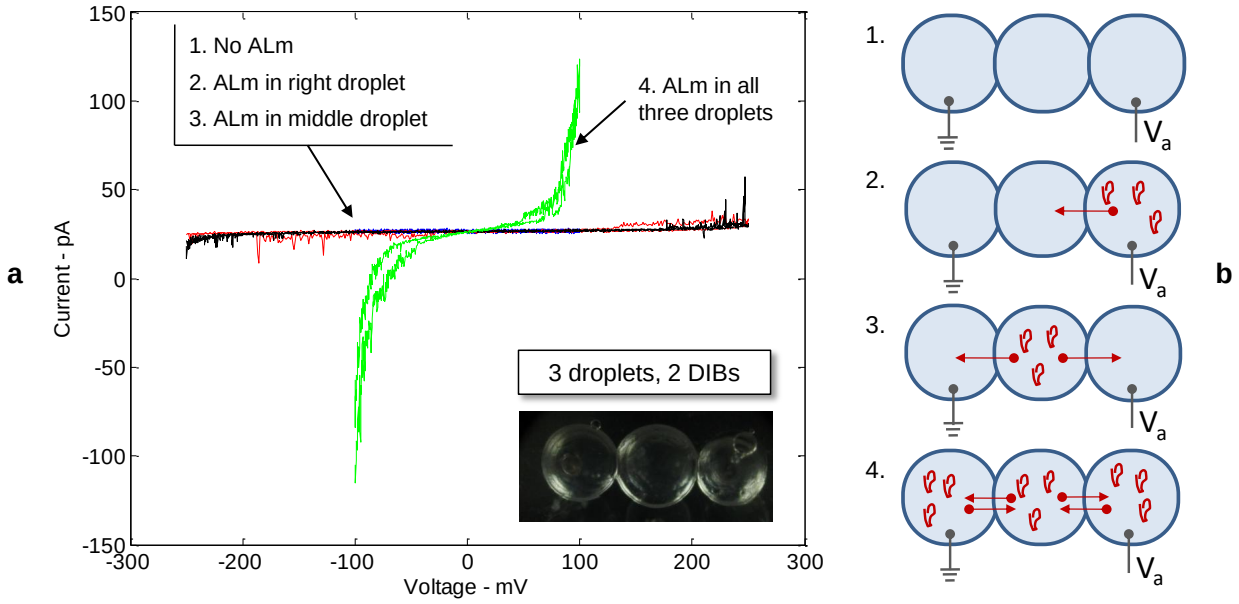

Figure 3.9: Current-voltage relationships measured with CV for multiple, *lipid-in* droplet interface bilayers with and without proteins (a). The arrows in droplet diagrams corresponding for the four tests cases indicate the direction of protein insertion (b).

are performed to verify bilayer formation prior to the CV measurements. In all four trials, the electrical impedance at low frequency ($<$ 10mHz) approaches 100GΩ while the high-frequency ($>$ 100kHz) asymptote of the measured impedance signature reflects the resistance of the electrolyte–implying that both interfaces are indeed lipid bilayers since at high frequency the capacitance of each membrane shorts, leaving the electrolyte as the dominant term in measured circuit. The current measurements shown in Figure 3.9a indicate that only when alamethicin proteins insert into all interfaces in the same direction (e.g. all interfaces have proteins oriented the same way) does the conductance of the membrane change significantly as a function of the applied potential. The insertion of proteins in both directions into both interfaces occurs when alamethicin is present in all three droplets and thus the conductance of the three-droplet network is sensitive to both positive and negative applied potentials. The insertion directions of the proteins are indicated with red arrows in the droplet diagram shown in Figure 3.9b.

Electrically, the additional lipid membrane in a three droplet network acts as a voltage divider in the circuit shown in Figure 3.10a. When no alamethicin is added to the droplets, the voltage drop across each interface is approximately half of the applied voltage assuming the resistance of each interface is equal. In the case where alamethicin inserts into one or both membranes in only a single direction (i.e. Cases 2 and 3), the applied voltage is again split across the two membranes. However, at positive potentials greater than 60mV for Case 2 (and at both positive and negative potentials greater than 60mV for Case 3), the presence of a second, highly resistive membrane limits the current flowing in the circuit. Even though proteins are present in both interfaces in Case 3, the opposite insertion direction causes the two membranes to be triggered by voltages of opposite polarity. Applying a larger potential across both interfaces to trigger the proteins in one bilayer may begin to increase the conductance of a given membrane, but this reduction in resistance causes the other bilayer to carry more of the voltage load, thus preventing a sufficient voltage drop across the interface with alamethicin from occurring. The measurements in Figure 3.9 show brief increases in the measured current at large potentials applied to networks with alamethicin inserted into interfaces in a single direction, but never show the large change in conductance seen for single DIB networks containing alamethicin in Figure 3.8.

Only when alamethicin inserts into both interfaces in the same direction does a significant change in the conductance of the network occur. The symmetric change in conductance about 0V measured for Case 4, when both bilayers contain proteins, illustrates this point. The voltage-induced change in conductance measured for this configuration arises at larger potentials than were required to trigger alamethicin proteins in a single DIB. Figure 3.10b directly compares the currents measured for a single DIB with alamethicin in both droplets and a two-DIB network with alamethicin in all three droplets. Consistent with expectations, the change in conductance for a two-DIB network occurs at roughly twice the applied

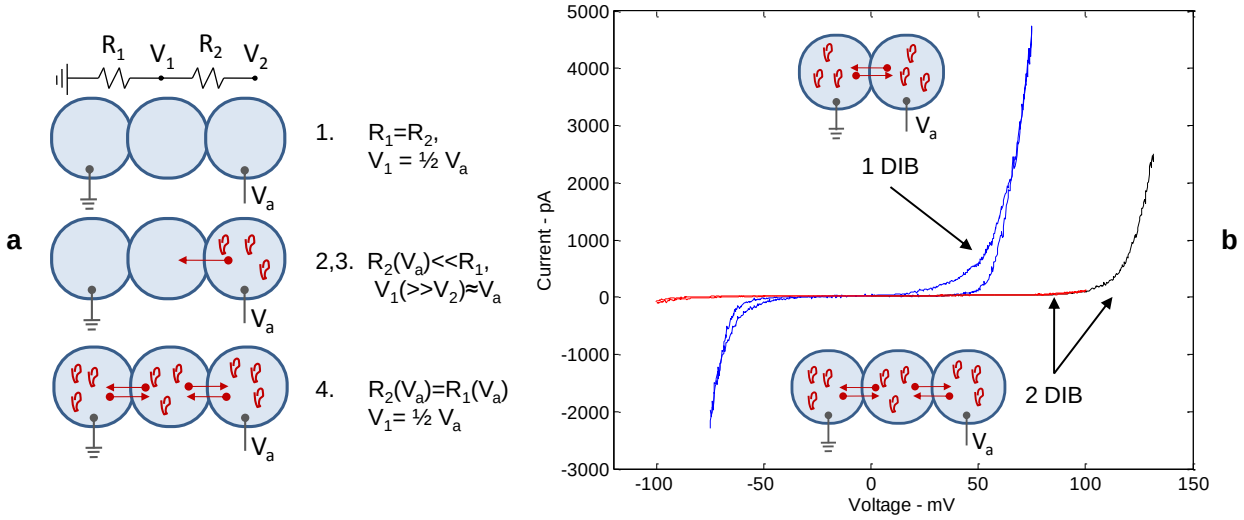

Figure 3.10: Equivalent circuits for the four cases presented in Figure 3.9 (a) and comparison of the voltage-dependent current measured for a single DIB and a two-DIB network with alamethicin present in all droplets (b). Note, only the resistance of the bilayer is considered since the CV measurements were taken at a low scan rate (2.5mV/s) and since the resistance of the electrolyte is small in comparison to the electrical resistance values of the lipid interfaces.

potential–indicating the two lipid membranes share the total applied potential. The circuit analysis also suggests that the *ON* conductance state of a two-DIB network would be lower than that for a single DIB due to the additional resistance of the second lipid bilayer in the line of current flow. The *ON* resistances of the single and two-DIB networks (approximated from the data to be 3.7MΩ at +70mV and 5.5MΩ at +130mV, respectively) appear to confirm this behavior, though this comparison does not account for unequal bilayer resistance in the *OFF* state or different numbers of proteins residing in each interface.

3.4 Feedback Control of Droplet Interface Bilayers

Feedback control offers an additional, previously-unexplored route for tailoring ion transport across lipid bilayers. The previous section demonstrated that the inherent properties of

biomolecules, including proteins, can be used to impart selective functionality to the membrane. The following section examines how concepts of external feedback control of electrical signals can provide an additional tool for obtaining controllable transport in droplet networks. Potential applications of this type of approach include use as nano-reactors or bio-communication devices, where the transport of species and the amplification of signals, respectively, provides device-level functionality. Two specific types of feedback control[2], integral current control and proportional-integral (PI) voltage control, are demonstrated on a two-droplet pair adjoined by a single bilayer interface.

3.4.1 Feedback Current Control through a Lipid Bilayer

Feedback current control of a droplet interface bilayer without proteins demonstrates that a desired current through a lipid bilayer can be prescribed. First, the electrical impedance of the lipid bilayer is measured in order to obtain estimates of the bilayer resistance and capacitance. These values provide a way to simulate the closed-loop system admittance and iteratively select an appropriate integral gain value necessary for achieving accurate current tracking.

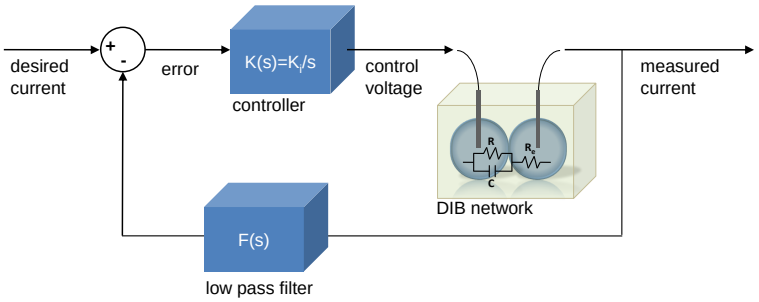

Figure 3.11: Block diagram of feedback current control applied to a droplet interface bilayer.

[2]A detailed discussion of the experimental setup for performing feedback control of droplet interface bilayers is provided in Appendix B. The control analysis used in the selection and design of each compensator is included for additionally clarity.

Controlling the flow of ions through a droplet interface bilayer is performed electrically via the Ag/AgCl electrodes inserted into the droplets for positioning and electrical measurements. An integral compensator (shown in Figure 3.11) is used in this scheme to compute a corrective control voltage applied to drive the error between the measured current and the desired value toward zero. A 100pA sinusoidal waveform is selected for the amplitude of the desired current signal in this demonstration. The ability to track this waveform is measured experimentally at four driving frequencies, f_d, using a constant integral control gain.

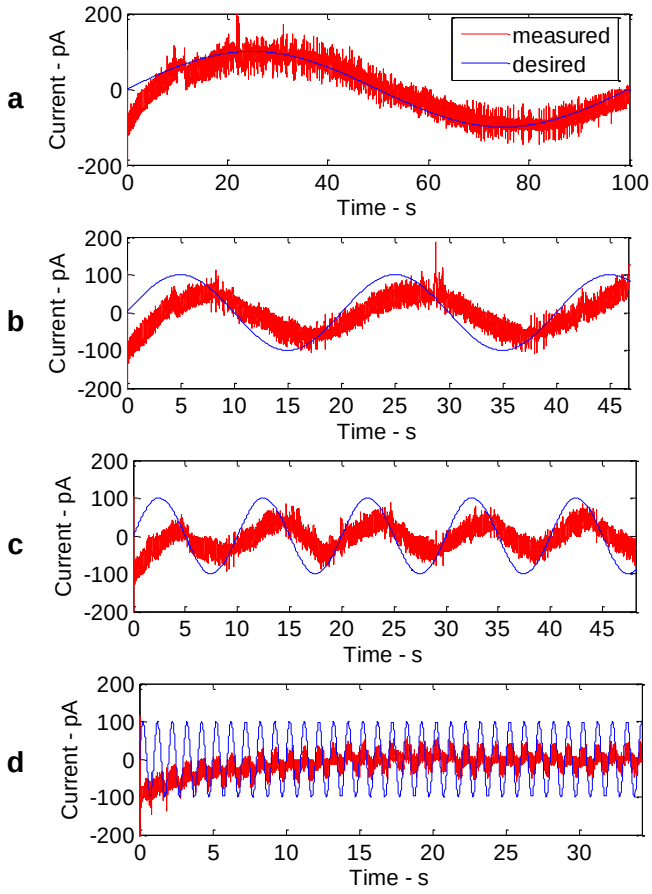

Figure 3.12: Measured current tracking versus driving frequency, f_d, of a droplet interface bilayer without proteins (a-d).

The measured current traces plotted in Figure 3.12 confirm the simulated closed-loop dynamics that as the driving frequency increases above 10mHz, the actual current flowing through

the bilayer does not track the desired current waveform accurately. The measured current for a driving frequency of 50mHz has a slightly smaller amplitude and lags the desired current by $2-3$ seconds in time. At 100mHz, the amplitude of the measured signal is roughly half of the 100pA desired amplitude and a similar phase lag exists. Lastly, the measurement at 1Hz shows significant attenuation of the measured current, even though it is able to keep pace in time with the desired current.

While the performance of the current tracking routine is limited to low frequency tracking (below 10mHz), this approach does demonstrate the ability to prescribe desired current flow across a bilayer. Increasing the control gain is one way to achieve better tracking at higher driving frequencies, though at the expense of a larger control voltage (this trade-off must be considered since bilayers rupture a larger potentials). Eliminating the external low-pass filter from the feedback loop would also increase the operational bandwidth but requires being able to measure current within a lower current range in Autolab in order to increase the magnitude of the voltage proportional to the measured current. Nonetheless, this analysis provides evidence that biological systems and their dynamics can be tailored in ways other than by component selection. Feedback current control provides an alternative method to regulate ion flux across a lipid membrane and in a system consisting of multiple connected droplets, closed-loop current control may provide a way to carry out precise chemical reactions within specific droplets at desired rates.

3.4.2 Feedback Voltage Control for Tunable Resonance

The second closed-loop control strategy investigates the use of proportional-integral voltage control to create a tunable voltage resonance across a bilayer. This form of feedback control transforms the first-order impedance response of the lipid bilayer into a second-order

closed-loop response, characterized by a resonance peak whose properties depend on both the electrical properties of the bilayer and the applied control gains. The proportional and integral gains used in feedback voltage control are computed from measured values of electrical resistance, R, and capacitance, C, of a lipid bilayer obtained from impedance spectroscopy and the prescribed values of natural frequency, f_n (or ω_n in rad/s), and damping ratio, ζ, for the closed-loop system. Expressions for these gains derived from the open-loop electrical impedance (see Appendix B for complete analysis) of the bilayer are given by

$$K_P = \frac{\omega_n RC(2B\zeta - A\omega_n) - B}{A^2\omega_n^2 - 2\zeta\omega_n AB + B^2} \tag{3.1}$$

and

$$K_I = \frac{\omega_n^2(RCB - A)}{A^2\omega_n^2 - 2\zeta\omega_n AB + B^2} \tag{3.2}$$

where, $A = R_e \cdot R \cdot C$, $B = R + R_e$, and recall that R_e is the resistance of the electrolyte solution within the droplets. The closed-loop transfer function of the voltage across the membrane relative to the desired voltage is measured during feedback voltage control on several droplet interface bilayers with and without proteins. A 50mV (RMS) white noise waveform is used as the input for measuring closed-loop transfer functions.

Voltage control of lipid-only DIBs

Closed-loop voltage control transforms the open-loop transfer function of the electrical impedance of a pure lipid DIB (Figure 3.2a) to a second-order, closed-loop system (Figure 3.13a). In each trial, the electrical resistance and capacitance of the membrane are approximated from impedance measurements. The proportional and integral control gains, K_P and K_I, are then computed in order to produce a closed-loop system with a desired natural frequency and damping ratio.

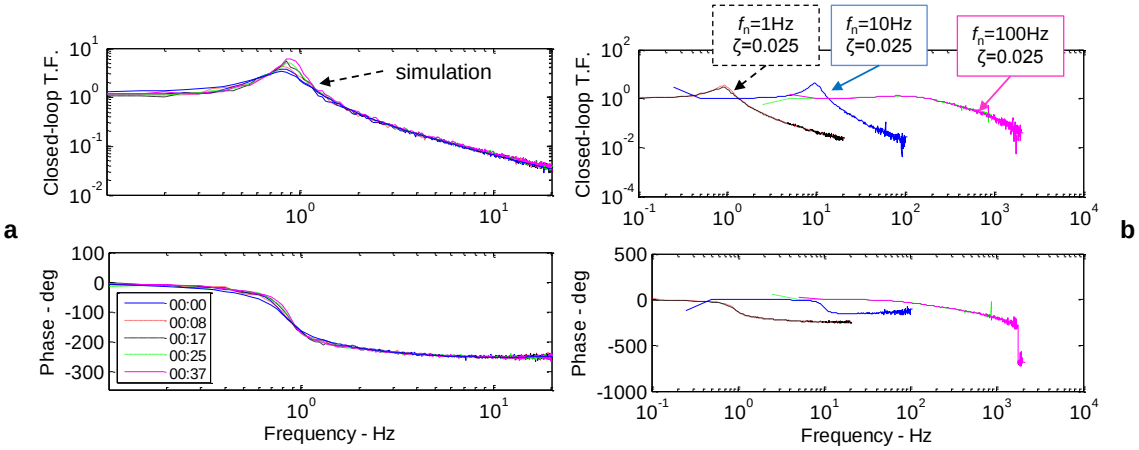

Figure 3.13: Measured closed-loop frequency response functions of a droplet interface bilayer without proteins for a natural frequency at 1Hz and a damping ratio of 0.1(a). Measured closed-loop FRFs on a single DIB demonstrate the ability to place the resonance and that the bandwidth of operation can be increased from less than 1Hz to more than 100Hz.

Figure 3.13a shows successive measurements of the frequency response function (FRF) for a bilayer with the closed-loop natural frequency and damping ratio set at 1Hz and 0.1, respectively. The measured FRFs of the bilayer in closed-loop control match the simulated response fairly well in the location of the resonance peak, but the measured result has more damping than expected from the simulation as indicated by the reduced magnitude of the FRF near resonance. These differences are attributed to inaccurate estimates of the membrane resistance and capacitance from EIS data but also due to non-linear decreases in the resistance and increases in the capacitance [154] of the bilayer with respect to a larger potential developed across the membrane at resonance. The magnitude of the measured resonance peak increases over time which is attributed to the increased resistance of the bilayer due to continual lipid packing into the membrane (as seen in the EIS and CV data of *lipid-out* DIBs in Figures 3.2 and 3.3).

Additional trials show that the natural frequency of the closed-loop system can be set at frequencies higher than 1Hz. Figure 3.13b presents the frequency response functions of a

single droplet interface bilayer in which the proportional and integral gains are adjusted to set the closed-loop natural frequency at 1, 10, and 100Hz. The measurements of the closed-loop systems confirm that through feedback control the dynamics of a changing voltage across the bilayer can be operated at much higher frequencies than for an uncontrolled bilayer. The electrical impedance spectra plotted in Figure 3.2a and Figure 3.5a show that the bandwidth of the electrical impedance ranges from $0.1 - 10$Hz, but at higher frequencies the magnitude of the impedance drops off and the phase delay increases. This open-loop response indicates that a voltage developed across a lipid bilayer as the result of current flowing through it, attenuates at frequencies higher than 1Hz. Through feedback control however, a desired voltage across the bilayer can even be prescribed at frequencies within the lower end of the audible range (20Hz-20kHz). The measurements also show that at natural frequencies of 100Hz and higher, the bilayer exhibits significantly higher damping evident by the diminished peak height. This behavior may indicate a possible frequency-dependence of the electrical resistance and capacitance of the bilayer. Physically, the operation bandwidth is limited by amount of increasing level of current required to develop a potential across the bilayer at higher frequencies which can cause bilayer failure. Several feedback control trials in which the natural frequency was set to 200Hz or higher resulted in immediate bilayer rupture.

Voltage control of alamethicin-doped bilayers

Coupling the current-voltage relationship of a bilayer containing alamethicin proteins with feedback voltage control provides a way of reversibly controlling the magnitude of the resonance peak. In a biocommunication-inspired application, the use of a bias potential to regulate the resistance of the membrane by triggering the proteins changes the amplification of the voltage across the membrane. The same feedback PI control scheme is applied to droplet interface bilayers in which one of the two droplets contained alamethicin.

a

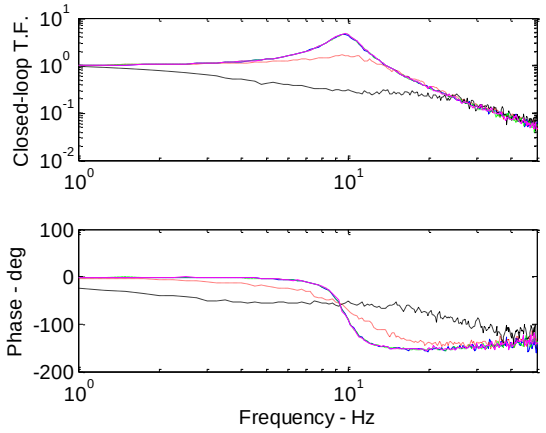

b

Run	Bias Voltage, V (mV)	Natural Frequency, f_n (Hz)	Damping Ratio, ζ
1	0	9.79	0.115
2	-25	10.91	0.336
3	-50	2.81	2.362
4	0	9.80	0.114
5	0	9.79	0.111

Figure 3.14: Measured closed-loop FRFs of a bilayer with alamethicin proteins biased at different levels (a). Estimates of the natural frequency and damping ratio by fitting the measured frequency responses (using INVFREQS in Matlab) confirm that toggling the bias voltage alters the membrane resistance, which primarily affects the damping ratio of the system.

Figure 3.14a shows the measured frequency response functions of a single bilayer containing alamethicin (EIS and CV data for this same DIB are shown in Figure 3.7). A natural frequency of 1Hz and a damping ratio of 0.025 are selected and the control gains are computed using resistance and capacitance values (775MΩ and 750pF, respectively) measured at 0mV bias. A bias voltage is added to the white noise input during the measurement at different potentials in order to vary the membrane resistance between 800MΩ and 8MΩ as discussed in Section 3.3.2. The change in the membrane resistance inversely affects the damping ratio of the closed-loop system and results in a significant change in the magnitude of the resonance peak in the frequency response function. With 0mV bias and the alamethicin channels closed, the high resistance of the membrane results in lower damping and a higher resonance peak. Partial protein activation by the resonance voltage may explain the additional damping (0.11 vs. 0.025) in the measurements taken at 0mV bias. Conversely, the height of the resonance peak is reduced partially with a −25mV bias (some alamethicin channels open) and then nearly eliminated at −50mV (all alamethicin channels open). Estimates of natural

frequency and damping ratio in Figure 3.14b confirm that the damping ratio increases at the negative bias potentials when the alamethicin ion channels are opened. These measurements demonstrate that coupling external feedback control with the voltage-gating characteristics of alamethicin provides a way to reversibly control the amplification of the voltage across the bilayer.

3.5 Chapter Summary and Conclusions

The droplet interface bilayer provides a relatively-simple, yet uniquely-generic environment for assembling networks of lipid bilayers through controlled self-assembly and phase-separated liquid-liquid interfaces. The ability to customize the composition and arrangement of the droplets highlights the potential for building bio-networks that display collective utility and which form the basis for a new class of active material.

As the first part of effort to develop robust, encapsulated biomolecular material systems, this chapter focused on the building block of such systems: a single liquid-supported, droplet interface bilayer. The electrical properties, including resistance and capacitance, and failure potentials of DPhPC droplet interface bilayers were characterized and methods for tailoring the current-voltage relationships of these bilayers were also investigated. The incorporation of transmembrane proteins, such as alpha-hemolysin or alamethicin, into DIBs showcased the convenience of self-insertion and produced bilayers with drastically-different current-voltage relationships. In a completely different approach, external feedback control strategies were used to demonstrate that the transport of species and the amplification of signals in biomolecular assemblies provides an alternative to changing the molecular composition of the network.

This initial set of studies establishes a basic understanding of liquid-supported bilayers and

expands the toolkit for creating customizable biomolecular networks through control of the properties of specific interfaces. Droplet interface bilayers characterized in this chapter were all formed in a relatively larger amount of oil and as a result, these systems often displayed the limits of unconstrained liquid-in-liquid platforms. Many times, the observed stability of droplet interface bilayers was as much a function of the quality of the membrane as it was on developing and using gentle methods for inserting electrodes and arranging droplets and eliminating mechanical perturbations to the network. The limitations of these unencapsulated droplet interface bilayers are discussed in more detail in Chapter 4 and techniques for building more robust networks through encapsulation within a durable material matrix are introduced.

Chapter 4

Physical Encapsulation of Droplet Interface Bilayers within Durable Materials

In its original embodiment, the DIB method provided an innovative approach for creating durable arrays of lipid bilayers in-house to study genetically-modified ion channels (namely alpha-hemolysin, αHL). And while this technique provides a suitable platform for conducting controlled laboratory studies, DIB platforms do not intuitively translate into robust material technologies.

Hagan Bayley, in a recent review article on the same topic, recognized that improvements are needed for creating more-sophisticated and more-durable droplet networks [101]. Making smaller droplets (potentially using micro-fluidic platforms), devising better ways to arrange droplets, and creating a material system in which to encase droplet networks such that the entire network could then be used in an aqueous environment, perhaps within the body for drug-delivery, were noted as specific areas in need of refinement.

The reasons to pursue these types of improvements are founded on the premise that liquid-supported biomolecular networks offer a unique set properties that have yet to be fully utilized for creating novel functional materials. Specific goals that must first be met in order to realize this potential include increasing the durability and portability of the networks through refined methods of packaging. Whereas droplets in the original embodiment of DIB networks have little interaction with the solid supporting substrate, we propose that by developing more-complex substrates to properly support the liquid contents, enclosed biomolecular material systems can demonstrate increased durability and portability and preserve the basic properties and functions of the lipid bilayers [1]. The focus of this chapter is to initiate the design and development of solid substrates that enable the use of packaged biomolecular networks for use in engineering applications.

4.1 Encapsulation Approach and Definitions

We denote the original form of the droplet interface bilayer as the *liquid-in-liquid* form due to the fact that lipid-encased aqueous droplets are surrounded by a large volume of oil contained in a shallow well of a supporting substrate. As demonstrated by Holden, et al, the liquid-in-liquid form enables easy reconfiguration of multi-droplet networks by rearrangement of individual droplets [98, 101]. However, modifications are required for the use of assembled biomolecular networks in applications that necessitate more durable and portable assemblies.

In order to create durable biomolecular materials, we need to first define the term *durability*. The word durability, as defined by Merriam-Webster, means to be "able to exist for a long time without significant deterioration." In the context of this research, we use the term

[1] Note: This chapter presents findings reported in a recent journal paper published in *Lab on a Chip* entitled, "Physical encapsulation of droplet interface bilayers for durable, portable biomolecular networks" [155].

durability to specifically characterize the capacity of a network to retain stable lipid bilayer interfaces under influences of time and other physical perturbations. This definition, then, includes the concept of longevity but also encompasses the notion that useful biomolecular networks can be constructed to resist failure when handled, shaken, inverted, or dropped. In another instance, durability may even be used to describe the resistance to bilayer failure caused by changes in operating conditions, such as temperature, pressure, or even chemical environment. Nonetheless, durable interface bilayers are necessary for preserving the desired separation and composition of each volume for hosting selective transmembrane biomolecules that regulate the transport of signals and species within the network. If a bilayer fails, either by rupturing or completely unzipping, then a vital connection in the network is lost, discrete volumes become contaminated, and proteins are no longer supported in a manner that allows them to function.

The concept of packaging, or *encapsulating*, droplet interface bilayers within an external material matrix is purely geared toward making functional biomolecular assemblies more usable than the original form of the droplet interface bilayer. Successful methods of encapsulation must contain the contents and protect the enclosed interface bilayers such that longevity is not a function of how gentle the network can be handled, but instead of how long the assembled molecules can survive. We envision that in more-complex embodiments, encapsulation may even provide methods for even constructing the network *in situ* such that the reconfigurability of original DIBs will also apply to encapsulated interface bilayer networks.

4.1.1 Methods for Encapsulating Interface Bilayers

The approach for creating encapsulated interface bilayers presented in this dissertation is a direct product of recognizing the strengths and limitations of the original droplet interface

bilayer. Particularly, we noticed that the inherent stability of lipid bilayers formed at the interface of connected water droplets results from the fact that lipid monolayers in these systems are not formed on a rigid support, but instead at a fluid oil/water interface. We believe that this type of assembly produces a forgiving boundary condition on the molecular length scale, one that promotes free diffusion of lipids from the separated monolayers into the thinned bilayer as needed for maintaining a minimal surface tension in the membrane. And to its credit, droplet interface bilayers created by Holden exhibited considerably greater longevity (on the order of weeks) [98] than bilayers assembled directly on a supporting substrate which typically last only a few hours (references).

Interestingly, however, the glaring limitation of this system is also found at the same liquid-interface, though at larger length scales. Lipid-encased aqueous droplets are not well-supported (i.e. constrained to a fixed location) by an oil phase alone and we have observed that the surrounding oil phase is ill-equipped to prevent large motions of the droplets when the system is moved and that such actions readily result in bilayer failure and droplet coalescence. Simple actions such as inverting the droplet network are also not possible since droplets are arranged in an open well and loosely-suspended on externally-fixed electrodes. It is this limitation that calls for better methods to support the network so as to preserve both structure and function.

The formation of encapsulated networks can be carried out in one of two ways: First, the network is assembled and then encapsulated by a surrounding material phase or second, the encapsulation material is created prior to the arrangement of the network. An example of the first approach is *chemical encapsulation*, in which a solid encapsulating material is produced directly by solidifying (i.e. curing, polymerizing) the oil phase that surrounds the aqueous droplets. In this strategy, the droplets are arranged first within the liquid precursor of the curable phase to form the desired DIB network and then polymerization is triggered

to transition the exterior media into a durable solid. We explored this type of encapsulation approach in a study presented in Appendix B and the results of the trials indicate that while it is possible to chemically-encapsulate droplet interface bilayers within curable materials, the use of a curable oil phase results in the loss of a fluid oil/water interface upon hardening. As a result, only a single droplet interface bilayer survived the entire curing period.

We term the second method for encapsulating DIBs *physical encapsulation*, since this approach relies on the physical constructs of a preformed solid substrate networks to confine and support both liquid phases of the network. Physical encapsulation, then, must simultaneously support the network on length-scales similar to the sizes of the droplets ($10-1000\mu$m), while not interfering with self-assembly processes that occur on much smaller scales ($1-10$nm). Accordingly, the primary difference of encapsulated networks compared to the original DIB technique is in the reduced amount of oil that separates the droplets from the substrate (see Figure 4.2). With less oil between the aqueous phases and the substrate, physically-encapsulated droplets are held more-tightly within specific regions of a solid substrate for the specific purpose of minimizing relative motions of the droplets that often lead to bilayer failure.

4.1.2 Quantifying Levels of Encapsulation

So what actually constitutes encapsulation? From the discussion so far, one could argue that the original DIB method is an encapsulated system, just one with a larger amount of oil and less restrictive solid substrate. As a way to quantify the differences in substrate design, we define a term called the *packing factor*, which relates the volume of the aqueous phase to the total volume of space within the substrate that the aqueous phase can occupy. Therefore, low packing factor substrates are predominantly oil, allowing the relatively small aqueous

droplets to move freely within the substrate. In contrast, high packing factor substrates have less oil that separates the substrate from the aqueous phase which helps to restrict movement. The trade-off in this spectrum is having a packing factor that is large enough to adequately support the droplets while still ensuring a sufficient amount of oil for supporting lipid monolayer formation. To better illustrate this concept, Figure 4.1 shows the spectrum of packing factors for a single spherical droplet encapsulated by oil within a spherical region.

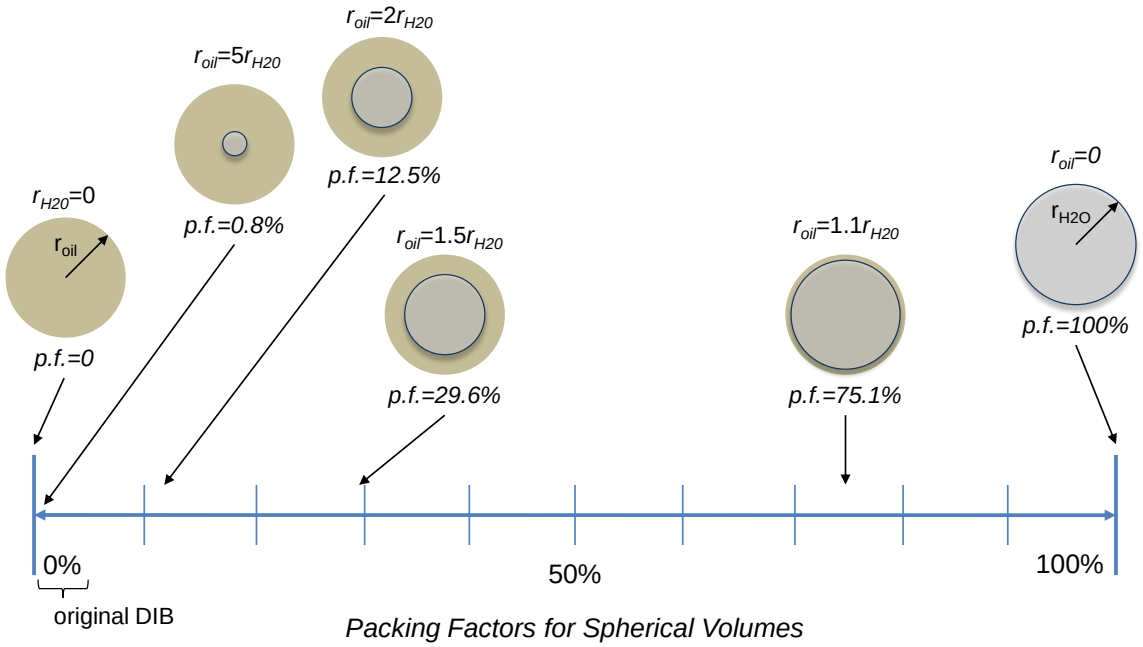

Figure 4.1: Packing factor spectrum for single spherical aqueous volumes contained within a spherical outer volume of oil.

When the surrounding oil phase has a radius that is five times larger than the internal droplet, the packing factor is a mere 0.8%, but when the oil phase has a radius that is only 1/10th bigger than the droplet, the packing factor is greater than 75%. The original droplet interface bilayers that Holden created (and that we studied in Chapter 3, shown in Figure 3.1) had low packing factors on the order or $1-5\%$ and accordingly, we observed that droplets easily moved laterally within the well in the substrate. Since such a low packing factor translates into minimal support, we will refer to the liquid-in-liquid form of the DIBs

as *unencapsulated* DIBs.

Since the packing factor is determined by a volume ratio that is independent of the geometry of the substrate, it is difficult to mark a specific transition value of packing factor to differentiate unencapsulated networks, where droplets are poorly restrained, from encapsulated networks.

As a starting point for understanding the contributions of increased packing factor, two significantly different packing factors are studied in this chapter to ascertain the key aspects of unencapsulated and encapsulated substrates. A *low packing factor*, on the order of 1%, is shown for the substrate illustrated in Figure 4.2a. This substrate has properties that are similar to those studied by Holden, et al, in their original work and which require the use of suspended electrodes for probing the network [98, 156]. Droplets are placed in small divots in the solid substrate and surrounded by a large volume of organic solvent.

A two-droplet high-packing factor substrate shown in Figure 4.2b consists of two wells drilled into a solid PMMA substrate. The bottom of each compartment is rounded to mimic the divots that are placed in the low-packing factor substrate. The packing factor for a 350nl droplet (875μm in diameter) residing in each droplet compartment in this substrate is approximately 32%, when only the total volume of the droplet compartments is considered. It is estimated that a $50-75\mu$m layer of hexadecane resides between each droplet and the surrounding acrylic substrate as measured along the droplet perimeter. For this work a packing factor of $> 30\%$ is denoted "high", and we have fabricated substrates that have packing factors on the order of $50-60\%$ depending on the depth of the wells and the size of the droplets. The remainder of this chapter focuses on demonstrating that physically-encapsulated DIB networks can be formed in solid substrates that feature integrated electrodes and that through encapsulation approach retains the appropriate phase segregration and provides suitable interactions between biomolecules and the surrounding substrate. The properties of two- and three-

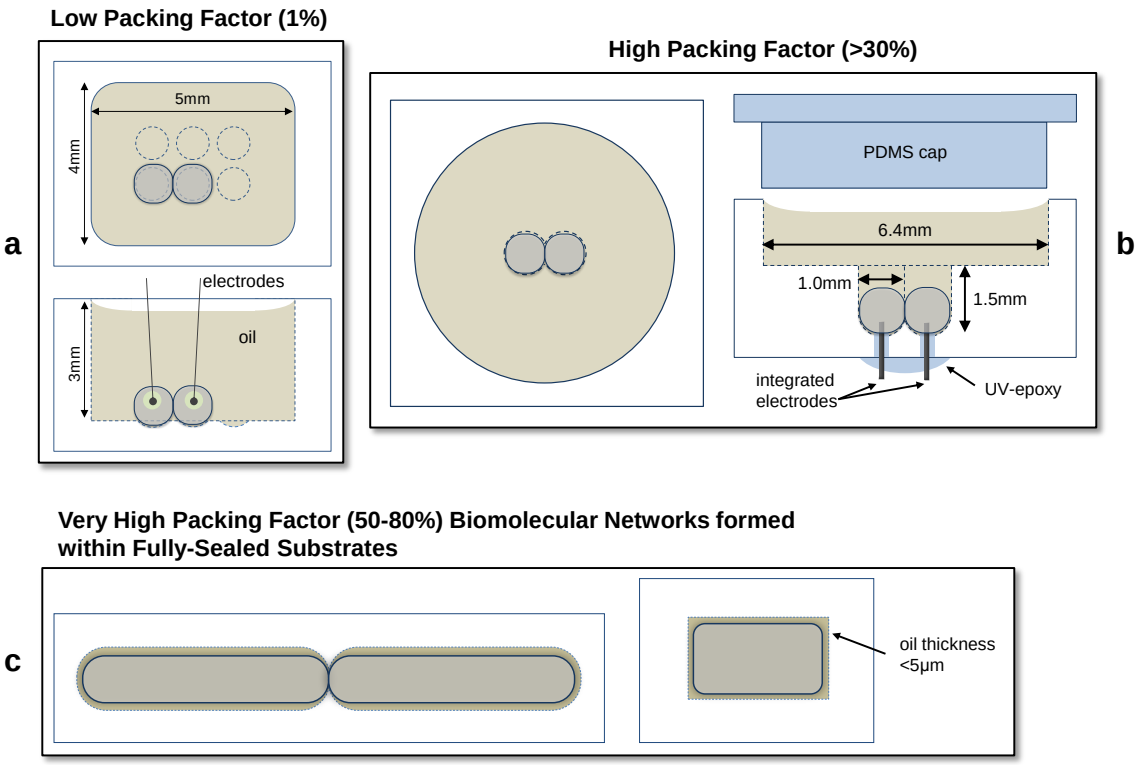

Figure 4.2: Unencapsulated DIBs are formed in a low packing factor substrate (a), while physically-encapsulated droplet interface bilayers are formed in a new high packing factor substrate that confines aqueous droplets submerged in oil to specific positions and features integrated electrodes for electrical interrogation (b).

droplet networks are quantified in a series of electrical and mechanical tests, and the results are compared to baseline results on an unencapsulated two-droplet network to demonstrate that encapsulated networks retain the critical properties of unencapsulated droplet interface bilayers.

More importantly, the initial substrate design studied in this chapter sets the stage for producing substrates with even higher packing factors, as shown in Figure 4.2c, where volumes of aqueous solution are encased by a very thin layer of oil within a fully-sealed substrate. Such a design produces encapsulated networks with packing factors as high as $80 - 90\%$, depending on the thickness of the oil phase. Methods that address how to fabricate these

types of susbstrates, as well how to form lipid bilayers within a closed material element such that critical elements of biomolecular networks formed at liquid interfaces can be retained are presented in the following chapters. And while this work builds on the basics of liquid-supported self-assembly demonstrated first with the DIB, encapsulated interface bilayers stand apart in both how they are formed and packaged.

4.2 Methodology

4.2.1 Substrate Fabrication

Physically-encapsulated droplet interface bilayers are formed in a prototype high packing factor supporting substrate (Figure 4.2b) made from an acrylic sheet (PMMA, McMaster-Carr). The initial concept pairs the shape of the simple two-droplet well made by Funakoshi, et al [97] with the hemispherical divots machined by Holden, et al [98]. The resulting substrate houses a single droplet within each compartment (1.02mm in diameter and 1.5mm deep) where the relative positioning of the overlapping compartments allows for intimate contact between neighboring droplets that leads to bilayer formation. An upper reservoir in the fixture is designed for holding separated droplets during monolayer formation. Custom silver-silver chloride (Ag/AgCl) electrodes built into the initial substrate are fabricated from 125μm diameter silver wire (Goodfellow) that is chlorided in household bleach for one hour before being coated in 5% agarose gel (Sigma) in order to render the surface of the electrode hydrophilic [98]. The two electrodes are inserted through 300μm diameter holes drilled through the substrate and held in place with a low-viscosity, light cure adhesive (Loctite 3104, Ellsworth Adhesives). The packing factor for 350nl droplets within this substrate exceeds 30%, when only the total volume of the droplet compartments is considered.

4.2.2 Formation of Physically-Encapsulated Droplet Interface Bilayer

The materials and methods of preparation used to form unencapsulated, *lipid-in* droplet interface bilayers in hexadecane (Chapter 3, Section 3.1.1) are also used herein to evaluate the concept of physically-encapsulated DIBs. In addition, the incorporation and measurement of protein activity within encapsulated bilayers relies on the procedures for introducing alamethicin channels into droplet interface bilayers (Section 3.3.2).

The formation of physically-encapsulated droplet interface bilayers must account for the immediate contact between neighboring droplets that occurs when the droplets are placed into adjacent compartments. Therefore, a single droplet is first injected into the hexadecane and moved into one of the droplet compartments where it is pierced by a fixed, wire-type Ag/AgCl electrode that extends vertically into the droplet compartment roughly 0.5mm from the bottom surface of the well. Additional droplets are injected into the hexadecane and held in the upper reservoir to allow for monolayer formation to occur before network assembly. Droplets are moved into the remaining vacant droplet compartments in the lower region of the substrate after $15 - 20$ minutes for monolayer formation. Electrode insertion again occurs as each droplet descends into its respective compartment. Bilayer formation between neighboring droplets occurs spontaneously within $2 - 3$ minutes of initial contact. Electrical recordings are performed as described in Section 2.3 of Chapter 2.

4.2.3 Mechanical Characterization of Bilayer Durability

In order to understand how the use of a high-packing factor substrate may provided added durability, physically-encapsulated droplet interface bilayers are subjected to mechanical characterization in which the substrate is violently shaken and the status of the bilayer is

monitored. This form of evaluation is chosen since the use of encapsulated biomolecular networks in device concepts must also be able to resist moderate mechanical disturbances. A Brüel and Kjaer 4810 mini-shaker is used to vibrate the droplets horizontally in a direction perpendicular to the bilayer interface. The shaker attaches directly to a platform on which the DIB substrates are mounted and is excited by a sinusoidal voltage waveform that is the output of a Siglab 20-42 data acquisition system and which is amplified using a Proton AA-1150 stereo power amplifier. The acceleration and displacement of the substrate are measured using an accelerometer (Piezotronics U352C22 and accompanying PCB Piezotronics 482A16 PZT charge coupler) and laser vibrometer (Polytec PDV-100), respectively. Durability tests are performed on the microscope stage of a Zeiss AxioVert 40CFL inverted microscope. Images and video are obtained through the objective lens of the microscope during and between tests using a Canon G6 digital camera and digital camera adapter.

4.3 Results and Discussion

4.3.1 Measured Durability of Unencapsulated Droplet Interface Bilayers

Only electrical characterization techniques have been employed up to this point for studying droplet interface bilayer formation and function. Apart from anecdotal observations [98], the durability of this systems has yet to be specifically studied or quantified.

In this section, the durability of unencapsulated droplet interface bilayers formed between two adjacent aqueous droplets surrounded by hexadecane is quantitatively characterized using a mechanical excitation test. Each trial consists of droplets formed from a 350nl volume of aqueous lipid solution and positioned in the same two hemispherical divots in the low

packing factor substrate (Figure 4.3a). The durability of the interface bilayer is characterized by gradually increasing the displacement of the applied vibration at a fixed frequency of oscillation until failure occurs. Observed failure modes include complete separation of the droplets or rupturing of the interface causing immediate droplet coalescence. Both cases are deemed DIB failure as the DIB no longer exists after these events.

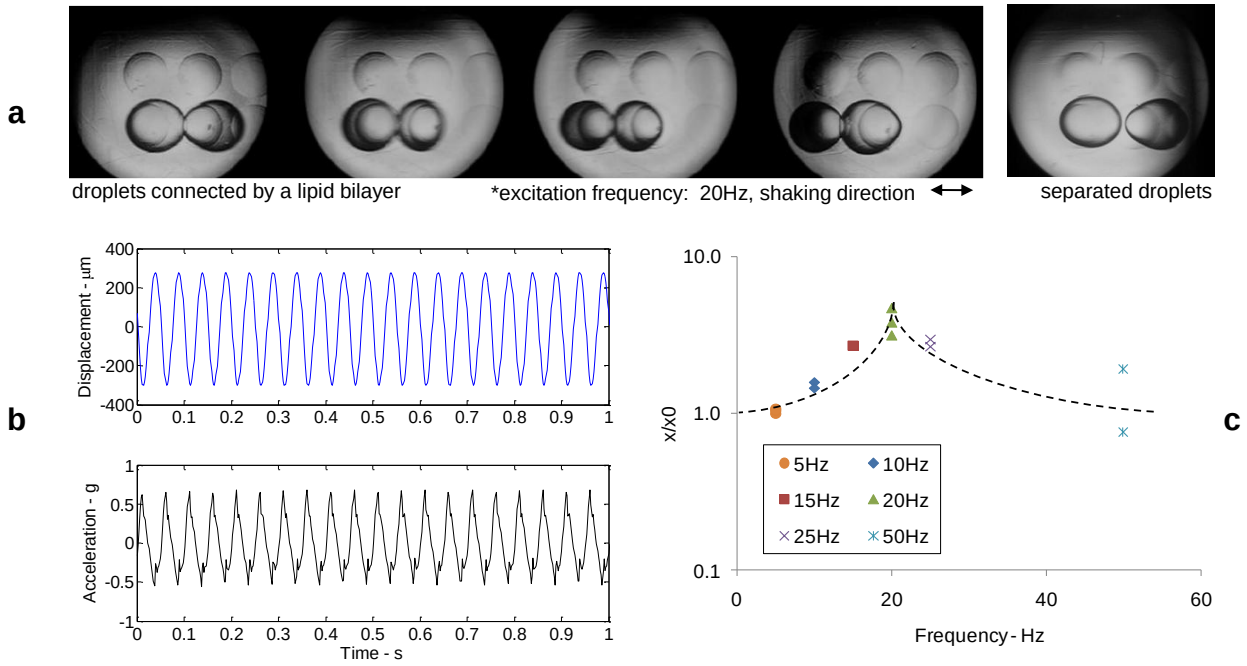

Figure 4.3: Unencapsulated DIBs undergo larger shaking displacements (and accelerations) (a) than are measured (b) for the supporting substrate when vibrated at 20Hz. Individual frames of a video recorded at 15 frames per second (fps) show how the droplets oscillate and deform throughout the cycle without causing either droplet separation or bilayer rupture (a). Image processing performed in Matlab allows the position of the droplets to be tracked throughout each video. The measured amplification of the droplet displacement per the measured displacement of the tray, x/x_0, is plotted against the driving frequency (Hz) in the transmissibilty plot (c).

Shaking tests on unencapsulated droplets are performed at frequencies of 5, 10, 15, 20, 25, and 50Hz. The images and data presented in Figure 4.3 show the response of the connected droplets undergoing vibration at 20Hz with 0.1V applied to the shaker. The accelerometer and laser vibrometer signals of the substrates movement indicate that the supporting

substrate experiences a peak-to-peak displacement of approximately 550μm and 0.6g of maximum acceleration. The frames from the video show that the connected droplets undergo a larger peak-to-peak displacement than the substrate (i.e. the side-to-side movement of the droplets is larger than the movement of features in the substrate, such as vacant hemispherical divots also shown in the images). An image processing routine that includes edge detection (for defining the boundaries of the droplets in each frame) and boundary tracing (returns the pixel coordinates of the droplets) is used to track the motion in pixels of the droplets during oscillation. The peak-to-peak displacements of the droplets in pixels is then converted to values of length (μm) using the known dimensions of the hemispherical divots on the bottom surface of the well. Analysis of videos taken at 20Hz indicate that the droplets experience peak-to-peak displacements (and maximum accelerations) of nearly $3-5$ times that measured for the substrate (Figure 4.3c. Amplification of the substrate movement is less though at frequencies less than and greater than 20Hz, with measurements at both 5 and 50Hz indicating a transmissibility ratio of approximately 1. The peak located near 20Hz represents the experimentally measured resonance peak of transmissibility for a two-droplet, single DIB network in the low-packing factor substrate. It is expected that by reducing the volume of hexadecane surrounding the droplets and confining the droplets to specific positions through physical encapsulation this resonance location will shift to a much higher frequency.

The data presented in Figure 4.4 highlights the ability of even unencapsulated droplet-pairs to undergo significant accelerations and displacements while retaining an interface lipid bilayer. Unencapsulated droplet interface bilayers finally fail when the relative motion of the droplets causes complete droplet separation. Single droplet-pairs remain connected up to measured accelerations and displacements of approximately $2-5$g and $5-7$mm, respectively, at low frequencies ($5-15$Hz). At higher excitation frequencies ($20-50$Hz),

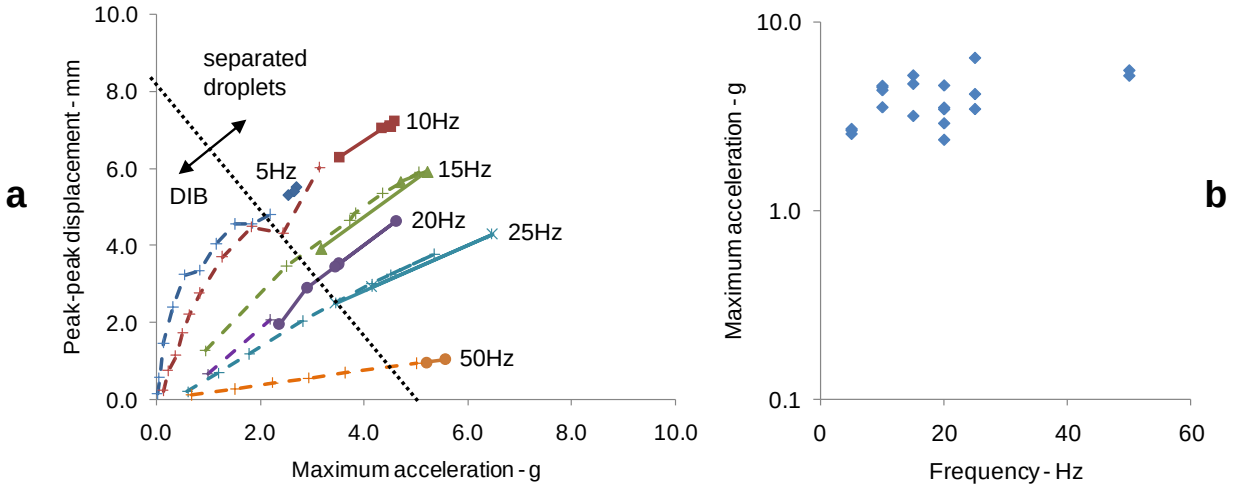

Figure 4.4: Peak-to-peak displacement (mm) versus maximum acceleration (g) data of unencapsulated DIBs formed in the low packing factor substrate are plotted for all driving frequencies (a). The filled markers and solid connecting lines represent data points at which failure due to droplet separation occurs, whereas the plus markers connected by dashed lines indicate measurements where the droplets are still connected via a bilayer. Maximum acceleration (g) experienced by the droplet pair at failure is plotted versus driving frequency (b).

however, less displacement ($1-4$mm) and higher experienced accelerations of $3-7$g causes droplet separation (measured accelerations that cause failure are also shown in Figure 4.4b). Interestingly, rupturing of the bilayer and droplet coalescence is not observed for DIBs shaken within the low packing factor substrate. Instead, droplet separation is repeatedly observed for multiple trials conducted at all six frequencies. At values of displacement near the failure point, the droplets deform from their original spherical geometry and the interface visible shrinks as the opposing lipid monolayers unzip. We believe that these deformations, in addition to the resulting forces on the interface due to out-of-phase motions of the two droplets, result in the creation of new oil/water interface that effectively raises the surface tension of each droplet and acts to unzip the bilayer at the interface.

4.3.2 Physical Encapsulation in a High Packing Factor Substrate

Physically-encapsulated droplet interface bilayers are constructed in a high packing factor substrate that contains individual droplet compartments and integrated electrodes (Figure 4.5a). The initial design of this substrate pairs the shape of the two-droplet well made by Funakoshi, et al [97] with the hemispherical divots machined by Holden, et al [98]. The resulting substrate houses a single droplet within each compartment where the overlapping compartments are positioned in order to promote bilayer formation between neighboring droplets. The presence of the oil phase prevents direct contact with the PMMA substrate evident by the face that the droplets do wet the substrate surfaces. An upper reservoir in the fixture is designed for holding separated droplets in oil during monolayer formation. Custom Ag/AgCl electrodes built into the initial substrate provide access for interrogating specific interfaces within the network and simplify network assembly, where droplets are connected to one another and electrodes are inserted by merely "dragging and dropping" them into their respective compartments.

EIS data shows that the low-frequency impedance of a droplet interface bilayer is typically higher than 1GΩ and is often on the order of 100GΩ (Figure 4.5a). Fifteen different bilayers are formed between droplet pairs using the same high packing factor substrate in this study. Initial resistance values of the membranes prior to mechanical testing yields a distribution in which five bilayers had a resistance greater than 100GΩ, five had nominal resistances between $1 - 100$GΩ, and five had resistances between $0.1 - 1$GΩ. The size of the interface varied from 80μm in diameter to more than 340μm in diameter (the average equivalent bilayer diameter was $267 \pm 67\mu$m ($n = 15$)), even though a constant droplet volume of 350nl is used in all trials. The initial specific membrane resistance (*resistance* $\times$ *area*) for physically-encapsulated DIBs formed in this study ranges from $0.1 - 100$M$\Omega\cdot$cm^2, which compares well to previously published values for normalized bilayer resistance [50, 57, 69].

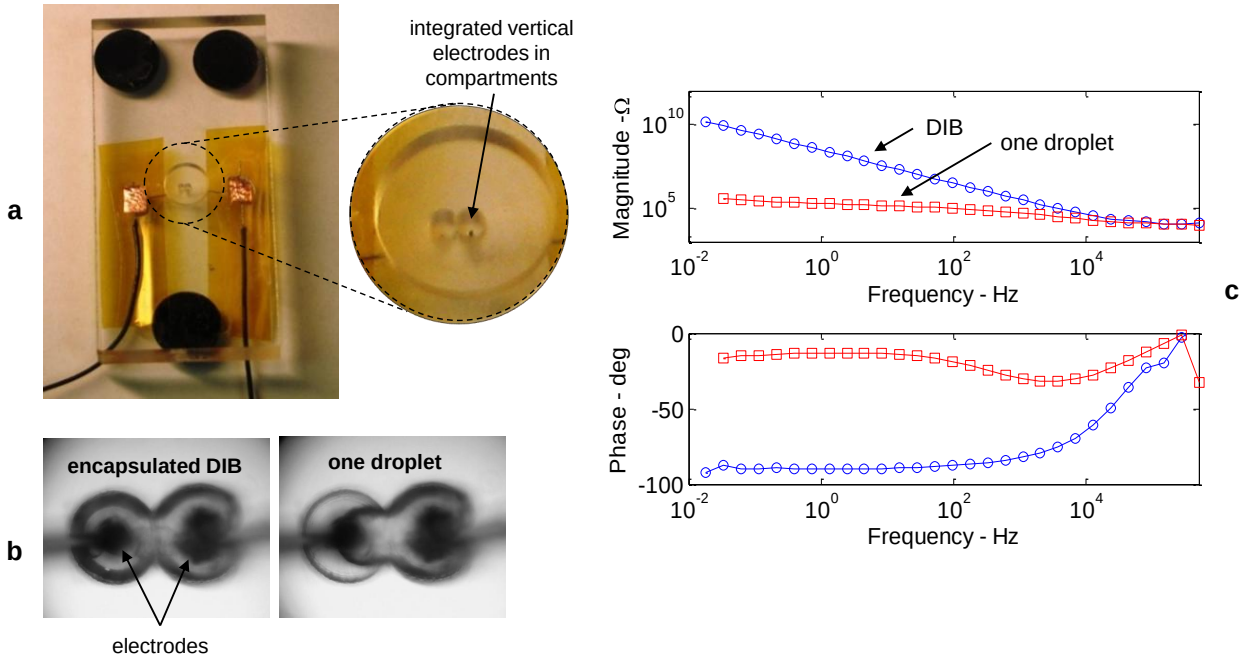

Figure 4.5: Images of the high packing factor substrate show individual droplet compartments with integrated electrodes that extend vertically from the bottom of each well (a). An image of a DIB formed between two droplets within this substrate (left) is compared to the image of a ruptured bilayer that results in droplet coalescence (b). EIS measurements confirm both bilayer formation and interface rupture (c).

The incorporation of voltage-sensitive alamethicin channels into physically-encapsulated droplet interface bilayers further confirms the formation of a lipid bilayer within the confined droplet compartments. Current-voltage traces presented in Figure 4.6b show a marked change in the ability for ions to pass through the bilayer containing alamethicin channels versus the highly-resistive response of a pure lipid membrane (see Figure 3.4). Specifically, an alamethicin-doped bilayer is highly-resistive in the "closed" state at applied potentials more positive than approximately −80mV, but "turns on" at potentials more negative than −80mV when aggregated alamethicin proteins form conductive pores through the bilayer that result in a large increase in the magnitude of current flowing through the membrane. Linear regressions applied to each of these regions shows that the bilayer containing alamethicin has a "off" resistance of approximately 17GΩ that reduces by four orders of magnitude to a

value of 1.9MΩ in the "on" state. The rectification ratio for this membrane is approximately 10000, much greater than a rectification of 60 measured for $10 - 15$ genetically-modified alpha hemolysin (αHL) channels in DIBs [157].

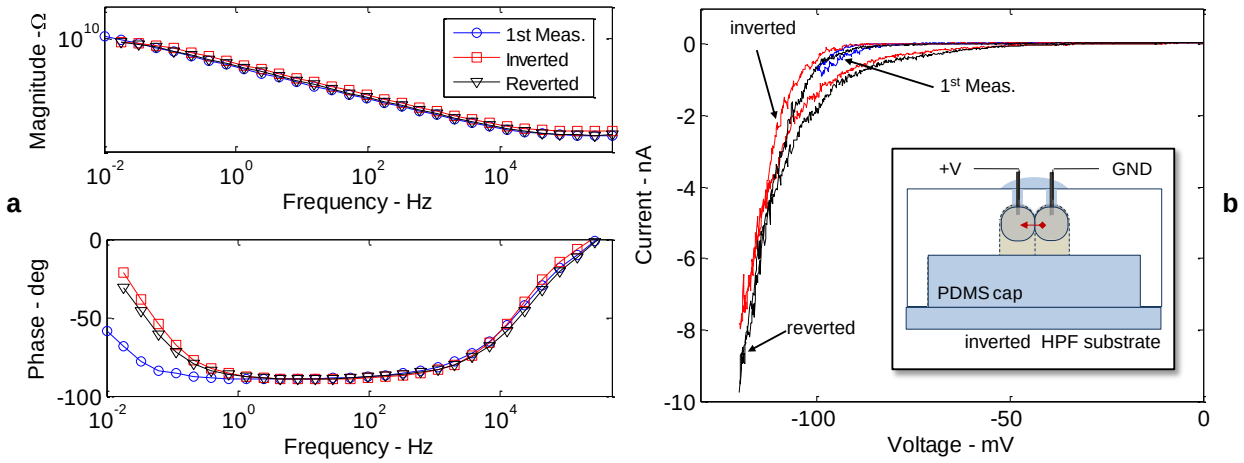

Figure 4.6: A PDMS plug is used to seal the droplets in their compartments after removing excess oil from the upper reservoir, permitting the entire substrate to be completely inverted. EIS (a) and CV (b) measurements confirm that the bilayer survives these actions, preserving alamethicin activity in the membrane.

A distinct improvement over unencapsulated DIBs is that physically-encapsulated droplet interface bilayers can survive handling and even inversion of the entire substrate after bilayer formation. A press-fit, molded PDMS plug is used to seal the droplet networks in the lower droplet compartments of the substrate (shown in the inset in Figure 4.6b) during inversion. Electrical measurements obtained via the integrated electrodes show that the interfacial lipid bilayer survives. The initial resistance of 38.4GΩ, reduces to 5.5GΩ after inversion and the size of the membrane also changes, reducing from an initial equivalent diameter of 430μm to 326μm. Both the resistance and diameter then increase to 7.5GΩ and 390μm, respectively, upon reversion to the initial orientation. These measurements suggest that the droplets sag vertically when the substrate is inverted due to the higher density of the aqueous phase compared to the oil. As a result, the bilayer unzips slightly but is retained since the

droplets remain anchored to the electrodes via the hydrophilic agarose coating. The voltage-dependent responses of the proteins measured in both the upright and inverted orientations add additional proof that physical encapsulation protects the structure and functions of the system.

4.3.3 Quantifying the Durability of Encapsulated DIBs

Preliminary qualitative tests demonstrate that physical encapsulation of DIBs provides increased portability by limiting relative droplet movement. The geometry of the solid substrate confines the droplets to specific positions within the network that are maintained even when the solid substrate is manually handled, tilted, and inverted. The reduced volume of organic solvent surrounding the droplet, while only $10 - 100\mu$m thick, provides the necessary oil/water interface required for monolayer adsorption (which occurs on a length scale of $1 - 10$nm) and acts as physical buffer between the liquid droplets and the solid exterior material.

The durability of physically-encapsulated bilayers is quantified using a mechanical shaker to vibrate the droplets horizontally in a direction perpendicular to the bilayer interface. Impedance measurements using the integrated electrodes show that after low levels ($<\tilde{}0.5$g) of acceleration, shaking the DIBs results in a significant increase in the resistance of the bilayer 4.8 [2]. We attribute this increase in resistance to the incorporation of additional lipid molecules present within the aqueous droplet volume into the interfacial membrane and the continued self-ordering and packing of molecules residing in the fluid bilayer that occurs as the droplets are gently shaken. Representative measurements taken at three different frequencies on different DIBs show that this change in resistance is not necessarily accompanied by a change in the size of the bilayer as indicated by a nearly constant estimated interface

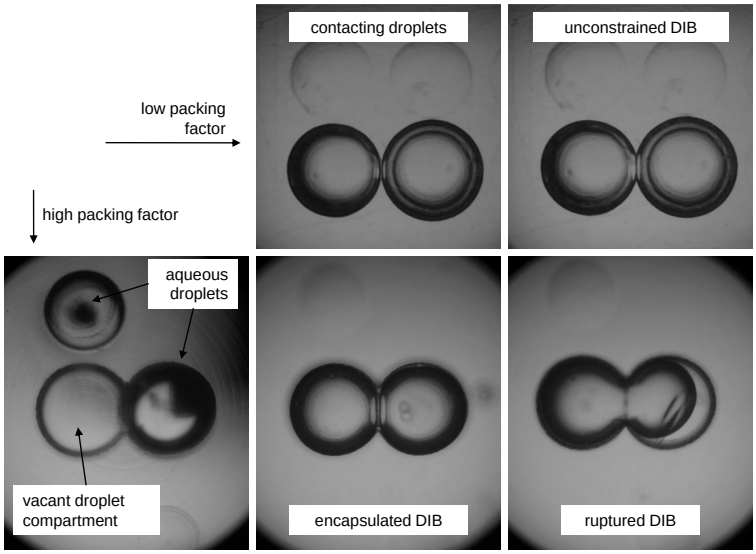

Figure 4.7: The interfacial region between adjacent droplets lightens as the two monolayers zip together to form a bilayer, whereas the shadowed regions that trace the perimeters of the droplets result from the difference in refractive index at the oil/water interface. The top two images show the formation of an unencapsulated DIB while the bottom row of images show droplets used to form a physically-encapsulated DIB with a packing factor of 30%.

diameter. Further, the measurements also show that at higher acceleration levels, the induced vibration reduces the resistance of the interface (again, a process independent of the bilayer size). This increase in bilayer resistance is observed consistently throughout the study, as shown in the histogram in Figure 4.8b, though changes in bilayer size were significantly more varied. The size of the bilayer as estimated from capacitance values increased by an average of 100μm in diameter from the initial measurement to the final measurement taken prior to bilayer failure, but with a large standard deviation of 220μm.

The observed failure mode for encapsulated DIBs in the high packing factor substrate with electrodes is bilayer rupture, whereas similar tests performed on unencapsulated DIBs resulted in droplet separation. When fixed electrodes are not present, physically-encapsulated

[2]Impedance measurements are not performed during the shaking tests since the induced droplet motion results in a flow of electrolyte ions (current) inside of the droplets that artificially decreases the measured impedance.

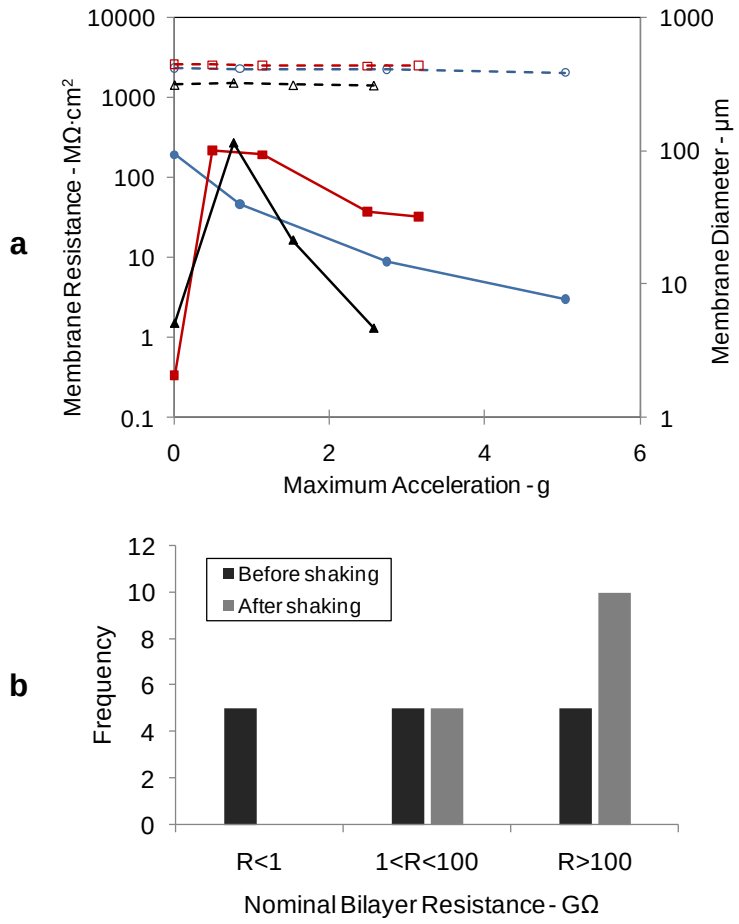

Figure 4.8: The membrane resistance ($M\Omega \cdot cm^2$) and equivalent diameter (μm) extracted from EIS measurements of physically-encapsulated DIBs show that the resistance of the bilayer is affected differently at different levels of acceleration (a). A distribution of the initial (before shaking) values of nominal bilayer resistance versus the maximum values of measured nominal resistance after shaking for all fifteen trials (c).

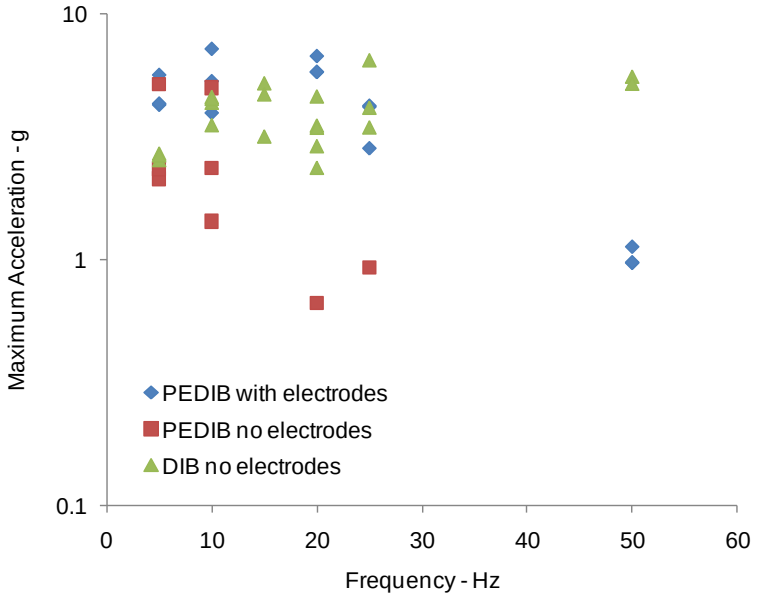

Figure 4.9: Measured values of maximum accelerations at failure for physically-encapsulated droplet interface bilayers (PEDIB) formed in similar high packing factor substrates with and without electrodes are compared to measured critical accelerations obtained for unencapsulated DIBs in the low packing factor substrate.

DIBs exhibit either separation or rupture. Failure consistently occurs between 1 and 10g of acceleration within the tested substrate geometries and frequency range. Droplet separation occurred several times in the high packing factor substrate when no electrodes were present. We observed that one of the droplets would move vertically into the upper reservoir, eventually separating from the other droplet. The integrated electrodes provide additional anchoring of the droplets, preventing separation of the droplets. The data points show that physical encapsulation of droplet interface bilayers positioned on integrated electrodes does not greatly decrease the survivability of the bilayer. While physically-encapsulated droplet interface bilayers rupture at lower acceleration levels than those that cause separation of unencapsulated DIBs at frequencies higher than 20Hz, they sustain larger accelerations than their unencapsulated counterparts at 5, 10, and 20Hz. For comparison, Kang, et al demonstrated that hydrogel-encapsulated bilayers were capable of surviving 5 min of shaking at

90RPM (1.5Hz), though no values of acceleration experienced by the substrate were reported [158].

The different mode of bilayer failure observed for encapsulated DIBs is attributed to the small amount of organic solvent that encases the droplets. In a low packing factor substrate, the droplets experience minimal contact with the rigid PMMA substrate and separation is induced due to deformations of the droplets that unzip the interface. Physically-encapsulated droplets, however, undergo less relative motion and are buffered by a much smaller volume of organic solvent. The reduced amount of organic solvent surrounding physically-encapsulated DIBs absorbs less energy, allowing more to be transmitted directly to the droplets. We believe that this interaction also causes physically-encapsulated droplet interface bilayers to be less resistant to failure at higher frequencies (Figure 4.9). It is further suggested that with lower displacements and higher accelerations experienced at higher frequencies, the vibration begins to affect the molecules more than the the droplets–whereupon the vibration essentially sonicates the system.

4.3.4 Physical Encapsulation of Multiple DIB Networks

This approach for physically-encapsulating DIB networks establishes a foundation on which larger, more-complex networks can be readily assembled given appropriate substrate design. A three-droplet network, featuring two droplet interface bilayers and integrated electrodes present in all compartments, is formed within a three-compartment substrate to showcases this point. In the same manner that two-droplet networks are formed, three-droplet networks are assembled using the "drag and drop" technique for connecting droplets and inserting electrodes. The results presented in Figure 4.10 show that the ability to tailor specific interfaces can still be achieved when the droplets are physically encapsulated. The upper-right

droplet shown in Figure 4.10a contains a mixture of lipid vesicles and alamethicin channels, while the other two droplets contain only the lipid vesicle solution. Impedance measurements performed across the interfaces individually and collectively ensure the formation of two lipid bilayers in the network (Figure 4.10b). The resulting network displays different current-voltage behavior across each interface due to the incorporation of proteins into only one bilayer (Figure 4.10c). The pure lipid membrane exhibits a typical resistive response in the CV measurement, while the second interface exhibits the voltage-dependent nature of a bilayer containing alamethicin channels.

4.4 Chapter Summary and Conclusions

The droplet interface bilayer is a method that takes full advantage of the principles of phase separation and molecular self-assembly. Each aqueous volume naturally remains submerged in the oil phase due to its higher density and conveniently takes on a spherical shape in order to minimize its surface area with the surrounding oil. Bilayers are formed between contacting droplets because phospholipid molecules first readily assemble at the oil/water interface of the droplets. This chapter introduced concepts of how biomolecular networks formed from DIBs can be constructed within durable materials through *physical encapsulation*, an approach selected for its ability to preserve phase separation and promote self-assembly.

The goal of encapsulation is to support the assemblies in a manner that reduces large-scale relative motions of the droplets which may adversely affect bilayer stability. Previous experience showed that unencapsulated DIB networks last days to weeks when left undisturbed, but assembled network structures quickly breakdown as soon as the system is moved. Physical encapsulation uses the constructs of a preformed solid substrate to support the droplet network. The results of this study show that high packing factor substrates containing DIB

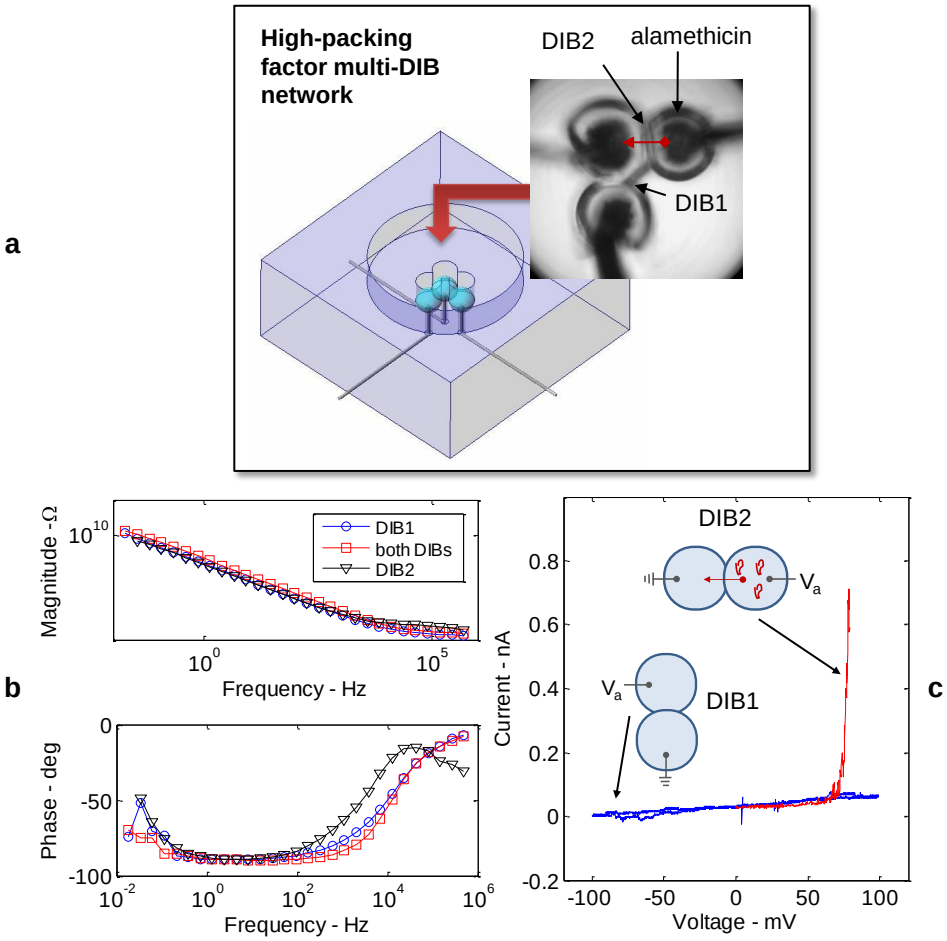

Figure 4.10: A three-droplet network is formed that demonstrates the scalability of this technique for producing larger networks (b). The integrated electrodes provide access for investigating the electrical impedance (b) and current-voltage relationships (c) of each interface individually.

networks can be moved, tilted, shaken, and even inverted while retaining the original molecular assembly and protein activity of the network. This approach overcomes the limited mobility of unencapsulated droplet networks and prevents droplet separation by reducing the volume of organic solvent that surrounds each droplet through substrate design. Integrated electrodes further simplify network formation and provide the necessary insertion into the aqueous phase for interrogating DIBs, all while retaining system mobility. The results of the mechanical testing both highlight (and quantify) the inherent durability of the droplet interface bilayers and suggest that substrate design can be used to minimize gross droplet movements which can limit the use of DIB networks in devices.

The work in this chapter demonstrates that liquid-supported biomolecular assemblies can be preserved inside of solid materials and that through encapsulation techniques, durable and portable material systems can be obtained. However, better methods for assembling fully-encapsulated networks and fabricating more-complex substrates that feature internal reservoirs are still needed. A primary limitation of physically-encapsulated droplet interface bilayers is that individual droplets still must be dispensed and arranged into compartments in the substrate. And while this is a process that could conceivably be automated, are there more elegant possibilities for creating material systems that enable controlled interface formation inside a material? Chapter 5 builds on the benefits of physical encapsulation for constructing portable biomolecular material systems and shows that reconfigurable liquid-supported bilayer networks can be formed *in situ* when supporting substrate is made from a flexible material.

Chapter 5

Regulated Attachment Method for *In Situ* Bilayer Formation

The observed [98] and now quantified (Chapter 4) durability of droplet interface bilayers is a key advantage of the DIB method compared to the traditional suspended lipid bilayer. The droplet interface bilayer eliminates the use of a supporting substrate in favor of an oil/water interface to host self-assembled phospholipids and as a result, promotes the formation of a continuous lipid monolayer that completely encapsulates each aqueous volume. The uninterrupted nature of liquid-supported lipid monolayers is a key delineation from traditional suspended or supported lipid bilayer techniques that feature a "patch" of phospholipid solution spread across discrete regions of a substrate [60, 129]. Consequently, the durability of bilayers formed via methods such as lipid folding or painting is limited, whereas the continuity of lipids that self-assemble at an oil/water interface allows DIBs to last for weeks while supporting functional biomolecules.

It is the opinion of this document that further refinement and integration of DIB-based platforms is impeded by four challenges: First, positioning and interrogating droplet interface

bilayers requires careful insertion of custom electrodes into droplets, a process that requires skill and/or the use of a micromanipulator and is one which can damage the adsorbed lipid monolayer. Second, the contents of each droplet are established prior to bilayer formation, preventing the introduction of species into droplets after network assembly [159]. Third, the size of the interface between two droplets is determined by both the size of the droplets, their relative positions, and the ability of the organic solvent molecule to reside in the hydrocarbon region of the bilayer [37], therefore precise control of droplet volume and positioning within the network is required in order to produce consistently-sized interfaces. Last, the dispensing and droplet positioning techniques developed by Holden, et al [98] can be used to easily form and manipulate droplets that are $0.1 - 100\mu$l in volume ($100 - 1000\mu$m in diameter), but constructing small-droplet networks that feature bilayer interfaces less than 1μm in diameter remains a challenge. Specifically, the need for reducing the size of the droplets in the network to achieve higher volumetric packing, smaller interfacial areas, and additional structural stability poses challenges to accurately dispense and controllably manipulate sub-nl ($< 60\mu$m in diameter) aqueous volumes.

In this chapter[1], an alternative method for bilayer formation, called the regulated attachment method (RAM), is presented in which the attachment of liquid-supported lipid monolayers is regulated by controlling the dimensions of an aperture formed in a flexible supporting substrate. First, a mechanical force is applied to the deformable substrate in order to close the aperture to separate a single aqueous volume submersed in oil into multiple volumes that then become encased with continuous lipid monolayers. The mechanical force on the substrate is reduced after a few minutes in order to open the aperture and allow the opposing lipid monolayers to come into contact. Regulating the dimensions of the aperture,

[1]Note: This chapter presents findings reported in a recent journal paper published in *Analytical Chemistry* entitled, "Regulated Attachment Method for Reconstituting Lipid Bilayers of Prescribed Size within Flexible Substrates" [160].

then, provides direct control over the size of the lipid bilayer which forms spontaneously after initial contact. The regulated attachment method is used to form lipid bilayers in a high packing factor (30%) flexible substrate made from polydimethylsiloxane (PDMS) and through experimental evaluation, we show that the areal size of the bilayer can be precisely prescribed by regulating the amount of contact between opposing monolayers via the applied force. The contributions of this particular study demonstrate that physically-encapsulated interface bilayers can be arranged and constructed *in situ* without the need to first dispense and arrange individual droplets. The following study is organized to highlight several advantages of bilayer formation using RAM compared to the original DIB technique.

5.1 Experimental Methods

5.1.1 Fabrication of Flexible Substrate

The prototype shown in Figure 5.1a features two connected compartments for holding aqueous volumes, where the design of the substrate is inspired by the overlapping droplet compartments used by Funakoshi [97]. The compartments (1.02mm in diameter and 1.52mm deep, with hemispherical bottom surfaces) are separated by a 500μm-wide by 1mm-tall aperture that spans the window formed between the circular compartments. The features that define the droplet compartments and aperture dimensions of the substrate are first machined into an acrylic (PMMA) substrate using a vertical end-mill. Uncured Sylgard 184 (Dow-Corning) PDMS (10 : 1 wt-wt ratio of base to curing agent) is poured into the acrylic substrate and crosslinked at $80 - 90^{o}$C for 1 hour in a benchtop oven in order to create the geometrical negative of the original high-packing factor acrylic substrate (Figure 5.1b). The cured PDMS negative is soaked in a 0.15% (w/w) [1.5mg/ml] solution of hydoxypropylmethylcel-

lulose (HPMC, Sigma) in 5mM phosphate, pH3 buffer (Fluka) for 10 minutes, rinsed with water, and then dried under nitrogen in order to prevent the cured negative from adhering to the PDMS replica upon subsequent curing of the PDMS replica [161] (Figure 5.1c). After curing in the oven at the same conditions, the PDMS negative is peeled from the flexible PDMS substrate (replica), which is then removed from the acrylic tray (Figure 5.1d). Silver-silver chloride (Ag/AgCl) electrodes made from 125μm-thick silver wire (Goodfellow) are then pierced through the sides of the PDMS substrate such that the tip of each electrode is positioned approximately in the center of a compartment (Figure 5.1a).

5.1.2 *In Situ* Bilayer Formation

Lipid solutions used in this chapter consist of 2mg/ml DPhPC phospholipid vesicles (purchased as lyophilized powder, Avanti Polar Lipids, Inc.) suspended in either 10mM MOPS (Sigma), 100mM NaCl (Sigma), pH7 or 10mM MOPS, 100mM KCl (Sigma), pH7 buffer solution. These solutions as well as mixtures of alpha-hemolysin αHL and alamethicin proteins are prepared for use as described in Chapter 3, Section 3.1.1.

Hexadecane ($> 10\mu$l) is first pipetted into the droplet compartments in order to provide the necessary oil/water interface surrounding the aqueous volumes. Then, 1.2μl of aqueous lipid vesicle solution is pipetted into the droplet compartments. The aqueous volume spans both droplet compartments as shown in Figure 5.2a and the silver-silver chloride electrodes insert easily into the aqueous phase without the need for a hydrophilic surface treatment such as the one used by Holden, et al [98, 93].

An electrode holder (M3301EH, World Precision Instruments, Inc.) mounted to the motorized micromanipulator is used to compress the soft substrate in order to fully close the aperture between the neighboring compartments. Upon compression the closing aperture di-

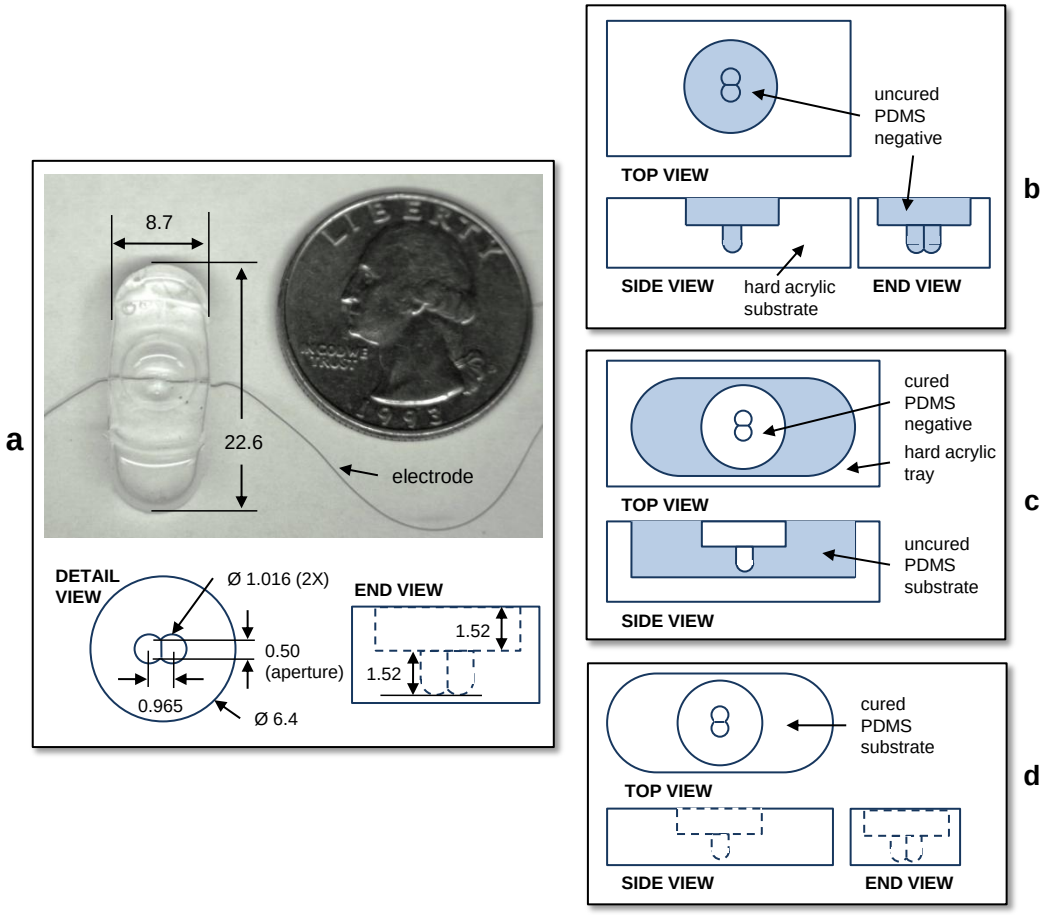

Figure 5.1: A flexible replica (a) of the original high packing factor substrate used in Chapter 4 is made with Sylgard 184 PDMS through a double molding procedure (b-d). 125μm silver-silver chloride electrodes are inserted through the completed PDMS substrate such that the tip of each electrode resides within a compartment.

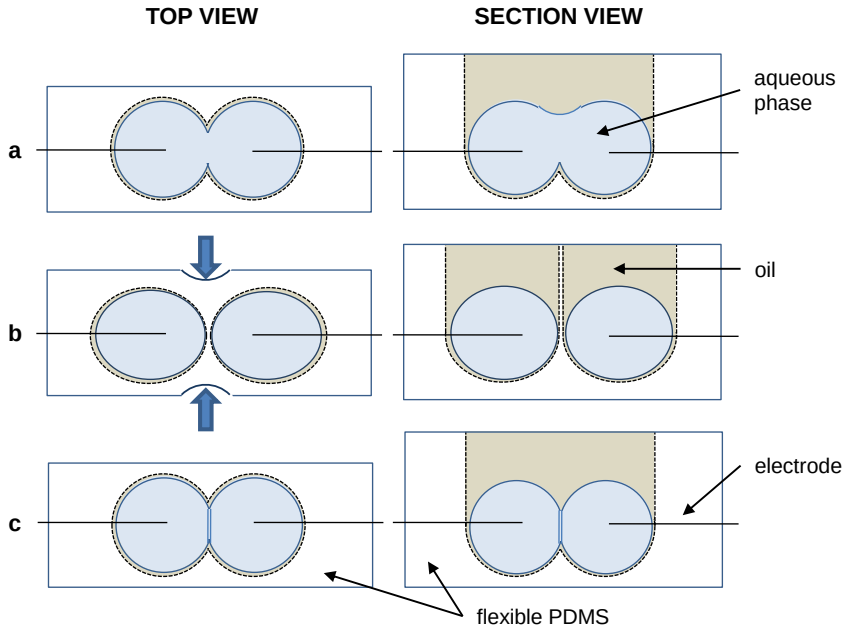

Figure 5.2: A flexible substrate is used to form interface bilayers *in situ* by the regulated attachment method, which divides a single aqueous volume (a) into multiple volumes (b) and then reattaches them after lipid monolayer adsorption (c). A prototype substrate made from PDMS provides a soft, flexible, and translucent support for separating and then reattaching lipid-encased aqueous volumes.

vides the single aqueous volume into two separate volumes submersed in hexadecane (Figure 5.2b). Complete separation is maintained for $5-10$ minutes in order to allow for monolayer adsorption to occur at the oil/water interface surrounding each aqueous volume (phospholipids adsorb from the aqueous phase in this study [93], though lipids can also adsorb from the oil phase [98]). Lastly, the compression force on the substrate is slowly reduced by moving the electrode holder in the opposite direction in order to open the aperture. A bilayer forms spontaneously after the aqueous volumes come into contact and excess oil is removed, allowing for the hydrocarbon tails of the lipids to zip together (Figure 5.2c).

Bilayers formed using RAM are again characterized using a variety of electrical techniques (see Chapter 2). In addition to EIS and CV measurements, unfiltered single channel recordings of bilayers containing αHL are measured at a fixed sampling rate of 10Hz using the Auto-

lab and GPES software (chronoamperometry mode) and AxoPatch recordings of alamethicin channels are conducted with a sampling rate of 250kHz and low-pass filtered at 1kHz.

5.2 Bilayer Formation using RAM

Lipid bilayers are formed using the regulated attachment method within the flexible, PDMS prototype substrate (Figure 5.1a). A motorized manipulator is used to produce incremental compression of the substrate for opening and closing the aperture in this study, though other methods could be used to separate and rejoin the adjacent aqueous volumes including magnetically-controlled valves [162], electro-rheological fluids [163], and directed electric fields [164, 156]. The prototype substrate fabricated for and used in this initial is made of a commercial silicone-elastomer that readily imbibes the oil phase, which may leach impurities back into the liquid phases. However, our initial results do not indicate that either the absorption or possible leaching affects either the formation or the resulting quality of the bilayers that are formed using RAM. We acknowledge that many different flexible, hydrophobic materials such as a new class of photocurable and solvent-resistant perfluoropolyethers (PFPEs) developed by DeSimone's group [165] could be used instead of PDMS.

Electrical impedance spectroscopy measurements obtained using the inserted electrodes confirm the changes in molecular ordering that occur during each step (Figure 5.3a). While our own experiences in forming DIBs reveal that monolayer-covered droplets can be difficult to pierce, the insertion of untreated electrodes into the single aqueous volume in the regulated attachment method occurs immediately and simultaneously before the monolayer has time to assemble. The EIS data presented in Figure 5.3b shows that the magnitude of the electrical impedance measured for a single aqueous volume is on the order of $0.1 - 1\text{M}\Omega$ due to the combined electrical conductivity of the aqueous solution and the interactions of this

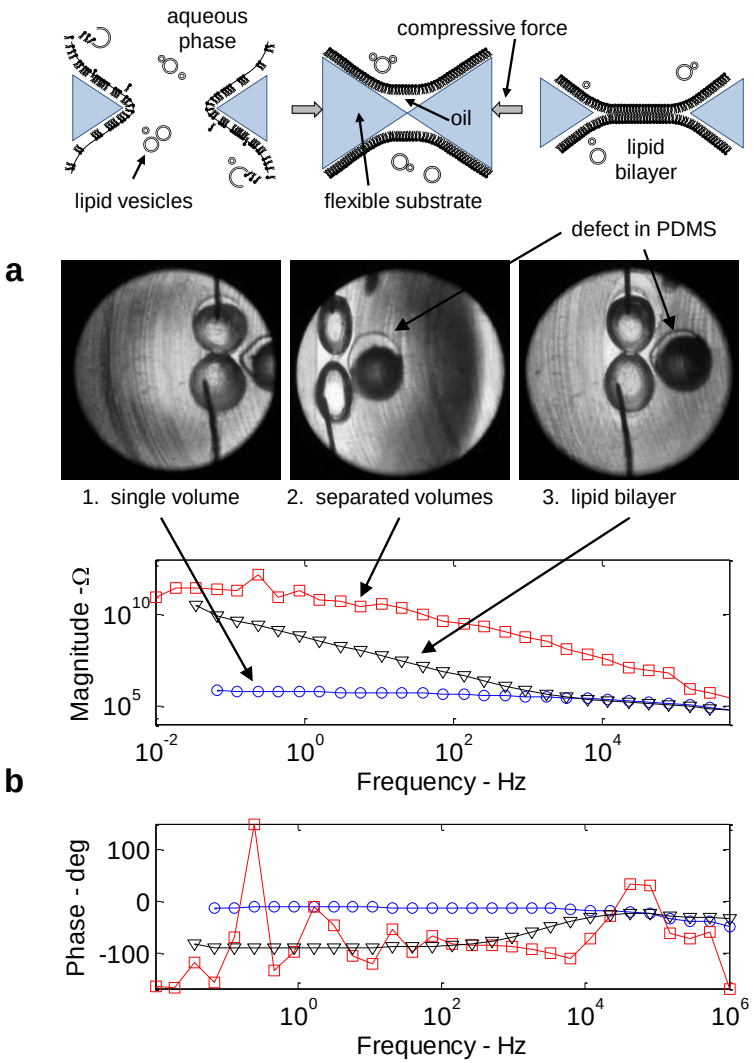

Figure 5.3: Lipid monolayer adsorption begins immediately when the aqueous volume containing lipid vesicles is injected into the surrounding hexadecane and continues after the aperture is closed (a). The droplet compartments move across the viewing range of a digital camera mounted to an inverted microscope due to the compression of the PDMS. EIS measurements are used to confirm complete separation and successive bilayer formation using RAM (b).

solution with the electrodes (blue circles). Once the aperture is closed due to the application of the mechanical force, the magnitude of the electrical impedance increases to a value that indicates there is no conducting path between the two aqueous volumes (red squares). This response verifies that the single aqueous volume has been completely divided into two separate volumes and ensures that lipid monolayer adsorption can occur along the entire oil/water interface surrounding both volumes. In the third stage, a lipid bilayer (black triangles) forms after the compression force is relaxed to promote contact between the adjacent lipid-encased volumes. The EIS measurement of a lipid bilayer demonstrates a DC resistance of more than 10GΩ due to the hydrocarbon core of the bilayer, which is consistent with previous impedance measurements on DIBs (Section 3.2).

The measured electrical properties of bilayers formed using RAM showcase the reproducibility of this method for forming high-quality lipid membranes. Values of electrical resistance for more than 10 different bilayers formed within the same substrate using RAM range from $10 - 500$GΩ, easily providing the giga-Ohm seal necessary for measuring single channel recordings [106]. Maximum equivalent diameters for lipid bilayers formed in the uncompressed prototype substrate are estimated to be 350 ± 27pF ($n = 3$). Bilayers formed using RAM consistently for more than three to four hours during the course of testing, even under applied potentials as high as $100 - 120$mV.

5.2.1 Control of Bilayer Size

The regulated attachment method offers a new approach for prescribing the areal size of an interface bilayer. For comparison, the size of a traditional supported/suspended lipid bilayer is bound, but not controlled, by the dimensions of the supporting substrate and the volume of the annulus of excess lipid solution that surrounds the thinned region of

the bilayer. The dimensions of this annulus are subsequently determined by the surface tension of the lipid monolayer–a function of both the physical properties of the phospholipid molecules and the molecular size of the organic solvent [37]–and the contact angle between the surface of the support and the lipid solution. Moreover, the sizes of unsupported lipid bilayers (DIB, DHB [100, 96, 125], etc) are constrained by the sizes of the droplets and the relative spacing between adjacent lipid-encased aqueous media which is maintained by precise electrode positioning. The regulated attachment method, however, enables precise control over bilayer size by controlling the amount of mechanical force that is applied to the aperture. This control mechanism for the bilayer size is completely independent of the size or shape of the aqueous volumes, or the type of organic solvent used at the oil-water interface. And while the molecular interactions of the organic solvent with the hydrocarbon tails still exist, size control is obtained by merely regulating the extent to which opposing lipid monolayers on neighboring volumes can zip together. A key distinction of this approach from previous bilayer formation methods is that control of the substrate is used to regulate the size of the bilayer even though the lipid monolayers are supported by the oil/water interface (shown in the top diagram of Figure 5.3). The regulated attachment method is further aided by the hydrophobic nature of the PDMS which ensures a small amount of the hexadecane remains between the lipid monolayers. This separation is crucial for allowing the size of the bilayer to be changed without causing disruption to the monolayers that could result in bilayer failure.

The results of the initial test presented in Figure 5.4 demonstrates control of bilayer size on a single lipid bilayer, showing that the membrane area (as measured by the bilayer capacitance) can be modulated reversibly by varying the level of compression applied to the substrate. The images in Figure 5.4a correspond to values of bilayer capacitance plotted in Figure 5.4b for Positions $5 - 8$ (moving from left to right) and show that increases in compression

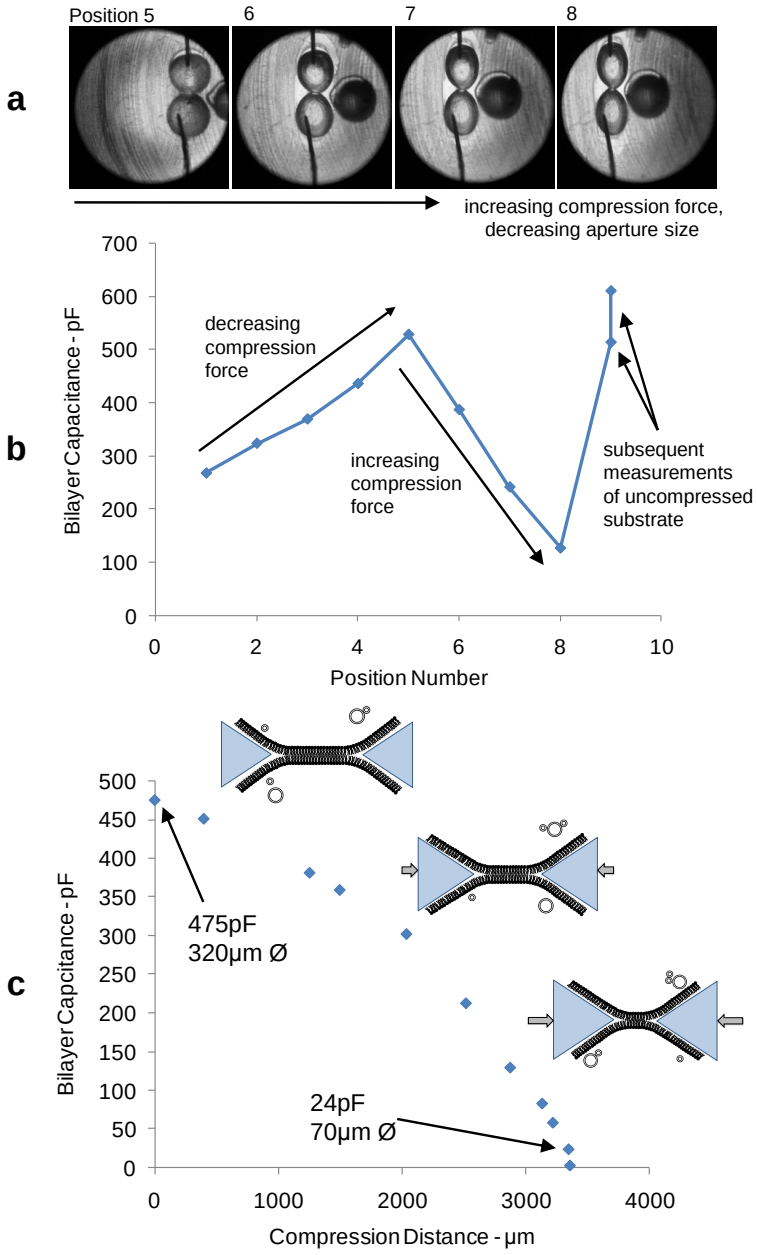

Figure 5.4: Images taken show the visible changes that occur to the aqueous volumes as the size of the aperture is consecutively reduced (a). The measured capacitance at each aperture setting confirms that the interfacial area between the two aqueous volumes changes as a result of a mechanical force applied to the supporting substrate (b). The last two data points taken at Position 9 reveal that the rate at which a growing bilayer thins is on the order of minutes. Measured bilayer capacitance versus recorded compression distance showcases the full range of sizes of bilayers that can be formed in the prototype flexible substrate (c).

result in both large-scale compression of the substrate indicated by the left-ward shift in the compartment positions and partial aperture closing. The capacitance of the bilayer varied from approximately 125pF at Position 8 to more than 600pF with the aperture fully open (recorded at Position 9), a 4.8-fold change in bilayer area.

This same experiment is repeated and the position coordinates for the electrode holder are tracked in order to correlate the applied deformation to the substrate to the change in the size of the membrane (Figure 5.4). The data presented in Figure 5.4c shows the full range of bilayer sizes that can be formed using the regulated attachment method in the prototype flexible substrate. The first measurement taken at a compression distance of 0μm (i.e. no applied force on the fixture) results in a bilayer with a capacitance of 475pF. The equivalent diameter for the membrane at this position is approximately 320μm. At a compression distance of approximately 3350μm, the smallest sustainable bilayer had a capacitance of 24pF, which translates to a diameter of 70μm-a nearly 5-fold decrease in diameter and a more than 30-fold decrease in bilayer area from the maximum state. The last data point taken yielded a capacitance of 2pF (equivalent to a diameter of only 23μm), though the droplets separated during the EIS measurement. Complete separation of the formed bilayer does not result in rupturing of the interface; instead, the lipid monolayers merely unzip. At this point, opening the aperture leads to new contact between the adjacent aqueous volumes that reestablishes a lipid bilayer interface. We believe that this ability to connect, disconnect, and reconnect the lipid monolayers creates a platform where the contents within each aqueous volume can be prescribed and safely maintained without undesired contamination of the opposite volume.

5.2.2 Incorporation of Proteins into RAM Bilayers

Lipid bilayers formed using the regulated attachment method provide a suitable and tunable environment for studying transmembrane proteins since both the size and composition of the bilayer can be prescribed. Furthermore, proteins can be introduced into RAM bilayer systems in several ways–both before and after bilayer formation. In the first scheme, prior to bilayer formation, separate volumes consisting of different compositions can be placed into adjacent compartments with the dividing aperture closed. Second, with the aperture open, the single volume that spans both compartments can contain proteins in order to prescribe protein insertion from both sides of the bilayer. The following results illustrate these separate introduction tactics and highlight the ability to form high-quality lipid bilayers and tailor their properties using proteins.

One-sided protein insertion is first demonstrated by pipetting different vesicle solutions into each compartment divided by the closed aperture. Similar to Hwang's demonstration of asymmetric bilayer formation using DIBs [93], one volume consists of alpha-hemolysin channels in DPhPC-KCl vesicle solution, while the second volume contains only DPhPC-KCl vesicle solution. The bilayer forms once the aperture is opened following monolayer formation and αHL channels insert into the membrane spontaneously via two mechanisms: through monomer aggregation and insertion directly from the aqueous solution [106, 98] or through vesicle fusion events that incorporate channels into the bilayer that had previously inserted into suspended DPhPC vesicles [80, 83]. We observe that each of these event types creates measurable transient currents, and the fusion of vesicles containing reconstituted αHL pores with the bilayer results in multiple αHL-conductance level increases in current. At low ($\leq$ 100ng/ml) final concentrations of αHL, single insertion and desorption events are seen in current traces measured after bilayer formation. Step-wise current variations of $3 - 5$pA correspond to conductance levels of $80 - 100$pS (shown in Figure 5.5a), agreeing

well with published conductances for alpha-hemolysin channels measured in bilayers formed in 100mM KCl electrolytes [46, 166]. The ability capture these single molecule activities further confirms that the regulated attachment method produces high quality lipid bilayers. At higher concentrations ($\geq 1\mu$g/ml αHL), a larger number of channels insert into the bilayer, causing a gradual reduction in the resistance of the membrane (corresponding to the increasing slope of the current-voltage traces shown in Figure 5.5b) and resulting in partial rectification of ion currents at positive potentials. This gross electrical behavior of a membrane containing alpha-hemolysin channels agrees well with several published works where similar concentrations of alpha-hemolysin were used [148, 47].

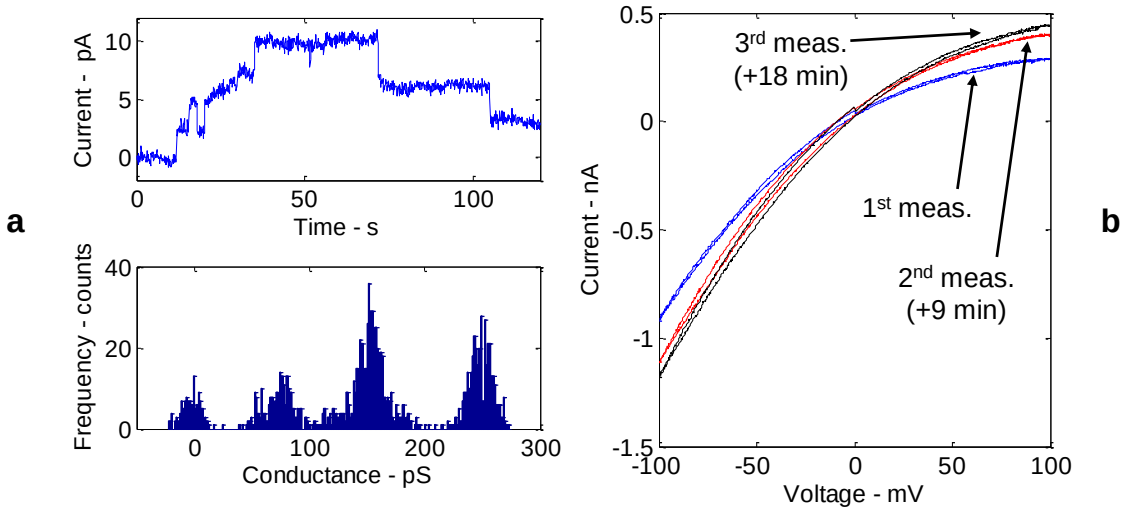

Figure 5.5: Single channel recordings of αHL channels are measured with an applied potential of +40mV (a) and gross current-voltage relationships of a bilayer containing a larger number of αHL channels are measured with CV (b).

Alamethicin channels are used to demonstrate two-sided insertion into bilayers formed using RAM as they demonstrate a well-known voltage-dependent conduction based on direction of insertion. In these tests, a single volume of alamethicin/DPhPC-NaCl solution is pipetted into the flexible substrate. The aperture is subsequently closed and then reopened after monolayer adsorption to form a bilayer. Alamethicin channels spontaneously insert into the

resulting bilayer from both sides following membrane formation.

The incorporation of alamethicin channels into the aqueous volumes at a fairly low concentration of 100ng/ml in DPhPC vesicle solution (prepared with 500mM KCl salt concentration to amplify the measured currents) enables the recording of single channel gating events and once again showcases the quality of the bilayers formed using RAM. Figure 5.6 shows that the alamethicin oligomers, or bundles of alamethicin monomers, form in the membrane upon the application of voltage. The step-wise measured increases in current are attributed to the multiple conductance states that alamethicin oligomers adopt as alamethicin monomers join (and leave) the bundle [167, 91, 69]. The conductance levels shown in Figure 5.6 are lower than those reported by others for the same salt concentration: $O_1 = 23 - 30$pA, $O_2 = 110 - 113$pA, $O_3 = 220 - 245$pA, $O_4 = 330 - 400$pA, and $O_5 = 590$pA [69, 106]. These differences in measured conductance may in fact be due to slight differences in either membrane thickness and/or membrane tension [168, 169] caused by differences in the amount of oil retained within the hydrophobic core of the interface [37] or additional tension induced on the membrane through deformation of the aqueous phases by the flexible substrate.

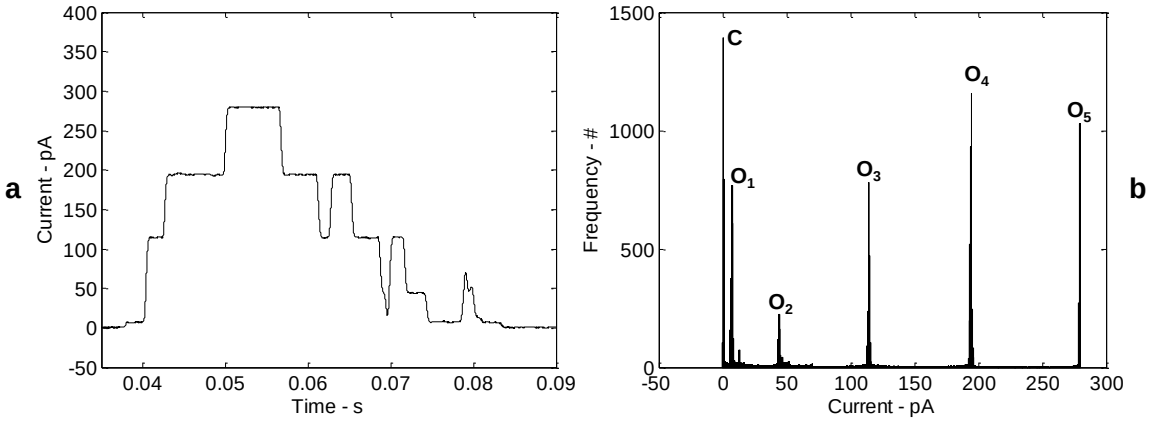

Figure 5.6: Single channel recordings of alamethicin proteins are obtained with the AxoPatch200B at an applied potential of +100mV (a). The step-wise current trace corresponds to the first five conductances levels: $O_1 = 7$pA, $O_2 = 44$pA, $O_3 = 115$pA, $O_4 = 195$pA, and $O_5 = 280$pA. (b)

At higher alamethicin concentrations, cyclic voltammetry measurements show the cumulative, voltage-dependent current flowing through the bilayer at potentials greater than |70mV| (Figure 5.7). The magnitude of the measured current upon channel opening agrees well with current-voltage traces obtained by Vodyanoy, et al on bilayers containing alamethicin channels at a similar solution concentration of 2μg/ml [151].

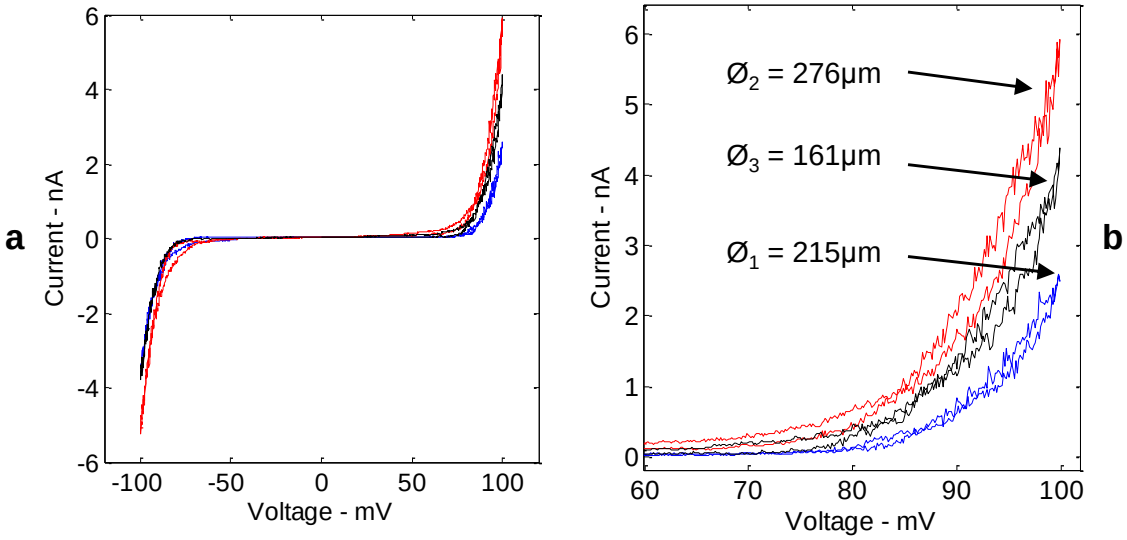

Figure 5.7: Alamethicin channels incorporated into the initial single aqueous phase that is separated and reattached to form a bilayer results in symmetric voltage-dependent gating at potentials greater than approximately |70mV| (a) and which is a function of prescribed bilayer size (b).

The symmetry of the current-voltage traces is attributed to the membrane containing alamethicin channels which have inserted into the bilayer from both sides (much like those measured in DIBs, Figure 3.8). Figure 5.7b shows that the magnitude of the current flowing through the membrane when the channels are 'open' ($>$ |70mV|) is a function of bilayer size and time. As the force applied to the substrate is decreased, the size of the membrane increases from an initial diameter of 215μm to 276μm and the measured current above the gating potential of $\approx$ 70mV increases as more proteins insert into the larger interface. This change is partially reversible, as seen in the reduced magnitude of measured current when

the bilayer size is reduced to 161μm for the third measurement. Some hysteresis between the first and third measurement is observed as alamethicin proteins continue to insert into the membrane area after initial bilayer formation. We believe further that repeated expansion and shrinking of the interface may also serve to consolidate proteins into a smaller interface, thus achieving higher protein concentrations within the bilayer.

5.2.3 Introduction of Species into Preformed Networks

A distinct advantage of partitioning the aqueous volumes with a controllable aperture is that it allows specific species to be introduced into specific regions of the network even after bilayer formation. This added feature provides the unique capability for merging RAM with microfluidics for introducing species into the connected volumes via micro-channels or syringes. Unlike the original droplet interface bilayer where the compositions of the droplets remain fixed, the introduction of species into a preformed bilayer can be studied and used for a variety of high-throughput screening applications [170, 171, 129, 172]. Furthermore, the addition of species can occur at two different times: before the attachment of adjacent aqueous volumes or after bilayer formation (Figure 5.8a).

A blunt-tip needle (34-gage NanoFil needle, WPI, Inc.) and syringe pump (10μl NanoFil syringe, WPI, Inc.) are used to incorporate alamethicin proteins into an aqueous volume on one side of a preexisting lipid bilayer. Prior to the test, a small channel routed into one droplet compartment is formed by piercing the needle through the PDMS substrate. The needle is then retracted slightly in order to prevent unwanted contact with the aqueous volume that could result in uncontrolled diffusion of species from within the syringe into the droplet. The first photograph in Figure 5.8b was taken after bilayer formation with the needle tip located to the lower right of the lower aqueous volume. The syringe contained a 100μg/ml

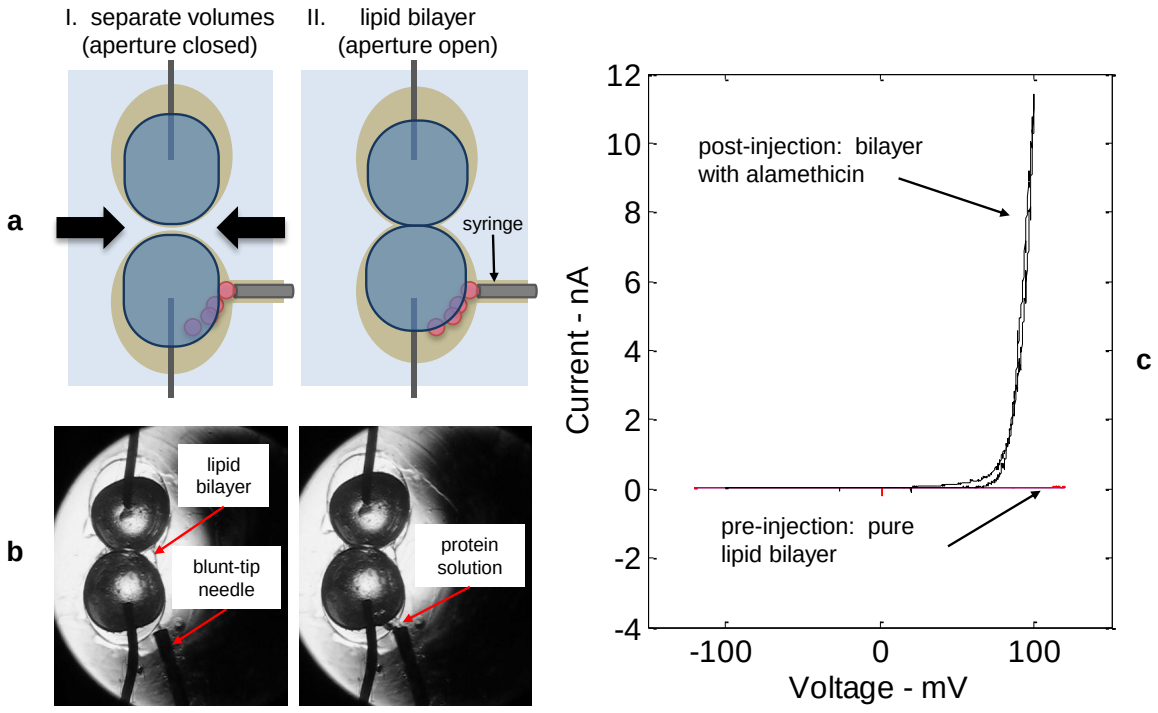

Figure 5.8: Alamethicin channels dissolved in an aqueous buffer are incorporated into a preformed lipid bilayer formed using RAM, by injection through a 10μl NanoFil syringe (WPI, Inc.) with a 34-gage blunt-tip NanoFil needle (WPI, Inc.) pierced through the soft PDMS substrate. The injection can be preformed both before bilayer formation with the aperture closed (a.I.) or as in this case, after bilayer formation (a.II, b.). The insertion of a large number of proteins occurs within $10 - 20$ minutes after the injection.

solution of alamethicin channels dissolved in 10mM MOPS, 100NaCl, pH7 buffer. Lipids were not incorporated into this phase in order to promote the coalescence and incorporation of contents of the injected volumes into the preexisting lipid-encased volume. During injection, the protein solution flows through the small channel at the end of the syringe and is directed toward the lower droplet shown in the second photograph. The small volumes (< 10nl each) of protein solution coalesce with the large lipid-encased droplet $1 - 2$ seconds after contact and release their contents into the larger volume.

In total, we estimate that approximately $50 - 100$nl of protein solution are incorporated into the lower 500nl aqueous volume consisting of lipid vesicle solution. Electrical measurements confirmed the incorporation of channels into just one droplet when, approximately $10 - 15$ minutes after injection, the current-voltage behavior of the membrane demonstrated an asymmetric voltage-dependent response. Unlike earlier tests where alamethicin proteins were incorporated into the initial single aqueous volume and resulted in the insertion of channels in both directions into the membrane (see Figure 5.7a), this method successfully incorporates species into just one aqueous volume, thus leading to single-sided insertion evident by the voltage-dependent behavior occurring only at potentials greater than +50mV. Moreover, we found that we were able to successfully incorporate $100 - 200$nl of alamethicin solution from the syringe into preformed networks in three out of three separate trials. The importance of this result is that for the first time external species and solutions can be introduced into preformed lipid bilayers to form modified lipid bilayers that can easily be compared with pre-injection membrane properties. Simply, this capability allows membranes to be constructed one component at a time.

In this experiment we added voltage-dependent ion channels to an existing bilayer in a controllable fashion, enabling the study of the roles of specific molecules on the entire assembly. As an example, the electrical impedance measurements, in addition to the differences ob-

served in the current-voltage relationship of the bilayer before and after alamethicin is added, show that the capacitance of the interface decreases by more than 100pF (three separate trials) upon channel insertion. We attribute this difference to changes in composition, rather than size, of the membrane and estimate, using the post-injection values of capacitance and normalized capacitance for DPhPC bilayers, that approximately $20 - 50\%$ of the area of the bilayer consists of alamethicin channels. We acknowledge the same technique could be used to transport species into droplet interface bilayers as formed by Holden, et al, though the designed partitioning of aqueous volumes that occurs in our prototype substrate aids in directing the injected solution toward the desired aqueous volume and prevents unwanted contamination of the other volumes. Further, because the sizes of bilayers formed using RAM are not determined by the size or shape of each aqueous volume, the addition of species contained in a carrier solvent allows for the composition of the bilayer to be tailored independently from the size of the interface.

5.3 Chapter Summary and Conclusions

In this chapter we have demonstrated that a flexible substrate can be used to control the attachment of opposing lipid monolayers which provides a novel and effective method for forming interface bilayers *in situ*. The study used the regulated application of a mechanical force to controllably open and close an aperture that separates two aqueous volumes, permitting large changes in the size of the bilayer (from more than 360μm in diameter to less than 70μm in diameter—a change of $>$ 5X in equivalent diameter and $>$ 30X in area) while retaining bilayers with high-quality electrical seals ($R > 10\text{M}\Omega\cdot\text{cm}^2$) necessary for monitoring single and few protein activities. This approach stands apart from previous bilayer formation methods in that both an immiscible liquid interface and a solid supporting substrate are used

in tandem to support molecular assembly and regulate bilayer thinning. Our results provide credible evidence that the regulated attachment method offers the unique capability to control the composition of lipid bilayers independently from the size of the interface, and in this light, we demonstrated alamethicin channels into preformed lipid bilayers. Moreover, the ability to partition aqueous volumes, preventing unwanted contamination of species, allows for asymmetric lipid bilayers to be formed much like with droplet interface bilayers [93].

The prototype flexible substrate fabricated and used for the studies performed in this chapter is a high packing factor substrate, similar to the one made from acrylic in Chapter 4, that features two connected compartments for housing both the oil and aqueous phases. Much like the rigid substrate used to demonstrate physical encapsulation of DIBs, this flexible substrate made from PDMS also constrains the aqueous volumes to prevent unwanted, and potentially damaging, relative motions and features integrated electrodes for portability. Through the durability of bilayers formed in situ was not quantitatively measured, we anticipated that interface bilayers formed in the PDMS substrate demonstrate similar resistance to failure as physically-encapsulated DIBs formed in Chapter 4 since both the aqueous volume sizes and substrate geometries are very similar. However, the substrate is open to the air and requires that a solid cap be inserted in order to create a fully-encapsulated network. In the following chapter, microfabrication techniques are used to develop a new form of flexible substrates that creates completely embedded interface bilayers. With this approach, the appropriate liquid phases are first injected into the material and then automatic phase separation occurs due to proper material selection and substrate surface treatments. The regulated attachment method is again used to demonstrate controlled bilayer formation *in situ* in microchannels between non spherical lipid-encased aqueous volumes.

Chapter 6

Encapsulated Interface Bilayers within Sealed Substrates

The two previous chapters demonstrate that interface bilayers can be contained, and even formed, within solid substrates in ways that produce durable, portable, and even reconfigurable interface bilayers. As a result, these contributions clearly distinguish the nature and approach of the work presented in this dissertation from the original droplet interface bilayer. This chapter expands on these specific efforts to create encapsulated interface bilayers within sealed substrates. The regulated attachment is again used to induce the necessary subdivision and reattachment of lipid-encased aqueous solutions, which, as Chapter 5 illustrated, eliminates the need to dispense and arrange individual aqueous droplets. Instead, continuous volumes of aqueous solutions contained within internal compartments of a solid material are manipulated locally within the material to create interface bilayers at desired locations.

In this chapter, fully-sealed flexible substrates made from PDMS are fabricated using microfabrication techniques for creating encapsulated interface bilayers. However, as this chapter

explains, stabilizing the necessary oil and water liquid phases within sealed PDMS substrates is not as straightforward as the initial tests in the open PDMS flexible substrate may have indicated. Through surface modifications to the substrate, we demonstrate that high quality lipid bilayers can be formed internally within higher packing factor substrates as long as a sufficient amount of oil can be retained between the aqueous phases and the solid material.

6.1 An Internally-Structured Substrate for Encapsulating Interface Bilayers

Recent advances in forming and stabilizing droplet interface bilayers within solid materials provides a foundation for designing internally-structured materials to house biomolecular assemblies. Physical encapsulation of droplet interface bilayers uses the constructs of a solid substrate to contain individual droplets and allow for contact between neighboring volumes to form interface bilayers (Chapter 4). By reducing the amount of organic solvent that surrounds the droplets, a solid substrate is better suited for restraining large-scale droplet motions that can lead to bilayer rupture. Additionally, integrated electrodes held by the solid substrate provide consistent electrical contact with the network and make the encapsulated biomolecular networks quite portable.

The regulated attachment method (RAM) introduced in Chapter 5 provides a convenient method for creating DIB-like interface bilayers *in situ* within flexible materials that avoids the formation and arrangement of discrete water droplets. This technique relies on the geometry of a flexible material to promote the division of a single aqueous volume and then allow for subsequent reattachment of the lipid-encased volumes to form lipid bilayers at specific locations in the material. The supporting substrate is designed to "pinch" the single aqueous

volume into multiple volumes, whereupon the self-assembly of a lipid monolayer encases each volume. The initial work demonstrated that an applied external mechanical force can be used to open and close a dividing aperture in a soft polydimethylsiloxane (PDMS) substrate. Incremental regulation of this applied force to controllably open and close the aperture even allowed for $20 - 30$X reversible changes in the area of the bilayer.

In the following sections, we present the design, fabrication, and surface modification of a flexible supporting substrate for creating encapsulated interface bilayers within sealed substrates. Our approach combines state-of-the-art microfabrication techniques with the demonstrated success of forming liquid-supported interface bilayers using RAM within flexible materials.

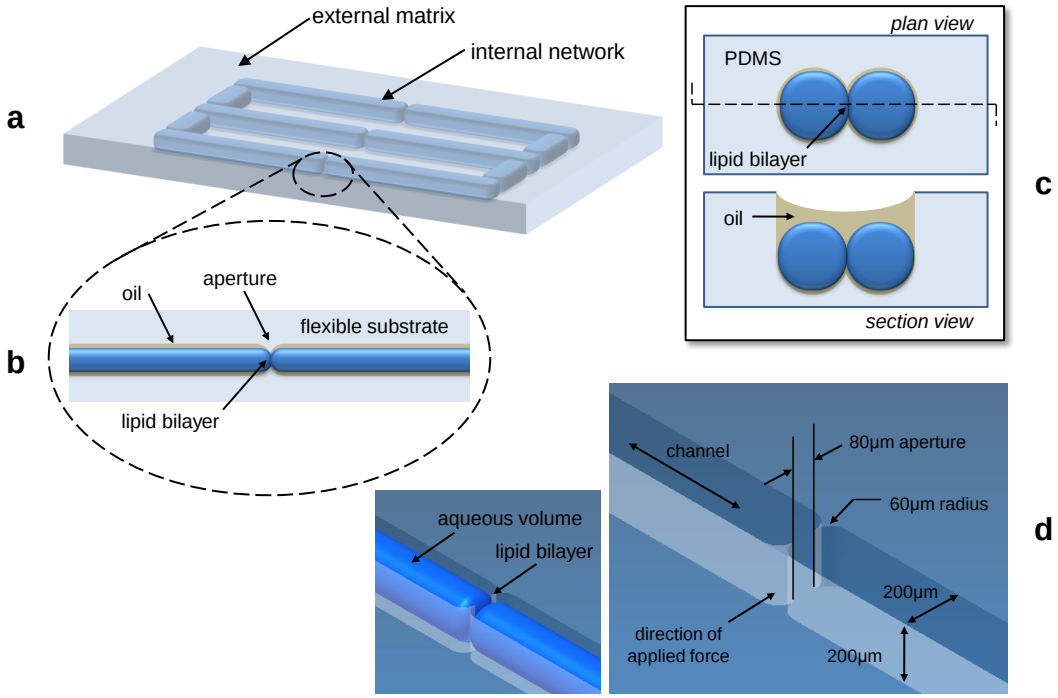

Figure 6.1: An illustration of a fully-encapsulated biomolecular material system contained within an external material matrix shows multiple aqueous volumes of various shapes and sizes connected via lipid bilayer interfaces (a). The building blocks of this concept rely on the self-assembly of lipid molecules at oil/water interfaces and demand proper phase separation within the internal reservoirs (b). The open droplet compartments (c) used in our previous work [155] provided inspiration for the design of microfluidic channels created in flexible materials using soft-lithography processes (d). Note: Dimensions are not to scale.

6.1.1 Candidate Material Requirements and Selection

Figure 6.1a shows one representation of a biomolecular material system, where internal reservoirs hold the necessary aqueous and organic phases needed for lipid self-assembly. The internal features of this structure are preformed such that the contents are injected after fabrication and the surface properties of the substrate then promote phase segregation of the two liquids, yielding a thin layer of oil that surrounds the aqueous volumes (Figure 6.1b). Therefore, it is crucial for the substrate to be made from a material that meets the following criteria.

- A candidate material must not absorb either the aqueous or oil phase since an oil/water interface is vital for obtaining fluid lipid monolayers required for durable bilayer formation.
- This material must also not leach material back into the fluid phases which may adversely affect composition or stability [173] of the network.
- The encapsulating material also needs to be flexible in order to use RAM for separating and reattaching the aqueous volumes.
- Lastly, an electrically insulating and optically transparent material is required to permit interrogation of the network and for both visualization and optical stimulation of internal biomolecules, respectively.

A polydimethylsiloxane (PDMS) elastomer (Sylgard 184, Dow Corning) is selected to fabricate the external material matrix. This material has been used widely in recent years in the field of microfluidics where many of the microfabrication techniques used have been developed for specifically processing this material [174, 175, 176, 177, 178]. Microstructures

in PDMS can easily be made via soft lithography on a silicon master that contains the geometric inverse of the features. However, two of the primary obstacles encountered when using PDMS in microfluidic applications are its hydrophobic nature that reduces wetting by aqueous solutions and its propensity to absorb small hydrophobic molecules such as those of many organic solvents (decane, hexane, pentane, hexadecane, etc.) [179]. While exposure to air or oxygen plasma during the PDMS bonding does lower the contact angle and increase wetting by aqueous volumes [180, 181, 174, 182], a hydrophobic surface is required for the proposed water-in-oil system studied in this work. Overcoming oil absorption into PDMS is critical for stabilizing the water-in-oil emulsion, since absorption of the oil phase not only hinders lipid monolayer assembly and reduces fluidity, but may also causing leaching of uncrosslinked PDMS chains back into the aqueous volumes.

As a solution to these challenges, a non-swelling fluorocarbon oil phase (perfluorodecalin) is used to eliminate loss of the oil phase through absorption into the bulk and a surface modification of the channel walls is performed to maximize the wetting of the oil phase on the channel surfaces. Together, these modifications allow for a thin layer of the oil phase to be retained upon subsequent injection of the aqueous phase into the material, providing the necessary fluid oil/water interface required for assembling lipid monolayers.

6.2 Materials and Methods

6.2.1 Substrate Fabrication

Silicon masters are fabricated from a 4-inch, p-type, boron-doped <100> orientation, 0.005−0.02Ω-cm, 500μm-thick silicon wafer (University Wafer). A negative photoresist (AZP9260 Photoresist, MicroChemicals GmbH) is first spun onto a clean wafer to a final thickness of

$15 - 16\mu$m. Channel features are then transfered to the photoresist layer with a 50-second UV hard cure using a Karl-Suss mask aligner. The unmasked regions of the photoresist are removed from the wafer surface using a 1:3 (v:v) solution of AZ400K developer (MicroChemicals GmbH) in deionized water (DI). The wafer is plasma etched using a Bosch process, which consists of alternating flows of plasma, sulfur hexafluoride (SF_6), and a passivation layer, octafluorocyclobutane (C_4F_8) to halt etching, in an Alcatel AMS 100 Deep Reactive Ion Etcher (see Appendix D for more details on wafer photolithography and etching processes). A total etching time of 56 minutes produces channel feature heights of approximately 200μm. The remaining photoresist on the raised features is removed with acetone and the wafer is then rinsed with DI.

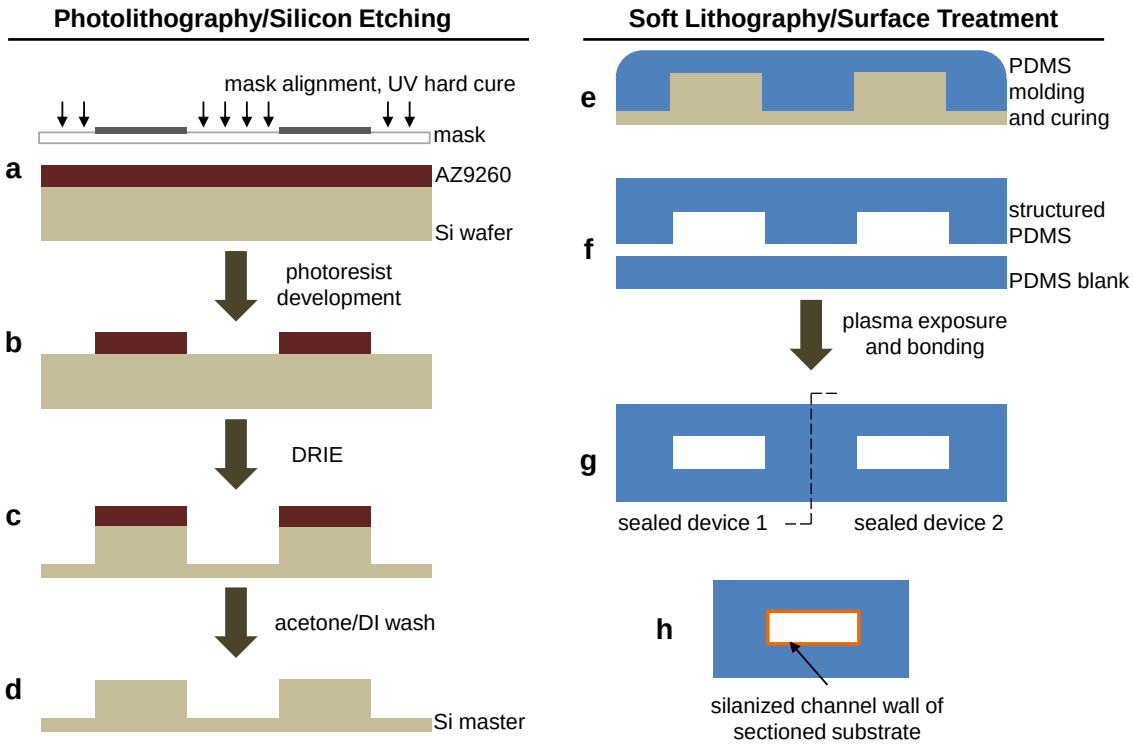

Figure 6.2: Raised features are fabricated on a silicon master through photolithography and DRIE processes (a-d) such that microchannels are formed in PDMS using soft-lithography (e). Subsequent bonding, sectioning, and silanization steps (f-h) produce individual test structures, each with an internal channel.

The etched wafer is treated with a fluorosilane prior to PDMS soft-lithography to aid in the release of the PDMS from the wafer surface after curing [174]. A few drops of (tridecafluoro-1,1,2,2-tetrahydrooctyl) trichlorosilane (SIT8174.0, Gelest Inc.) are placed along side the etched wafer in a clean Petri dish and placed under vacuum for 30 minutes to deposit a monolayer of the fluorocarbon on the surface of the etched wafer. Microchannels in PDMS are produced from Sylgard 184 (Dow Corning) at a 10:1 mass ratio of monomer to curing agent. The liquid PDMS precursor is thoroughly mixed by hand, degassed under vacuum, poured onto the treated wafer, and placed into a shallow aluminum foil tray formed to hold the 4-inch wafer. The PDMS is cured at 165^{o}C on a hot plate for 20 minutes. After cooling, the PDMS mold is gently peeled away from the silicon wafer.

Injection ports are punched through the PDMS at both ends of each channel using a 0.75mm-diameter punch. The microstructured PDMS and flat PDMS blank of similar thickness ($2 - 3$mm) are exposed to air plasma for five minutes on high in a plasma cleaner (PDC-001, Harrick Plasma), after which the two PDMS pieces are immediately pressed together to form an irreversible bond. Individual test structures, each containing a single 200μm-wide $\times$ 200μm-deep channel, are then sectioned from the original sealed PDMS substrate and excess PDMS material is removed near the pinch-points of each structure to facilitate force concentration necessary for adequate closing of the channel apertures. A 300μm micro-drill bit (McMaster) is used to pierce two vertical channels from the top of the substrate downward, intersecting the channel on both sides of the channel aperture.

6.2.2 Channel Surface Modification

The PDMS channel walls are treated with the same fluorosilane (SIT8174.0, Gelest, Inc.) in order to obtain sufficient wetting and retention of the oil phase along the channels. This

process is crucial for achieving the necessary liquid phase separation shown in Figure 6.1b. A technique based on the work by Sui, et al to surface treat intact PDMS-based microfluidic devices is used to deposit a monolayer of fluorocarbon on the channel walls through solution-phase modification [183]. A 5:1:1 (by volume) solution of deionized water, hydrogen peroxide (Sigma), and hydrochloric acid (Sigma) (H_2O:H_2O_2:HCl) is flowed continuously through the channel for 5 minutes to cause solution oxidation of the PDMS surface. The channel is then rinsed with deionized water and dried with nitrogen (N_2), yielding hydrophilic, silanol-covered surfaces. Solution oxidization is required even after plasma exposure because silanization is often performed hours after device bonding and PDMS is known to recover a non-oxidized (hydrophobic) surface in a few hours upon exposure to air [179]. Sequential silanization is achieved by injecting neat fluorosilane into the channel and allowing it to react with the silanol (Si-OH) sites for $3 - 5$ minutes. The fluorocarbon-covered channel is lastly rinsed with ethanol (Sigma) and dried with N_2.

Contact angle measurements for water, hexadecane, and perfluorodecalin are performed on native, oxidized, and silanized PDMS coupons treated in same manner as the enclosed channels in order to quantify the effect of the silanization procedure. Static contact angle measurements are recorded using a FTA125 Contact Angle Analyzer (First Ten Angstroms). For each type of PDMS treatment, the static contact angle of a droplet is measured on five separate samples and the average contact angle is reported. All data are collected at room temperature.

6.2.3 Encapsulated Bilayer Formation

Perfluorodecalin ($C_{10}F_{18}$, Sigma) is used without further purification as the oil phase in the treated microchannels. A 2mg/ml solution of 1,2-diphytanoyl-*sn*-glycero-3-phosphocholine

(DPHPC, Avanti Polar Lipids, Inc.) vesicles in 10mM MOPS (Sigma), 100mM $CaCl_2$ (Sigma), pH7 is prepared and stored as described in Chapter 3. First, perfluorodecalin is injected with a micropipette (Socorex Calilbra 822, $1 - 10\mu$l) to fill the channel. After a few minutes to allow for sufficient wetting of the channel surfaces by the oil phase, aqueous lipid solution is injected into the channel, displacing most of the oil from channel, causing it to flow out of the open exit port. 125μm silver-silver chloride (Ag/AgCl) electrodes are inserted into the vertical channels such that the tips of each electrode come into contact with the aqueous solution in the channel. As with the previous study (Chapter 5), an electrode holder attached to the motorized micromanipulator is used to compress the flexible substrate laterally against a rigid backstop (Figure 6.7a). The applied compression enables controlled closing and re-opening of the aperture, which is used to separate a continuous aqueous volume into multiple neighboring volumes and then reattach them to form a lipid bilayer within the channel. The bilayer forms as the the compression force is relaxed (by moving the electrode holder away from the structure) and the two lipid-encased aqueous volumes come into contact. Electrical recordings are performed to verify formation and characterize the quality of encapsulated interface bilayers formed with sealed PDMS substrates. Real-time capacitance measurements, EIS, CV, and single channel recordings are conducted as described in Chapter 2.

6.3 Results and Discussion

6.3.1 Fabrication and Silanization of Microstructured Substrates

PDMS supporting structures are fabricated by soft-lithography on an etched silicon wafer and then bonded to a flat PDMS blank to produce sealed, internal channels. The sealed

structures are sectioned for testing so that each substrate features one internal channel having either one or three constriction points (Figure 6.3a). Figure 6.3d shows two sealed PDMS structures for supporting internal biomolecular assemblies. The device on the left with colorless channel walls has not been silanized, while the device on the right displays an opaque, white channel. The inlet and outlet ports of this device are also white in color due to presence of the fluorocarbon grafted onto the PDMS surfaces. The silanized device also shows the wedge-shaped sections of PDMS removed from both sides of the channel to help concentrate applied loads when using the regulated attachment method for bilayer formation.

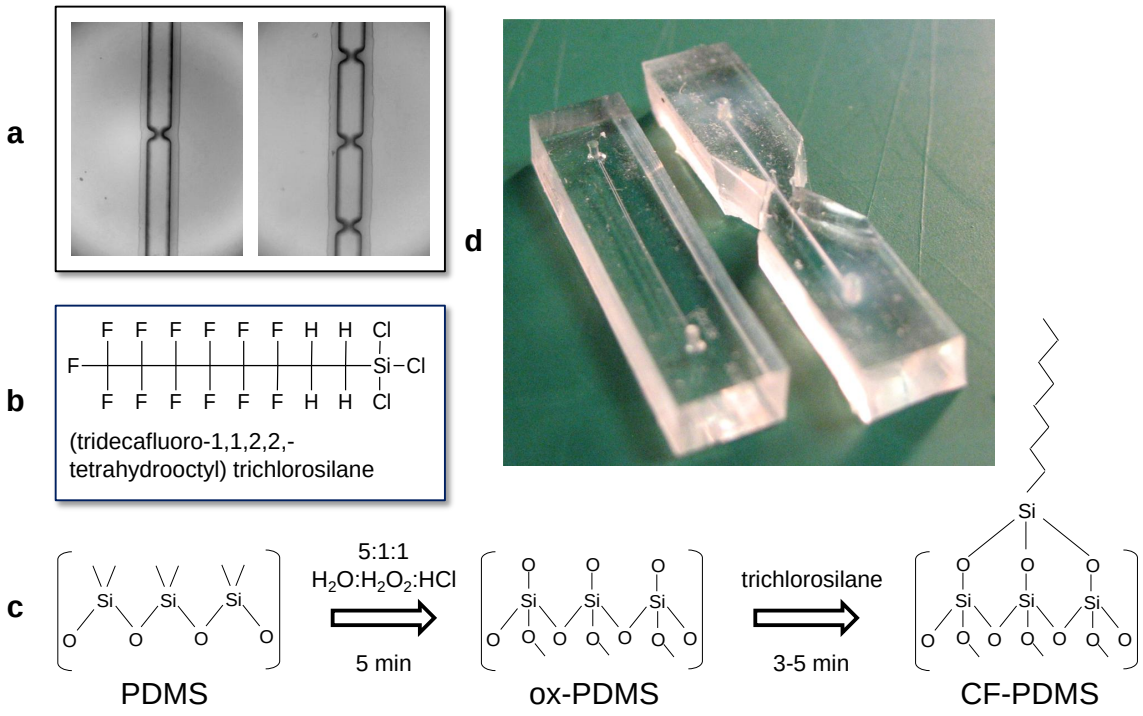

Figure 6.3: Single-aperture and three-aperture test structures (a) are used in this initial study for demonstrating controlled phase separation and bilayer formation using RAM. Surface modification using a fluorinated trichlorosilane (b-c) is performed in a two-step process designed to first oxide and then silanize the PDMS surfaces of the channel walls. The grafted fluorosilane layer appears white along the length of the channel wall and in the inlet and outlet ports (right structure, d).

Silanization via a two-step procedure (Figure 6.3c) adopted from the work of Sui, et al [183] is necessary to help recover a hydrophobic surface after the plasma bonding process that leaves the surfaces of the PDMS hydrophilic [182]. In the first step the acid cleaves the methyl (CH_3) group on the siloxane backbone, leaving behind exposed silanol (Si-OH) sites. Sui, et al demonstrated the permanent attachment of poly(ethylene glycol) (PEG) and amine (NH_2) functional groups with the second, silanization step in order to tailor surface hydrophobicity for controlling nonspecific protein absorption and biomolecule attachment. The trichlorosilane used in this work (Figure 6.3b) covalently binds to the silanol sites on the PDMS in the same manner but with the intent to render the surface hydrophobic for improved wetting by the oil phase and decreased wetting by the aqueous phase. We expect that channel wall wetting by the oil phase is further encouraged by the fact that the fluorosilane selected has a similar chemical structure to the perfluorodecalin molecule.

The relationship between the tendency of the outer fluid, called the *carrier fluid* in systems that involve fluid flow, to wet a surface versus its propensity to swell the substrate material is discussed in context to Figure 6.4. In our application, the outer fluid is the oil phase needed to provide an oil/water interface for self-assembly of phospholipids. Our choice of perfluorodecalin versus hexadecane for use in a PDMS substrate can be visualized graphically when the swelling ratio, S, of each is compared. The swelling ratio is the ratio of an arbitrary dimension, D, of a swollen PDMS sample soaked in a solvent versus the same dimension, D_0 for the original, unswollen PDMS sample. Therefore, a swelling ratio of 1 means that a solvent does not increase the size of the material sample, while values of S greater than 1 indicate the absorption of a given solvent. Hexadecane has a swelling ratio of approximately 1.4, versus water and non-swelling fluorocarbon oils such as perfluorodecalin, which both have swelling ratios of 1.00 [179].

The contact angle of each liquid on the substrate surface is equally important in the choice

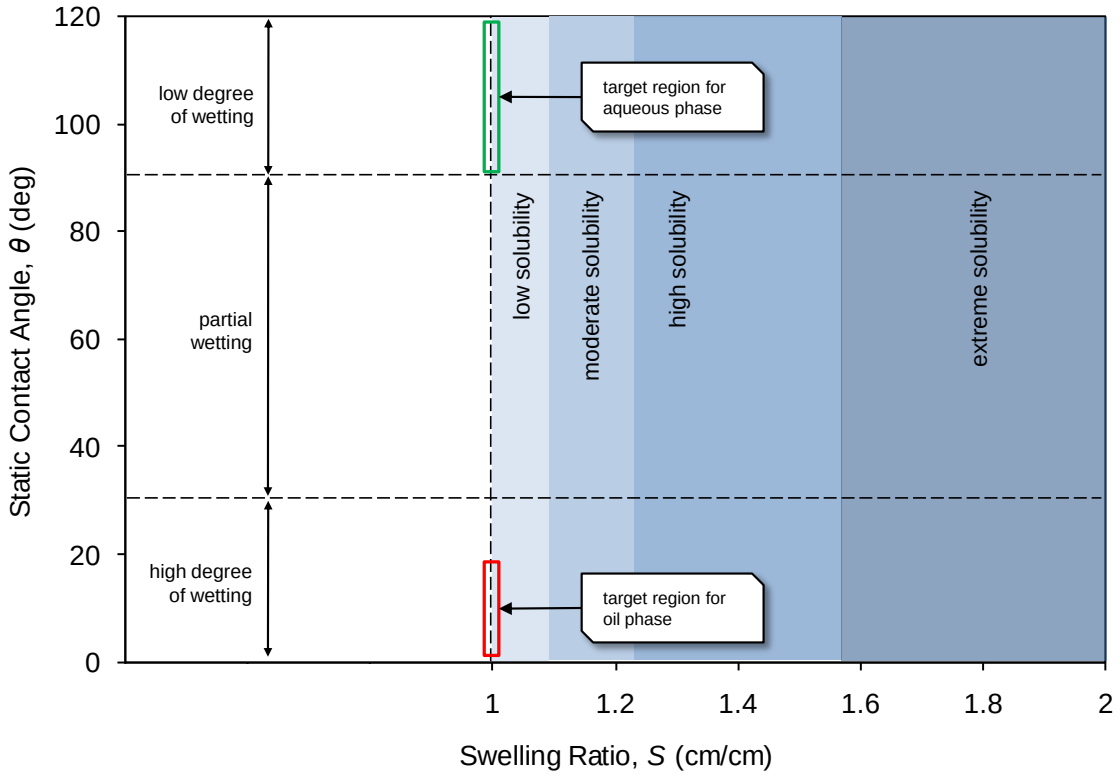

Figure 6.4: A material design space for selecting appropriate liquid and solid phases for encapsulated interface bilayers compares the tendency for each liquid phase to swell the supporting substrate versus its ability to wet the substrate surface. Regions of low, moderate, high, and extreme solubility are marked according to a study on the compatibility of various solvents with PDMS [179].

of both the liquid phases and the substrate material for creating encapsulated interface bilayers. Specifically, an ideal oil phase must freely wet the surface of the substrate such that the aqueous phase does not come into direct contact with the substrate. Said differently, the oil phase needs to have a low contact angle with the substrate while the aqueous phase should have a very high contact angle.

These two design criteria suggest that an ideal oil phase for creating stable encapsulated interface bilayers within PDMS substrates exists in a region near a swelling ratio of 1 and at contact angle values much less than 30^o. Additionally, the aqueous phase should have

a contact angle close to or above 100^o and a swelling ratio of 1 with this same material surface. Both target regions marked in Figure 6.4 provide a graphical means for interpreting the effectiveness of pair liquid phases and substrate materials.

Contact angle measurements on four varieties of PDMS samples provide quantification of the effect of each treatment (Figure 6.5). Native PDMS has a contact angle of water greater than 100^o [179], while both hexadecane and perfluorodecalin (PFD) have much lower contact angles of 23^o and 27^o, respectively. The effect of the plasma treatment used for PDMS bonding creates silanol (Si-OH) groups on the surface of the PDMS that results in a lower contact angle of water on the more-hydrophilic oxidized surface. Freshly plasma-oxidized PDMS can have contact angles for water as low as $10 - 30^o$ [179, 184], which is why plasma-treatment of PDMS channels for device bonding is commonly performed to promote wetting of aqueous solutions within microchannels. However, this hydrophilic surface reverts back to a more-hydrophobic surface upon exposure to air with contact angles approaching that of native PDMS within several hours. The measurements of contact angle for both plasma-oxidized and solution-oxidized PDMS conducted approximately 5 hours after initial oxidation still show reduced contact angles of $67 - 80^o$ for water. In contrast, the solution-phase silanization procedure produces a highly-hydrophobic fluorocarbon surface with water contact angles greater than 100^o and perfluorodecalin contact angles less than 5^o.

The images and contact angle measurements in Figure 6.5 confirm that without silanization, the aqueous phase is not greatly repelled from the plasma-treated PDMS surface. In the context of forming phase separated water-in-oil assemblies within PDMS microchannels, an aqueous phase that even partially wets the surface reduces the ability for the oil to reside between the aqueous phase and the PDMS, thereby preventing suitable lipid monolayer formation. By grafting the fluorosilane onto the PDMS, the contact angle water increases to that measured for native PDMS. But more importantly, silanization greatly increases

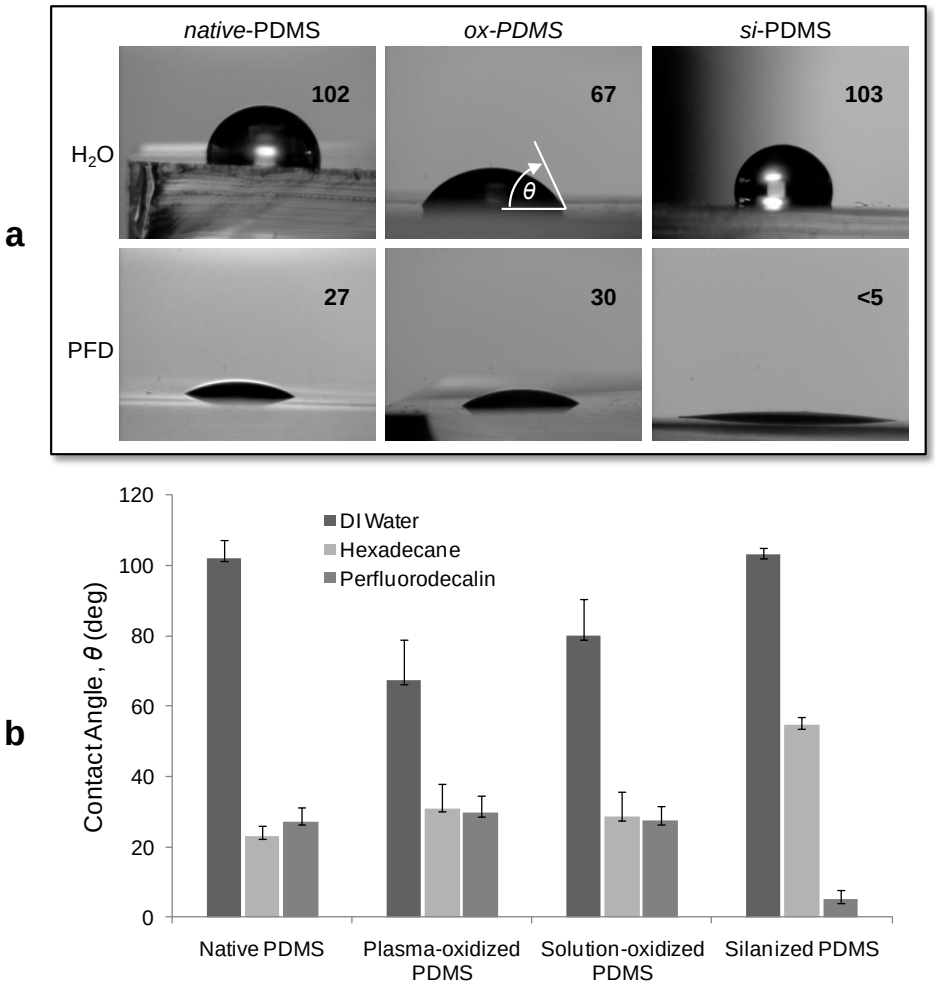

Figure 6.5: Contact angle measurements for water (H_2O), hexadecane, and perfluorodecalin (PFD) of the various types of PDMS provide quantitative differences for each surface treatment. The images illustrate that a lower contact angle results when a liquid wets, or spreads itself along a surface, while higher contact angles result in droplet beading (a). The silanization of the PDMS recovers a high contact angle for water, but more importantly it greatly increases wetting by the perfluorodecalin (b).

wetting by the perfluorodecalin needed for retaining a thin layer of fluorocarbon oil along the channel surfaces. The error bars shown in Figure 6.5 also indicate that this treatment produces a more uniform surface in comparison to the oxidized PDMS surfaces that become more hydrophobic over time.

Others have used silanization to achieve increased hydrophobicity of PDMS surfaces, but none with the intent to increase wetting by a fluorocarbon oil. Bhushan, et al worked with the same silane in studies to show that vapor phase deposition of silane on flat plasma-oxidized PMDS surfaces (not in channels) increases the hydrophobicity of the surface [185, 184]. In addition, Wang, et al demonstrated solution phase grafting of perfluoronated alkoxysilane on PDMS microchannels as an alternative to plasma-exposure for device bonding, but found that the silanization step produced weaker, reversible PDMS sealing [186, 187]. To overcome this drawback, others have demonstrated solution phase silanization after PDMS bonding (where the bond strength of plasma-exposed PDMS is irreversible) through a similar two step process with octadecyltrichlorosilane (ODTS) [188, 189] in PDMS devices used to produce aqueous plugs in flowing oil within the channels. The combination of methods and materials described herein specifically expands the use of PDMS materials for obtaining a hydrophobic surface suitable for stabilizing water-in-fluorocarbon oil assemblies in zero-flow applications, where the liquid phases are not replenished by continuous injection.

The measured contact angles on the various PDMS samples (native PDMS, Na-PDMS, oxidized PDMS, Ox-PDMS, and silanized PDMS, Si-PDMS) are plotted against known swelling ratios for each liquid in Figure 6.6 to emphasize the benefit of the silanization procedure. The earlier discussion concluded that ideal liquid phases should exhibit swelling ratios near 1 for both water and oil and that the substrate should be much more easily wet by the oil phase than the water phase. While a contact angle of $27 - 30^o$ indicates that perfluorodecalin wets the plasma-oxidized PDMS fairly well, a contact angle of approximately

70^o for water also means that an oxidized surface does not simultaneously repel the aqueous phase. After silanization, the contact angles for the perfluorodecalin and water are $< 5^o$ and $> 100^o$, respectively. Moreover, these data points fall on the $S = 1$ dashed line, since neither phase has a tendency to absorb into the material.

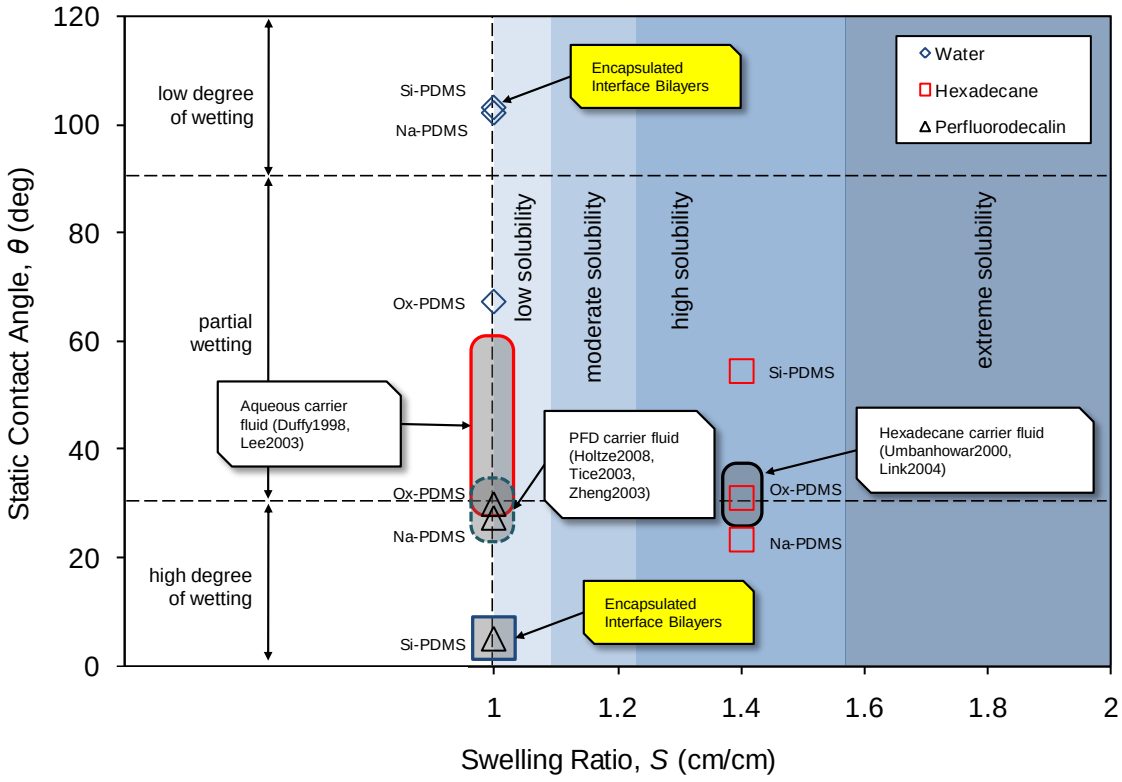

Figure 6.6: Measured contact angles for the three liquid phases on the various PDMS treatments are plotted against the respective swelling ratio, S, for each liquid in PDMS [179]. The results are compared to a variety of microfluidics work that use various carrier fluids within PDMS substrates in order to show that creating encapsulated interface bilayers within sealed PDMS substrates requires different operating conditions than when the liquid contents are flowed through the device. Common flow velocities of the carrier fluids used in these works ranges from $0.1 - 100$mm/s [174, 179, 190, 191, 192, 193, 194].

In comparison, operating regions for other microfluidic systems are also shown in Figure 6.6. Each block represents common operating conditions for three carrier fluids, water, hexadecane, and perfluorodecalin, that are in contact with the PDMS substrate. In each of these

cases, flow is present, therefore the liquid phase is continually replenished within the channels and, in the case of hexadecane, the fact that PDMS absorbs the oil is negligible—much like the work in Chapter 5 where hexadecane could be added as needed into the PDMS substrate. The ranges of acceptable contact angles ($25 - 60^o$) for these groupings also show that extreme wetting by the oil phase is not critical for applications that involve flow. However, in our case, where the contents are injected into the material once and subsequent bilayer formation is induced in a static (no-flow) condition, the interactions between the substrate and the two liquid phases are even more important. The silanization procedure allows us to meet this requirement for both the aqueous and oil phases—both have low solubilities in PDMS and the ratio of contact angles confirms that the oil will remain along the channel, separating the aqueous phase from the substrate.

6.3.2 Regulated Attachment Method

The formation of lipid bilayers in PDMS microchannels using RAM is based on principles of phase separation and self-assembly. In our previous work, hexadecane, which is known to readily absorb into PDMS, was used as the oil phase and the open design of the original RAM substrate allowed for additional oil to be added as needed in order to retain a sufficient amount of oil in the droplet compartments. The use of hexadecane in smaller, closed channels is not an option since the absorbed oil cannot easily be replenished. Therefore, a non-swelling perfluorocarbon solvent is selected to circumvent this limitation [179, 192]. After successive injections of perfluorodecalin and the aqueous lipid solution into the channel, the channel aperture is closed by moving a modified electrode holder laterally into the sample (Figure 6.7a). The aqueous solution is divided into separated volumes on either side of the closed aperture and excess oil in the channel fills in the evacuated space near the aperture (Figure 6.7b). The channel is reopened by moving the electrode holder away from the

sample following approximately $30 - 60$ seconds of stabilization time. A bilayer forms when the separated, lipid-encased volumes come into contact.

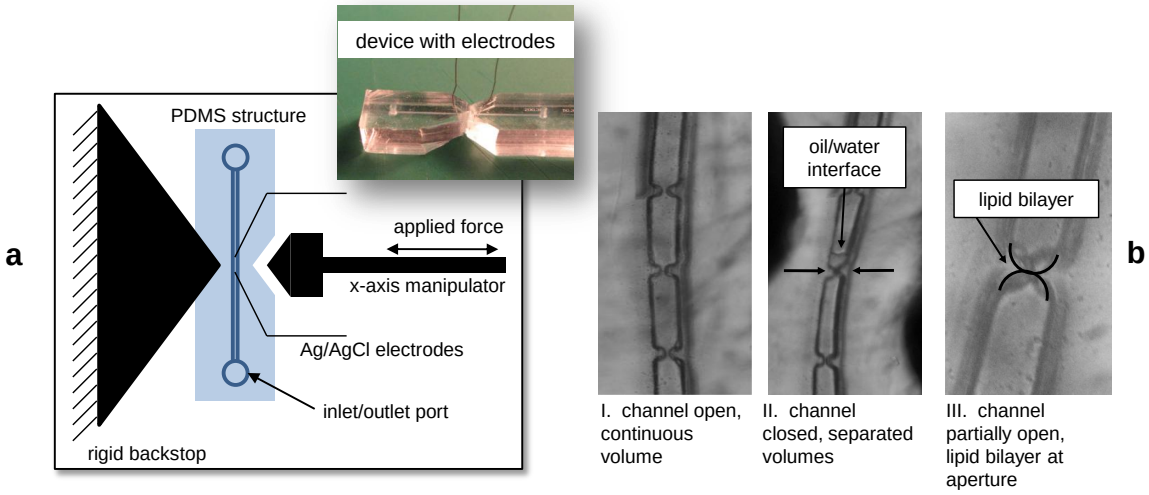

Figure 6.7: The regulated attachment method via an applied mechanical force (a) that closes the aperture separates the continuous aqueous volume (b.I) into adjacent aqueous plugs in the channel (b.II). A bilayer forms and then expands when the two plugs come into contact once the aperture is reopened (b.III).

Although the observed separation of the volumes consistently occurs at the point of the closed aperture, bilayer formation sometimes occurs away from this location, resulting in bilayers with areas nearly equal to the cross-sectional area of the channel. We attribute this shift in bilayer formation location to small pressure gradients that can exist along the length of the channel and which cause the solutions to flow slightly. In contrast to the treated channel surfaces, we observe that unmodified PDMS channels remain too hydrophilic following plasma bonding, causing the aqueous solution to sufficiently wet the channel surface. The injected aqueous solution completely evacuates the oil phase from the channel in this case, preventing separation of the aqueous phase from occurring upon aperture closure.

Real-time capacitance measurements provide quantitative evidence of bilayer thinning and subsequent expansion (Figure 6.8a) after initial contact of the separated volumes. A 10mV, 100Hz triangular voltage waveform is applied to the electrodes prior to bilayer formation with

the aqueous plugs separated. The amplitude of the measured square wave current (directly proportional to the capacitance of the interface) increases sharply due to an increase in capacitance that occurs when excess perfluorodecalin is removed from between the advancing aqueous plugs, allowing bilayer thinning. The capacitance of the bilayer increases to a steady-state value as the area of the thinned bilayer grows radially. Similar measurements on a stable lipid bilayer show that the areal size of the bilayer decreases and finally drops to the noise floor when the aperture is closed (see Figure 6.8b).

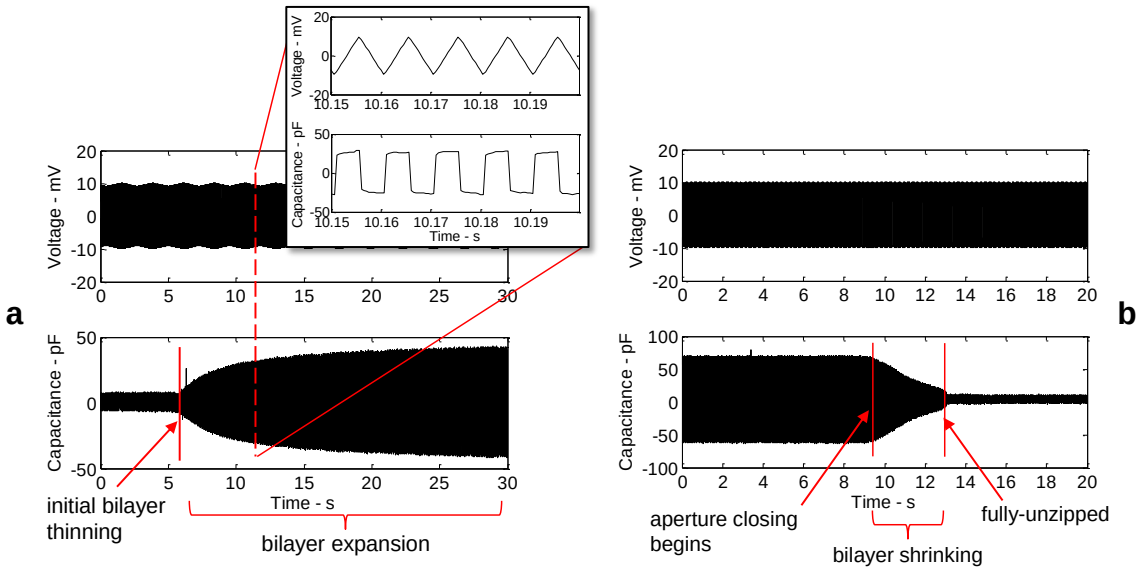

Figure 6.8: Both the attachment of separated plugs to form a bilayer when the aperture is opened (a) and the complete unzipping of a bilayer as the channel is re-closed (b) are recorded with real-time capacitance measurements.

6.3.3 Characterization of Encapsulated Interface Bilayers

Previous works with liquid-supported interface bilayers have used either decane or hexadecane for the oil phase [97, 98, 93, 101, 172, 157]. Perfluorodecalin is used in the study in order prevent unwanted absorption of the oil phase from the channel into the PDMS bulk, which not only depletes the necessary oil water interface for self-assembly, but can also cause

delamination of the bonded PDMS layers [179]. Reducing the tendency of the two PDMS layers to separate due to oil absorption is critical in this application since the substrates are additionally stressed by the applied force to open and close the apertures. Bilayers formed in perfluorodecalin form almost immediately after two lipid-encased aqueous volumes come into contact and then expand rapidly (see Figure 6.9a). Our own experience in forming droplet interface bilayers in hexadecane show that bilayer formation typically occurs after $1-2$minutes following initial droplet contact. We attribute this difference to the bulkier perfluorodecalin molecule that is more readily excreted from the hydrocarbon core of the bilayer [37]. The use of a bulkier solvent molecule likewise results in a lower lipid monolayer surface tension and larger contact angle, corresponding to the observed rapid expansion and larger final area of contact between adjacent aqueous plugs . As a result, we expect that bilayers formed in perfluorodecalin contain less solvent and are slightly thinner than those formed in smaller molecule solvents like hexadecane.

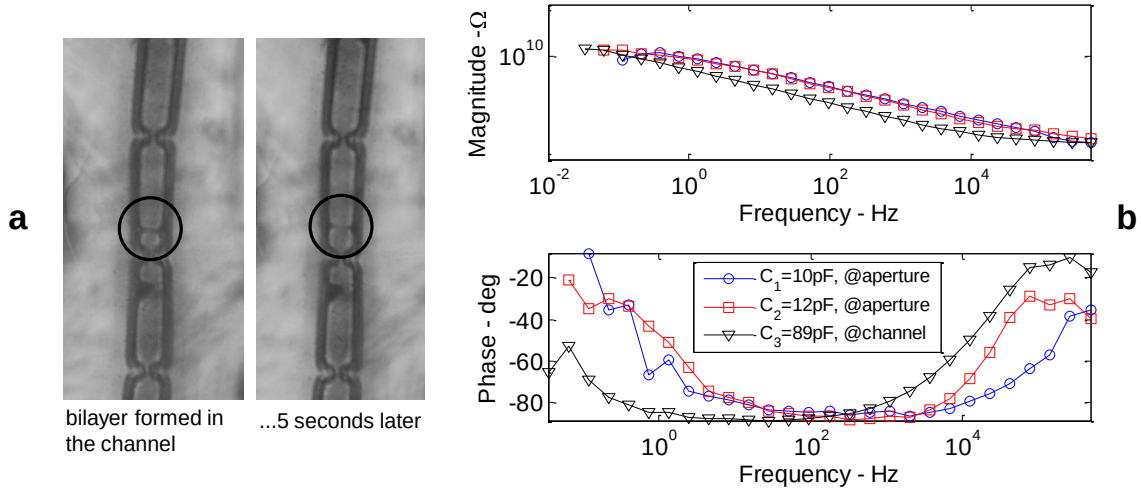

Figure 6.9: Rapid bilayer expansion is observed after the initial contact of lipid-encased aqueous plugs in perfluorodecalin (a). The magnitude of the electrical impedance of bilayers formed using RAM demonstrate the high resistance at low frequency associated with high-quality lipid bilayers (b). The range in estimated capacitance (proportional to the area of the interface) from the EIS data shows that bilayers can form across the partially open aperture or across the full channel.

Figure 6.9b shows the magnitude and phase of the measured impedance versus frequency for three bilayers formed within the PDMS substrates. The first two bilayers formed at the location of the aperture have estimated capacitance values of $10 - 12$pF. The third bilayer has a much larger capacitance of 89pF, indicating that the two separated aqueous solutions came into contact away from the constriction and were able to expand to a larger areal size. In general bilayers formed across the aperture have capacitance values ranging from $10 - 50$pF, while bilayers that stabilize in the main part of the channel have capacitances on the order of $80 - 200$pF. The measured electrical resistances for more than 20 different lipid bilayers formed in this fashion are all greater than 1GΩ, with a large percentage having values of resistance greater than 10GΩ. The failure potential for many of these membranes was also measured using cyclic voltammetry. The average measured failure potential of 243 ± 45mV ($n = 11$) compares well with measurements of unencapsulated droplet interface bilayers formed in hexadecane [141].

Electrical recordings of protein insertion using the AxoPatch200B/Digidata provide additional proof of bilayer formation and an indirect measure of the quality of the assembled membrane. Alpha-hemolysin (αHL, Sigma) proteins stored in 10mM MOPS, 100mM KCl (Sigma), pH7 buffer solution are incorporated into a 2mg/ml DPhPC vesicle solution prepared in the same buffer and this mixture is injected into the microchannel in PDMS. These proteins incorporate into the bilayer either through direct insertion from the aqueous lipid solution or via vesicle fusion events. Figure 6.10 shows the step-wise changes of $\pm$6pA in the measured current across the bilayer for an applied voltage of +40mV, corresponding to channel conductances of 150nS. The current shift of 11pA marks the insertion of two channels into the membrane. These values compare well to previously measured single channel alpha-hemolysin insertion events of $3 - 6$pA in 100mM KCl-based buffer solutions [166].

Single channel recordings are also conducted on encapsulated interface bilayers containing

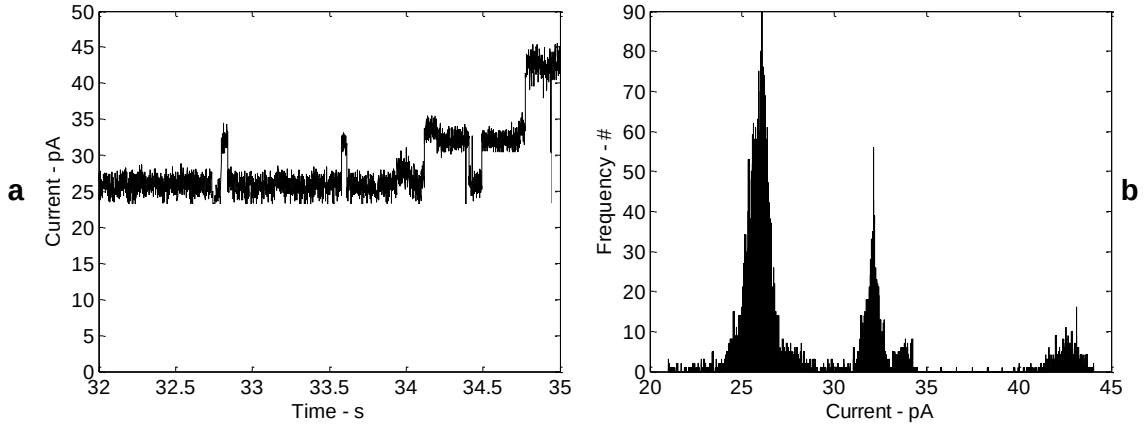

Figure 6.10: Current recordings and the corresponding histogram of αHL channels show the step-wise increases and decreases in current due to protein insertion and removal measured at +40mV (a-b). Measurements are obtained at a sampling rate of 5kHz and low-pass filtered at 1kHz with the AxoPatch/Digidata.

alamethicin proteins (Figure 6.11). As before, the protein molecules are incorporated into the aqueous lipid vesicle solution injected into the mircochannel. Alamethicin channels present on both sides of the membrane self-insert into the interface as monomers (single units) and then form conductive transmembrane channels as multiple monomers group together to form an oligomer [195, 167, 69]. The conductance of the aggregate is dependent on the number of molecules present, and single channel recordings of alamethicin exhibit rapid, step-wise changes in current due to the entrance and exit of individual monomers from an aggregate (Figure 6.11a). The current fluctuates between a closed state to several open conductance states of O_1 = 24pA, O_2 = 90pA, O_3 = 180pA, O_4 = 276pA, and O_5 = 380pA for an applied potential of +100mV. The corresponding conductance levels are less than but of similar relative size to those measured by Romer, et al and Wong, et al: $0.23 - 0.3$nS (O_1), $1.1 - 1.13$nS (O_2),$2.2 - 2.45$nS (O_3), $3.34 - 4.02$nS (O_4), and 5.93 (O_5) [69, 106]. We attribute the reduced conductance levels of each state to the presence of lipid vesicles in the aqueous solution that creates a solution conductivity slightly less than that of pure 500mM KCl.

Interestingly, the measured conductance levels for alamethicin channels formed with perfluorodecalin as the oil phase differ from those recorded for the same protein in DPhPC interface bilayers formed in the same electrolyte concentration with hexadecane in the original RAM substrate (Figure 5.6). It is suspected that these differences may stem from differences in either bilayer thickness or surface tension caused by the change in the oil phase [37], or due to deformation of the shape of droplets in the original RAM substrate that may affect interface tension. And though we did not perform a regimented study of how tension affects alamethicin conductance in this work, the physical state of the membrane is known to directly affect protein function [169] and, in the case of alamethicin, the gating behavior has been shown to be directly dependent on the tension of the membrane [168].

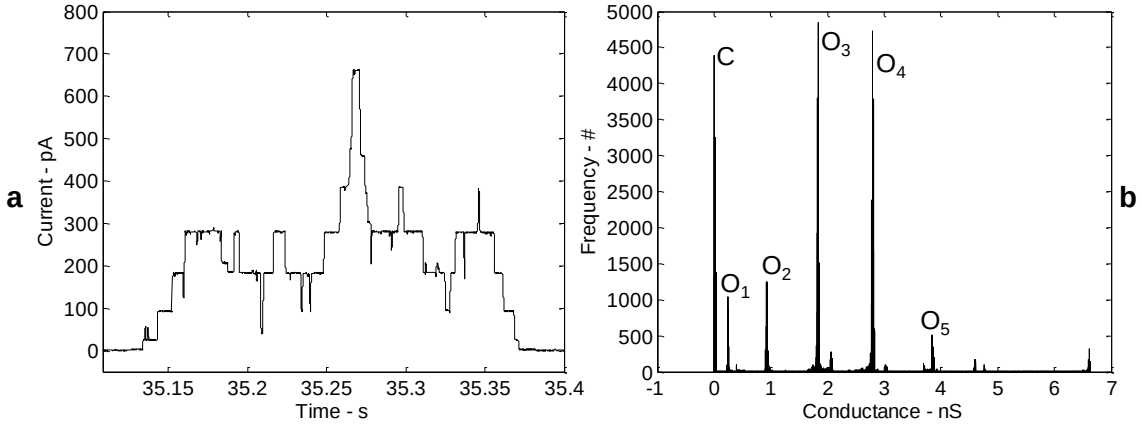

Figure 6.11: Current measurements of a bilayer containing alamethicin at 100mV (a) and the associated histogram of the distinct current levels (b) illustrate the voltage-driven, stepwise increases in current attributed to the formation of alamethicin oligomers that span the membrane. The aqueous lipid solution contains 100ng/ml of alamethicin incorporated into a 2mg/ml suspension of DPhPC vesicles in 10mM MOPS, 500mM KCl, pH7 buffer solution. Measurements are obtained at 250kHz and low-pass filtered at 1kHz using the AxoPatch200B/Digidata 1440A.

6.4 Comments on Durability of Encapsulated Interface Bilayers

Despite the measured quality of lipid bilayers formed within the sealed substrates, encapsulated interface bilayers demonstrate significantly shorter lifetimes than those formed using the regulated attachment method in the flexible PDMS substrate shown in Figure 5.1 that features an open design. We observe that encapsulated bilayers formed within the sealed PDMS substrates typically survive only $10 - 20$ minutes, whereas bilayers formed in the previous substrate consistently last several hours. And while the notion that physical encapsulation provides improved durability by increasing the packing factor of the aqueous volumes within the substrate, the observed durability of encapsulated interface bilayers, which have packing factors upwards of 80%, is limited.

The reduced durability is attributed to several factors that differentiate how the substrates used in this chapter interact with the liquid contents from the ways in which the prototype substrate introduced in Chapter 5 supported the contents. The primary difference stems from the fact that the liquid contents held in the microchannels are not open to air, and as a result, small pressure gradients that can develop within the channel are not canceled as readily, causing the contents to flow along the length of the channel. We observed that differences in pressure can arise from uneven levels of liquid contained in the inlet/exit ports that feed the channels as well as from the actuation of the pinch point, which locally collapses the channel and displaces the aqueous volumes. In this study, the inlet and exit ports were not fully-closed during testing which may have contributed to small differences in pressure along the length and the resulted in a shift in the bilayer location. A moving interface is potentially damaging to the bilayer since self-assembly processes along the oil/water interfaces must keep pace with the varying location of the membrane.

A second difference between these substrates and the previous design is the amount of oil that is retained between the aqueous volumes and the substrate. In Chapter 5, hexadecane was used as the oil phase and while this readily absorbs into the substrate, additional oil was added in order to provide a sufficient depth of oil within the substrate for submersing the aqueous droplets. In the sealed microchannels, retention of the oil phase is improved by silanization step through increased wetting by the fluorocarbon oil but is also decreased by the manner in which the contents are injected into the channel. The aqueous solution displaces a large percentage of the oil phase from the channel upon its injection into the channel, and so the amount of oil that separates the aqueous phase from the substrate is reduced. This has multiple consequences on durability: First, without a sufficient layer of oil, monolayer formation may be spotty resulting in a bilayer with compromised mechanical integrity. Secondly, less oil phase separation increases interactions of the bilayer with the substrate, which in effect produces a suspended bilayer instead of a durable liquid-supported interface. By retaining a thicker oil phase between the aqueous volumes and the substrate, we anticipate the encapsulated interface bilayers can exhibit durability similar to physically-encapsulated DIBs.

Our initial design was aimed at demonstrating that aqueous volumes need not be spherical droplets in order to create similar liquid-supported interface bilayers. However, this photomask design may have deviated too far from the previous geometry and, in doing so, introduced additional effects that mask the inherent durability of the system.

6.5 Chapter Summary and Conclusions

The concept of physically-encapsulated DIB networks was extended to fully-encapsulated biomolecular material systems featuring encapsulated interface bilayers formed within inter-

nal microchannels. This study highlighted several key differences in forming fully-encapsulated interface bilayers within enclosed compartments in PDMS as opposed to the initial high packing factor design discussed in Chapter 5. First, the ability to retain a fluid oil/water interface is not only critical for allowing proper separation of the aqueous solution but is a must for promoting adequate lipid monolayer formation needed for creating interface bilayers. Initial tests using hexadecane as the oil phase were quickly abandoned due to the loss of the oil from the channel through absorption into the PDMS. We observed in these trials that once the oil phase left the channel it led to delamination of the bonded PDMS halves used to make a sealed device, subsequently preventing the aqueous phase from being subdivided at the pinch point. These processes were further inhibited by the mildly hydrophilic surface of the channel walls produced during plasma-bonding.

A fluorocarbon oil, perfluorodecalin, was chosen to circumvent absorption of the oil phase into the bulk material of the substrate, though we found that surface effects of the substrate are equally important in retaining oil in the channel. A silanization step performed to decrease wetting of the aqueous phase on channel walls also greatly increased the wetting by the fluorocarbon oil, such that oil remains along the channel surfaces after introduction of the aqueous volume into the channel. These combined modifications proved successful in keeping enough oil in the channel to both separate and reattach aqueous volumes in the channel using regulated attachment. Furthermore, the bilayers formed at the perfluorodecalin/water interface exhibited similar properties to those measured in previous interface bilayer studies with hexadecane and were of high enough quality to examine single channel gating events for two different proteins. Unfortunately the observed durability of encapsulated lipid bilayers was not on par with other interface bilayer systems but we anticipate that with a more-appropriate design of the internal compartments and complete sealing of the internal volumes that encapsulated bilayers can experience significant gains in durabil-

ity. Even still, the demonstrated success of forming lipid bilayers completely within durable materials marks continued progress of the development of usable and efficiently packaged bilayer-based systems.

Chapter 7

Summary and Conclusions

7.1 Overview of the Research

The primary focus of the work presented in this document is to create new types of material systems that make use of the inherent functions of biomolecules. We started with the droplet interface bilayer (DIB) because this system exhibits key properties not found in other bilayer formation methods: simplicity, stability, and modularity. In short, droplet interface bilayer networks offer a unique method for constructing functional networks from active biomolecules, where the compositions and arrangement of the droplets determines the overall utility of the network. The goals of the work are to demonstrate that the primary limitations of the DIB method, the limited portability of such a liquid-in-liquid system and the need to independently dispense and arrange each droplet, can be overcome through *physical encapsulation* in a durable substrate.

The initial studies in Chapter 3 focused on developing the capability to form droplet interface bilayers using the methods developed by Holden, et al and establishing an understanding of

how the transport properties of interface bilayers can be tailored. In this work, a variety of electrical measurements on single droplet interface bilayers formed by incorporating the phospholipid molecules into either organic or aqueous phase provided comparative data on the electrical resistances and capacitances of the membranes, the current-voltage relationships of pure lipid interfaces, and the failure potentials of each method of assembly. Protein molecules, including alpha-hemolysin (αHL) and alamethicin, were added to the droplets in relatively high concentrations in order to show that the gross current-voltage characteristic of an interface can be altered with biomolecules. In an alternative approach, feedback control provided a novel means for controlling transport properties of DIBs. Feedback current control proved that ion current flowing through a lipid-only interface bilayer can be tailored using external control. This method provided limited results, with accurate current tracking occurring at frequencies less than 100mHz. The second application of control demonstrated that feedback voltage control can be used to generate a tunable voltage resonance across the bilayer. Both strategies coupled the electrical properties of the interface to the control gains for achieving a desired closed loop response.

In Chapter 4, the formation and characterization of physically-encapsulated droplet interface bilayers demonstrated that, through confinement of the aqueous volumes, more-portable DIB networks can be achieved. This work first introduced the concept of a substrate *packing factor* as a method for quantifying the differences in substrates that tightly confine droplets versus substrates like the one used by Holden, et al, which provided little support to the network and which had a packing factor of approximately 1% [98]. A high packing factor substrate ($> 30\%$) made from PMMA that features overlapping droplet compartments and integrated electrodes was fabricated for evaluating the effectiveness of increased droplet support. Droplet interface bilayers were formed by dragging and dropping individual droplets into neighboring compartments, where each droplet descends to the bottom of the com-

partment and sat on a fixed, wire-type electrode. The resulting interfaces were examined through electrical measurements in order to confirm that confinement (i.e. less oil separating the droplets from the solid substrate) does not adversely affect bilayer formation. Substrates containing physically-encapsulated DIBS were also subjected to a variety of handling conditions to qualitatively demonstrate the portability and durability of the confined droplet pairs. Quantitative shaking tests were also performed on both unencapsulated droplet interface bilayers and physically-confined DIBs in order to compare how the level of confinement affects the durability of the interface and the mode of interface failure.

Following our work with rigid acrylic substrates for physically confining DIBs, we found that the use of a flexible substrate has additional advantages. A high packing factor replica of the acrylic substrate used in Chapter 4 was made from PDMS, a soft silicone elastomer. The deformability of this material enabled the two droplet compartments to be fully separated by compressing the substrate with a mechanical force. We discovered that this action permits the formation of physically-confined droplet interface bilayers *in situ* by first separating a single aqueous volume through compression of the substrate and then reattaching the separated volumes by relaxing the applied force to open the dividing aperture. The results presented in Chapter 5 emphasized that interface bilayers form using RAM retain the same properties of unencapsulated DIBs, but with several additional aspects for controlling the formation process and final composition of the membrane. Namely, by modulating the applied force on the flexible substrate to control the dimensions of the dividing aperture, the size of the bilayer can be modulated reversibly. In the same fashion, the aperture can be fully closed after bilayer formation to completely unzip the attached lipid monolayers. This work also showcased that, with the aqueous volumes intimately confined by the flexible substrate, additional species can be added to a preformed DIB pair by delivery of discrete aqueous volumes containing the desired species through the oil phase. These “material

packets" incorporate their contents through coalescence with the monolayer-encased aqueous volume. Tests were performed to confirm that protein molecules can be added to a pure-lipid bilayer through the incorporation of alamethicin molecules from a lipid-free, external aqueous solution. Measurements of the bilayer both before and after the addition of these molecules demonstrated the change in composition of the membrane and confirmed that via controlled coalescence, species can be added to the network one element at a time and without causing bilayer rupture.

The research culminated in Chapter 6 where encapsulated interface bilayers were formed within fully-sealed PDMS substrates. This work builds on the use of physical encapsulation to support aqueous volumes surrounded by an oil phase and the regulated attachment method for *in situ* bilayer formation, marking a significant departure from the original DIB technique. Whereas physically-confined droplets in Chapter 4 could be fully enclosed within the substrate through the use of a solid cap, this work demonstrates that a fully-enclosed material system can be constructed to facilitate proper phase separation of the two liquid phases and bilayer formation completely within the closed material element. No longer are droplets first dispensed and arranged to form an interface. Instead, non-spherical aqueous volumes are subdivided and reattached locally within a fully-sealed material system for inducing bilayer formation.

Key aspects of this section of research were to identify suitable materials for preventing unwanted absorption of the oil phase and retaining a sufficient amount of oil in the channel upon injection of the aqueous solution. A non-swelling fluorocarbon oil, perfluorodecalin, was used to overcome the first challenge, while a silanization procedure produced a fluorinated surface on the channel walls increased wetting of the oil phase to maintain a fluid oil/water interface within the substrate. These modifications enabled proper phase separation within the substrates, allowing the regulated attachment method to be used to induce bilayer for-

mation at discrete locations within the channels. These experiments further revealed that bilayers formed within perfluorodecalin demonstrate high electrical resistance and the ability to support transmembrane proteins much like those formed with hexadecane in the original DIB method.

7.2 Conclusions

Physical encapsulation is used in this research to appropriately increase the interactions between the substrate and the aqueous volumes for added physical support while still allowing vital self-assembly processes to occur at the oil/water interface. This concept specifically asserts that by increasing the so-called packing factor of a substrate, a relationship of the degree of interaction between the substrate and the aqueous volumes, liquid phases can be constrained for building portable material systems and the substrate itself can even be used to manipulate the positions of the volumes contained within for *in situ* interface bilayer formation. Key conclusions of the work that support this thesis are provided below:

7.2.1 Characterizing and Tailoring Transport in Droplet Interface Bilayers

- We conclude from EIS and CV measurements that the incorporation of phospholipids as vesicles into the aqueous phase results in more complete and quicker lipid monolayer assembly at the oil/water interface surrounding each droplet. Electrical resistances of *lipid-in* DIBs are consistently greater than 10GΩ and failure potentials range from $|250 - 330|$mV, while those measured for *lipid-out* DIBs are quite lower.

- The current-voltage relationships of DIBs can be tailored with proteins that self-insert into liquid-supported interface bilayers from the aqueous phases. The type of protein determines the nature of the measured response. Alpha-hemolysin proteins, for example, demonstrate slight rectification at negative membrane potentials, while alamethicin proteins exhibit much greater forward rectification for positive potentials across the bilayer.

- The use of feedback control offers an alternative method for tailoring the transport of ions across an interface bilayer. This strategy couples the electrical properties of the membrane to tunable feedback control gains in order to adjust the closed loop performance of the system. As demonstrated, feedback current control of the flow of ions through an interface bilayer is limited to low driving frequencies, where the interface behaves like a pure resistor. However, results of feedback voltage control of a DIB showed that the potential developed across the bilayer can be driven at much higher frequencies ($10 - 100$Hz).

7.2.2 Physical Encapsulation of Droplet Interface Bilayers

- We conclude from electrical measurements made with fixed electrodes in the high packing substrate that even a $50 - 100\mu$m thick layer of oil around the droplets is sufficient for promoting lipid monolayer assembly needed for high quality bilayer formation.

- This study also proved that by restraining the droplets, more portable DIB networks can be achieved. Notably, physically-encapsulated droplet interface bilayers supported by a solid acrylic substrate can withstand considerable shaking and, when a solid cap is used to seal the liquid contents in the substrate, encapsulated DIBs can survive multiple inversions without loss of the bilayer interface.

- Lateral shaking tests demonstrated that liquid-supported DIBs can withstand $3-7$g of acceleration prior to failure of the interface. The organization of the lipid monolayers in these systems compared to lipid bilayers formed directly on a synthetic support shows that the continuity of the lipid monolayers provides increased bilayer resilience. We conclude that this continuity is key in establishing an assembly environment in which the bilayer has no limiting boundary condition. Instead, the monolayer within each leaflet of the bilayer merely continues to trace the perimeter of a given droplet.

- Unencapsulated DIBs arranged in a low packing factor substrate routinely failed as a result of relative motions of the connected droplets that led to complete separation of the droplets. We conclude from these observations that as the unconstrained droplets deform under acceleration, the increasing tensions of each monolayer overcome the energy that holds the bilayer together and act to unzip the interface.

- Confined droplets also fail at acceleration levels ranging from $3-7$g, though the mode of failure is bilayer rupture. Since the droplets are more-tightly restrained by the solid substrate, relative droplet motions and shape deformations that would otherwise lead to interface unzipping are minimized. Instead, a thinner oil phase surrounding the system reduces fluid damping, essentially stiffening the connection between the submerged droplets and the solid substrate. We conclude from these data that as more energy is transferred directly to the interface in physically-encapsulated DIBs bilayer rupture occurs as a way to minimize the total energy of the system.

7.2.3 Regulated Attachment Method for *In Situ* Bilayer Formation

- We conclude that flexible substrates, such as those made from PDMS, can be used to create confined systems of droplet interface bilayers using the regulated attachment method without the need for wire-type probes to be used for droplet positioning.

- Measured electrical resistances of $> 10\text{G}\Omega$ and single channel protein currents from αHL and alamethicin channels for interface bilayers formed in a flexible substrate suggest that RAM creates bilayers of similar quality to the original droplet interface bilayer.

- The regulated attachment method enables reversible control over the size of the interface formed between adjacent compartments. Bilayers ranging from approximately 70μm in equivalent diameter to more than 300μm show that, by adjusting the size of the aperture through a modulated mechanical force applied to the substrate, $20-30X$ changes in area and $4-5X$ change in equivalent diameter of the interface are possible within the high packing factor (30%) PDMS substrate.

- We conclude from the syringe tests in Chapter 5 that additional species can be successfully incorporated into preformed interface bilayers from an external aqueous solution. The images and data presented in Figure 5.8 demonstrate that small volumes of an external aqueous solution containing alamethicin proteins can be delivered through the oil phase and coalesce with preexisting lipid-encased aqueous volumes in order to change the composition of a preformed membrane. The voltage-dependent current-voltage relationship of the interface approximately 10 minutes after the adding contents confirms the incorporation of alamethicin molecules into the bilayer via delivery through the oil phase.

7.2.4 Encapsulated Interface Bilayers in Sealed PDMS Substrates

- Microfabrication techniques such as soft-lithography and silicon etching (DRIE) provides an alternative method for constructing flexible PDMS substrates that have internal compartments for housing biomolecular assemblies.

- The use of perfluorodecalin, which has a swelling ratio of 1 in PDMS, versus a traditional hydrocarbon oil such as hexadecane ($S \approx 1.4$) is an effective substitute for eliminating the absorption of the oil phase from the internal fluid compartments into the substrate bulk.

- A solution-phase silanization procedure of the internal surfaces of the substrate can be used to produce a hydrophobic PDMS surface following plasma-bonding. The specific treatment performed in Chapter 6 produced a fluorinated surface with a water contact angle of $> 100^o$ and a reduced perfluorodecalin contact angle of $< 5^o$. We conclude from these data that the silanization step is key to simultaneously minimizing the tendency for the aqueous phase to wet the substrate and maximizing the ability for the oil phase to wet the same surface.

- Encapsulated interface bilayers exhibit high electrical resistance values ($> 1\text{G}\Omega$) and average failure potentials of approximately $|240|$mV. Single channel measurements of αHL and alamethicin channels confirm a lipid bilayer structure at the interface. These results allow us to conclude that encapsulated interface bilayers can be formed within sealed PDMS substrates by using the regulated attachment method.

7.3 Contributions

The contributions of this research highlight the evolution of how interface bilayers are both supported and formed using concepts of physical encapsulation.

- External feedback control was demonstrated on droplet interface bilayers to provide tailored transport properties across the interface. This work is the first of its kind to affect biomolecular assemblies with established control methodologies.

- Physical encapsulation enables droplet interface bilayers formed in high packing factor substrates to have increased portability and durability. This contribution confirms that large-scale droplet support and undisturbed phospholipid assembly at the oil/water interface can be simultaneously balanced to provide increased usability of DIBs through more-intimate packaging.

- The durability of unencapsulated and physically-encapsulated droplet interface bilayers was quantified for the first time through a controlled set of mechanical shaking experiments. Both the level of acceleration that causes interface failure and the manner in which the interface fails (i.e. separation or rupture) was established per the different levels of packing factor.

- This work also demonstrated that interface bilayer formation at an oil/water interface can be performed *in situ* using the regulated attachment method. This concept takes advantage of a flexible substrate to manipulate the locations of the aqueous volumes, and even subdivide aqueous volumes into multiple volumes, by opening and closing an aperture in the substrate. Compared to the original DIB technique, RAM eliminates the need to dispense and arrange individual droplets. Furthermore, RAM provides unique control of the size of the bilayer and allows for the introduction of species

through the oil phase into preformed interfaces.

- Static water-in-oil emulsions are stabilized within sealed PDMS devices by using a fluorocarbon oil in tandem with a silanized channel surface. These combined modifications are crucial for simultaneously eliminating oil absorption into the bulk and maximizing wetting of the oil phase needed to retain oil in the channel during injection of the aqueous volume into the material. This contribution overcomes the tendency for PDMS substrates, which are widely used in constructing a variety of micro-scale devices, to absorb the oil phase in dual-phase systems.

- A final contribution of this work is the proof of encapsulated interface bilayer formation and characterization within a completely closed material element. High-quality interface bilayer formation and single channel recordings in perfluorodecalin is also demonstrated for the first time.

Appendices

Appendix A

Estimation of Bilayer Resistance and Capacitance from EIS Data

A.1 Methodology

The electrical resistance and capacitance of interface bilayers are extracted from electrical impedance spectroscopy data using an unconstrained nonlinear optimization process that minimizes errors between the measured data points and a simulated impedance response (given by Equation 2.5). Specifically, the *fminsearch* command in Matlab is used to determine optimal values of electrical resistance and capacitance that provide the best fit between the model and data. The optimization procedure requires an initial guess for each parameter and also a function that defines the error of the approximation. The fit error definition takes into account error in both the real and imaginary values of the impedance and uses a vector of weighing factors to allow for each measurement point to contribute equally to the entire fit [138].

The following example codes shows how data fitting using the described method is performed in Matlab. This same procedure is used through the dissertation for extracting bilayer properties from measured EIS data.

A.2 Top-level Script

```
clear all;clc;close all
path=cd;

%--------------------------- Experimental Data --------------------------
%Find all files that have .dfr file type for batch processing
D=dir([path,'\*.dfr']);
%Use the size of D to determine the number of .dfr files found
size_D=size(D);num_files=size_D(1);
%Create a vector of the filenames-useful for seeing order of processing
filename_vec=char(D(:,1).name);

%Initialize plot of the electrical impedance of fitted model guesses
figure(2);clf reset

%Run through the for loop for each .dfr file found
for jj=1:num_files
    %Name files:
    eval(['file',num2str(jj),'=D(',num2str(jj),',1).name;']);

    %-----------------------------------------------------------------
    %Extract data using 'read_dfr.m':
    eval(['data',num2str(jj),'=read_dfr(file',num2str(jj),');']);
    %-----------------------------------------------------------------

    %Assign names to frequency, magnitude, and phase data:
    eval(['freq',num2str(jj),'=data',num2str(jj),'(:,1);']);
    eval(['mag',num2str(jj),'=abs(data',num2str(jj),'(:,2)-j.*data',...
        num2str(jj),'(:,3));']);
    eval(['phs',num2str(jj),'=atan2(-data',num2str(jj),'(:,3),data',...
        num2str(jj),'(:,2))*180/pi;']);
    %Complex impedance:
```

```
eval(['Z',num2str(jj),'=data',num2str(jj),'(:,2)-j.*data',...
    num2str(jj),'(:,3);']); %Ohms

eval(['freq=freq',num2str(jj),';']);
eval(['mag=mag',num2str(jj),';']);
eval(['phs=phs',num2str(jj),';']);
eval(['Zexp=Z',num2str(jj),';']);

%---------------------------- Initial Guesses -------------------------
%Bilayer Resistance (Ohms):
Rblm=max(mag);  %use the maximum value of the magnitude
as the initial guess for bilayer resistance
%Bilayer Capacitance (F):
Cblm=400e-12;  %400pF is a reasonal guess for interface bilayers
formed in this work

%Electrolyte/Test Cell (Ohms):
Re=mag(1); %pick the first data point, since frequency
is swept from high to low during the measurement

%Frequency range (rad/s):
w=2*pi*freq; %this determines the frequency values
used to compare the model to the data
%----------------------------------------------------------------------

%[R(RC)] Electrical equivalent model
%----------------------------------------------------------------------
%Simulated response from 'model_def.m' using the initial guesses:
[Z_m0,mag_m0,phs_m0]=model_def(Rblm,Cblm,Re,w);
%Initial guess vector:
X0=[Rblm,Cblm,Re];
%Run 'fminsearch.m' to minimize error in 'error_def.m' by varying X
[Xf,err]=fminsearch('error_def',X0,[],w,Zexp);
%Compute the simulated impedance using optimized parameters:
[Z_fit,mag_fit,phs_fit]=model_def(Xf(1),Xf(2),Xf(3),w);
%----------------------------------------------------------------------

%Plot experimental data and fitted model
subplot 211;loglog(freq,mag,'b*-',freq,mag_fit,'ro-');
hold on
legend('Experimental Data','Model');ylabel('Magnitude - \Omega');
subplot 212;semilogx(freq,phs,'b*-',freq,phs_fit,'ro-');
```

```
    xlabel('Frequency - Hz');ylabel('Phase - deg');
    hold on

    %Compute approximate BLM area and equivalent diameter
    eval(['R_BLM(',num2str(jj),')=Xf(1)/1e9;']); %GOhms
    eval(['C_BLM(',num2str(jj),')=Xf(2)*1e12;']); %pF
    eval(['R_H20(',num2str(jj),')=Xf(3);']); %Ohms
    eval(['area_BLM(',num2str(jj),')=...
    (C_BLM(',num2str(jj),')/1e12)/c_blm;']); %cm^2
    eval(['diam_BLM(',num2str(jj),')=sqrt(area_BLM(',num2str(jj),...
        ')*4/pi)*1e4;']); %microns
end
%-------------------------------------------------------------------
%Display results in
fit_data=vpa([R_BLM' C_BLM' area_BLM' diam_BLM'],'5')
```

A.3 EIS Model Definition, *model_def.m*

```
function[Z,mag,phs]=model_def(R1,C1,R2,w);
%Impedance model [R(RC)]:
%
%Inputs:
%---------------------------
%1. R1 = resistance (Ohms)
%2. C1 = capacitance (Farads)
%3. R2 = resistance (Ohms)
%
%Outputs:
%---------------------------
%1. Z = complex impedance signature
%2. mag = magnitude of Z (Ohms)
%3. phs = phase angle of Z (deg)

Z=R1./(1+j.*w*R1*C1)+R2;
mag=abs(real(Z)+j.*imag(Z));
phs=atan2(imag(Z),real(Z))*180/pi;
```

A.4 Error Definition for Optimization, *error_def.m*

```
function[err]=error_def(X,w,Z_exp);
%
%Computes the norm of the square of error between experimental data
%(magnitude and phase) and the simulated response for 'model_def.m':
%       where,  Model 1: Z(w)=R2+(R1||C1);
%
%Inputs:
%-------------------------------------------------------
%1. X = initial guesses for [R1 C1 R2];
%2. w = frequency range (rad/s)
%3. Z_exp = measured complex impedance (experimental)
%-------------------------------------------------------
%
%Outputs:
%-------------------------------------------------------
%1. err = norm of the square of the error in magnitude and phase

%Experiment:
real_exp=real(Z_exp); %real part of experimental impedance
imag_exp=imag(Z_exp); %imaginary part of impedance


%Model:
R1=X(1);
C1=X(2);
R2=X(3);
[Z,mag,phs]=model_def(R1,C1,R2,w);
real_mod=real(Z);
imag_mod=imag(Z);

%Error Calculation:
err_real=(real_mod-real_exp).^2;
err_imag=(imag_mod-imag_exp).^2;
%weights (same weighting as used in Autolab, developed by:
%B.A. Boukamp, Solid State Ionics, Vol. 20 (1986), 31-44)
we=1./(real_exp.^2+imag_exp.^2);
err=we'*(err_real+err_imag);
```

Appendix B

Feedback Control of Droplet Interface Bilayers

B.1 Experimental Setup

Feedback control of droplet-interface bilayers requires the ability to continually compare a measured quantity (current or voltage) with a desired signal. The Autolab PGSTAT12, controlled externally, is used to produce and measure current and voltage during the study (Figure B.1). The feedback control algorithms for both integral current control and proportional-integral voltage control are computed in Simulink, and the appropriate control signals, in the form of voltages, are output to Autolab via a dSPACE CP1104, 4-channel control board. Autolab accepts the control signal and produces the appropriate voltage or current applied to the electrodes inserted into the droplets. The Autolab system is configured to also output voltage signals back to dSPACE that are proportional to the current flowing through the bilayer and the voltage across it in order to complete the feedback loop. It should be noted that during feedback current control, Autolab is operated in potentiostatic mode, regulating

the voltage across the membrane. During the feedback voltage control tests, Autolab is operated in galvanostatic mode, such that it regulates the current flowing through the bilayer, and a Tektronix 2630 Fourier Analyzer is used to compute the frequency response functions of the closed-loop system. A 50mV (RMS) random white noise voltage is generated by Tektronix and added to the bias potential created in Simulink for exciting the bilayer systems. Closed-loop transfer functions are recorded with 5kHz sampling rate in dSpace and consist of 10 averages of 1024 frequency points within the tested range. Also, an Ithaco 4302 low pass filter (4-pole Butterworth filter) with a cutoff frequency at 50Hz is used to filter noise from the voltage signal proportional to the measured current only during feedback current control.

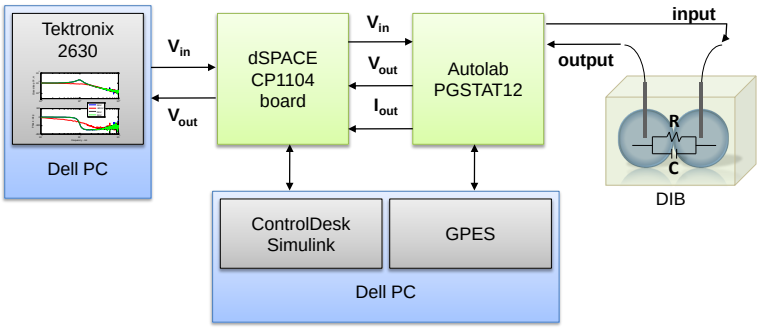

Figure B.1: Schematic of the equipment and software used for feedback control of droplet-interface bilayers. The Tektronix 2630 was used for measuring frequency response functions of the bilayers only during closed-loop voltage control.

B.2 Compensator Design for Integral Current Control

The goal in feedback current control is to minimize the error between a desired current signal and the current flowing through the membrane (Figure 9). The transfer function of the integral controller is

$$K(s) = \frac{K_I}{s} \tag{B.1}$$

where, K_I is the integral gain used to increase or decrease the control authority and s is the Laplace variable. Since the input to the system is an applied voltage and the output is a current flowing through the bilayer, the plant is described by the electrical admittance, $Y(s)$, of the system. The electrical impedance, $Z(s)$, of two-droplet network written in the s-domain, which is modeled as a resistor, R, and capacitor, C, connected in parallel for the bilayer in series with a resistance, R_e, for the aqueous solution, is given by

$$Z(s) = [R||C] + R_e = \frac{R}{1 + j\omega RC} + R_e. \tag{B.2}$$

Simplifying the expression for electrical impedance, gives

$$Z(s) = \frac{As + B}{1 + j\omega RC} \tag{B.3}$$

where, $A = R_e = R = C$, $B = R + R_e$, and $Z(s) = 1/Y(s)$. Therefore, the admittance of the system can be written as

$$Y(s) = \frac{1 + j\omega RC}{As + B} \tag{B.4}$$

The transfer function for the 4-pole, low-pass Butterworth filter with a cutoff frequency at 50Hz is

$$F(s) = \frac{\alpha_0}{s^4 + \alpha_3 s^3 + \alpha_2 s^2 + \alpha_1 s + \alpha_0} \tag{B.5}$$

where, the coefficients that were determined experimentally are $\alpha_0 = 9.741 \times 10^9$, $\alpha_1 = 8.102 \times 10^7$, $\alpha_2 = 3.370 \times 10^5$, and $\alpha_3 = 820.9$.

The closed-loop transfer function for integral control, $H_I(s)$, is

$$H_I(s) = \frac{F(s)\,Y(s)}{1 + F(s)\,K(s)\,Y(s)} = \frac{K_I(1 + sRC)}{As^2 + Bs + F(s)\,K_I(1 + sRC)} \tag{B.6}$$

The selection of the K_I gain determines how much control effort is afforded in order to drive the actual current toward the desired current. Simulated closed-loop responses were generated using Equation B.6 and compared with current measurements performed at five frequency points.

B.3 Compensator Design for Proportional-Integral Voltage Control

Feedback voltage control of droplet-interface bilayers demonstrates that the natural dynamics of lipid membranes can be modified to provide desired closed-loop dynamics such as damping ratio and natural frequency using pole-placement. The plant in this case is the electrical impedance, $Z(s)$, given in Equations B.2 and B.3. Proportional-integral (PI) control applied to the impedance of the bilayer, creates a second-order closed-loop system, that can be characterized by a natural frequency, ω_n, and damping ratio, ζ. The transfer function of a PI controller is defined as

$$K_{PI}(s) = K_P + \frac{K_I}{s} \tag{B.7}$$

where, K_P is the proportional gain and K_I is again the integral gain. Since the plant is defined by the electrical impedance of the bilayer system, the closed-loop transfer function, H_{PI}, can be written as

$$H_{PI}(s) = \frac{K_{PI}(s)\,Z(s)}{1 + K_{PI}(s)\,Z(s)} \tag{B.8}$$

and then expanded, using the relations in Equations B.3 and B.7, to

$$H_{PI}(s) = \frac{AK_P s^2 + (AK_I + BK_P)\,s + BK_I}{(RC + AK_P)\,s^2 + (AK_I + BK_P + 1)\,s + BK_I} \tag{B.9}$$

The characteristic equation that defines the closed-loop dynamics of the system is

$$s^2 + \left(\frac{AK_I + BK_P + 1}{RC + AK_P}\right)s + \left(\frac{BK_I}{RC + AK_P}\right) = 0 \tag{B.10}$$

where,

$$2\zeta\omega_n = \left(\frac{AK_I + BK_P + 1}{RC + AK_P}\right) \tag{B.11}$$

$$\omega_n^2 = \left(\frac{BK_I}{RC + AK_P}\right). \tag{B.12}$$

Equations B.11 and B.12 relate the electrical parameters of the DIB network as well as the two gains for the controller, $K_{PI}(s)$, to the natural frequency and damping ratio of the closed-loop system. These expressions can also be written in matrix form

$$\begin{bmatrix} \omega_n^2 A & -B \\ 2\zeta\omega_n A - B & -A \end{bmatrix} \begin{bmatrix} K_P \\ K_I \end{bmatrix} = \begin{bmatrix} -\omega_n^2 RC \\ 1 - 2\zeta\omega_n RC \end{bmatrix} \tag{B.13}$$

where, the control gains can be computed for measured electrical properties of the DIB network and for desired closed-loop natural frequency, ω_n, and damping ratio, ζ. Analytical expressions for the two control gains are given by

$$K_P = \frac{\omega_n RC\left(2B\zeta - A\omega_n\right) - B}{A^2\omega_n^2 - 2\zeta\omega_n AB + B^2} \tag{B.14}$$

and

$$K_I = \frac{\omega_n^2\left(RCB - A\right)}{A^2\omega_n^2 - 2\zeta\omega_n AB + B^2} \tag{B.15}$$

Equations B.14 and B.15 illustrate that feedback control can provide a way to tailor the closed-loop electrical impedance of droplet-interface bilayers. The connection between the closed-loop dynamics and the electrical properties of the membrane for fixed control gains makes it possible to detect changes to the resistance and capacitance of the membrane due to lipid packing and/or ion channel insertion. Values for K_P and K_I are computed for each bilayer system and for prescribed values of damping ratio and natural frequency.

Appendix C

Chemical Encapsulation of Droplet Interface Bilayers

A supplementary study is presented on the viability of achieving complete encapsulation of droplet interface bilayers through *chemical encapsulation*. Unlike physical encapsulation (see Chapter 4) where aqueous droplets are completely surrounded by a thin layer of oil contained within in a solid substrate, chemical encapsulation substitutes the oil phase for a curable material system to form a solid material around the network. In this approach, encapsulated biomolecular networks are achieved by first dispensing and arranging aqueous droplets to form a desired DIB network in the liquid precursor and then the exterior phase is cured solid. While the end result of achieving durable, encapsulated biomolecular networks is not been realized using this approach, some success is demonstrated and so the findings are presented.

In this appendix, several curable material systems are identified and then tested for their ability to enable DIB formation and then cure in a manner that leaves the DIBs intact. An initial set of criteria is established for guiding candidate material selection. Finally, a revised

set of criteria for candidate curable materials is then derived from the results of the study.

C.1 Identification of Candidate Curable Materials

Criteria that candidate materials must meet for possible substitution of the oil phase are first defined. These physical attributes help to determine the ability whether or not a candidate curable material first will allow for droplet formation and phospholipid self-assembly and then remain completely phase separated during material solidification (polymerization). The following list outlines the key attributes a material system must meet:

- Miscibility/Hydrophobicity - The formation of droplet-interface bilayers first requires that the surrounding medium be nonpolar and immiscible with water. Otherwise the necessary phase separation can not occur and there would be no "oil/water" interface to support lipid monolayer self-assembly. An ideal a candidate material is hydrophobic both before and after curing.

- Viscosity - A low viscosity of the prospective curable phase is needed to enable droplet positioning during network arrangement and then promote the removal of the "oil" phase from between opposing monolayers upon bilayer formation.

- Density - Candidate material systems must have a density less than or equal to that of the aqueous droplets (1 g/ml) in order to prevent droplets from surfacing prior to curing of the exterior phase.

- Curing Temperature - Phospholipid molecules undergo phase transitions in which they transition from a liquid crystalline state to more fluid phases. As a result, the ability to induce and achieve complete curing of the encapsulation phase at room temperature

helps to maintain stability of the bilayers in addition to reducing protein denaturation that can occur at elevated temperature.

Additional considerations for material selections include optical transparency to allow for visual droplet positioning, desired mechanical properties of the cured encapsulant, and the effect of the curing initiator (heat, UV, chemical) on the assembled biomolecules.

C.2 Candidate Materials

Silicone-based polymeric materials form basis of the material set initially tested for chemical encapsulation of droplet-interface bilayers. Polydimethylsiloxane (PDMS) materials are commonly used in a variety of microfluidics applications [175, 176] where through soft-lithography processing, this conforming elastomer can be used to create sub-micron features. McDonald and Whitesides highlighted many of the advantageous qualities of PDMS for use in microfluidics applications including: optical clarity (transparent down to 240nm), low electrical (breakdown voltage of 2×10^7 V/m) and thermal conductivities, low surface energy (≤ 20 dyn/cm), negligible water absorption, inertness, and non-toxicity.

Many of these properties, namely the natural hydrophobicity, low-density, and optical transparency, make PDMS-based materials good candidates for encapsulating DIBs. While others have also shown that perfluoropolyethers (PFPEs) have many of the same qualities as PDMS with an added resistance to organic solvents [165], the more-dense PFPE materials ($1.5-2.0$ g/ml) are considered to be too heavy for chemically-encapsulating aqueous droplets (PDMS-based materials have densities less than 1.2 g/ml).

Table C.1 provides a complete list of curable materials chosen for this study. The material names, along with key physical attributes and curing information are presented in the order

of testing.

Table C.1: Candidate silicone-based materials for encapsulating droplet interface bilayers

Number	Product	Vendor	Material Description	Density (g/ml)	Viscosity (cP)	Molecular Weight (g/mole)	Curing Mechanism	Comments
1	Sylgard 184	Dow-Corning	2-part, 10:1 (w:w) of monomer to curing agent, monomer is a vinyl-terminated PDMS that crosslinks via a platinum addition reaction	1.10	3500		addition curing reaction, curing occurs in ~24h @ R.T., 1 hour @ 90°C	One of the most widely-used PDMS elastomers in the literature
2	SS5293	Silicone Solutions	1-part (dual cure) PDMS, no chemical structure provided	1	400-800		dual cure: UV, moisture cure in shadowed areas	
3	DMS-U21	Gelest, Inc	(3-Acryloxy-2-hydroxypropoxypropyl) Terminated PolyDimethylsiloxanes-terminated PDMS, CAS: 128754-61-0	0.99	60-140	600-900	UV-cure with the addition of 1% w/vol of diphenyloxymethacrylate (DPMA) or benzophenone dissolved in xylene	Curing with an LED UV source (@365nm) occurs in less than 20 seconds
4	DMS-R05		Methacryloxypropyl Terminated PolyDimethylsiloxanes, CAS: 58130-03-3	0.97	4-6	380-550		Curing with an LED UV source (@365nm) occurs in less than 1 minute
5	DMS-R11		Methacryloxypropyl Terminated PolyDimethylsiloxanes, CAS: 58130-03-3	0.98	8-14	900-1200		
6	DMS-R18		Methacryloxypropyl Terminated PolyDimethylsiloxanes, CAS: 58130-03-3	0.98	50-90	4500-5000		
7	DMS-V00		Vinyl Terminated PolyDimethylsiloxanes, CAS: 68083-19-2	0.81	0.7	180	addition cure with the addition of a crosslinker and platinum catalyst	

C.3 Evaluation Methodology

Each candidate material is evaluated on the basis of whether it allows for droplet dispensing and arrangement and lipid monolayer assembly and bilayer formation. Single, *lipid-in* droplet interface bilayers are formed from two, 300nl aqueous droplets using the protocols established in Chapter 3 for forming DIBs in a machined well filled with the liquid precursor (uncured). The standard set of electrical impedance spectroscopy (EIS) and cyclic voltammetry measurements (CV) used to verify and characterize DIBs in hexadecane is again used in this study in the cases where stable droplet interface bilayers are achieved. For multi-part precursors such as Sylgard 184, the monomer and curing agent are mixed thoroughly by hand prior to droplet submersion and attempted bilayer formation.

While several of the candidate curable materials are two-part systems that cure at room temperature, several of the materials undergo an ultraviolet light-triggered (UV) polymerization step. A hand-held, LED-powered UV light source (LED-100, Electro-Lite Corp.) is

used to polymerize UV-curable materials during this study. The device emits UV light at a constant wavelength (365nm) and intensity (1mW/cm^2 at the bulb) for durations ranging from $20 - 300$ seconds.

C.4 Chemical Encapsulation Results

The results of this study are presented in the order of the tested candidate materials. Electrical measurements are provided for those material systems that allow the formation of a DIB.

C.4.1 Sylgard 184

The first material system investigated for encapsulating droplet interface bilayers is the two-part silicone elastomer Sylgard 184 (Dow-Corning) which cures via a platinum addition reaction at room temperature. Hexadecane (Sigma) is added to Sylgard 184 (10:1 w:w monomer:curing agent) in order to reduce the viscosity and density of the uncured elastomer. A 32%:68% volume ratio of hexadecane:mixed Sylgard provides a solution with an approximate viscosity and density of 210cP and 0.997, respectively, which allowed for the submersion and arrangement of the aqueous droplets. This relative hexadecane quantity is the minimum amount required to achieve a specific gravity less than of water. Larger amounts of the organic solvent further reduce density and viscosity with the trade-off of increased curing time.

A droplet-interface bilayer was formed during one of the first trials using this material and survived the $1 - 2$ day curing schedule at room temperature. Electrical impedance spectroscopy measurements via silver-silver chloride electrodes inserted into each droplet confirm

the presence of the interfacial lipid membrane and are used to track changes to the bilayer during cure at room temperature (Figure C.1). Specific membrane resistance (MΩ·cm^2) and equivalent membrane diameter (μm) obtained from the EIS measurements provide information about the quality and size of the interface, respectively. A specific membrane capacitance of 0.6μF/cm^2 [140, 98] is used to approximate the areal size of the interface.

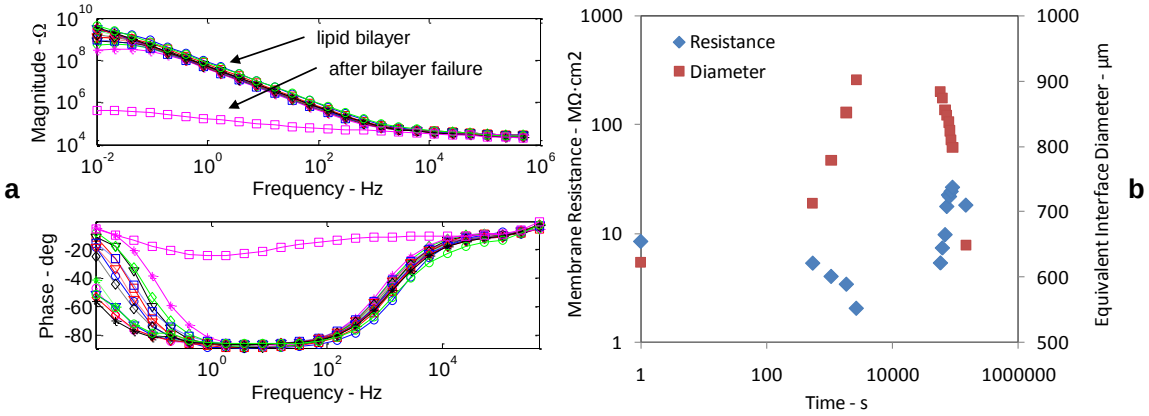

Figure C.1: Magnitude and phase of the electrical impedance of a bilayer lipid membrane formed at the interface of droplets submerged in PDMS/hexadecane curable fluid (a). Specific membrane resistance (MΩ·cm^2) and equivalent interface diameter (μm) values versus time for a droplet-interface bilayer formed in a curable PDMS/hexadecane solution (b).

The electrical impedance measurements of the membrane during the curing of the PDMS/hexadecane mixture indicate that the size of the bilayer increases in the first few hours after BLM formation and then reduces in size later during cure. This change in area is also confirmed by a decrease in the resistance of the membrane in the first few hours as well as the visible increase in the size of the interface (Figure C.2.

The data and the images both confirm that as the PDMS cures the droplets "zip" together further to produce a larger interface. As this occurs, the measured capacitance increases while the resistance of the membrane lowers. The increase in resistance and decrease in interface size later in the curing duration are attributed to shrinking in the PDMS that may have exerted a compressive, separating force on the droplets. The bilayer interface survived

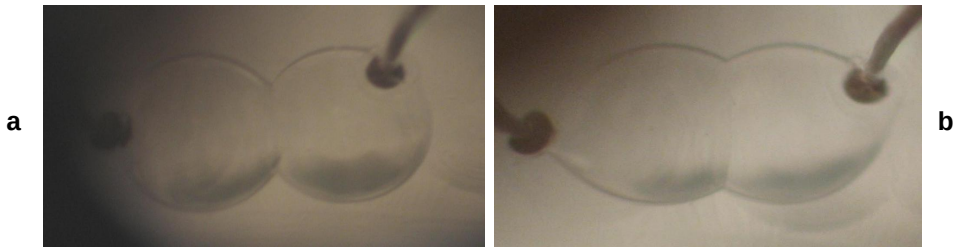

Figure C.2: Photographs taken through the eyepiece of a low-power stereo microscope show that the bilayer size (a) grows to a significantly larger interface (b) during the 2-day cure schedule.

the entire room temperature curing period and only ruptured when until it was attempted to sever the electrodes from their holders in order to move the cured sample. The last EIS measurement confirms the rupture of the bilayer shown in the greatly-reduced low-frequency impedance response.

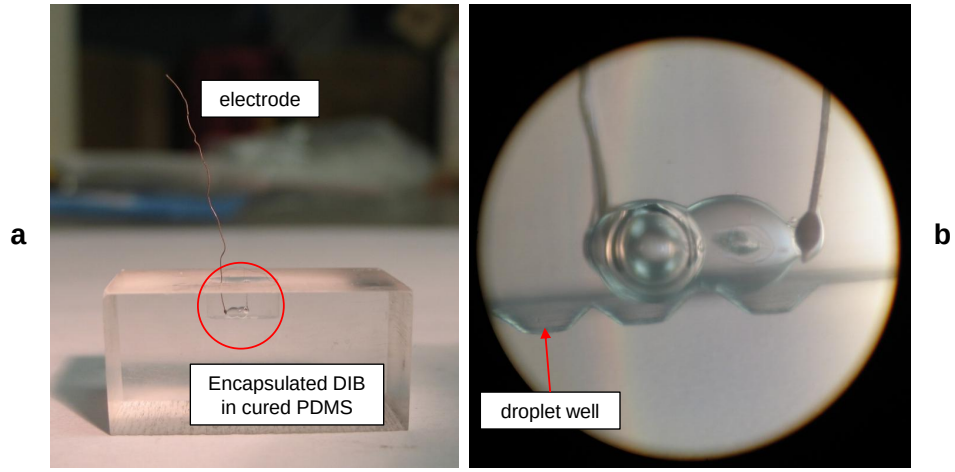

Figure C.3: Side view images of a chemically-encapsulated droplet interface bilayer pair after interface failure show the internal space within the cured PDMS occupied by the droplets. An air bubble was introduced into the internal volume upon removing an electrode (b).

Figure C.3 provides additional views of the cured PDMS/droplet material system. The cured PDMS creates a clear, solid material that intimately traces the profile of the connected droplets. The images also show the as the interface grew larger prior to the setting (upon which the viscosity of the curing material no longer permitted droplet motion), the

two droplets pulled away from the electrodes and lift out of the machined droplet wells (Figure C.3b). The miscibility of the hexadecane in Sylgard precursor resulted in a homogeneous, rather than phase-separated, encapsulating material. This observation agrees well with published data that indicates hexadecane also readily absorbs into cured PDMS of the same type [179].

Incorporation of alamethicin into DIBs in PDMS

In a subsequent trial, alamethicin channels were incorporated into the aqueous lipid vesicle solution encapsulated in a mixture of hexadecane/PDMS. After demonstrating the formation and survival of a DIB formed within a mixture of PDMS and hexadecane, it was desired to demonstrate protein activity in order to further verify that the interface is a lipid bilayer. Alamethicin proteins (1μg/ml alamethicin in 10mM MOPS, 100mM NaCl, pH7) are added to the lipid vesicle solution ($1 - 2$mg/ml DPhPC vesicles in the same buffer) at a $1:1$ volume ratio to produce a final protein concentration of 500ng/ml (comparable to the level used in Chapter 3). As before, a single droplet interface bilayer is formed in a liquid mixture of hexadecane and mixed PDMS precursor. Following an initial impedance measurement to verify formation, CV data confirms protein insertion (Figure C.4).

The data in Figure C.4b shows that at potentials less than approximately -20mV, the proteins create pathways for ion conduction through the membrane which is measured directly as an increase in electrical current. This measurement indicates that the high electrical impedance measured between the droplets is not a thin film of curable material, but rather a fluid lipid membrane capable of hosting proteins for the regulation of ion conduction and controlled transport of species between droplets. The bilayer formed in this experiment ruptured within $30 - 40$ minutes after formation.

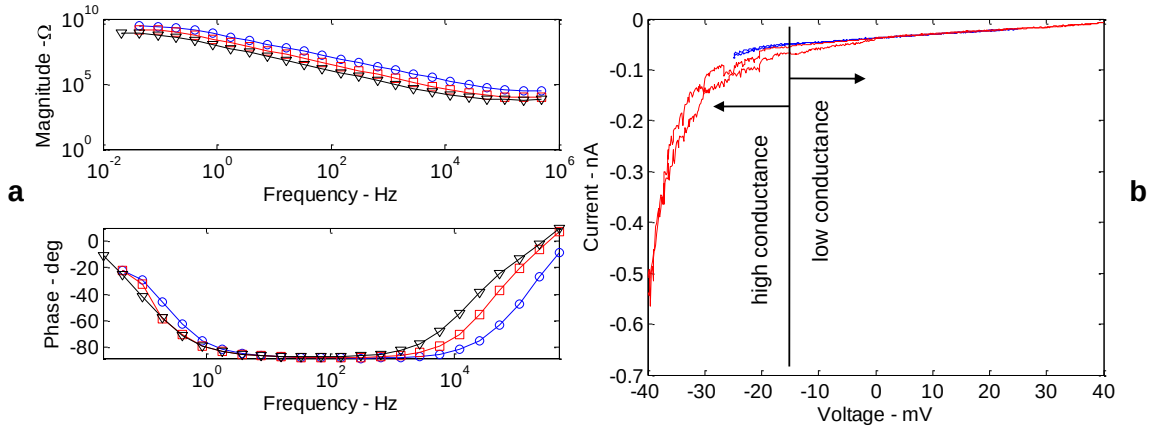

Figure C.4: EIS (a) and CV (b) measurements indicating the formation of a DIB and presence of functioning proteins within a bilayer encased in PDMS.

This preliminary study confirms the ability to form droplet-interface bilayers within a curable surrounding material matrix, however all subsequent trials ended in bilayer rupture before the PDMS cured. It was observed that the droplets zipped together quickly in each of these trials, producing a large, unstable interface that eventually ruptured within the first hour after formation. Following a set of experiments in which the ratio of PDMS to hexadecane was varied, it was determined that the relatively large molecule of the PDMS monomer (compared to that of hexadecane) results in the rapid growth and consistent rupture of DIBs formed in PDMS mixtures. This result is consistent with a study performed by Needham and Haydon in 1983 in which they correlated the size of the surrounding solvent molecule to the surface tension of the lipid bilayer and the contact angle of a lens of organic solvent trapped on the surface of a lipid bilayer [37]. The growth of the interface of DIBs formed in PDMS mixtures is attributed to the lowered surface tension of the lipid monolayer that allows the droplets to zip together further in order to balance the energy of London van der Waals forces exerted by water molecules on opposite sides of the bilayer [133, 135, 37]. Observations from experiments using large-molecule solvents consistent show that as the size of the interface grows, the likelihood of membrane rupture also increases. Furthermore,

we attribute the single success to the fact that the two electrodes used for positioning and measurement likely anchored the droplets just enough to prevent additional zipping and/or bilayer failure.

C.4.2 Additional Curable Materials

In favor of brevity, the first material set was the only system to result in successful chemical encapsulation of droplet interface bilayers within a cured, solid matrix.

The first (and only successful) attempt to encapsulate DIBs in Sylgard 184 provided initial encouragement that DIB networks can be formed in a curable matrix. However, all subsequent trials resulted in bilayer rupture prior to complete PDMS polymerization. The image in Figure C.2 shows that after the initial formation, the droplets continue to "zip" together, forming a noticeably larger interface and pulling the droplets away from the fixed electrodes. While subsequent and parallel studies of the effect that solvent molecule size plays on the equilibrium dimension and stability of the resulting lipid interface explain the observed change in interface size, it is the presence of the fixed electrodes that prevented further bilayer thinning and eventual rupture, leading to the success of this trial.

The motivation for moving away from the Sylgard to other curable materials was to identify a material that could be cured more quickly (see Table C.2). In this way, it was thought that the DIB network can first be assembled and then locked in place before the interface grows too large or fails. However, both the preformulated SS5293 and the functional acrylate- and methacrylate-terminated PDMS monomers from Gelest demonstrate the importance of hydrophobicity in the uncured state as these materials either cure locally in the presence of water or prevent the necessary lipid self-assembly required for DIBs.

The vinyl-terminated PDMS from Gelest allows for consistent formation of droplet-interface

Table C.2: Results of material evaluation study

No.	Name	Description	Curing Mechanism	Result	Comments
1	Dow Sylgard 184/hexadecane	2-part vinyl-terminated PDMS (10:1 base: curing agent) mixed with hexadecane (68% PDMS/32% hexadecane	Room temperature cure over 1-2 days via a platinum reaction	1 successful encapsulation of a single DIB (2 droplets). Alamethicin activity was recorded in a bilayer formed in PDMS/hex., though the bilayer failed during before solidification.	Large molecule size resulted in large contact angle (and thus large interface area). Fixed electrodes prevented complete zipping of droplets, which prevented droplet coalescence before curing
2	Silicone Sol. 5293	unknown composition (methacyroloxy, or acryloxy-PDMS most likely)	Dual cure (UV/moisture in shadowed areas)	Local curing occurred at the oil/water interface, which prevented the exclusion of excess solvent during droplet positioning.	No measure of monolayer formation observed, since the polymer cured between droplets
3	Silicone Sol. 6002S	unknown composition	Room temperature cure in ~60 min.	Large BLM, eventual droplet coalescence	Large molecule size results in a large interface size and resulted in droplet coalescence
4	Gelest DMS-U21	Acryloxypropyl-terminated PDMS, MW~800	UV cure with the addition of 1%wt DPMA, or benzophenone in xylol	Very fast UV curing (<20 seconds) to produce a clear, slightly-yellow hard polymer. In the monomer state, the droplets became white and blurry. No DIB formation attempted	Amphiphilic nature of the A-PDMS resulted in the migration and absorption of the monomer into the droplet interior.
5	Gelest DMS-R05, DMS-R11, DMS-R18	Methacryloxypropyl-terminated PDMS. R05: MW~400, R11: MW~1000, R18: MW~5000	UV cure with the addition of 1% wt DMPA, or benzophenone in xylol	UV curing to give softer, more brittle clear polymer. Slower curing than the A-PDMS. Droplets fused almost immediately after solvent exclusion upon attempted DIB formation. No measurements of a bilayer were obtained.	Again, the amphiphilic nature of the MA-PDMS seemed to prevent the formation of a lipid monolayer at the oil water interface. The droplets remained clear, indicating absorption into the aqueous droplets did not occur, though all tests seemed to indicate that the lipid monolayers were not present to support the interface upon solvent excretion. Varying molecular weights were tested try to reduce the effects of the polar functional endgroups, though at the expense of increasing molecular weight.
6	Gelest DMS-V00	Vinyl-terminated PDMS, MW~180	Cures through a platinum addition reaction. UV cure is not an option	DIB formation attempts yielded quality bilayers and the activity of ALm proteins was measured in DIBs formed in v-PDMS. Curing the matrix was attempted via UV, though not successful.	The small, hydrophobic monomer molecules resulted in stable DIBs with small-medium interface sizes. However, a quick curing procedure for the matrix was not determined.

bilayers that can support transmembrane biomolecules due to its completely hydrophobic chemical structure. Further, the small molecule size of the lowest available molecular weight version of this monomer prevents significant growth in the interface. As a result, the membranes formed between adjacent droplets demonstrated very high electrical resistances and were observed to be resistant to rupture during testing. The downside to this material system is additional components required to create a crosslinkable matrix. Whereas A-PDMS and MA-PDMS cure rapidly under UV radiation when a photo-initiator is added, vinyl-PDMS does not crosslink.

C.5 Revised Criteria for Candidate Encapsulants

The results in this paper present a chronological study of candidate materials for encapsulating droplet-interface bilayers. Each material system tested demonstrated some of the criteria, though none matched all of the conditions necessary to create stable DIB networks contained with a cured solid matrix. These tests prove that all conditions must be met in order to create durable, encapsulated droplet-interface bilayers and as a result of the observations from this study, a revised set of primary criteria for a suitable encapsulation material is presented.

Table C.3: Revised material criteria for chemical encapsulation of DIBs

Parameter	Acceptable Range/Comments
Miscibility/Hydrophobicity	Hydrophobic both in the uncured and cured state to allow for proper phase separation and promote adequate phospholipid self-assembly
Specific Gravity	< 1
Molecule Size	< 300 g/mole, for reasonable interface size and sufficient stability
Viscosity	< ~200 cP
Curing Mechanism	Photocuring preferred, though quick room termperature cure also acceptable
Optical Transparency	Optically transparent for initial droplet-positioning and for optical signaling/excitation of encapsulated DIBs after formation

C.6 Viability of Chemical Encapsulation

Permanent chemical encapsulation of droplet-interface bilayers seeks to extend the durability and portability of this technology by creating a novel material system that features aqueous liquid droplets contained within the solid exterior matrix. The true challenge in creating robust methods to chemically-encapsulated droplets lie in the details of molecular size and assembly in the presence of a changing "oil" phase. Unlike DIBs formed in hexadecane, where the sizes of the solvent molecules that surround the lipid-encased droplets do not change, the transition from a liquid to a solid through polymerization is by nature a process by which the size of the molecule grows infinitely large. Without a small buffer of a traditional oil phase (i.e. decane, hexadecane) to buffer the droplets, the larger polymer molecules effect monolayer fluidity and surface tension–both of which directly affect bilayer stability.

Possible methods to achieve chemical encapsulated networks may include multi-phase-separated systems (e.g., like water-in-oil-in-water emulsions) that can retain a small amount of oil between the droplets and the supporting substrate. Physical encapsulation (presented in Chapter 4 provides clear evidence that encapsulation of biomolecular network can be readily obtained as long as this notion of proper phase composition and arrangement are preserved.

Appendix D

Photolithography and Deep Reactive Ion Etching of Silicon Wafers

The fabrication procedure for developing etched silicon wafers used to create microchannels within PDMS is described in detail in this appendix. The work was performed under the assistance of Mr. Donald Leber in the Micron Lab (Whittemore Hall) at Virginia Tech and the following procedures were obtained directly from Don Leber.

D.1 Photoresist Spin Coating and UV Exposure

The following recipe creates a $7-8\mu$m thick layer of AZP9260 Photoresist (MicroChemicals GmbH) onto a clean silicon wafer. For etching processes approaching depths of 200μm, it is advised to repeat the spin coating and soft bake steps in order to create a thicker, $15-16\mu$m layer of photoresist such that the photoresist is not etched away during long-duration wafer etching.

D.1.1 Preparations

1. Take PR9260 out of the refrigerator the night before to allow it to reach room temperature
2. Place silicon wafer in wafer container and label it
3. Clean photoresist beaker and wafer tweezers
4. Set the hot plat to 114^{o}C (actual 110^{o}C)
5. Turn on gases and power for the Karl-Suss MA-6 UV source (exposure tool)
6. Make sure you have acetone, isopropyl alcohol (IPA), hexamethyldisilane (HMDS), photoresist developer (AZ400K)
7. Have pipettes and wipes on hand

D.1.2 Wafer Clean (Solvent Clean)

1. Caution: Do not allow any fluid to enter the vacuum chuck or under the chuck assembly
2. Center the wafer on spin coat processor
3. Set the processor to a cleaning program (1.5 min @ 3000 rpm for 8μm thickness) or (1.5 min @ 2000 rpm for $>$ 8μm thickness)
4. Spray acetone + IPA for 30 seconds onto spinning wafer
5. Spray IPA for 30 seconds
6. DO NO ALLOW ACETONE TO DRY ON SAMPLE BEFORE RINSING WITH IPA
7. Let it spin for the last 30 seconds with no spray
8. Dehydrate the wafer by backing at 130^{o}C for 2 minutes

D.1.3 Photoresist Coating

1. Pour PR in a clean beaker and cover it
2. Spin a few drops of HMDS for 30 seconds to promote adhesion of the PR to the wafer
3. Bake again at 120^{o}C for 3 minutes to dehydrate the surface
4. Allow to cool before applying the photoresist

5. Set the processor to a coating program
6. Dispense PR (10 sec @ 500 rpm)
7. Spin PR (45 sec @ 3000 rpm)
8. Visually inspect sample for uniform resist layer. (Resist coating should appear to be smooth, with no bubbles or particles)
9. Edge Bead Removal: wipe the edge of the wafer with a wipe or applicator stick while turning the wafer by hand
10. Clean the backside of the wafer

D.1.4 UV Exposure and Development

1. Soft bake PR-coated wafer for 3 min @ 110^{o}C
2. Turn on MA-6, follow operating procedure
3. Clean photomask
4. Load photomask, dark side up
5. Select program #5, set exposure to 40 seconds (50 seconds for a $15 - 16\mu$m-thick photoresist layer)
6. Load wafer, make sure the wafer is clean
7. Expose to UV
8. Pour 1 part by volume developer (AZ400K) + 3 parts deionized (DI) water water in shallow dish
9. Place wafer in the developer for $5 - 6$ minutes ($8 - 9$ minutes for double layer of photoresist
10. Rinse wafer thoroughly with DI water and dry with nitrogen

D.2 Deep Reactive Ion Etching

The photomask geometries transfered to the photoresist layer defines which areas of the wafer will not be etched during deep reactive ion etching (DRIE). In the case where the wafer

is used as a master for soft-lithography of PDMS microchannels, the photomask prevents etching in the areas that define the channels such that raised features in the shapes of the channels are produced on the silicon wafer surface. Again, DRIE was performed under the guidance of Mr. Don Leber in the Micron Lab using an Alcatel AMS100 Deep Reactive Ion Etcher. Prior to etching it is advised to obtain an initial mass of the wafer with photoresist and measure the photoresist thickness using a Dektak3 Surface Profilometer.

D.2.1 Wafer Etching

1. Sign in
2. Vent load lock, F9
3. Place wafer into holder
4. Etch for desired time
5. F3 to run the process (after running use F10 for visual status, F3 for numerical status)
6. Vent load lock to get the wafer
7. Pump load lock, F9
8. Check the setting of thermalization (F12), logout, sign out
9. Dip wafer in acetone for 30min to strip away remaining photoresist
10. Wash with acetone and then IPA
11. Dry with nitrogen
12. O_2 cleaning for 10 min
13. Sign out

D.2.2 Alcatel Operating Parameters

The etching process was performed in stages in order to first determine the etch rate for the given etching parameter shown in Figure D.1 and the specific photomask design since

Recipe							
Gas							
Pulsed							
	Inact. State (sccm)	**Active State (sccm)**	**Priority**	**Duration (s)**			
SF6(1000)	0	300	2	7			
C4F8(400)	0	150	1	**2**			
Power/Pressure							
Source gen	Load	Tune	SH gen.2				
checked	650	800	checked				
	Regulation mode						
	Pressure						
C4F8	4.50E-02						
SF6	4.50E-02						
Power	**Source G (W)**		**LF. Gene Pulsed**				
C4F8	1800		H. Pow (W)	H. Time (ms)	L. Pow (W)	L. Time (ms)	
SF6	1800	C4F8	**80**	20	0	8**0**	
Step Time							
Process Duration							
10 min							
SH Option							
He Pressure	**SH Position from source (mm)**						
Center	200						
1.50E+01							

Figure D.1: Operating parameters used to etch silicone wafers.

the etch rate is dependent on the area of the wafer being etched. Typically, a 3-minute etch is performed and then the wafer is weighed and the step height is measured from a PR-covered region down to the etched wafer level. The total etch height then is computed by subtracting the initial photoresist thickness from the total measured step height. Etch rate is subsequently determined by dividing by the prescribed etching time. Multiple etch/measurement cycles can be repeated in order to monitor etch rate for the wafer. Once the etch rate is determined, the wafer is etched for the remaining time needed to obtain desired feature heights (or etch depths) on the wafer. For total etching distances of less than 60μm, the DekTak profilometer can be used to measure the final feature heights. Otherwise,

measurements of feature height are obtained indirectly by measuring the dimensions of the resulting PDMS channels. Scanning electron microscopy (SEM) is another option for measuring feature heights on both the wafer or the PDMS materials, but this technique was not explored in this work.

Bibliography

[1] Trisha Creekmore. The science channel's 100 greatest discoveries. Discovery Communications, LLC., 2008.

[2] Thomas J. Mueller and James D. DeLaurier. Aerodynamics of small vehicles. *Annual Review of Fluid Mechanics*, 35(1):89–111, 2003.

[3] Jae-Sung Bae, Michael T. Seigler, Daniel Inman, and In Lee. Aerodynamic and aeroelastic considerations of a variable-span morphing wing. AIAA, 2004.

[4] Robert D. Dowling, Steven W. Etoch, Karla A. Stevens, Amy C. Johnson, and Jr Gray, Laman A. Current status of the AbioCor implantable replacement heart. *Ann Thorac Surg*, 71(90030):S147–149, 2001.

[5] Robert D. Dowling, Jr Gray, Laman A., Steven W. Etoch, Hillel Laks, Daniel Marelli, Louis Samuels, John Entwistle, Greg Couper, Gus J. Vlahakes, and O. H. Frazier. The AbioCor implantable replacement heart. *Ann Thorac Surg*, 75(90060):S93–99, 2003.

[6] S. Hofmann, C. T. Wong Po Foo, F. Rossetti, M. Textor, G. Vunjak-Novakovic, D. L. Kaplan, H. P. Merkle, and L. Meinel. Silk fibroin as an organic polymer for controlled drug delivery. *Journal of Controlled Release*, 111(1-2):219–227, 2006.

[7] Jonathan A. Kluge, Olena Rabotyagova, Gary G. Leisk, and David L. Kaplan. Spider silks and their applications. *Trends in Biotechnology*, 26(5):244–251, 2008.

[8] Charu Vepari and David L. Kaplan. Silk as a biomaterial. *Progress in Polymer Science*, 32(8-9):991–1007, 2007.

[9] Philip Ball. Synthetic biology for nanotechnology. *Nanotechnology*, 16:R1–R8, 2005.

[10] B. A. Cornell, V. L. B. Braach-Maksvytis, L. G. King, P. D. J. Osman, B. Raguse, L. Wieczorek, and R. J. Pace. A biosensor that uses ion-channel switches. *Nature*, 387(6633):580–583, 1997.

[11] Hagan Bayley and Paul S. Cremer. Stochastic sensors inspired by biology. *Nature*, 413(6852):226–230, 2001.

[12] Yan-lei Su, Jin-ru Li, Long Jiang, and Jie Cao. Biosensor signal amplification of vesicles functionalized with glycolipid for colorimetric detection of escherichia coli. *Journal of Colloid and Interface Science*, 284(1):114–119, 2005.

[13] Vishnu B. Sundaresan. *Biological Ion Transporters as Gating Devices for Chemomechanical and Chemoelectrical Energy Conversion*. Dissertation, Virginia Tech, Blacksburg, VA, May 15, 2007 2007.

[14] Ryohei Yasuda, Hiroyuki Noji, Kazuhiko Kinosita, and Masasuke Yoshida. F1-ATPase is a highly efficient molecular motor that rotates with discrete 120^o steps. *Cell*, 93(7):1117–1124, 1998.

[15] Henry Hess and Viola Vogel. Molecular shuttles based on motor proteins: active transport in synthetic environments. *Reviews in Molecular Biotechnology*, 82(1):67–85, 2001.

[16] Yann Astier, Hagan Bayley, and Stefan Howorka. Protein components for nanodevices. *Current Opinion in Chemical Biology*, 9(6):576–584, 2005.

[17] Rupa Das, Patrick J. Kiley, Michael Segal, Julie Norville, A. Amy Yu, Leyu Wang, Scott A. Trammell, L. Evan Reddick, Rajay Kumar, Francesco Stellacci, Nikolai Lebedev, Joel Schnur, Barry D. Bruce, Shuguang Zhang, and Marc Baldo. Integration of photosynthetic protein molecular complexes in solid-state electronic devices. *Nano Letters*, 4(6):1079–1083, 2004.

[18] Tzy-Jiun M. Luo, Ricky Soong, Esther Lan, Bruce Dunn, and Carlo Montemagno. Photo-induced proton gradients and ATP biosynthesis produced by vesicles encapsulated in a silica matrix. *Nat Mater*, 4(3):220–224, 2005.

[19] Leland H. Hartwell, John J. Hopfield, Stanislas Leibler, and Andrew W. Murray. From molecular to modular cell biology. *Nature*, 402:C47–C52, 1999.

[20] Wikipedia. Eukaryote. Wikipedia, December 20, 2008 2008.

[21] Franklin M. Harold. *The Way of the Cell: Molecules, Organisms and the Order of Life*. Oxford University Press, New York, NY, 2001.

[22] Stephen R. Bolsover, Jeremy S. Hyams, Elizabeth A. Shephard, Hugh A. White, and Claudia G. Wiedemann. *Cell Biology: A Short Course*. John Wiley & Sons, Inc., Hoboken, NJ, 2nd edition, 2004.

[23] H. T. Tien and A. L. Ottova. The lipid bilayer concept and its experimental realization: from soap bubbles, kitchen sink, to bilayer lipid membranes. *J. of Membrane Science*, 189:83–117, 2001.

[24] S. J. Singer and Garth L. Nicolson. The fluid mosaic model of the structure of cell membranes. *Science*, 175(4023):720–731, 1972.

[25] Pieter R. Cullis and Michael J. Hope. Physical properties and functional roles of lipids in membranes. In D. E. Vance and J. Vance, editors, *Biochemistry of Lipids, Lipoproteins and Membranes*, volume 20 of *New Comprehensive Biochemistry*, chapter Chapter 1, page 596. Elsevier Science Publishers B. V., Amsterdam, The Netherlands, 1991.

[26] Wikipedia. Surfactant. Wikipedia: The Free Encyclopedia, December 28, 2008 2008.

[27] B. L. Smiley and G. L. Richmond. Alkyl chain ordering of asymmetric phosphatidylcholines adsorbed at a liquid-liquid interface. *J. Phys. Chem. B*, 103(4):653–659, 1999.

[28] Charles Tanford. The hydrophobic effect and the organization of living matter. *Science*, 200(4345):1012–1018, 1978.

[29] Charles Tanford. *The Hydrophobic Effect: Formation of Micelles and Biological Membranes*. John Wiley & Sons, Inc., New York, NY, 2 edition, 1980.

[30] David Chandler. Interfaces and the driving force of hydrophobic assembly. *Nature*, 437(7059):640–647, 2005.

[31] Sol M. Gruner. Intrinsic curvature hypothesis for biomembrane lipid composition: A role for nonbilayer lipids. *Proceedings of the National Academy of Sciences of the United States of America*, 82(11):3665–3669, 1985.

[32] P. J. Booth. Sane in the membrane: designing systems to modulate membrane proteins. *Curr. Opin. in Struct. Biol.*, 15:435–440, 2005.

[33] E. Ruckenstein and R. Nagarajan. Aggregation of amphiphiles in nonaqueous media. *J. Phys. Chem.*, 84:1349–1358, 1980.

[34] Jens A. Lundbaek, M. Mae, Andreia, and O. S. Andersen. Lipid bilayer electrostatic engery, curvature stress, and assembly of gramicidin channels. *Biochemistry*, 36(19):5695–5701, 1997.

[35] J. McIntosh, Thomas and Sidney A. Simon. Roles of bilayer material properties in function and distribution of membrane proteins. *Annu. Rev. Biophys. Biomol. Struct.*, 35:177–198, 2006.

[36] Evan. Evans and David. Needham. Physical properties of surfactant bilayer membranes: thermal transitions, elasticity, rigidity, cohesion and colloidal interactions. *The Journal of Physical Chemistry*, 91(16):4219–4228, 1987.

[37] D. Needham and D. A. Haydon. Tensions and free energies of formation of "solventless" lipid bilayers. measurement of high contact angles. *Biophys. J.*, 41(3):251–257, 1983.

[38] D. Needham and E. Evans. Structure and mechanical properties of giant lipid (dmpc) vesicle bilayers from 20.degree.c below to 10.degree.c above the liquid crystal-crystalline phase transition at 24.degree.c. *Biochemistry*, 27(21):8261–8269, 1988.

[39] D Needham and R S Nunn. Elastic deformation and failure of lipid bilayer membranes containing cholesterol. *Biophys. J.*, 58(4):997–1009, 1990.

[40] S. Lee, D. H. Kim, and D. Needham. Equilibrium and dynamic interfacial tension measurements at microscopic interfaces using a micropipet technique. 2. dynamics of phospholipid monolayer formation and equilibrium tensions at the water-air interface. *Langmuir*, 17(18):5544–5550, 2001.

[41] Jens A. Lundbaek. Regulation of membrane protein function by lipid bilayer elasticityâe"a single molecule technology to measure the bilayer properties experienced by an embedded protein. *J. Phys.: Condens. Matter*, 18:S1305–S1344, 2006.

[42] J. R. Silvius. Thermotropic phase transitions of pure lipids in model membranes and their modification by membrane proteins. In P. C. Jost and O. H. Griffith, editors, *Lipid-Protein Interactions*, volume 2, pages 239–281. Wiley-Interscience, New York, NY, 1982.

[43] R. A. Walker, J. A. Gruetzmacher, and G. L. Richmond. Phosphatidylcholine monolayer structure at a liquid-liquid interface. *J. Am. Chem. Soc.*, 120(28):6991–7003, 1998.

[44] Andrew D. Robertson and Kenneth P. Murphy. Protein structure and the energetics of protein stability. *Chemical Reviews*, 97(5):1251–1268, 1997.

[45] H. Bayley. Pore-forming proteins with built-in triggers and switches. *Bioorganic Chemistry*, 23(4):340–354, 1995.

[46] Langzhou Song, Michael R. Hobaugh, Christopher Shustak, Stephen Cheley, Hagan Bayley, and J. Eric Gouaux. Structure of staphylococcal alpha -hemolysin, a heptameric transmembrane pore. *Science*, 274(5294):1859–1865, December 13, 1996 1996.

[47] Aleksij Aksimentiev and Klaus Schulten. Imaging alpha-hemolysin with molecular dynamics: Ionic conductance, osmotic permeability, and the electrostatic potential map. *Biophys. J.*, 88(6):3745–3761, 2005.

[48] Vishnu Baba Sundaresan, Christopher Homison, Lisa M. Weiland, and Donald J. Leo. Biological transport processes for microhydraulic actuation. *Sensors and Actuators B: Chemical*, 123(2):685–695, 2007a.

[49] Vishnu Baba Sundaresan and Donald J. Leo. Modeling and characterization of a chemomechanical actuator using protein transporter. *Sensors and Actuators B: Chemical*, 131(2):384–393, 2008.

[50] P. Mueller, D. O. Rudin, H. T. Tien, and W. C. Wescott. Reconstitution of excitable cell membrane structure in vitro. *Circulation*, 26:1167–1171, 1962.

[51] A. Ottova and H. T. Tien. The 40th anniversary of bilayer lipid membrane research. *Bioelectrochemistry*, 56:171–173, 2002.

[52] P. Mueller, D. O. Rudin, H. T. Tien, and W. C. Wescott. Chapter 11 - formation and properties of bimolecular lipid membranes. In J. F. Danielli, K. G. A. Pankhurst, and A. C. Riddiford, editors, *Recent Prog. Surf. Sci.*, volume 1, pages 379–393. Academic Press, 1964.

[53] Angelica L. Ottova and H. Ti Tien. Self-assembled bilayer lipid membranes: from mimicking biomembranes to practical applications. *Bioelectrochemistry and Bioenergetics*, 42(2):141–152, 1997.

[54] E. Sackmann. Supported membranes: Scientific and practical applications. *Science*, 271:43–48, 1996.

[55] Agnes Pockels. Surface tension. *Nature*, 43:437–439, 1891.

[56] E. Gorter and F. Grendel. On bimolecular layers of lipoids on the chromocytes of the blood. *J. Exp. Med.*, 41(4):439–443, March 31, 1925 1925.

[57] P. Lauger, W. Lesslauer, E. Marti, and J. Richter. Electrical properties of bimolecular phospholipid membranes. *Biochim. Biophys. Acta*, 135:20–32, 1967.

[58] M. Naumowicz, A. D. Petelska, and Z. A. Figaszewski. Impedance analysis of phosphatidylcholine-cholesterol system in bilayer lipid membranes. *Electrochimica Acta*, 50:2155–2161, 2005.

[59] M. Naumowicz, A. D. Petelska, and Z. A. Figaszewski. Capacitance and resistance of the bilayer membrane formed of phosphatidylcholine and cholesterol. *Cellular & Molecular Biology Letters*, 8:5–18, 2003.

[60] M. Montal and P. Mueller. Formation of bimolecular membranes from lipid monolayers and a study of their electrical properties. *Proc. Nat. Acad. Sci. USA*, 69(12):3561–3566, 1972.

[61] M. Mayer, J. K. Kriebel, M. T. Tosteson, and G. M. Whitesides. Microfabricated teflon membranes for low-noise recordings of ion channels in planar lipid bilayers. *Biophys. J.*, 85:2684–2695, 2003.

[62] D. P. Nikolelis and C. G. Siontorou. Bilayer lipid membranes for flow injection monitoring of acetylcholine, urea, and penicillin. *Anal. Chem.*, 67:936–944, 1995.

[63] M. Thompson, R. B. Lennox, and R. A. McClelland. Structure and electrochemical properties of microfiltration filter-lipid membrane systems. *Anal. Chem.*, 54:76–81, 1982.

[64] K. Yoshikawa, H. Hayashi, T. Shimooka, H. Terada, and T. Ishii. Stable phospholipid membrane supported on porous filter paper. *Biochem. Biophys. Res. Comm.*, 145(3):1092–1097, 1987.

[65] Y. Kobatake, A. Irimajiri, and N. Matsumoto. Studies of electric capacitance of membranes. I. a model membrane composed of a filter paper and a lipid analogue. *Biophys. J.*, 10(8):728–744, 1970.

[66] K. P. O'Boyle, F. A. Siddiqi, and H. T. Tien. Antigen-antibody-complement reaction studies on micro bilayer lipid membranes. *Immunol. Comm.*, 13(2):85–103, 1984.

[67] M. A. Dhoke, P. J. Ladha, F. J. Boerio, L. B. Lessard, D. H. Malinowska, J. Cuppoletti, and D. S. Wieczorek. Porous membranes for reconstitution of ion channels. *Biochim. Biophys. Acta*, 1716:117–125, 2005.

[68] J. Drexler and C. Steinem. Pore-suspending lipid bilayers on porous alumina investigated by electrical impedance spectroscopy. *J. Phys. Chem. B*, 107:11245–11254, 2003.

[69] Winfried Romer and Claudia Steinem. Impedance analysis and single-channel recordings on nano-black lipid membranes based on porous alumina. *Biophys. J.*, 86(2):955–965, 2004.

[70] R. Naumann, T. Baumgart, Graber P., A. Jonczyk, Offenhausser A., and W. Knoll. Proton transport through a peptide-tethered bilayer lipid membrane by the h+-atp synthase from chloroplasts measured by impedance spectroscopy. *Biosensors & Bioelectronics*, 17:25–34, 2002.

[71] T. Cassier, A. Sinner, Offenäuser A., and Möhwald H. Homogeneity, electrical resistivity and lateral diffusion of lipid bilayers coupled to polyelectrolyte multilayers. *Colloids and Surfaces B: Biointerfaces*, 15:215–225, 1999.

[72] M. C. Peterman, J. M. Ziebarth, O. Braha, H. Bayley, H. A. Fishman, and D. M. Bloom. Ion channels and lipid bilayer membranes under high potentials using microfabricated apertures. *Biomedical Microdevices*, 4(3):231–236, 2002.

[73] G. Wiegand, N. Arribas-Layton, H. Hillebrandt, E. Sackmann, and P. Wagner. Electrical properties of supported lipid bilayer membranes. *J. Phys. Chem. B*, 106:4245–4254, 2002.

[74] C. Schmidt, M. Mayer, and H. Vogel. A chip-based biosensor for the functional analysis of single ion channels. *Angewandte Chemie (International Ed.)*, 39(17):3137–3140, 2000.

[75] K. B. Blodgett. Monomolecular films of fatty acids on glass. *J. Am. Chem. Soc.*, 56:495, 1934.

[76] K. B. Blodgett. Films built by depositing successive monomolecular layers on a solid surface. *J. Am. Chem. Soc.*, 57:1007–1022, 1935.

[77] K. B. Blodgett and I. Langmuir. Built-up films of barium stearate and their optical properties. *Phys. Rev.*, 51:964–982, 1937.

[78] C. P. L. Rubinger, R. L. Moreira, L. A. Cury, G. N. Fontes, B. R. A. Neves, A. Meneguzzi, and C. A. Ferreira. Langmuir–Blodgett and Langmuir–Schaefer films of poly(5-amino-1-naphthol) conjugated polymer. *Applied Surface Science*, 253:543–548, 2006.

[79] W. M. Reichert, C. J. Bruckner, and J. Joseph. Langmuir–Blodgett films and black lipid membranes in biospecific surface-selective sensors. *Thin Solid Films*, 152:345–376, 1987.

[80] E. Kalb, S. Frey, and L. K. Tamm. Formation of supported planar bilayers by fusion of vesicles to supported phospholipid monolayers. *Biochim. Biophys. Acta.*, 1103:307–316, 1992.

[81] Susan Ferro-Novick and Reinhard Jahn. Vesicle fusion from yeast to man. *Nature*, 370(6486):191–193, 1994.

[82] Z. V. Leonenko, A. Carnini, and D. T. Cramb. Supported planar bilayer formation by vesicle fusion: the interaction of phospholipid vesicles with surfaces and the eÂ¡ect of gramicidin on bilayer properties using atomic force microscopy. *Biochimica et Biophysica Acta*, 1509:131–147, 2000.

[83] M. R. R. de Planque, G. P. Mendes, M. Zagnoni, M. E. Sandison, K. H. Fisher, R. M. Berry, A. Watts, and H. Morgan. Controlled delivery of membrane proteins to artificial lipid bilayers by nystatin-ergosterol modulated vesicle fusion. *IEE Proceedings Nanobiotechnology*, 153(2):21–30, 2006.

[84] R Langer. New methods of drug delivery. *Science*, 249(4976):1527–1533, 1990.

[85] Ning Z. Wu, Daphne Da, Tracy L. Rudoll, David Needham, A. Richard Whorton, and Mark W. Dewhirst. Increased microvascular permeability contributes to preferential accumulation of stealth liposomes in tumor tissue. *Cancer Res.*, 53(16):3765–3770, 1993.

[86] David Needham and Mark W. Dewhirst. The development and testing of a new temperature-sensitive drug delivery system for the treatment of solid tumors. *Advanced Drug Delivery Reviews*, 53(3):285–305, 2001.

[87] P. Y. Bolinger, D. Stamou, and H. Vogel. Integrated nanoreactor systems: Triggering the release and mixing of compounds inside single vesicles. *J. Am. Chem. Soc.*, 126(28):8594–8595, 2004.

[88] P. Nollert, H. Kiefer, and Jähnig F. Lipid vesicle adsorption versus formation of planar bilayers on solid surfaces. *Biophys. J.*, 69:1447–1455, 1995.

[89] T. Okazaki, K. Morigaki, and T. Taguchi. Phospholipid vesicle fusion on micropatterned polymeric bilayer substrates. *Biophys. J.*, 91:1757–1766, 2006.

[90] A. A. Brian and H. M. McConnell. Allogeneic stimulation of cytotoxic T cells by supported planar membranes. *Proc. Natl. Acad. Sci. USA*, 81:6159–6163, 1984.

[91] S J Archer and D S Cafiso. Voltage-dependent conductance for alamethicin in phospholipid vesicles. a test for the mechanism of gating. *Biophys. J.*, 60(2):380–388, 1991.

[92] Robert C. MacDonald, Felecian D. Jones, and Ruozi Qui. Fragmentation into small vesicles of dioleoylphosphatidylcholine bilayers during freezing and thawing. *Biochimica et Biophysica Acta (BBA) - Biomembranes*, 1191(2):362–370, 1994.

[93] William L. Hwang, Min Chen, Brid Cronin, Matthew A. Holden, and Hagan Bayley. Asymmetric droplet interface bilayers. *J. Am. Chem. Soc.*, 130(18):5878–5879, 2008.

[94] Stephen H. White. Chapter 1 - the physical nature of planar bilayer membranes. In Christopher Miller, editor, *Ion Channel Reconstitution*, pages 3–35. Plenum Press, New York, NY, 1986.

[95] S. H. White. Formation of "solvent-free" black lipid bilayer membranes from glyceryl monooleate dispersed in squalene. *Biophys. J.*, 23(3):337–347, 1978.

[96] J. R. Thompson, A. J. Heron, Y. Santoso, and M. I. Wallace. Enhanced stability and fluidity in droplet on hydrogel bilayers for measuring membrane protein diffusion. *Nano Lett.*, 7(12):3875–3878, 2007.

[97] K. Funakoshi, H. Suzuki, and S. Takeuchi. Lipid bilayer formation by contacting monolayers in a microfluidic device for membrane protein analysis. *Anal. Chem.*, 78(24):8169–8174, 2006.

[98] M. A. Holden, D. Needham, and H. Bayley. Functional bionetworks from nanoliter water droplets. *J. Am. Chem. Soc.*, 129(27):8650–8655, 2007.

[99] W. L. Hwang, M. A. Holden, S. White, and H. Bayley. Electrical behavior of droplet interface bilayer networks: Experimental analysis and modeling. *J. Am. Chem. Soc.*, 129(38):11854–11864, 2007.

[100] A. J. Heron, J. R. Thompson, A. E. Mason, and M. I. Wallace. Direct detection of membrane channels from gels using water-in-oil droplet bilayers. *J. Am. Chem. Soc.*, 129(51):16042–16047, 2007.

[101] John Hagan Pryce Bayley, Matthew Holden, Andrew John Heron, and David Needham. Formation of bilayers of amphiphatic molecules, 2008.

[102] H. T. Tien, S. H. Wurster, and A. L. Ottova. Electrochemistry of supported bilayer lipid membranes: background and techniques for biosensor development. *Bioelectrochemistry and Bioenergetics*, 42:77–94, 1997.

[103] O. S. Andersen. Ion movement through gramicidin a channels. single-channel measurements at very high potentials. *Biophys. J.*, 41(2):119–133, 1983.

[104] M. Misakian, J. J. Kasianowicz, B. Robertson, and O. Petersons. Frequency response of alternating currents through the staphylococcus aureus alpha-hemolysin ion channel. *Bioelectromagnetics*, 22(7):487–493, 2001.

[105] P. C. Jordan. Fifty years of progress in ion channel research. *NanoBioscience, IEEE Transactions on*, 4(1):3–9, 2005.

[106] Denise Wong, Tae-Joon Jeon, and Jacob Schmidt. Single molecule measurements of channel proteins incorporated into biomimetic polymer membranes. *Nanotechnology*, 17(15):3710, 2006.

[107] J. Sabo, A. Ottova, G. Laputkova, M. Legin, L. Vojcikova, and H. T. Tien. A combined ac-dc method for investigating supported bilayer lipid membranes. *Thin Solid Films*, 306:112–118, 1997.

[108] F. Bordi, C. Cametti, and A. Gliozzi. Impedance measurmements of self-assembled lipid bilayer membranes on the tip of an electrode. *Bioelectrochemistry*, 57:39–46, 2002.

[109] Stephen A. Sarles, Vishnu B. Sundaresan, and Donald J. Leo. Electrical impedance analysis of phospholipid bilayer membranes for enabling engineering design of bio-based devices. In *MRS Fall Meeting*, volume 1016E of *Biomolecular and Biologically Inspired Interfaces and Assemblies*, page in press, Boston, MA USA, 2007. Tok, H., MRS.

[110] Vishnu Baba Sundaresan, Stephen Andrew Sarles, and Donald J. Leo. Characterization of porous substrates for biochemical energy conversion devices. volume 6928, page 69280K. SPIE, 2008.

[111] Mineo Ikematsu, Masahiro Iseki, Yukihiro Sugiyama, and Atsuo Mizukami. Lipid bilayer formation in a microporous membrane filter monitored by ac impedance analysis and purple membrane photoresponses. *Journal of Electroanalytical Chemistry*, 403(1-2):61–68, 1996.

[112] W. Romer and et al. Channel activity of a viral transmembrane peptide in micro-blms: Vpu_{1-32} from HIV-1. *J. of Am. Chem. Soc.*, 126:16267–16274, 2004.

[113] H. T. Tien. Cyclic voltammetry of bilayer lipid membranes. *J. Phys. Chem.*, 88:3172–3174, 1984.

[114] J. M. Mountz and H. T. Tien. Photoeffects of pigmented lipid membranes in a microporous filter. *Photochem. Photobiol. Sci.*, 28:395–400, 1978.

[115] X. K. Zhao, S. Baral, and J. H. Fendler. Electrochemical characterization of bilayer lipid membrane-semiconductor junctions. *J. Phys. Chem.*, 94:2043–2052, 1990.

[116] P. Krysinki, H. T. Tien, and A. Ottova. Charge-transfer processes and redox reactions in planar lipid monolayers and bilayers. *Biotechnol. Prog.*, 15:974–990, 1999.

[117] R Kwok and E Evans. Thermoelasticity of large lecithin bilayer vesicles. *Biophys. J.*, 35(3):637–652, 1981.

[118] David P. Hopkinson. *Measurements and Modeling of the Failure Pressure of Bilayer Lipid Membranes*. Dissertation, Virginia Tech, Blacksburg, VA, December 6, 2007 2007.

[119] N. R. Pallas and B. A. Pethica. Liquid-expanded to liquid-condensed transition in lipid monolayers at the air/water interface. *Langmuir*, 1(4):509–513, 1985.

[120] S. Lee, D. H. Kim, and D. Needham. Equilibrium and dynamic interfacial tension measurements at microscopic interfaces using a micropipet technique. 1. a new method for determination of interfacial tension. *Langmuir*, 17(18):5537–5543, 2001.

[121] L. K. Tamm and H. M. McConnell. Supported phospholipid bilayers. *Biophys. J.*, 47:105–113, 1985.

[122] Taekjip Ha. Single-molecule fluorescence resonance energy transfer. *Methods*, 25(1):78–86, 2001.

[123] Albert Cha, Gregory E. Snyder, Paul R. Selvin, and Francisco Bezanilla. Atomic scale movement of the voltage-sensing region in a potassium channel measured via spectroscopy. *Nature*, 402(6763):809–813, 1999.

[124] V. Borisenko, T. Lougheed, J. Hesse, E. Fureder-Kitzmuller, N. Fertig, J. C. Behrends, G. A. Woolley, and G. J. Schutz. Simultaneous optical and electrical recording of single gramicidin channels. *Biophys. J.*, 84:612–622, 2003.

[125] Andrew J. Heron, James R. Thompson, Bríd Cronin, Hagan Bayley, and Mark I. Wallace. Simultaneous measurement of ionic current and fluorescence from single protein pores. *Journal of the American Chemical Society*, 131(5):1652–1653, 2009.

[126] B. L. Smiley and G. L. Richmond. Assembly of long chain phosphatidylcholines at a liquid-liquid interface. *Biopolymers*, 57(2):117–125, 2000.

[127] R. A. Walker, D. E. Gragson, and G. L. Richmond. Induced changes in solvent structure by phospholipid monolayer formation at a liquid-liquid interface. *Colloids and Surfaces A: Physicochemical and Engineering Aspects*, 154(1-2):175–185, 1999.

[128] E. T. Castellana and P. S. Cremer. Solid supported lipid bilayers: From biophysical studies to sensor design. *Surface Science Reports.*, 61:429–444, 2006.

[129] Erik Reimhult and Karthik Kumar. Membrane biosensor platforms using nano- and microporous supports. *Trends in Biotechnology*, 26(2):82–89, 2008.

[130] Ricky K. Soong, George D. Bachand, Hercules P. Neves, Anatoli G. Olkhovets, Harold G. Craighead, and Carlo D. Montemagno. Powering an inorganic nanodevice with a biomolecular motor. *Science*, 290(5496):1555–1558, 2000.

[131] Yannick Rondelez, Guillaume Tresset, Takako Nakashima, Yasuyuki Kato-Yamada, Hiroyuki Fujita, Shoji Takeuchi, and Hiroyuki Noji. Highly coupled ATP synthesis by F1-ATPase single molecules. *Nature*, 433(7027):773–777, 2005.

[132] A. Bernards, Daniel, G. Malliaras, George, E. S. Toombes, Gilman, and Sol M. Gruner. Gating of an organic transistor through a bilayer lipid membrane with ion channels. *Applied Physics Letters*, 89(5):053505, 2006.

[133] D. A. Haydon and J. L. Taylor. Contact angles for thin lipid films and the determination of london-van der waals forces. *Nature*, 217(5130):739–740, 1968.

[134] J. Requena, D. F. Billett, and D. A. Haydon. Van der waals forces in oil-water systems from the study of thin lipid films. i. measurement of the contact angle and the estimation of the van der waals free energy of thinning of a film. *Proceedings of the Royal Society of London. Series A, Mathematical and Physical Sciences (1934-1990)*, 347(1649):141–159, 1975.

[135] J. Requena and D. A. Haydon. Van der waals forces in oil–water systems from the study of thin lipid films. ii. the dependence of the van der waals free energy of thinning on film composition and structure. *Proceedings of the Royal Society of London. Series A, Mathematical and Physical Sciences (1934-1990)*, 347(1649):161–177, 1975.

[136] Tatsuya Kitade, Keisuke Kitamura, Shigehiko Takegami, Yoko Miyata, Miwa Nagatomo, Tomomi Sakaguchi, and Michiko Furukawa. Needle-type ultra micro silver/silver chloride reference electrode for use in micro-electrochemistry. *Analytical Sciences*, 21(8):907–912, 2005.

[137] Brian J. Polk, Anna Stelzenmuller, Geraldine Mijares, William MacCrehan, and Michael Gaitan. Ag/agcl microelectrodes with improved stability for microfluidics. *Sensors and Actuators B: Chemical*, 114:239–247, 2006.

[138] Bernard A. Boukamp. A nonlinear least squares fit procedure for analysis of immittance data of electrochemical systems. *Solid State Ionics*, 20:31–44, 1986.

[139] R. Fettiplace, D. M. Andrews, and D. A. Haydon. The thickness, composition and structure of some lipid bilayers and natural membranes. *Journal of Membrane Biology*, 5(3):277–296, 1971.

[140] T. Baba, Y. Toshima, H. Minamikawa, M. Hato, K. Suzuki, and N. Kamo. Formation and characterization of planar lipid bilayer membranes from synthetic phytanyl-chained glycolipids. *Biochimica et Biophysica Acta (BBA) - Biomembranes*, 1421(1):91–102, 1999.

[141] Stephen A. Sarles and Donald J. Leo. Tailored current–voltage relationships of droplet-interface bilayers using biomolecules and external feedback control. *Journal of Intelligent Material Systems and Structures*, 20(10):1233–1247, 2009.

[142] Stephen A. Sarles, Pegah Ghanbari Bavarsad, and Donald J. Leo. Incorporation and characterization of biological molecules in droplet-interface bilayer networks for novel active systems. In Ahmadian Mehdi and N. Ghasemi-Nejhad Mehrdad, editors, *Active and Passive Smart Structures and Integrated Systems 2009*, volume 7288, page 72880H, San Diego, CA, 2009. SPIE.

[143] A. Ottova, V. Tvarozek, J. Racek, J. Sabo, W. Ziegler, T. Hianik, and H. T. Tien. Self-assembled blms: biomembrane models and biosensor applications. *Supramolecular Science*, 4(1-2):101–112, 1997.

[144] Mauro Robello and Alessandra Gliozzi. Conductance transition induced by an electric field in lipid bilayers. *Biochimica et Biophysica Acta (BBA) - Biomembranes*, 982(1):173–176, 1989.

[145] Jeremy P. Wilburn, David W. Wright, and David E. Cliffel. Imaging of voltage-gated alamethicin pores in a reconstituted bilayer lipid membrane via scanning electrochemical microscopy. *The Analyst*, 131(2):311–316, 2006.

[146] Sarah E. Henrickson, Martin Misakian, Baldwin Robertson, and John J. Kasianowicz. Driven dna transport into an asymmetric nanometer-scale pore. *Physical Review Letters*, 85(14):3057, 2000.

[147] Petr G. Merzlyak, Maria-Fatima P. Capistrano, Angela Valeva, John J. Kasianowicz, and Oleg V. Krasilnikov. Conductance and ion selectivity of a mesoscopic protein nanopore probed with cysteine scanning mutagenesis. *Biophys. J.*, 89(5):3059–3070, 2005.

[148] Gianfranco Menestrina. Ionic channels formed by staphylococcus aureus alpha-toxin: Voltage-dependent inhibition by divalent and trivalent cations. *Journal of Membrane Biology*, 90(2):177–190, 1986.

[149] B. Bechinger. Structure and functions of channel-forming peptides: Magainins, cecropins, melittin and alamethicin. *Journal of Membrane Biology*, 156(3):197–211, 1997.

[150] K He, S J Ludtke, W T Heller, and H W Huang. Mechanism of alamethicin insertion into lipid bilayers. *Biophys. J.*, 71(5):2669–2679, 1996.

[151] I. Vodyanoy, J. E. Hall, and T. M. Balasubramanian. Alamethicin-induced current-voltage curve asymmetry in lipid bilayers. *Biophys. J.*, 42(1):71–82, 1983.

[152] Igor Vodyanoy, James E. Hall, and Vitaly Vodyanoy. Alamethicin adsorption to a planar lipid bilayer. *Biophys. J.*, 53:649–658, 1988.

[153] Takashi Okazaki, Machiko Sakoh, Yasuo Nagaoka, and Koji Asami. Ion channels of alamethicin dimer n-terminally linked by disulfide bond. *Biophys. J.*, 85(1):267–273, 2003.

[154] O Alvarez and R Latorre. Voltage-dependent capacitance in lipid bilayers made from monolayers. *Biophys. J.*, 21(1):1–17, 1978.

[155] Stephen A. Sarles and Donald J. Leo. Physical encapsulation of droplet interface bilayers for durable, portable biomolecular networks. *Lab on a Chip*, 10(6):710–717, 2010.

[156] Sara Aghdaei, Mairi E. Sandison, Michele Zagnoni, Nicolas G. Green, and Hywel Morgan. Formation of artificial lipid bilayers using droplet dielectrophoresis. *Lab on a Chip*, 8(10):1617–1620, 2008.

[157] Giovanni Maglia, Andrew J. Heron, William L. Hwang, Matthew A. Holden, Ellina Mikhailova, Qiuhong Li, Stephen Cheley, and Hagan Bayley. Droplet networks with incorporated protein diodes show collective properties. *Nat Nano*, 4(7):437–440, 2009.

[158] Xiao-feng Kang, Stephen Cheley, Allison C. Rice-Ficht, and Hagan Bayley. A storable encapsulated bilayer chip containing a single protein nanopore. *Journal of the American Chemical Society*, 129(15):4701–4705, 2007.

[159] Hagan Bayley, Brid Cronin, Andrew Heron, Matthew A. Holden, William L. Hwang, Ruhma Syeda, James Thompson, and Mark Wallace. Droplet interface bilayers. *Molecular BioSystems*, 4(12):1191–1208, 2008.

[160] Stephen A. Sarles and Donald J. Leo. Regulated attachment method for reconstituting lipid bilayers of prescribed size within flexible substrates. *Analytical Chemistry*, 82(3):959–966, 2010.

[161] Leonid Gitlin, Philipp Schulze, and Detlev Belder. Rapid replication of master structures by double casting with PDMS. *Lab on a Chip*, 9(20):3000–3002, 2009.

[162] Attila Gaspar, Menake Piyasena, Lajos Daroczi, and Frank Gomez. Magnetically controlled valve for flow manipulation in polymer microfluidic devices. *Microfluidics and Nanofluidics*, 4(6):525–531, 2008.

[163] Xize Niu, Mengying Zhang, Jinbo Wu, Weijia Wen, and Ping Sheng. Generation and manipulation of "smart" droplets. *Soft Matter*, 5(3):576–581, 2009.

[164] Sung Kwon Cho, Yuejun Zhao, and Chang-Jin "CJ" Kim. Concentration and binary separation of micro particles for droplet-based digital microfluidics. *Lab on a Chip*, 7(4):490–498, 2007.

[165] J. P. Rolland, R. M. VanDam, D. A. Schorzman, S. R. Quake, and J. M. DeSimone. Solvent-resistant photocurable "Liquid Teflon" for microfluidic device fabrication. *J. Am. Chem. Soc.*, 126(8):2322–2323, 2004.

[166] G. Oukhaled, L. Bacri, J. Mathe, J. Pelta, and L. Auvray. Effect of screening on the transport of polyelectrolytes through nanopores. *EPL (Europhysics Letters)*, (4):48003, 2008.

[167] L. G. M. Gordon and D. A. Haydon. Potential-dependent conductances in lipid membranes containing alamethicin. *Philosophical Transactions of the Royal Society of London. Series B, Biological Sciences*, 270(908):433–447, 1975.

[168] L. R. Opsahl and W. W. Webb. Transduction of membrane tension by the ion channel alamethicin. *Biophysical Journal*, 66(1):71–74, 1994.

[169] Olaf S. Andersen and Roger E. Koeppe. Bilayer thickness and membrane protein function: An energetic perspective. *Annual Review of Biophysics and Biomolecular Structure*, 36(1):107–130, 2007.

[170] Amir Aharoni, Gil Amitai, Kalia Bernath, Shlomo Magdassi, and Dan S. Tawfik. High-throughput screening of enzyme libraries: Thiolactonases evolved by fluorescence-activated sorting of single cells in emulsion compartments. *Chemistry & Biology*, 12(12):1281–1289, 2005.

[171] Jason L. Poulos, Tae-Joon Jeon, Robert Damoiseaux, Eugene J. Gillespie, Kenneth A. Bradley, and Jacob J. Schmidt. Ion channel and toxin measurement using a high throughput lipid membrane platform. *Biosensors and Bioelectronics*, 24(6):1806–1810, 2009.

[172] Ruhma Syeda, Matthew A. Holden, William L. Hwang, and Hagan Bayley. Screening blockers against a potassium channel with a droplet interface bilayer array. *Journal of the American Chemical Society*, 130(46):15543–15548, 2008.

[173] Noah Malmstadt, Michael A. Nash, Robert F. Purnell, and Jacob J. Schmidt. Automated formation of lipid-bilayer membranes in a microfluidic device. *Nano Letters*, 6(9):1961–1965, 2006.

[174] David C. Duffy, J. Cooper McDonald, Olivier J. A. Schueller, and George M. Whitesides. Rapid prototyping of microfluidic systems in poly(dimethylsiloxane). *Analytical Chemistry*, 70(23):4974–4984, 1998.

[175] J. Cooper McDonald and George M. Whitesides. Poly(dimethylsiloxane) as a material for fabricating microfluidic devices. *Accounts of Chemical Research*, 35(7):491–499, 2002.

[176] Johana Kuncova-Kallio and Pasi J. Kallio. PDMS and its suitability for analytical microfluidic devices. In *Engineering in Medicine and Biology Society, 2006. EMBS '06. 28th Annual International Conference of the IEEE*, pages 2486–2489, 2006.

[177] Adam C. Siegel, Sergey S. Shevkoplyas, Douglas B. Weibel, Derek A. Bruzewicz, Andres W. Martinez, and George M. Whitesides. Cofabrication of electromagnets and microfluidic systems in poly(dimethylsiloxane). *Angewandte Chemie International Edition*, 45(41):6877–6882, 2006.

[178] Andrea Bubendorfer, Xianming Liu, and Amanda V Ellis. Microfabrication of PDMS microchannels using SU-8/PMMA moldings and their sealing to polystyrene substrates. *Smart Materials and Structures*, (2):367, 2007.

[179] Jessamine Ng Lee, Cheolmin Park, and George M. Whitesides. Solvent compatibility of poly(dimethylsiloxane)-based microfluidic devices. *Analytical Chemistry*, 75(23):6544–6554, 2003.

[180] Manoj K. Chaudhury. Surface free energies of alkylsiloxane monolayers supported on elastomeric polydimethylsiloxanes. *Journal of Adhesion Science and Technology*, 7:669–675, 1993.

[181] Manoj K. Chaudhury. Self-assembled monolayers on polymer surfaces. *Biosensors and Bioelectronics*, 10(9-10):785–788, 1995.

[182] Dhananjay Bodas and Chantal Khan-Malek. Hydrophilization and hydrophobic recovery of PDMS by oxygen plasma and chemical treatment–an SEM investigation. *Sensors and Actuators B: Chemical*, 123(1):368–373, 2007.

[183] Guodong Sui, Jinyi Wang, Chung-Cheng Lee, Weixing Lu, Stephanie P. Lee, Jeffrey V. Leyton, Anna M. Wu, and Hsian-Rong Tseng. Solution-phase surface modification in intact poly(dimethylsiloxane) microfluidic channels. *Analytical Chemistry*, 78(15):5543–5551, 2006.

[184] Bharat Bhushan and Michal Cichomski. Nanotribological characterization of vapor phase deposited fluorosilane self-assembled monolayers deposited on polydimethylsiloxane surfaces for biomedical micro-/nanodevices. *J. Vac. Sci. Technol. A*, 25(4):1285–1293, 2007.

[185] Bharat Bhushan, Derek Hansford, and Kang Kug Lee. Surface modification of silicon and polydimethylsiloxane surfaces with vapor-phase-deposited ultrathin fluorosilane films for biomedical nanodevices. *J. Vac. Sci. Technol. A*, 24(4):1197–1202, 2006.

[186] Dan Wang, Richard D. Oleschuk, and J. Hugh Horton. Surface modification of poly(dimethylsiloxane) with a perfluorinated alkoxysilane for selectivity toward fluorous tagged peptides. *Langmuir*, 24(3):1080–1086, 2008.

[187] Dan Wang, Michelle Douma, Brenna Swift, Richard D. Oleschuk, and J. Hugh Horton. The adsorption of globular proteins onto a fluorinated PDMS surface. *Journal of Colloid and Interface Science*, 331(1):90–97, 2009.

[188] Brian J Adzima and Sachin S Velankar. Pressure drops for droplet flows in microfluidic channels. *Journal of Micromechanics and Microengineering*, (8):1504, 2006.

[189] J T Schumacher, A Grodrian, C Kremin, M Hoffmann, and J Metze. Hydrophobic coating of microfluidic chips structured by SU-8 polymer for segmented flow operation. *Journal of Micromechanics and Microengineering*, (5):055019, 2008.

[190] P. B. Umbanhowar, V. Prasad, and D. A. Weitz. Monodisperse emulsion generation via drop break off in a coflowing stream. *Langmuir*, 16(2):347–351, 2000.

[191] D. R. Link, S. L. Anna, D. A. Weitz, and H. A. Stone. Geometrically mediated breakup of drops in microfluidic devices. *Physical Review Letters*, 92(5):054503, 2004.

[192] Joshua D. Tice, Helen Song, Adam D. Lyon, and Rustem F. Ismagilov. Formation of droplets and mixing in multiphase microfluidics at low values of the reynolds and the capillary numbers. *Langmuir*, 19(22):9127–9133, 2003.

[193] Bo Zheng, L. Spencer Roach, and Rustem F. Ismagilov. Screening of protein crystallization conditions on a microfluidic chip using nanoliter-size droplets. *Journal of the American Chemical Society*, 125(37):11170–11171, 2003.

[194] C. Holtze, A. C. Rowat, J. J. Agresti, J. B. Hutchison, F. E. Angile, C. H. J. Schmitz, S. Koster, H. Duan, K. J. Humphry, R. A. Scanga, J. S. Johnson, D. Pisignano, and D. A. Weitz. Biocompatible surfactants for water-in-fluorocarbon emulsions. *Lab on a Chip*, 8(10):1632–1639, 2008.

[195] Gnther Boheim. Statistical analysis of alamethicin channels in black lipid membranes. *Journal of Membrane Biology*, 19(1):277–303, 1974.